Thesis by Publication

Development of Aggregation-Resistant Monoclonal Antibodies Through Antibody Engineering and Formulation Approaches

Mouhamad Reslan

This thesis is submitted in full satisfaction of the requirements for the degree of Doctor of Philosophy at the University of Sydney.

School of Pharmacy

Faculty of Medicine and Health

2018

Statement of Authentication

This thesis is submitted to the University of Sydney in fulfilment of the requirement for the degree of Doctor of Philosophy. The work presented in this thesis is, to the best of my knowledge and belief, original except as acknowledged in the text. I hereby declare that I have not submitted this material, either in full or in part, for a degree at this or any other institution.

Signature:

Date: 13th of August 2018

Acknowledgements

I start by acknowledging the traditional owners of this land - the Gadigal people of the Eora nation - on which I have spent the last three to four years conducting research and developing new friendships. To my supervisor, Associate Professor Veysel Kayser, I thank you for your patience, support and guidance during this time. I thank you for embarking on this journey with me, while giving me the freedom to decide my own path. To my co-supervisor Associate Professor Serdar Kuyucak and the Biophysics Team, thank you for the time we worked together, the words of support as we hit roadblocks along the way, and the celebrations as we broke through and graduated. To my colleagues, Vicki, Esteban, Yusuf and the many students I met on the way, I could not have asked for a better network of friends to work alongside and to enjoy this experience with. Thank you for all the laughter and fun we had together (and all those games of ping pong!). To the amazing people I met along the way including Meryem, Zehra and David – thank you for being mentors, your time and effort has been invaluable to myself and others and has contributed significantly to the success of the work within this thesis. Thank you to everyone in the office, and the wonderful staff and academics at the School of Pharmacy, for your continued support and words of encouragement. Thank you to Sheng and Donna for your time training me and assisting with my research at MBF. Thank you to Mario, for sharing your expertise with us when we first began and supporting us throughout. Finally, thank you to my family for your constant support during the challenges and moments of joy; I can now close this chapter of my life, having gained new insights, experiences, and ideas. I look forward to writing the next chapter.

Authorship attribution statement

Chapter 1 of this thesis (with omitted sections) is published as:

Elgundi, Z., Reslan, M., Cruz, E., Sifniotis, V., Kayser, V. (2017). The state-of-play and future of antibody therapeutics. Advanced Drug Delivery Reviews, 122:2-19.

M. Reslan wrote several sections of the review including: parts of the section 'Biobetters', all 'Physical and chemical degradation of antibodies' including 'Computational design tools', made minor edits to 'optimisation of antibody bioavailability and delivery' and contributed to writing the abstract, introduction, and conclusion. He also critically reviewed and edited the entire manuscript to prepare it for submission. In the thesis introduction, he updated the information in each included section with current literature.

Chapter 2 of this thesis is published as:

Reslan, M., Demir, Y., Trout, B., Chan, H., Kayser, V. (2017). Lack of a synergistic effect of arginine-glutamic acid on the physical stability of spray-dried bovine serum albumin. Pharmaceutical Development and Technology, 22:785-791.

M. Reslan co-designed the study, prepared the formulations and performed most of the formulation characterisation. He analysed most of the data and wrote the manuscript.

Chapter 3 of this thesis is published as:

Reslan, M., Kayser, V. (2016). The effect of deuterium oxide on the conformational stability and aggregation of bovine serum albumin. Pharmaceutical Development and Technology, 1-7.

M. Reslan co-designed the study, performed all experiments and data analysis, and wrote the manuscript.

Chapter 4 of this thesis is published as:

Reslan, M., Kayser, V. (2018). Ionic liquids as biocompatible stabilizers of proteins. Biophysical Reviews. doi:10.1007/s12551-018-0407-6

M. Reslan performed the literature searches and co-wrote the review.

Chapter 5 of this thesis is prepared for publication as:

Reslan, M., Kayser, V. (2018). Analysis of the aggregation kinetics of Herceptin® (trastuzumab). European Journal of Pharmaceutics and Biopharmaceutics.

M. Reslan co-designed the study, performed all experiments and data analysis, and wrote the manuscript.

Chapter 6 of this thesis published as:

Reslan, M., Vijayaraghavan R., Macfarlane D. R., Kayser, V. (2018). Choline ionic liquid enhances the stability of Herceptin® (trastuzumab). Chemical Communications, 54:10622-10625.

M. Reslan co-designed the study, prepared the formulations, performed all stability characterisation experiments and data analysis, and wrote the manuscript.

Chapter 7 of this thesis is published as:

Elgundi, Z., Sifniotis, V., Reslan, M., Cruz, E., Kayser, V. (2017). Laboratory Scale Production and Purification of a Therapeutic Antibody. Journal of Visualized Experiments, 119: e55153.

M. Reslan assisted with the writing of the manuscript. He designed and wrote all sections relating to the purification and characterisation of the antibody following expression, performed those experiments and prepared the figures.

Chapter 8 of this thesis is prepared for publication as:

Reslan, M., Sifniotis, V., Cruz, E., Sumer-Bayraktar, Z., Kayser, V. (2018). Enhancing the stability of adalimumab by engineering additional glycosylation motifs. European Journal of Pharmaceutics and Biopharmaceutics.

M. Reslan co-designed the experiments and conducted most of the experimental work including mutagenesis, sequencing analysis, expression of the antibody variants, purification and characterisation. He also wrote most sections of the manuscript and compiled it together for publication.

In addition to the statements above, in cases where I am not the corresponding author of a published item, permission to include the published material has been granted by the corresponding author.

Mouhamad Reslan, Signature: *13th of August 2018*

As supervisor for the candidature upon which this thesis is based, and corresponding author for the publications, I can confirm that the authorship attribution statements above are correct.

Veysel Kayser, Signature: *13th of August 2018*

Table of Contents

Thesis abstract

Monoclonal antibodies (mAbs) have an invaluable role in the treatment of cancers, auto-immune and inflammatory conditions. Since their advent, approximately 80 antibodies and antibody-based therapeutic products have gained marketing approval, quickly earning their positions in the list of top ten selling prescription products worldwide. One of the major challenges associated with the development of mAbs and novel antibody-based therapies, is protein aggregation - a degradation phenomenon which results in 'clumping' of proteins together, and subsequent loss of protein activity. Furthermore, antibody aggregates have been associated with immunogenic reactions experienced by patients undergoing immunotherapy with antibody products. Preventing antibody aggregation has major implications for the future of biopharmaceutical development; not only are immunogenic reactions minimised, the shelf-life of therapeutic antibodies is significantly increased thus reducing manufacturing costs, there is increased flexibility in the type of antibody formulations that can be manufactured - including non-invasive options - and the half-life of antibodies *in vivo* may be increased. Other types of degradation can also occur including deamidation, oxidation and fragmentation, although less commonly.

We tackled the challenge of protein aggregation via two main approaches – 1) investigating novel additives and formulation approaches to suppress protein aggregation of model proteins and antibodies; 2) engineering structural changes to antibodies to enhance their stability and resistance to aggregation without compromising their therapeutic function. Protein unfolding and aggregation was accelerated by incubation at elevated temperatures or by using chemical denaturants and characterised using intrinsic and extrinsic fluorescence, size-exclusion-HPLC and light scattering techniques. This orthogonal approach allowed us to probe the conformational and colloidal stability of the protein at every step in the aggregation process.

Successful approaches discovered in our work include the use of novel stabilizing additives such as ionic liquids and an approach to engineering antibodies with additional glycosylation to strategically improve their conformational stability. The work described in this thesis paves the way for the development of next-generation therapeutic antibodies, or biobetters, which are resistant to aggregation.

Thesis introduction

Chapter 1 of this thesis explores current developments in the field of antibody therapy, the types of degradation processes that affect antibodies and their formulations, the development of biobetter antibodies engineered with improved biophysical properties, and the outlook of the antibody therapeutic landscape. This chapter was published in the Editor's issue of Advanced Drug Delivery Reviews:

Elgundi, Z., Reslan, M., Cruz, E., Sifniotis, V., Kayser, V. (2017). The state-of-play and future of antibody therapeutics. Advanced Drug Delivery Reviews, 122:2-19.

Amongst the many degradation processes affecting antibodies discussed in chapter 1, protein aggregation is one of the most common and challenging. One consequence of this degradation process is reduced flexibility in the types of formulations that can be developed and administered. As such, many biologics such as antibodies are administered via diluted infusion bags, resulting in added inconvenience to the patient. In chapter 2, we investigated the combination use of two amino acids (arginine and glutamic acid) as synergistic stabilizing additives for an inhalable dry powder protein formulation. The study found that the hypothesised synergistic effect of these additives was not observed for the protein tested. It was concluded that the synergy of these amino acids was protein and concentration-specific. Chapter 2 was published in the Pharmaceutical Development and Technology journal:

Reslan, M., Demir, Y., Trout, B., Chan, H., Kayser, V. (2017). Lack of a synergistic effect of arginine-glutamic acid on the physical stability of spray-dried bovine serum albumin. Pharmaceutical Development and Technology, 22:785-791.

In chapter 3 we replaced H_2O as the solvent for a protein formulation with deuterium oxide (D_2O) to induce in hydrogen-deuterium exchange and deuteration of the protein. This was hypothesised to enhance protein stability as the protein's intra-molecular interactions are strengthened by deuterium. We observed a modest improvement in the stability of the protein tested, however, the rate of aggregation was also increased. The work described in this chapter was published in the Pharmaceutical Development and Technology journal:

Reslan, M., Kayser, V. (2016). The effect of deuterium oxide on the conformational stability and aggregation of bovine serum albumin. Pharmaceutical Development and Technology, 1-7.

Rapid developments in the field of ionic liquids and their widespread applications prompted a literature review of their use as potential stabilizers of proteins, an area of research which had not yet received its deserved attention. In chapter 4, we summarised the literature available on the effect of ionic liquids on protein stability and screened for biocompatible ionic liquids with potential application for the stabilization of therapeutic antibodies. This invited review was published in the Biophysical Reviews journal:

Reslan, M., Kayser, V. (2018). Ionic liquids as biocompatible stabilizers of proteins. Biophysical Reviews. doi:10.1007/s12551-018-0407-6

Monoclonal antibodies (mAbs) are multi-domain proteins with more complex aggregation pathways than smaller, globular proteins. To aid the development of rational approaches to stabilise mAbs, a mechanistic understanding of the aggregation process is needed. In chapter 5, we thoroughly studied the aggregation kinetics of trastuzumab - a marketed therapeutic mAb - and developed a simple model to characterise the process of aggregation connecting data from accelerated studies at elevated temperature to long-term storage at lower temperature. This study was prepared for publication to the European Journal of Pharmaceutics and Biopharmaceutics:

Reslan, M., Kayser, V. (2018). Analysis of the aggregation kinetics of Herceptin® (trastuzumab). European Journal of Pharmaceutics and Biopharmaceutics.

In chapter 6, we formulated trastuzumab at high concentrations with a biocompatible ionic liquid – choline dihydrogen phosphate (CDHP) – discovered during our previous literature search (chapter 4). At ~50% w/v concentrations of CDHP, we were successful in stabilizing trastuzumab at concentrations 3-fold higher (60 mg/mL) than the concentration of the marketed product. The complex effect of different concentrations of CDHP on the stability of trastuzumab was detailed in this chapter, including its effect on the conformational stability of each domain and the process of aggregation. Chapter 6 was published as a communication article at Chemical Communications:

Reslan, M., Vijayaraghavan R., Macfarlane D. R., Kayser, V. (2018). Choline ionic liquid enhances the stability of Herceptin® (trastuzumab). Chemical Communications, 54:10622-10625.

Antibody engineering is another approach utilised to prevent protein aggregation and enhance antibody stability. In chapter 7, We developed and described a cost-effective, simple and high-yielding protocol to express, purify and characterise therapeutic antibodies in preparation for our antibody engineering work. Chapter 7 was published in the Journal of Visualized Experiments:

Elgundi, Z., Sifniotis, V., Reslan, M., Cruz, E., Kayser, V. (2017). Laboratory Scale Production and Purification of a Therapeutic Antibody. Journal of Visualized Experiments, 119: e55153.

In chapter 8, we rationally engineered blockbuster antibody adalimumab with additional N-linked glycans to stabilize an aggregation-prone region in the Fab domain. Amongst the mutants tested, several had significantly enhanced conformational stability in the Fab domain, attributed to the added pair of glycans. The binding affinity of the mutants to the antigen and Fc receptors was also checked to characterise any change in therapeutic function. Determination of the aggregation-prone region was based on computational methods, highlighting the significant role of computational tools for the future development of next-generation antibodies. Chapter 8 was prepared for publication to the European Journal of Pharmaceutics and Biopharmaceutics:

Reslan, M., Sifniotis, V., Cruz, E., Sumer-Bayraktar, Z., Kayser, V. (2018). Enhancing the stability of adalimumab by engineering additional glycosylation motifs. European Journal of Pharmaceutics and Biopharmaceutics.

Conferences and publications

Reslan, M., Sifniotis, V., Elgundi, Z., Yasmin, S., Patel, D. J., Kuyucak, S., Kayser, V. (2016). Development of a Trastuzumab (Herceptin) Biobetter with Enhanced Stability and Binding Affinity to HER2. *2016 Sydney Cancer Conference (SCC2016)*, Sydney, Australia.

Reslan, M., Vijayaraghavan R., Macfarlane D. R., Kayser, V. (2018). Choline ionic liquid enhances the stability of Herceptin® (trastuzumab). Chemical Communications, 54:10622-10625.

Reslan, M., Kayser, V. (2018). Ionic liquids as biocompatible stabilizers of proteins. Biophysical Reviews. doi:10.1007/s12551-018-0407-6

Elgundi, Z., Reslan, M., Cruz, E., Sifniotis, V., Kayser, V. (2017). The state-of-play and future of antibody therapeutics. Advanced Drug Delivery Reviews, 122:2-19.

Elgundi, Z., Sifniotis, V., Reslan, M., Cruz, E., Kayser, V. (2017). Laboratory Scale Production and Purification of a Therapeutic Antibody. Journal of Visualized Experiments, 119: e55153.

Reslan, M., Demir, Y., Trout, B., Chan, H., Kayser, V. (2017). Lack of a synergistic effect of arginine-glutamic acid on the physical stability of spray-dried bovine serum albumin. Pharmaceutical Development and Technology, 22:785-791.

Reslan, M., Kayser, V. (2016). The effect of deuterium oxide on the conformational stability and aggregation of bovine serum albumin. Pharmaceutical Development and Technology, 1-7.

CHAPTER 1

“The State-of-Play and Future of Antibody Therapeutics”

Graphical abstract

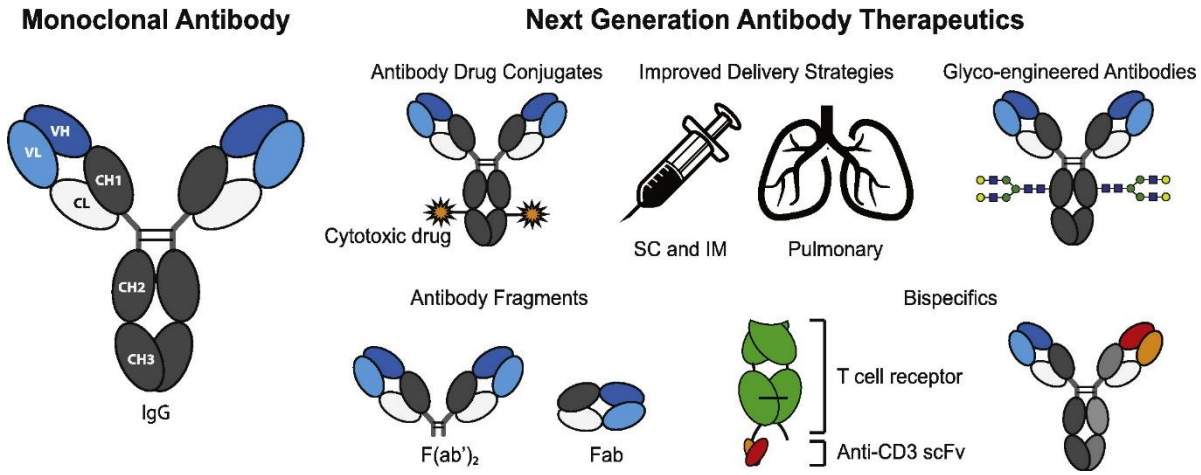

Chapter 1 was published in the Editor’s issue of Advanced Drug Delivery Reviews:

Elgundi, Z., Reslan, M., Cruz, E., Sifniotis, V., Kayser, V. (2017). The state-of-play and future of antibody therapeutics. Advanced Drug Delivery Reviews, 122:2-19.

Several sections were not included in the thesis introduction as they were outside the scope of this thesis. Additionally, minor content has been updated with new developments since publication in 2017.

Abstract

It has been over four decades since the development of monoclonal antibodies (mAbs) using a hybridoma cell line was first reported. Since then approximately 80 therapeutic antibodies have been marketed, mostly as oncology, autoimmune and inflammatory therapeutics. Innovations in antibody engineering are providing the opportunity to design biobetter antibodies with improved biophysical properties to maximize efficacy. The manufacturing process of antibodies is also moving forward with advancements relating to host cell production and purification processes. Studies into the physical and chemical degradation pathways of antibodies are contributing to the design of more stable proteins guided by computational tools. Moreover, the delivery and pharmacokinetics of antibody-based therapeutics are improving as optimized formulations are pursued through the implementation of recent innovations in the field.

1. Introduction

Over the past twenty years, therapeutic antibodies have rapidly become the leading product within the biopharmaceutical market. In 2013, therapeutic antibodies represented 50% of the $140 billion taken by the biopharmaceutical market with sales growing from $39 billion in 2008 to $75 billion in 2013 [1]. There are currently more than 70 therapeutic antibodies approved for established markets such as the United States and Europe with over three hundred antibody-based products in clinical development [1-3]. Therapeutic antibodies are no longer full-length, naked mouse antibodies; advancements in antibody engineering technologies, novel antigen discovery strategies and progress in deciphering disease pathways have all generated robust interest, resources and investment in antibody development. In this review, we will discuss developments in the field of therapeutic antibodies, the growth of biosimilars and pay particular attention to targeting degradation pathways of antibodies to produce more stable biobetter antibodies and formulations.

2. Antibody discovery strategies

The generation of early antibodies relied on the immunization of mice or other mammals with the desired antigen target. This resulted in multiple antibodies directed at different epitopes of the antigen secreted by a mixed population of B cells with each cell secreting only one specific antibody (i.e. polyclonal). Unfortunately, secreting B cells can only replicate a limited number of times, therefore rendering mass production

all but impossible. The ground-breaking hybridoma technology developed by Kohler and Milstein allowed antibody secreting cells from the spleen of immunized animals to be fused with immortalized non-antibody secreting cells, thus resulting in cells that would divide continuously when cultivated in permissive conditions [4, 5]. Although the first recombinant antibodies were produced using this technology, including the first approved therapeutic antibody muromonab-CD3 (Orthoclone OKT®3) in 1986 for preventing kidney transplant rejection, hybridoma production presented some drawbacks. Hybridomas can be labor intensive, low yielding or genetically unstable [6]. More importantly though, the antibody sequences originated from an immunized animal and consequently had the potential of triggering an immune response in humans. Therefore, further improvements were needed to yield antibodies more human-like and safe. These technologies have evolved from chimeric antibodies that is, grafting essential mouse amino acids needed for antigen binding onto a human antibody framework [7, 8] to both *in vitro* and *in vivo* techniques for generating humanized antibodies.

The XenoMouse™ (Abgenix) and HuMab-Mouse® (Medarex) are transgenic mice developed in parallel and in both, the endogenous murine heavy and kappa light chain genes are inactivated and replaced with the equivalent human germline sequences [9, 10]. Injection of antigens into these mice leads to development of 'fully human' antibodies that have undergone mouse somatic hypermutation and selection to relatively high affinity. Validation of this technology came with the regulatory approval of panitumumab (Vectibix®) in 2006; a fully human antibody directed against epidermal growth factor receptor (EGFR) as treatment for advanced colorectal cancer [11]. Since then, RANK ligand-specific denosumab (Prolia®) has been approved for bone loss and TNF-specific golimumab (Simponi®) for rheumatoid arthritis.

An *in vitro* method for generating fully human antibodies can be accomplished by cloning and screening large libraries of sufficiently diverse human antibody genes in combination with display technology. The concept of display technology provides a direct physical link between a gene (genotype) and the encoding antibody fragment (phenotype) to allow selection of genes that encode a protein with the desired binding function. Phage display technology remains the most widely used *in vitro* method for the display of large repertoires and for the selection of high affinity antibodies to biologically relevant targets [6]. Phage display involves the expression of proteins on

the surface of filamentous phage via fusion with phage coat protein with the genetic sequence packaged within, linking phenotype to genotype selection. When combined with antibody libraries, phage display allows for rapid *in vitro* selection of antigen-specific antibodies and recovery of their corresponding coding sequence [12-14]. This system is highly effective, robust and amenable to high throughput processes for screening of $>10^{10}$ specificities [15]. The diversity of phage display libraries is distinguishable by source and design: naïve [16], immune [12], synthetic [17] and semi-synthetic [18]. The technology was first demonstrated for a single chain variable fragment (scFv) [13] with screening of other formats also introduced including human antigen binding fragments (Fabs) [19], domain antibodies [20], camelid domain antibodies [21], single domain shark antibodies [22], diabodies [23] and even whole IgG [24]. The first approved human antibody isolated by phage display technology was adalimumab (Humira®) which binds the cytokine TNF. This antibody was first selected as a scFv expressed on the surface of phage and was further engineered in human IgG1 format, providing major validation for phage display technologies [25]. Adalimumab remains the most lucrative antibody product generating global sales of $18 billion in 2017 [1, 26]. The number of phage display-derived candidates currently in clinical development further demonstrates the value of phage display as an established and reliable drug discovery platform [27].

3. Manufacture of antibodies

Therapeutic antibodies are mainly produced in mammalian host cell lines because of their ability to introduce post-translational modifications. Chinese hamster ovary (CHO) cells remain the most widely used cell line for the manufacture of antibodies (20 of 39 FDA approved), followed by SP2/0 (8/39) and NS0 (7/39) mouse cell lines and hybridomas (2/28). Two of the three Fabs are produced in the bacterial strain *Escherichia coli*. As the clinical success of therapeutic antibodies grows, alternative and more cost-effective production platforms are being pursued including microbial hosts and plant systems. Microbial cells such as bacteria and yeast possess many advantages including fast growth, well-characterised genetics and low cultivation costs.

Antibody production in bacterial systems has focused on fragments due to the lack of post-translation glycosylation required on the Fc region of full length IgG antibodies,

specifically required for efficient FcγR interactions. A major advancement was recently achieved with the expression of active, full-length IgG in the cytoplasm of *E. coli* to generate 'cyclonals'. Robinson et al. used an engineered strain with an oxidative cytoplasmic environment to facilitate and promote the formation of disulphide bonds and efficient IgG folding and assembly [28]. Moreover, molecular engineering of cyclonal Fc domains with previously identified Fc mutations enabled FcγR interactions [29-31]. Conversely, yeast expression offers the advantages of post-translational modifications, disulphide bond formation as well as secretion of correctly-folded proteins. Antibody yields surpassing mammalian systems have been reported for a glyco-engineered strain of *P. pastoris* capable of producing human N-linked glycoproteins [32, 33]. Additionally, a series of experiments have demonstrated production of IgG at industrial scale to be robust and commercially viable [34]. The potential of yeast expression systems has not yet been fully realised with the most advanced antibodies otelixizumab (refer to Fc engineered section) and clazakizumab completing Phase II trials for psoriatic arthritis and rheumatoid arthritis.

Plant systems are also generating interest as an alternative production platform due to the absence of mammalian pathogens but too are subject to disadvantages given the different glycosylation profile to humans, subcellular localisation issues and decreased yield because of proteolytic degradation. Nevertheless, several antibodies have reached clinical development. For instance, CaroRX is an antibody that targets *Streptococcus mutans* and used for treating cavities, produced in *Nicotiana tabacum* and approved for use in Europe [35]. MB66 (or MAPP66) contains a combination of three monoclonal antibodies produced in *Nictiana benthamiana* designed to block distinct mechanisms of HIV which has entered Phase I trials. The clear advantages of using plant systems is the low cost, scalability and relative ease to deploy in developing countries [36, 37]. Interestingly, a biosimilar of trastuzumab produced in *N. benthamiana* is entering Phase I clinical trials. An efficacy study in mice has shown that biosimilar trastuzumab was as effective as originator trastuzumab (Herceptin®) in reducing the size and growth rate of breast cancer tumours [38].

The choice of expression system therefore depends on many factors in order to guarantee cost-effective high yields and meet safety criteria; from discovery stages with the precise sequence and mode of action of the specific antibody to development of the manufacturing cell line. Manufacturing cell lines to yield a therapeutic antibody

are initially generated by vector construction and transfection. A variety of different expression systems and transfection methods exist [39]. Following transfection, cells are subjected to a selection procedure where stable cell lines are cloned and expanded. Several strategies have since evolved from the limiting dilution approach that utilise automated cell sorting equipment [40, 41]. The screening and selection of stable clones with desired growth and production characteristics is a critical albeit time-consuming step in the process. Once conditions are defined, the process is often transferred to a pilot scale to test scalability and produce material for preclinical toxicology studies. Larger scale manufacturing for production of clinical material is performed under current good manufacturing practices (cGMP) regulations involving either fed-batch or continuous perfusion culture [42, 43]. For validation purposes, three (United States) or five (Europe) consecutive full-scale culture runs are required for BLA approval [44].

Therapeutic antibodies must have very high purity and be sterile, with the concentration of host cell proteins reduced to parts per million (ppm), DNA to parts per billion (ppb) and virus levels to less than one virus particle per million doses [45, 46]. The stringent purification of antibodies from mammalian cells is typically accomplished using a three column chromatography process; protein A affinity chromatography as an initial capture step followed by cation exchange (CEX) and anion exchange (AEX) chromatography [47]. These are followed by a virus clearance step after which the purified product is concentrated and diafiltered into the final formulation buffer. While the antibody is primarily captured during the affinity step, the consecutive ion exchange processes act as ‘polishing’ steps to remove impurities such as host cell protein, DNA, aggregates, endotoxin, adventitious and endogenous viruses [44]. With the growing demand and increasing market competition, attention is now being focused on reducing manufacturing costs and improving process efficiency. For example, Protein A affinity chromatography contributes a major cost to the purification process, therefore improved chromatography matrices, specifically non-affinity methods are gaining popularity such as; hydrophobic charge induction chromatography (HCIC), high performance tangential flow filtration (HPTFF) and MEP HyperCel [48-51].

4. Biobetter antibodies

Between 2015-2018 (June) close to 30 mAbs have received marketing approval by the US Food and Drug Administration (FDA) (Table 1), with the rate of approvals steadily increasing each year. Despite its success, antibody-based therapy still presents a long list of important shortcomings that need to be overcome to fully exploit their full therapeutic potential. Typical drawbacks in antibody-based therapy include limited efficacy due to poor tissue and tumor penetration, low *in vivo* efficacy, cumbersome administration, antibody aggregation, solubility as well as high production costs [52].

Table 1. Novel full-length monoclonal antibodies and fragments approved by the FDA in recent years

Name	**Commercial Name**	**Company**	**Target**	**Indication (FDA approved)**	**Format**
APPROVED BY FDA IN 2015					
Secukinumab	Costentyx®	Novartis	IL-17	Psoriasis	IgG1 (fully human)
Dinutuximab	Unituxin®	United Therapeutics Corporation	GD2	Neuroblastoma (pediatric patients)	IgG1 (chimeric)
Alirocumab	Praulent®	Sanofi	PCSK9	Hyperlipidemia	IgG1 (fully human)
Evolocumab	Repatha®	Amgen	PCSK9	Hyperlipidemia	IgG2 (fully human)
Idarucizumab	Praxbind®	Boehringer Ingelheim	Dabigatran	Anticoagulation reversal	Fab fragment (humanised)
Mepolizumab	Nucala®	Glaxo Smith Kline	IL-5	Asthma	IgG1 (humanised)

Necitumumab	Portrazza ®	Eli Lilly	EGFR	NSCLC	IgG1 (fully human)
Daratumumab	Darzalex ®	Janssen Biotech	CD38	Multiple myeloma	IgG1 (fully human)
APPROVED BY FDA IN 2016					
Reslizumab	Cinqair®	Teva	IL-5	Asthma	IgG4 (humanised)
Ixekizumab	Taltz®	Eli Lilly	IL-17a	Psoriasis	IgG4 (humanised)
Obiltoxaximab	Anthim®	Elusys Therapeutics	*Bacillus anthrax*	Anthrax	IgG3 (humanised)
Olaratumab	Lartruvo®	Eli Lilly	PDGFR -α	Soft tissue sarcoma	IgG1 (fully human)
Atezolizumab	Tecentriq ®	Roche/ Genentech	PD-L1	NSCLC, bladder cancers	IgG1 (humanised)
Bezlotoxumab	Zinplava®	Merck	*Clostridium difficile* toxin B	Prevention of recurrent *C. difficile* infection	IgG1 (fully human)
APPROVED BY FDA in 2017					
Brodalumab	Silliq®	Valeant Pharmaceuticals	IL-17R	Psoriasis	IgG1 (fully human)
Ocrelizumab	Ocrevus®	Genentech/ Roche	CD20	Multiple Sclerosis	IgG1 (humanised)

Durvalumab	Imfinzi®	AstraZeneca	PD-L1R	Urothelial and NSCLC	IgG1 (fully human)
Sarilumab	Kevzara®	Regeneron/ Sanofi	IL-6R	Rheumatoid arthritis	IgG1 (fully human)
Guselkumab	Tremfya®	Janssen Biotech/ Johnson & Johnson	IL-23/p19	Psoriasis	IgG1 (fully human)
Benralizumab	Fasenra®	Astra Zeneca	IL-5R	Asthma	IgG1 (humanised)
Dupilumab	Dupixent®	Regeneron/ Sanofi	IL-4R	Atopic Dermatitis	IgG4 (fully human)
Avelumab	Bavencio®	Pfizer/ Merck	PD-L1	NSCLC, gastric and Merkel-cell carcinoma	IgG1 (fully human)
APPROVED BY FDA in 2018 (as of June)					
Ibalizumab-uiyk	Trogarzo®	TaiMed Biologics/ Theratechnologies	CD4	Multi-drug resistant HIV-1	IgG4 (humanised)
Tildrakizumab-asmn	Ilumya®	Sun Pharmaceutical Industries/ Merck	IL-23/p19	Plaque psoriasis	IgG1 (humanised)
Burosumab-twza	Crysvita®	Ultragenyx Pharmaceutical	FGF-23	X-linked hypophosphatemia	IgG1 (fully human)

Erenumab-aooe	Aimovig®	Novartis/ Amgen	CGRPR	Prevention of migraines	IgG2 (fully human)

Abbreviations: GD = disialoganglioside; NSCLC = non-small cell lung cancer; PCSK = proprotein convertase subtilisin/kexin; EGFR = epidermal growth factor receptor; PD-L = programmed death-ligand; PDGFR = platelet-derived growth factor receptor; IL = interleukin; CD = cluster of differentiation; FGF = fibroblast growth factor; CGRPR = calcitonin gene-related peptide receptor

The use of antibody engineering to improve the properties of therapeutic antibodies has advanced greatly in the last decades giving rise to a varied set of novel formats that offer enhanced attributes for therapeutic and research purposes. These novel molecules are often referred to as biobetters or next-generation antibodies and include platforms such as: engineered antibodies for enhanced effector functions, antibody drug-conjugates (ADC), multi-specific antibodies and single-domain antibody fragments (sdAb or nanobodies®) (Fig. 1) [53, 54]. While full-length and IgG1 antibodies still dominate, novel formats such as bispecifics and ADCs are starting to enter the market. In 2017, inotuzumab ozogamicin an anti-CD22 humanized IgG4 antibody conjugated to calicheamicin was approved for acute lymphoblastic leukemia (ALL). The FDA also approved emicizumab, a bispecific IgG4 mAb targeting factor IXa and X [55].

A biobetter can have modifications to its chemical structure such as humanization, fusion/conjugation or be glyco-engineered to be less immunogenic or more efficacious. For instance, anti-CD20 ocrelizumab which was approved by the FDA in 2017 for multiple sclerosis, is a humanized version of rituximab (Rituxan®). A biobetter may be modified to have an improved formulation for improved treatment regimen so treatment is less evasive or have a simplified manufacturing process. This was demonstrated with novel subcutaneous (SC) formulations of trastuzumab (Herceptin®) and rituximab (Mabthera®) developed by co-formulating the antibody with hyaluronidase, an enzyme that increases the absorption and distribution of the injected product [56]. A biobetter may be engineered to have higher target affinity, bind at a different epitope or stronger effector function to enhance efficacy and potentially reduce any off-target side effects. Any such improvement means that the

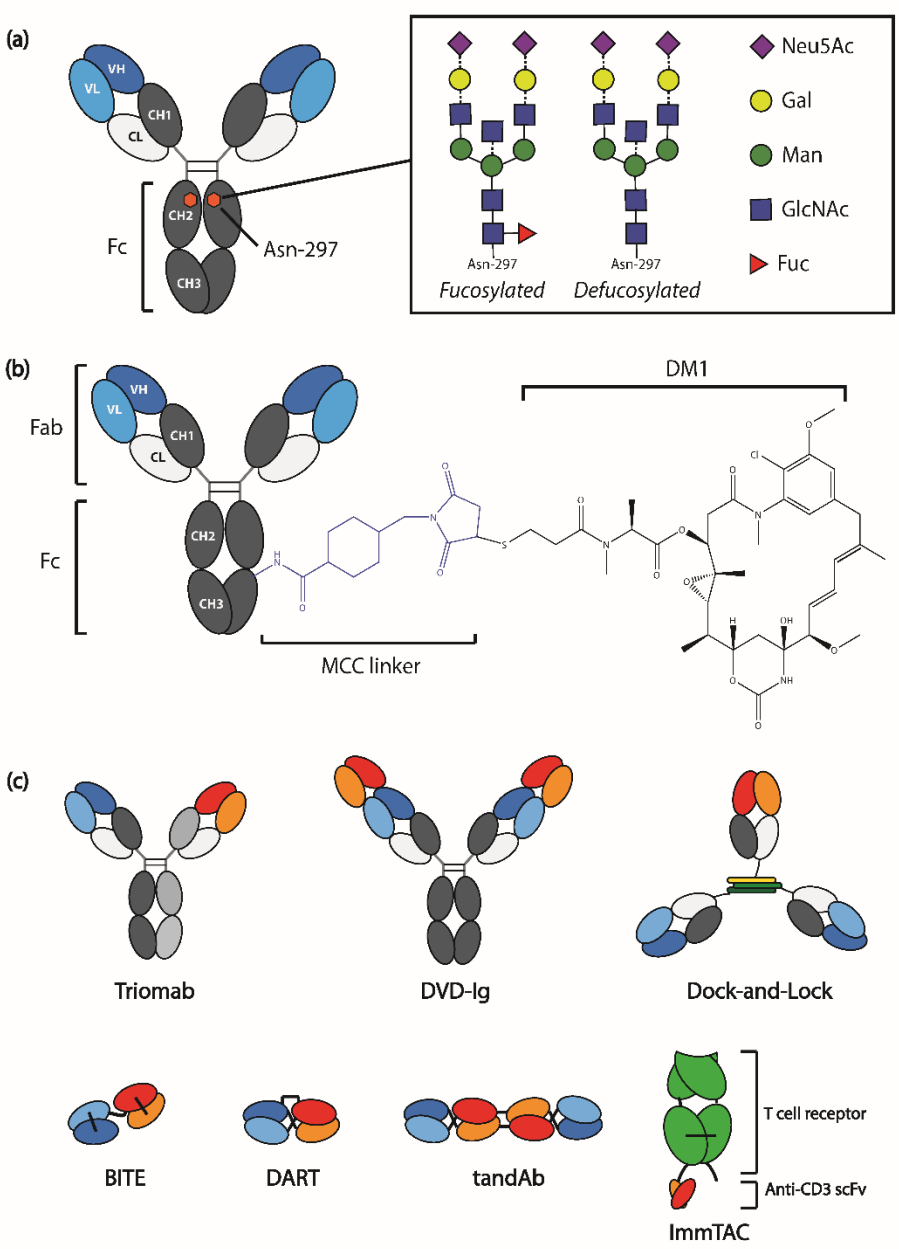

Figure 1. Schematic representation of biobetter antibody formats being pursued for clinical development. (a) Schematic structure of an IgG1 antibody with glycosylation sites at asparagine 297 (Asn-297) in C_H2 domains indicated by hexagons. The general structure of N-linked glycosylation is shown inset; core structures indicated by solid lines and variable structures by dotted lines comprising of Fucose (Fuc), N-Acetylglucosamine(GlcNAc), Mannose (Man), Galactose (Gal) or N-Acetylneuraminic acid (Neu5Ac). Glyco-engineering of antibodies can involve defucosylation which refers to the removal of core fucose to enhance Fc-mediated effector functions. (b) Schematic structure of an antibody drug conjugate (ado-trastuzumab emtansine; Kadcyla®) including N-maleimidomethyl) cyclohexane-1-carboxylate (MCC) linker and maytansinoid 1 (DM1) payload. (c) Prominent bispecific formats in development including: Triomab or Trifunctional antibody, Dual variable domain immunoglobulin (DVD-Ig), Dock-and-Lock (DNL) antigen binding fragments (Fabs), Bispecific T cell engager (BITE), Dual affinity re-targeting (DART) molecule, Tandem diabody (tandAb) and Immune-mobilizing monoclonal T cell receptors against cancer (ImmTAC).

therapeutic has been modified and incomparable to the original therapeutic; it is therefore classified as a new biological therapeutic and requires more laborious testing to obtain regulatory approval before market entry.

4.1. Fc engineered antibodies for enhanced effector functions

Antibody engineering has sought to improve the effector function of antibodies via the Fc region; namely ADCC, complement dependent cytotoxicity (CDC) and PK profile. Specifically, this has been mostly explored through modifications in the amino acid sequence or the glycosylation pattern in the Fc region to enhance the affinity towards Fcγ receptors (FcγR) on effector cells [53, 57]. The most prominent and successful technology so far has been the glycosylation approach, which has seen nearly twenty glyco-engineered antibodies enter clinical trials with three already approved for clinical use [58-60]. The first success came with the approval of mogamulizumab (Poteligeo®) in Japan in 2012, developed using the POTELLIGENT (Kyowa Hakko Kirin) platform which is indicated for CC-chemokine receptor 4 (CCR4)-expressing T cell leukaemia-lymphoma and peripheral T cell lymphoma (PTCL) in adult patients [61].

An ADCC enhanced version of rituximab, obinituzumab (Gazyva®) gained approval by the FDA in 2013 under breakthrough therapy designation [62]. Obinituzumab is an anti-CD20 monoclonal antibody that was originated by GlycArt Biotechnology (now GlycoMAb) and is approved for CCL [59]. Both POTELLIGENT® and GlycArt platforms are based on the manufacture of products using engineered cell lines that yield defucosylated antibodies; a structural modification that removes the core 1,6 fucose from the N-glycans attached to asparagine at amino acid position 297 of human IgG1 thereby greatly enhancing the affinity towards FcγRIII, and increasing ADCC induction by NK cells (Fig. 1a) [63, 64]. NK cells are not abundant in the tumor site, and human endogenous IgG can inhibit the elicitation of ADCC by therapeutic antibodies [65] therefore, increasing the affinity towards FcγRIII to preferentially interact with the therapeutic antibody is a valuable approach to improve the efficacy profile. This approach was demonstrated by Zhang et al. [66] by producing an anti-HER2 antibody with an identical sequence to trastuzumab but with superior binding affinity to FcyRIIIa and greater ADCC activity [66]. The antibody was produced using glyco-engineered *Pichia pastoris* and the differences were presumed to be due to absence of fucose in the N-glycans attached to the IgG1 product. Benralizumab is

another example of a defucosylated IgG1 mAb which received marketing approval by the FDA in 2017 for maintenance treatment of severe asthma [55].

Whereas the glyco-engineering approach generates defucosylated antibodies with FcγRIIIa-specific affinity improvement, variants generated by mutagenesis of Fc amino acid sequence can be enhanced for multiple FcγR interactions. A number of publications have identified specific Fc mutations to improve binding to the activating receptor FcγIIIa and reduce binding to the inhibitory receptor FcγIIb with corresponding improvement to ADCC activity [67-69]. The XmAb® concept is one such example that was investigated as an anti-CD30 in Phase I trials for Hodgkin lymphoma.

In an alternative approach, aglycosylated antibodies (without glycan structures) can be engineered to display effector functions that are distinct from those of glycosylated counterparts [29, 31, 70, 71]. The use of aglycosylated therapeutic antibodies offers manufacturing advantages by bypassing glycosylation and hence production can be performed in prokaryotic hosts. On the other hand, the importance of glycosylation on the structural stability of antibodies has been demonstrated [72, 73]. The first aglycosylated antibody to enter clinical trials, produced in yeast, is humanized rat-derived IgG1 otelixizumab directed against CD3 which is being assessed in Phase II trials for new onset autoimmune type I diabetes mellitus.

5. Physical and chemical degradation of antibodies

During manufacturing and storage, therapeutic antibodies are at risk of degradation via several pathways. Though these reactions may be kept under control by appropriate storage and formulation conditions of the final product, degradation that occurs during culture, downstream processing and *in vivo* cannot be controlled sufficiently. These degradation events may affect antigen recognition, hamper functionality and in severe cases lead to immunogenic responses [74-78]. Each antibody molecule seems to have a unique personality related to its requirements for stability; a phenomenon derived from the fact that differences in the CDR between antibodies are primarily dictated by the surface exposed amino acids that define antigen specificity [77]. The identification of degradation prone or unstable regions early in the antibody development process would ideally permit re-engineering of these problematic areas [79-82]. This approach is aided by recent developments in

computational modelling tools that predict regions of interest susceptible to physical, chemical degradation or influence other biophysical properties of antibodies. In the next section, degradation pathways commonly observed in therapeutic antibodies and an overview of predictive tools are discussed.

5.1. Aggregation

Protein aggregation is the most common and significant type of physical degradation associated with therapeutic antibodies, often leading to reduced activity and in some cases, formation of immunogenic products [83, 84]. Initial preparations of therapeutic antibodies were administered by intravenous (IV) infusion formulated at protein concentrations (1-25 mg/ml). As antibody-based therapeutics have become more widely used, high concentration formulations that allow SC injection (>50 mg/ml) became desirable giving rise to aggregation issues. Proteins are folded in such a way as to internalize hydrophobic regions and surface expose more hydrophilic regions. As protein-protein contact frequency increases at high concentrations, the opportunity for aggregation formation increases proportionally. Changes in extrinsic conditions including temperature, pH, salt, shaking, viscosity and concentration can transiently expose hydrophobic regions which in doing so promotes protein-protein interactions that lead to aggregation events [85-88]. Non-covalent aggregates can be formed via hydrophobic and/or electrostatic interactions and may be reversible, while covalent aggregates are usually formed by disulphide bonds and are difficult to reverse. Mechanisms of protein aggregation include: (1) aggregation of native state monomers; (2) aggregation of monomers with a modified conformation (non-native); (3) aggregation of chemically-modified monomers; (4) aggregation via a nucleation-dependant process; and (5) surface-induced aggregation via adsorption of protein to glass-liquid or air-liquid interfaces [89, 90].

5.2. Denaturation

Protein denaturation refers to the partial or complete unfolding of the native three-dimensional folded protein structure. A denatured antibody often loses its tertiary and perhaps secondary structure leading to loss of binding affinity and activity if an active site domain is affected, and may expose aggregation-prone regions leading to further degradation [86, 91, 92]. Several intermediate states may exist between the folded native structure of an antibody molecule and the denatured state, with some

intermediates thought to act as precursors or ‘nuclei’, attracting other protein species to exposed hydrophobic sites and forming irreversible aggregates. Denaturation may be induced by a number of stress conditions that arise during antibody manufacture including changes in solution pH or temperature, use of organic solvents or chaotropes, high salt concentrations, or shear force [85, 86, 93]. In general, the C_H3 domain of an antibody is often the most stable against denaturation at high temperatures (highest T_m) while the C_H2 domain is least stable and denatures first (lowest T_m) [94].

5.3. Fragmentation

Fragmentation of therapeutic antibodies can be a product of enzymatic or non-enzymatic hydrolysis that occurs at the peptide backbone of a number of regions, such as the hinge region, the C_H2-C_H3 interface or a region containing aspartic acid (Asp) or tryptophan (Trp) residues [85]. Asp-associated hydrolysis is affected by pH and the n+1 residue; for instance, a serine (Ser), valine (Val) or tyrosine (Tyr) adjacent to an Asp may increase the rate of Asp-hydrolysis. Hinge region hydrolysis can occur in the absence of Asp and occurs most commonly in the IgG1 isoform [85, 95, 96]. The rate of hydrolysis is dependent on the flexibility the peptide sequence at the hinge and occurs within a narrow range of residues. Hinge hydrolysis rates are affected by solution pH, with a minimum rate of hydrolysis observed near pH 6, and higher rates at a lower or higher pH [85, 96]. Fragmentation of full-length antibodies is a common occurrence and generally, cleaved forms are present in such low amounts that effect on efficacy would not likely be seen.

5.4. Deamidation

Deamidation is the most common chemical degradation pathway of therapeutic antibodies and results from the hydrolysis of the amide side-chain of amino acids glutamine (Gln) or asparagine (Asn) [85, 89, 97, 98]. Hydrolysis of the side-chain can occur at acidic pH (pH <4) resulting in the conversion of Asn to Asp and Gln to glutamic acid (Glu) [85]. However, at higher pH, deamidation occurs predominantly (and more slowly) via the formation of a cyclic imide intermediate For Asn, the cyclic intermediate (succinimide) leads to either the formation of Asp or an isomer of Asp. A similar process results in the deamidation of Gln to Glu; although Gln deamidation is much less frequent, due to the lower stability of the 6-membered cyclic intermediate formed. In short, deamidation events lead to more acidic forms of the antibody through the

acquisition of additional carboxylic acid groups. Conversely, it is also possible for Asp residues to undergo modification to a succinimide intermediate that produces a basic form of the antibody by removal of a carboxylic acid group [97].

Several factors can affect the rate of deamidation. For instance, Asn residues are more prone to deamidation if they are present in solvent-accessible or structurally-flexible regions, especially if followed by a small or flexible residue such as Gly, Ser, threonine (Thr) or Asn [85, 99]. Deamidation rate is also affected by extrinsic conditions including pH, temperature, buffer composition and concentration [100]. Gln deamidation is thought to be less common than Asp deamidation due to the lower stability of the 6-membered cyclic ring intermediate, which results in a much slower reaction rate [85]. Although Gln deamidation occurs less frequently, a study found that following incubation at pH 9, 7.8% of Gln82 of a recombinant IgG1 mAb had undergone deamidation, despite no deamidation of this residue occurring at neutral pH [98].

Deamidation of therapeutic antibodies is well characterised both *in vitro* and *in vivo*, and has been shown to decrease the potency, activity and stability of antibodies [97, 99-103]. The deamidation events appear to be highly selective for individual antibodies. For example, Harris et al. performed accelerated stability studies at elevated temperatures with rhuMAB HER2 antibody and found three labile Asn residues in the CDR region (Asn55, Asn30 and Asn102) [97]. These residues either formed aspartate, isoasparatate or a stable succinimide intermediate, resulting in a total of 7 species of the antibody being resolved. Deamidation of these Asn residues was shown to significantly affect the specific *in vitro* activity and potency of rhuMAb HER2.

5.5. Oxidation

Oxidation is another common degradation pathway which can occur during antibody production, formulation or storage. A number of amino acid residues may be affected, including methionine (Met), cysteine (Cys), histidine (His), tyrosine (Tyr) and Trp [85]. Specific Met residues within the Fc region (up to four residues) are prone to oxidation resulting in production of methionine sulfoxide [89, 104, 105]. Oxidation of these residues may affect the stability of an antibody, Fc-mediated effector function or Protein A binding affinity which is often used for purification from cell culture supernatant [106]. Wang et al. demonstrated that oxidation of Met252 can result in >4-

fold reduction in the half-life of an antibody in transgenic mice expressing human Fc neonatal receptor (FcRn). However, this was only observed when 80% of the antibody existed in the oxidized form, and not at 40% [107].

Oxidation can be dependent on intrinsic factors such as the degree of surface exposed residues as well as extrinsic factors including buffer composition, light exposure and pH, although Met oxidation appears to be almost pH-independent [85, 106, 108]. Oxidative stress has been observed during antibody production in mammalian expression systems where the formation of reactive oxygen species as a result of hypoxic conditions caused fragmentation of an IgG1 antibody [109].

Tryptophan oxidation of antibodies has been reported following light exposure. Sreedhara et al. [104] found that light induced oxidation of surface exposed Trp residues (Trp53, Trp108 and Trp94) in the Fab region of an IgG1 antibody leading to a loss in potency accompanied with a solution colour change [104]. In another example, oxidation of Trp residue in the H3 CDR loop (Trp135) of a humanized anti-respiratory syncytial virus (RSV) therapeutic antibody resulted in loss of antigen binding and biological function [110].

6. Computational design tools

In recent years, computational methods used to simulate and develop structural models of proteins have transformed into practical design tools for the development of biobetter and next-generation antibody therapeutics [80, 111]. Current computational design tools have evolved to allow rapid identification of specific amino acid sequences or regions on a protein of interest, that contribute to its observed *in vivo* properties such as binding affinity, efficacy, stability and half-life [111].

Some of the early computational tools used for protein modelling include TANGO, PAGE, AGGRESCAN, PASTA and Zyggregator all of which rely on the sequence of the protein of interest (Table 2) [81, 112-117]. These computational tools use force fields such as CHARMM or AMBER and exploit chemical properties of the amino acids such as hydrophobicity, β-sheet propensity, charge, and aromatic content to predict aggregation hot-spots and residues susceptible to chemical degradation. In some cases, multiple tools can be used in combination to improve the predictive power. For example, Wang et al. combined TANGO and PAGE to identify aggregation-prone

motifs and residues susceptible to deamidation or oxidation of 22 commercial and 20 non-commercial therapeutic antibodies [118].

Table 2. A representative list of computational tools for prediction of protein aggregation hot spots.

Name	**Properties**
Sequence-based methods	
TANGO [112]	Determines the secondary structure formation propensity
Aggrescan [113]	Uses amino acid aggregation propensity value
Zyggregator [115]	Compares a new peptide sequence to the database
PASTA [116]	Predicts amyloid structure aggregation by looking into sequences that are likely to stabilize the cross-beta core of fibrils
PAGE [117]	Uses physicochemical properties for prediction
Structure-based methods	
SAP [81]	Determines spatial effective surface accessible area
LIP [119]	Measures ratio of polar surface area to apolar surface area of buried interfaces
AGGRESCAN3D [120]	Based on original AGGRESCAN server with input from 3D structure and spatial arrangement of residues

Some structure-based computational tools have also been developed. One such method, Spatial Aggregation Propensity (SAP), predicts surface exposed aggregation-prone regions of a protein based on hydrophobicity, dynamic fluctuations and solvent accessibility of residues and regions [80]. The tool has been used to simulate entire antibodies and develop IgG1 antibody variants with enhanced physical stability to the wild type, by performing single or multiple mutations in either the Fab or Fc regions [80, 82].

Another method developed by Angarica and Sancho [119] predicts aggregation propensity based on the packing density and polarity ratio (ratio of polar surface area to apolar surface area) of buried interfaces [119]. The tool was designed to characterise “Light Interfaces of high Polarity” (LIPs) considered to be intrinsically unstable cores. The technology shows promise as a tool for engineering antibody variants with increased aggregation-resistance, especially as a complimentary method to surface- or sequence-based tools mentioned above.

One of the most recent developments in computational modelling is the evolution of AGGRESCAN to AGGRESCAN3D (A3D), an improved server which addresses many of the limitations of AGGRESCAN and other sequence-based methods. A3D takes into account the three-dimensional structure of the protein and the spatial arrangement of the residues when the protein is in its native folded state [120]. With the incorporation of a mutation module that allows the easy modelling of the detected aggregation-prone and surrounding residues, A3D looks to be a promising tool for predicting problematic regions and the same time, allowing for re-design of more stable proteins.

7. Optimization of antibody bioavailability and delivery

Antibody-based therapies are predominantly delivered intravenously (IV), though an increasing number are now being formulated and administered subcutaneously (SC). While the IV route offers 100% bioavailability, systemic distribution and physiological barriers greatly reduce the actual concentration of antibody achieved in target tissues [121]. What is more, IV infusions are time-consuming and inconvenient. Ideally, an antibody formulation should be non-invasive and increase local bioavailability. Limited alternatives have been implemented in the clinic since formulation requirements for such delivery often pose significant hurdles. For other parenteral administration routes, such as SC or intramuscular (IM), the most common limitation is poor antibody solubility at the high concentrations required, given that maximum volume of injection is restricted to 2 ml and 5 ml, respectively. When compared to IV formulations which range from 1-25 mg/ml, SC and IM products often require concentrations >100 mg/ml to deliver an effective dose [122]. Furthermore, these delivery routes involve an absorption step to enable systemic circulation. Two main approaches are being pursued to optimize bioavailability: 1) the design of aggregation-resistant antibodies

with higher solubility to prevent precipitation at higher concentrations; 2) the use of polymer matrix systems to develop controlled release formulations and improve PK profile.

As discussed in the previous section, the design of aggregation-resistant antibodies albeit challenging, has become possible with the implementation of computational tools and increasing understanding of antibody structure and degradation pathways. Formulation stability has also been improved by using stabilizing additives such as salts (e.g. citrates, sulfates), amino acids (e.g. glycine, alanine) and sugars (e.g. sorbitol, sucrose, trehalose) [85, 123-125]. The development of SC and IM products has been successful in the last decade because of the formulation of large doses in significantly smaller volumes without aggregation issues [56]. SC and IM formulations have significantly improved patient convenience enabling self-administration through the use of pre-filled syringes, a feature that is highly advantageous for treatment of chronic diseases. A novel approach to improving SC formulation and PK has been proposed by Yang et al. whereby, crystalline antibody preparations of infliximab (Remicade®) and trastuzumab (Herceptin®) were formulated at 200 mg/ml while maintaining low viscosities suitable for this delivery route [126]. Animal studies in rats showed a 2-fold increase of antibody half-life compared to non-crystallized antibody, demonstrating the potential of crystalline preparations as controlled release systems. Alginate polymers have also been explored for controlled release. Schweizer et al. [127] developed two polyanionic alginate matrices loaded with antibody through electrostatic interactions [127]. Both matrices were delivered to rats subcutaneously as hydrogels. After comparison with its liquid antibody counterpart, no significant differences in bioavailability were reported.

For many pathologies, local delivery could increase efficacy and reduce systemic exposure. In such cases, administration routes such as oral, topical, respiratory and intraocular become highly relevant. Controlled release systems based on polymer matrices are also being tested in preclinical studies for these delivery routes [121, 128]. For instance, liposomes and chitosan-alginate microparticles have been employed for oral delivery in order to protect antibodies from gastric inactivation and allow release in the small intestine [129, 130]. This is being explored in combination with the conjugation of targeting ligands to improve delivery and absorption in the gastro-intestinal tract. [131]. For topical application, a hydrofiber dressing/adhesive sheet

has been used to apply infliximab as a gel formulation for wound healing with improvements in 7/8 patients tested [132]. In another example, a Phase I trial has been completed with positive results for BIL-010t, a topically administered, sheep antibody therapy to treat Basal Cell Carcinoma (BCC). BIL-010t ointment was self-applied for 28 days; it was noted that 13/20 patients had decreases in the sizes of their lesions with only mild localized skin reactions reported. The respiratory route has been extensively studied for treatment of chronic obstructive pulmonary disease, lung cancer, asthma and other pulmonary pathologies. Liposomes and microspheres have shown potential to increase bioavailability of respiratory delivery by preventing proteolysis [133]. The PEGylation of antibody fragments was shown to increase lung lumen residence time in a murine model through decreased clearance of alveolar macrophages and increased mucoadhesion [134]. Other strategies being investigated to deliver antibodies via the respiratory tract include IgG-loaded lipid microparticles and nano-micelles [135-137]. The most advanced molecule in clinical development is ALX-0171, an anti-RSV nanobody administered through inhalation; demonstrating a positive safety and tolerability profile in a first-in-infant Phase I/II study with an anti-viral effect observed [138].

Overall, the IV route will likely remain the most prominent administration route in development due to ease of formulation. Still, the improvement of local bioavailability is an obvious requirement to fulfil the potential of antibody-based therapy, both in terms of efficacy and patient convenience. As such, strategies such as pursuing alternative administration routes and developing appropriate controlled release systems will gain relevance as their therapeutic potential continues to be explored in preclinical studies.

8. Conclusion

Antibody-based therapeutics have evolved from murine antibodies to humanized and fully human antibodies, developed with innovative technologies such as transgenic mice and phage display. In the coming years, next-generation antibodies with improved properties and formats including ADC and bispecifics are expected to gain popularity as biobetter antibody therapeutics. The advancement of next-generation biobetters is critical to address the shortcomings confronted with the use of these

antibodies such as poor efficacy and stability and most importantly, to provide greater patient benefit.

Acknowledgements

The authors would like to acknowledge the School of Pharmacy of the University of Sydney for financial contribution. E. Cruz acknowledges the Ministry of Science, Technology and Telecommunications of the Republic of Costa Rica for postgraduate scholarship. M. Reslan is a recipient of the Research Training Stipend provided by the University of Sydney on behalf of the Department of Education and Training to support his research training.

Disclosures

The authors declare that they have no competing financial interests.

References

[1] D.M. Ecker, S.D. Jones, H.L. Levine, The therapeutic monoclonal antibody market, mAbs, 7 (2015) 9-14.

[2] R.E. Kontermann, U. Brinkmann, Bispecific antibodies, Drug Discovery Today, 20 (2015) 838-847.

[3] P.M. Drake, D. Rabuka, An emerging playbook for antibody-drug conjugates: lessons from the laboratory and clinic suggest a strategy for improving efficacy and safety, Current Opinion in Chemical Biology, 28 (2015) 174-180.

[4] G. Kohler, C. Milstein, Continuous cultures of fused cells secreting antibody of predefined specificity, Nature, 256 (1975) 495-497.

[5] G. Kohler, C. Milstein, Derivation of specific antibody-producing tissue culture and tumor lines by cell fusion, European Journal of Immunology, 6 (1976) 511-519.

[6] W. Li, N.B. Caberoy, New perspective for phage display as an efficient and versatile technology of functional proteomics, Applied Microbiology and Biotechnology, 85 (2010) 909-919.

[7] P.T. Jones, P.H. Dear, J. Foote, M.S. Neuberger, G. Winter, Replacing the complementarity-determining regions in a human antibody with those from a mouse, Nature, 321 (1986) 522-525.

[8] L. Riechmann, M. Clark, H. Waldmann, G. Winter, Reshaping human antibodies for therapy, Nature, 332 (1988) 323-327.

[9] N. Lonberg, Human antibodies from transgenic animals, Nature Biotechnology, 23 (2005) 1117-1125.
[10] C.T. Scott, Mice with a human touch, Nature Biotechnology, 25 (2007) 1075-1077.
[11] A. Jakobovits, R. Amado, X. Yang, L. Roskos, G. Schwab, From XenoMouse technology to panitumumab, the first fully human antibody product from transgenic mice, Nature Biotechnology, 25 (2007) 1134-1143.
[12] W.D. Huse, L. Sastry, S.A. Iverson, A.S. Kang, M. Alting-Mees, D.R. Burton, S.J. Benkovic, R.A. Lerner, Generation of a large combinatorial library of the immunoglobulin repertoire in phage lambda, Science, 246 (1989) 1275-1281.
[13] J. McCafferty, A.D. Griffiths, G. Winter, D.J. Chiswell, Phage antibodies: filamentous phage displaying antibody variable domains, Nature, 348 (1990) 552-554.
[14] C.F. Barbas, 3rd, A.S. Kang, R.A. Lerner, S.J. Benkovic, Assembly of combinatorial antibody libraries on phage surfaces: the gene III site, Proceedings of the National Academy of Sciences, 88 (1991) 7978-7982.
[15] D.J. Schofield, A.R. Pope, V. Clementel, J. Buckell, S.D.J. Chapple, K.F. Clarke, J.S. Conquer, A.M. Crofts, S.R.E. Crowther, M.R. Dyson, G. Flack, G.J. Griffin, Y. Hooks, W.J. Howat, A. Kolb-Kokocinski, S. Kunze, C.D. Martin, G.L. Maslen, J.N. Mitchell, M. O'Sullivan, R.L. Perera, W. Roake, S.P. Shadbolt, K.J. Vincent, A. Warford, W.E. Wilson, J. Xie, J.L. Young, J. McCafferty, Application of phage display to high throughput antibody generation and characterization, Genome Biology, 8 (2007).
[16] J.D. Marks, H.R. Hoogenboom, T.P. Bonnert, J. McCafferty, A.D. Griffiths, G. Winter, By-passing immunization. Human antibodies from V-gene libraries displayed on phage, Journal of Molecular Biology, 222 (1991) 581-597.
[17] C.F.I. Barbas, J.D. Bain, D.M. Hoekstra, R.A. Lerner, Semisynthetic combinatorial antibody libraries: a chemical solution to the diversity problem, Proceedings of the National Academy of Sciences, 89 (1992) 4457-4461.
[18] H.R. Hoogenboom, G. Winter, By-passing immunisation. Human antibodies from synthetic repertoires of germline VH gene segments rearranged *in vitro*., Journal of Molecular Biology, 227 (1992) 381-388.
[19] H.R. Hoogenboom, A.D. Griffiths, K.S. Johnson, D.J. Chiswell, P. Hudson, G. Winter, Multi-subunit proteins on the surface of filamentous phage: methodologies for displaying antibody (Fab) heavy and light chains, Nucleic Acids Research, 19 (1991) 4133-4137.

[20] J. Davies, L. Riechmann, An antibody variable heavy domain with a lox-Cre site integrated into its coding region: bacterial recombination within a single polypeptide chain, FEBS Letters, 377 (1995) 92-96.
[21] M.M. Harmsen, H.J. De Haard, Properties, production, and applications of camelid single-domain antibody fragments, Applied Microbiology and Biotechnology, 77 (2007) 13-22.
[22] S.D. Nuttall, U.V. Krishnan, L. Doughty, K. Pearson, M.T. Ryan, N.J. Hoogenraad, M. Hattarki, J.A. Carmichael, R.A. Irving, P.J. Hudson, Isolation and characterization of an IgNAR variable domain specific for the human mitochondrial translocase receptor Tom70, European Journal of Biochemistry, 270 (2003) 3543-3554.
[23] K. Nakano, T. Kojima, K. Kasutani, C. Senoh, O. Natori, S. Ishii, H. Tsunoda, K. Hattori, Effective screening method of agonistic diabodies based on autocrine growth, Journal of Immunological Methods, 347 (2009) 31-35.
[24] Y. Mazor, T. Van Blarcom, R. Mabry, B.L. Iverson, G. Georgiou, Isolation of engineered, full-length antibodies from libraries expressed in Escherichia coli, Nature Biotechnology, 25 (2007) 563-565.
[25] L.S. Jespers, A. Roberts, S.M. Mahler, G. Winter, H.R. Hoogenboom, Guiding the selection of human antibodies from phage display repertoires to a single epitope of an antigen, Biotechnology (N Y), 12 (1994) 899-903.
[26] L. Urquhart, Top drugs and companies by sales in 2017, Nature Reviews Drug Discovery, 17 (2018) 232.
[27] A.E. Nixon, D.J. Sexton, R.C. Ladner, Drugs derived from phage display: from candidate identification to clinical practice, mAbs, 6 (2014) 73-85.
[28] M.P. Robinson, N. Ke, J. Lobstein, C. Peterson, A. Szkodny, T.J. Mansell, C. Tuckey, P.D. Riggs, P.A. Colussi, C.J. Noren, C.H. Taron, M.P. DeLisa, M. Berkmen, Efficient expression of full-length antibodies in the cytoplasm of engineered bacteria, Nature Communications, 6 (2015) 8072.
[29] S.L. Sazinsky, R.G. Ott, N.W. Silver, B. Tidor, J.V. Ravetch, K.D. Wittrup, Aglycosylated immunoglobulin G1 variants productively engage activating Fc receptors, Proceedings of the National Academy of Sciences, 105 (2008) 20167-20172.
[30] S.T. Jung, W. Kelton, T.H. Kang, D.T. Ng, J.T. Andersen, I. Sandlie, C.A. Sarkar, G. Georgiou, Effective phagocytosis of low Her2 tumor cell lines with engineered,

aglycosylated IgG displaying high FcgammaRIIa affinity and selectivity, ACS Chemical Biology, 8 (2013) 368-375.
[31] S.T. Jung, S.T. Reddy, T.H. Kang, M.J. Borrok, I. Sandlie, P.W. Tucker, G. Georgiou, Aglycosylated IgG variants expressed in bacteria that selectively bind FcgammaRI potentiate tumor cell killing by monocyte-dendritic cells, Proceedings of the National Academy of Sciences, 107 (2010) 604-609.
[32] H. Li, N. Sethuraman, T.A. Stadheim, D. Zha, B. Prinz, N. Ballew, P. Bobrowicz, B.K. Choi, W.J. Cook, M. Cukan, N.R. Houston-Cummings, R. Davidson, B. Gong, S.R. Hamilton, J.P. Hoopes, Y. Jiang, N. Kim, R. Mansfield, J.H. Nett, S. Rios, R. Strawbridge, S. Wildt, T.U. Gerngross, Optimization of humanized IgGs in glycoengineered Pichia pastoris, Nature Biotechnology, 24 (2006) 210-215.
[33] T.I. Potgieter, S.D. Kersey, M.R. Mallem, A.C. Nylen, M. d'Anjou, Antibody expression kinetics in glycoengineered Pichia pastoris, Biotechnology and Bioengineering, 106 (2010) 918-927.
[34] J. Ye, J. Ly, K. Watts, A. Hsu, A. Walker, K. McLaughlin, M. Berdichevsky, B. Prinz, D. Sean Kersey, M. d'Anjou, D. Pollard, T. Potgieter, Optimization of a glycoengineered Pichia pastoris cultivation process for commercial antibody production, Biotechnology Progress, 27 (2011) 1744-1750.
[35] J.K. Ma, T. Lehner, P. Stabila, C.I. Fux, A. Hiatt, Assembly of monoclonal antibodies with IgG1 and IgA heavy chain domains in transgenic tobacco plants, European Journal of Immunology, 24 (1994) 131-138.
[36] B. De Muynck, C. Navarre, M. Boutry, Production of antibodies in plants: status after twenty years, Plant Biotechnology Journal, 8 (2010) 529-563.
[37] G. Moussavou, K. Ko, J.H. Lee, Y.K. Choo, Production of monoclonal antibodies in plants for cancer immunotherapy, BioMed Research International, 2015 (2015) 306164.
[38] B.M. Grohs, Y. Niu, L.J. Veldhuis, S. Trabelsi, F. Garabagi, J.A. Hassell, M.D. McLean, J.C. Hall, Plant-produced trastuzumab inhibits the growth of HER2 positive cancer cells, Journal of Agricultural and Food Chemistry, 58 (2010) 10056-10063.
[39] F.M. Wurm, Production of recombinant protein therapeutics in cultivated mammalian cells, Nature Biotechnology, 22 (2004) 1393-1398.
[40] S.M. Browne, M. Al-Rubeai, Selection methods for high-producing mammalian cell lines, Trends in Biotechnology, 25 (2007) 425-432.

[41] S. Shi, R.G. Condon, L. Deng, J. Saunders, F. Hung, Y.S. Tsao, Z. Liu, A high-throughput automated platform for the development of manufacturing cell lines for protein therapeutics, Journal of Visualized Experiments, (2011).
[42] M. Chartrain, L. Chu, Development and production of commercial therapeutic monoclonal antibodies in Mammalian cell expression systems: an overview of the current upstream technologies, Current Pharmaceutical Biotechnology, 9 (2008) 447-467.
[43] L. Chu, D.K. Robinson, Industrial choices for protein production by large-scale cell culture, Current Opinion in Biotechnology, 12 (2001) 180-187.
[44] H.F. Liu, J. Ma, C. Winter, R. Bayer, Recovery and purification process development for monoclonal antibody production, mAbs, 2 (2010) 480-499.
[45] J.R. Birch, A.J. Racher, Antibody production, Advanced Drug Delivery Reviews, 58 (2006) 671-685.
[46] S.D. Jones, P. Seymour, H.L. Levine, CMC Activities for Development of MAbs, Contract Pharma, 2010, pp. 60-63.
[47] R.L. Fahrner, H.L. Knudsen, C.D. Basey, W. Galan, D. Feuerhelm, M. Vanderlaan, G.S. Blank, Industrial purification of pharmaceutical antibodies: development, operation, and validation of chromatography processes, Biotechnology and Genetic Engineering Reviews, 18 (2001) 301-327.
[48] W. Schwart, D. Judd, M. Wysocki, L. Guerrier, E. Birck-Wilson, E. Boschetti, Comparison of hydrophobic charge induction chromatography with affinity chromatography on protein A for harvest and purification of antibodies, Journal of Chromatography A, 908 (2001) 251-263.
[49] R. van Reis, S. Gadam, L.N. Frautschy, S. Orlando, E.M. Goodrich, S. Saksena, R. Kuriyel, C.M. Simpson, S. Pearl, A.L. Zydney, High performance tangential flow filtration, Biotechnology and Bioengineering, 56 (1997) 71-82.
[50] B. Lebreton, A. Brown, R. van Reis, Application of high-performance tangential flow filtration (HPTFF) to the purification of a human pharmaceutical antibody fragment expressed in Escherichia coli, Biotechnology and Bioengineering, 100 (2008) 964-974.
[51] T. Arakawa, M. Futatsumori-Sugai, K. Tsumoto, Y. Kita, H. Sato, D. Ejima, MEP HyperCel chromatography II: binding, washing and elution, Protein Expression and Purification, 71 (2010) 168-173.

[52] P. Chames, M. Van Regenmortel, E. Weiss, D. Baty, Therapeutic antibodies: successes, limitations and hopes for the future, British Journal of Pharmacology, 157 (2009) 220-233.
[53] R. Niwa, M. Satoh, The current status and prospects of antibody engineering for therapeutic use: focus on glycoengineering technology, Journal of Pharmaceutical Sciences, 104 (2015) 930-941.
[54] J.B. Evans, B.A. Syed, From the analyst's couch: Next-generation antibodies, Nat Rev Drug Discov, 13 (2014) 413-414.
[55] H. Kaplon, J.M. Reichert, Antibodies to watch in 2018, mAbs, 10 (2018) 183-203.
[56] O. Shpilberg, C. Jackisch, Subcutaneous administration of rituximab (MabThera) and trastuzumab (Herceptin) using hyaluronidase, British Journal of Cancer, 109 (2013) 1556-1561.
[57] S. Derer, C. Kellner, S. Berger, T. Valerius, M. Peipp, Fc engineering: design, expression, and functional characterization of antibody variants with improved effector function, Methods Mol Biol, 907 (2012) 519-536.
[58] A. Beck, J.M. Reichert, Marketing approval of mogamulizumab: a triumph for glyco-engineering, mAbs, 4 (2012) 419-425.
[59] M. Sachdeva, S. Dhingra, Obinutuzumab: A FDA approved monoclonal antibody in the treatment of untreated chronic lymphocytic leukemia, Int J Appl Basic Med Res, 5 (2015) 54-57.
[60] M. Ratner, Genentech's glyco-engineered antibody to succeed Rituxan, Nature Biotechnology, 32 (2014) 6+.
[61] J.M. Subramaniam, G. Whiteside, K. McKeage, J.C. Croxtall, Mogamulizumab: first global approval, Drugs, 72 (2012) 1293-1298.
[62] A.K. Kakkar, S. Balakrishnan, Obinutuzumab for chronic lymphocytic leukemia: promise of the first treatment approved with breakthrough therapy designation, J Oncol Pharm Pract, 21 (2015) 358-363.
[63] S.D. Liu, C. Chalouni, J.C. Young, T.T. Junttila, M.X. Sliwkowski, J.B. Lowe, Afucosylated antibodies increase activation of FcgammaRIIIa-dependent signaling components to intensify processes promoting ADCC, Cancer Immunol Res, 3 (2015) 173-183.
[64] T. Mizushima, H. Yagi, E. Takemoto, M. Shibata-Koyama, Y. Isoda, S. Iida, K. Masuda, M. Satoh, K. Kato, Structural basis for improved efficacy of therapeutic antibodies on defucosylation of their Fc glycans, Genes to Cells, 16 (2011) 1071-1080.

[65] S. Preithner, S. Elm, S. Lippold, M. Locher, A. Wolf, A.J. da Silva, P.A. Baeuerle, N.S. Prang, High concentrations of therapeutic IgG1 antibodies are needed to compensate for inhibition of antibody-dependent cellular cytotoxicity by excess endogenous immunoglobulin G, Mol Immunol, 43 (2006) 1183-1193.
[66] N. Zhang, L. Liu, C. Dan Dumitru, N.R.H. Cummings, M. Cukan, Y. Jiang, Y. Li, F. Li, T. Mitchell, M.R. Mallem, Y. Ou, R.N. Patel, K. Vo, H. Wang, I. Burnina, B.-K. Choi, H.E. Huber, T.A. Stadheim, D. Zha, Glycoengineered Pichia produced anti-HER2 is comparable to trastuzumab in preclinical study, mAbs, 3 (2011) 289-298.
[67] R.L. Shields, A.K. Namenuk, K. Hong, Y.G. Meng, J. Rae, J. Briggs, D. Xie, J. Lai, A. Stadlen, B. Li, J.A. Fox, L.G. Presta, High resolution mapping of the binding site on human IgG1 for Fc gamma RI, Fc gamma RII, Fc gamma RIII, and FcRn and design of IgG1 variants with improved binding to the Fc gamma R, The Journal of Biological Chemistry, 276 (2001) 6591-6604.
[68] G.A. Lazar, W. Dang, S. Karki, O. Vafa, J.S. Peng, L. Hyun, C. Chan, H.S. Chung, A. Eivazi, S.C. Yoder, J. Vielmetter, D.F. Carmichael, R.J. Hayes, B.I. Dahiyat, Engineered antibody Fc variants with enhanced effector function, Proceedings of the National Academy of Sciences, 103 (2006) 4005-4010.
[69] J.B. Stavenhagen, S. Gorlatov, N. Tuaillon, C.T. Rankin, H. Li, S. Burke, L. Huang, S. Vijh, S. Johnson, E. Bonvini, S. Koenig, Fc optimization of therapeutic antibodies enhances their ability to kill tumor cells in vitro and controls tumor expansion in vivo via low-affinity activating Fcgamma receptors, Cancer Research, 67 (2007) 8882-8890.
[70] M.J. Borrok, S.T. Jung, T.H. Kang, A.F. Monzingo, G. Georgiou, Revisiting the role of glycosylation in the structure of human IgG Fc, ACS Chemical Biology, 7 (2012) 1596-1602.
[71] R. Stewart, G. Thom, M. Levens, G. Guler-Gane, R. Holgate, P.M. Rudd, C. Webster, L. Jermutus, J. Lund, A variant human IgG1-Fc mediates improved ADCC, Protein Engineering Design and Selection, 24 (2011) 671-678.
[72] V. Kayser, N. Chennamsetty, V. Voynov, K. Forrer, B. Helk, B.L. Trout, Glycosylation influences on the aggregation propensity of therapeutic monoclonal antibodies, Biotechnology Journal, 6 (2011) 38-44.
[73] Y. Mimura, S. Church, R. Ghirlando, P.R. Ashton, S. Dong, M. Goodall, J. Lund, R. Jefferis, The influence of glycosylation on the thermal stability and effector function expression of human IgG1-Fc: properties of a series of truncated glycoforms, Molecular Immunology, 37 (2000) 697-706.

[74] M.K. Joubert, M. Hokom, C. Eakin, L. Zhou, M. Deshpande, M.P. Baker, T.J. Goletz, B.A. Kerwin, N. Chirmule, L.O. Narhi, V. Jawa, Highly aggregated antibody therapeutics can enhance the in vitro innate and late-stage T-cell immune responses, The Journal of Biological Chemistry, 287 (2012) 25266-25279.
[75] S. Hermeling, D.J. Crommelin, H. Schellekens, W. Jiskoot, Structure-immunogenicity relationships of therapeutic proteins, Pharmaceutical Research, 21 (2004) 897-903.
[76] D.S. Rehder, D. Chelius, A. McAuley, T.M. Dillon, G. Xiao, J. Crouse-Zeineddini, L. Vardanyan, N. Perico, V. Mukku, D.N. Brems, M. Matsumura, P.V. Bondarenko, Isomerization of a single aspartyl residue of anti-epidermal growth factor receptor immunoglobulin gamma2 antibody highlights the role avidity plays in antibody activity, Biochemistry, 47 (2008) 2518-2530.
[77] A.L. Daugherty, R.J. Mrsny, Formulation and delivery issues for monoclonal antibody therapeutics, Adv Drug Deliv Rev, 58 (2006) 686-706.
[78] Y. Yan, H. Wei, Y. Fu, S. Jusuf, M. Zeng, R. Ludwig, S.R. Krystek, G. Chen, L. Tao, T.K. Das, Isomerization and Oxidation in the Complementarity-Determining Regions of a Monoclonal Antibody: A Study of the Modification–Structure–Function Correlations by Hydrogen–Deuterium Exchange Mass Spectrometry, Analytical Chemistry, 88 (2016) 2041-2050.
[79] B. Moorthy, B. Xie, E. Moussa, L. Iyer, S. Chandrasekhar, J. Panchal, E. Topp, Structure of Monoclonal Antibodies, in: A. Rosenberg, B. Demeule (Eds.) Biobetters, Springer New York2015, pp. 81-89.
[80] N. Chennamsetty, V. Voynov, V. Kayser, B. Helk, B.L. Trout, Design of therapeutic proteins with enhanced stability, Proceedings of the National Academy of Sciences, 106 (2009) 11937-11942.
[81] N. Chennamsetty, V. Voynov, V. Kayser, B. Helk, B.L. Trout, Prediction of aggregation prone regions of therapeutic proteins, The Journal of Physical Chemistry B, 114 (2010) 6614-6624.
[82] F. Courtois, C.P. Schneider, N.J. Agrawal, B.L. Trout, Rational Design of Biobetters with Enhanced Stability, Journal of Pharmaceutical Sciences, 104 (2015) 2433-2440.
[83] M. Ahmadi, C.J. Bryson, E.A. Cloake, K. Welch, V. Filipe, S. Romeijn, A. Hawe, W. Jiskoot, M.P. Baker, M.H. Fogg, Small Amounts of Sub-Visible Aggregates

Enhance the Immunogenic Potential of Monoclonal Antibody Therapeutics, Pharmaceutical Research, 32 (2015) 1383-1394.
[84] J. Bessa, S. Boeckle, H. Beck, T. Buckel, S. Schlicht, M. Ebeling, A. Kiialainen, A. Koulov, B. Boll, T. Weiser, T. Singer, A.G. Rolink, A. Iglesias, The Immunogenicity of Antibody Aggregates in a Novel Transgenic Mouse Model, Pharmaceutical Research, 32 (2015) 2344-2359.
[85] M.C. Manning, D.K. Chou, B.M. Murphy, R.W. Payne, D.S. Katayama, Stability of Protein Pharmaceuticals: An Update, Pharmaceutical Research, 27 (2010) 544-575.
[86] E. Sahin, A.O. Grillo, M.D. Perkins, C.J. Roberts, Comparative effects of pH and ionic strength on protein–protein interactions, unfolding, and aggregation for IgG1 antibodies, Journal of Pharmaceutical Sciences, 99 (2010) 4830-4848.
[87] P. Arosio, S. Rima, M. Morbidelli, Aggregation Mechanism of an IgG2 and two IgG1 Monoclonal Antibodies at low pH: From Oligomers to Larger Aggregates, Pharmaceutical Research, 30 (2013) 641-654.
[88] S.N. Telikepalli, O.S. Kumru, C. Kalonia, R. Esfandiary, S.B. Joshi, C.R. Middaugh, D.B. Volkin, Structural Characterization of IgG1 mAb Aggregates and Particles Generated Under Various Stress Conditions, Journal of Pharmaceutical Sciences, 103 (2014) 796-809.
[89] F. Depreter, G. Pilcer, K. Amighi, Inhaled proteins: Challenges and perspectives, International Journal of Pharmaceutics, 447 (2013) 251-280.
[90] V. Kayser, N. Chennamsetty, V. Voynov, B. Helk, K. Forrer, B.L. Trout, Evaluation of a non-Arrhenius model for therapeutic monoclonal antibody aggregation, Journal of Pharmaceutical Sciences, 100 (2011) 2526-2542.
[91] N. Kim, R.L. Remmele Jr, D. Liu, V.I. Razinkov, E.J. Fernandez, C.J. Roberts, Aggregation of anti-streptavidin immunoglobulin gamma-1 involves Fab unfolding and competing growth pathways mediated by pH and salt concentration, Biophysical Chemistry, 172 (2013) 26-36.
[92] H. Wu, R. Kroe-Barrett, S. Singh, A.S. Robinson, C.J. Roberts, Competing aggregation pathways for monoclonal antibodies, FEBS Letters, 588 (2014) 936-941.
[93] S.B. Mehta, J.S. Bee, T.W. Randolph, J.F. Carpenter, Partial Unfolding of a Monoclonal Antibody: Role of a Single Domain in Driving Protein Aggregation, Biochemistry, 53 (2014) 3367-3377.

[94] V.I. Razinkov, M.J. Treuheit, G.W. Becker, Accelerated Formulation Development of Monoclonal Antibodies (mAbs) and mAb-Based Modalities: Review of Methods and Tools, Journal of Biomolecular Screening, 20 (2015) 468-483.
[95] H. Liu, G. Gaza-Bulseco, J. Sun, Characterization of the stability of a fully human monoclonal IgG after prolonged incubation at elevated temperature, Journal of Chromatography B, 837 (2006) 35-43.
[96] J. Vlasak, R. Ionescu, Fragmentation of monoclonal antibodies, mAbs, 3 (2011) 253-263.
[97] R.J. Harris, B. Kabakoff, F.D. Macchi, F.J. Shen, M. Kwong, J.D. Andya, S.J. Shire, N. Bjork, K. Totpal, A.B. Chen, Identification of multiple sources of charge heterogeneity in a recombinant antibody, Journal of Chromatography B: Biomedical Sciences and Applications, 752 (2001) 233-245.
[98] H. Liu, G. Gaza-Bulseco, C. Chumsae, Glutamine deamidation of a recombinant monoclonal antibody, Rapid Communications in Mass Spectrometry, 22 (2008) 4081-4088.
[99] Y.T. Zhang, J. Hu, A.L. Pace, R. Wong, Y.J. Wang, Y.-H. Kao, Characterization of asparagine 330 deamidation in an Fc-fragment of IgG1 using cation exchange chromatography and peptide mapping, Journal of Chromatography B, 965 (2014) 65-71.
[100] A.L. Pace, R.L. Wong, Y.T. Zhang, Y.-H. Kao, Y.J. Wang, Asparagine deamidation dependence on buffer type, pH, and temperature, Journal of Pharmaceutical Sciences, 102 (2013) 1712-1723.
[101] L. Yi, N. Beckley, B. Gikanga, J. Zhang, Y.J. Wang, H.-W. Chih, V.K. Sharma, Isomerization of Asp–Asp motif in model peptides and a Monoclonal Antibody Fab Fragment, Journal of Pharmaceutical Sciences, 102 (2013) 947-959.
[102] V. Timm, P. Gruber, M. Wasiliu, H. Lindhofer, D. Chelius, Identification and characterization of oxidation and deamidation sites in monoclonal rat/mouse hybrid antibodies, Journal of Chromatography B, 878 (2010) 777-784.
[103] L. Huang, J. Lu, V.J. Wroblewski, J.M. Beals, R.M. Riggin, In Vivo Deamidation Characterization of Monoclonal Antibody by LC/MS/MS, Analytical Chemistry, 77 (2005) 1432-1439.
[104] A. Sreedhara, J. Yin, M. Joyce, K. Lau, A.T. Wecksler, G. Deperalta, L. Yi, Y. John Wang, B. Kabakoff, R.S.K. Kishore, Effect of ambient light on IgG1 monoclonal

antibodies during drug product processing and development, European Journal of Pharmaceutics and Biopharmaceutics, 100 (2016) 38-46.
[105] A. Sreedhara, K. Lau, C. Li, B. Hosken, F. Macchi, D. Zhan, A. Shen, D. Steinmann, C. Schöneich, Y. Lentz, Role of Surface Exposed Tryptophan as Substrate Generators for the Antibody Catalyzed Water Oxidation Pathway, Molecular Pharmaceutics, 10 (2013) 278-288.
[106] R. Torosantucci, C. Schöneich, W. Jiskoot, Oxidation of Therapeutic Proteins and Peptides: Structural and Biological Consequences, Pharmaceutical Research, 31 (2014) 541-553.
[107] W. Wang, J. Vlasak, Y. Li, P. Pristatsky, Y. Fang, T. Pittman, J. Roman, Y. Wang, T. Prueksaritanont, R. Ionescu, Impact of methionine oxidation in human IgG1 Fc on serum half-life of monoclonal antibodies, Mol Immunol, 48 (2011) 860-866.
[108] W. Wang, S. Singh, D.L. Zeng, K. King, S. Nema, Antibody structure, instability, and formulation, Journal of Pharmaceutical Sciences, 96 (2007) 1-26.
[109] B. Yan, Z. Yates, A. Balland, G.R. Kleemann, Human IgG1 Hinge Fragmentation as the Result of H2O2-mediated Radical Cleavage, Journal of Biological Chemistry, 284 (2009) 35390-35402.
[110] Z. Wei, J. Feng, H.-Y. Lin, S. Mullapudi, E. Bishop, G.I. Tous, J. Casas-Finet, F. Hakki, R. Strouse, M.A. Schenerman, Identification of a Single Tryptophan Residue as Critical for Binding Activity in a Humanized Monoclonal Antibody against Respiratory Syncytial Virus, Analytical Chemistry, 79 (2007) 2797-2805.
[111] C.J. Wilson, Rational protein design: developing next-generation biological therapeutics and nanobiotechnological tools, Wiley Interdisciplinary Reviews: Nanomedicine and Nanobiotechnology, 7 (2015) 330-341.
[112] N. Cerda-Costa, A. Esteras-Chopo, F.X. Aviles, L. Serrano, V. Villegas, Early kinetics of amyloid fibril formation reveals conformational reorganisation of initial aggregates, Journal of Molecular Biology, 366 (2007) 1351.
[113] N. de Groot, I. Pallares, F. Aviles, J. Vendrell, S. Ventura, Prediction of "hot spots" of aggregation in disease-linked polypeptides, BMC Structural Biology, 5 (2005) 18.
[114] U. Ogmen, O. Keskin, S. Aytuna, R. Nussinoiv, A. Gursoy, PRISM: Protein interactions by structural matching, Nucleic Acids Research, 33 (2005) W331-W336.
[115] G.G. Tartaglia, M. Vendruscolo, The Zyggregator method for predicting protein aggregation propensities, Chemical Society Reviews, 37 (2008) 1395-1401.

[116] A. Trovato, F. Seno, S.C.E. Tosatto, The PASTA server for protein aggregation prediction, Protein Engineering Design and Selection, (2007) gzm042.
[117] G.G. Tartaglia, A. Cavalli, R. Pellarin, A. Caflisch, Prediction of aggregation rate and aggregation-prone segments in polypeptide sequences, Protein Science, 14 (2005) 2723-2734.
[118] X. Wang, T.K. Das, S.K. Singh, S. Kumar, Potential aggregation prone regions in biotherapeutics, mAbs, 1 (2009) 254-267.
[119] V.E. Angarica, J. Sancho, Protein Dynamics Governed by Interfaces of High Polarity and Low Packing Density, PLoS ONE, 7 (2012) e48212.
[120] R. Zambrano, M. Jamroz, A. Szczasiuk, J. Pujols, S. Kmiecik, S. Ventura, AGGRESCAN3D (A3D): server for prediction of aggregation properties of protein structures, Nucleic Acids Research, 43 (2015) W306-W313.
[121] D. Schweizer, T. Serno, A. Goepferich, Controlled release of therapeutic antibody formats, European Journal of Pharmaceutics and Biopharmaceutics, 88 (2014) 291-309.
[122] A.L. Daugherty, R.J. Mrsny, Formulation and delivery issues for monoclonal antibody therapeutics, Advanced Drug Delivery Reviews, 58 (2006) 686-706.
[123] L. Chang, D. Shepherd, J. Sun, X. Tang, M.J. Pikal, Effect of sorbitol and residual moisture on the stability of lyophilized antibodies: Implications for the mechanism of protein stabilization in the solid state, Journal of Pharmaceutical Sciences, 94 (2005) 1445-1455.
[124] L. Platts, R.J. Falconer, Controlling protein stability: Mechanisms revealed using formulations of arginine, glycine and guanidinium HCl with three globular proteins, International Journal of Pharmaceutics, 486 (2015) 131-135.
[125] S. Ohtake, Y. Kita, T. Arakawa, Interactions of formulation excipients with proteins in solution and in the dried state, Adv Drug Deliv Rev, 63 (2011) 1053-1073.
[126] M.X. Yang, B. Shenoy, M. Disttler, R. Patel, M. McGrath, S. Pechenov, A.L. Margolin, Crystalline monoclonal antibodies for subcutaneous delivery, Proceedings of the National Academy of Sciences, 100 (2003) 6934-6939.
[127] D. Schweizer, K. Schonhammer, M. Jahn, A. Gopferich, Protein-polyanion interactions for the controlled release of monoclonal antibodies, Biomacromolecules, 14 (2013) 75-83.
[128] D.W. Grainger, Controlled-release and local delivery of therapeutic antibodies, Expert Opinion on Biological Therapy, 4 (2004) 1029-1044.

[129] M. Shimizu, Y. Miwa, K. Hashimoto, A. Goto, Encapsulation of chicken egg yolk immunoglobulin G (IgY) by liposomes, Bioscience Biotechnology and Biochemistry, 57 (1993) 1445-1449.
[130] X.Y. Li, L.J. Jin, T.A. McAllister, K. Stanford, J.Y. Xu, Y.N. Lu, Y.H. Zhen, Y.X. Sun, Y.P. Xu, Chitosan-alginate microcapsules for oral delivery of egg yolk immunoglobulin (IgY), Journal of Agricultural and Food Chemistry, 55 (2007) 2911-2917.
[131] Y. Yun, Y.W. Cho, K. Park, Nanoparticles for oral delivery: Targeted nanoparticles with peptidic ligands for oral protein delivery, Advanced Drug Delivery Reviews, 65 (2013) 822-832.
[132] M. Streit, Z. Beleznay, L.R. Braathen, Topical application of the tumour necrosis factor-alpha antibody infliximab improves healing of chronic wounds, International Wound Journal, 3 (2006) 171-179.
[133] M. Smola, T. Vandamme, A. Sokolowski, Nanocarriers as pulmonary drug delivery systems to treat and to diagnose respiratory and non respiratory diseases, International Journal of Nanomedicine, 3 (2008) 1-19.
[134] S.J. Koussoroplis, G. Paulissen, D. Tyteca, H. Goldansaz, J. Todoroff, C. Barilly, C. Uyttenhove, J. Van Snick, D. Cataldo, R. Vanbever, PEGylation of antibody fragments greatly increases their local residence time following delivery to the respiratory tract, Journal of Controlled Release, 187 (2014) 91-100.
[135] L. Dellamary, D.J. Smith, A. Bloom, S. Bot, G.R. Guo, H. Deshmuk, M. Costello, A. Bot, Rational design of solid aerosols for immunoglobulin delivery by modulation of aerodynamic and release characteristics, Journal of Controlled Release, 95 (2004) 489-500.
[136] A.I. Bot, T.E. Tarara, D.J. Smith, S.R. Bot, C.M. Woods, J.G. Weers, Novel lipid-based hollow-porous microparticles as a platform for immunoglobulin delivery to the respiratory tract, Pharmaceutical Research, 17 (2000) 275-283.
[137] I.M. El-Sherbiny, N.M. El-Baz, M.H. Yacoub, Inhaled nano- and microparticles for drug delivery, Global Cardiology Science and Practice, 2015 (2015) 2.
[138] L. Detalle, T. Stohr, C. Palomo, P.A. Piedra, B.E. Gilbert, V. Mas, A. Millar, U.F. Power, C. Stortelers, K. Allosery, J.A. Melero, E. Depla, Generation and Characterization of ALX-0171, a Potent Novel Therapeutic Nanobody for the Treatment of Respiratory Syncytial Virus Infection, Antimicrobial Agents and Chemotherapy, 60 (2016) 6-13.

CHAPTER 2

“Lack of a Synergistic Effect of Arginine-Glutamic Acid on the Physical Stability of Spray-Dried Bovine Serum Albumin”

Chapter 2 was published in the Pharmaceutical Development and Technology journal:

Reslan, M., Demir, Y., Trout, B., Chan, H., Kayser, V. (2017). Lack of a synergistic effect of arginine-glutamic acid on the physical stability of spray-dried bovine serum albumin. Pharmaceutical Development and Technology, 22:785-791.

Abstract

Improving the physical stability of spray-dried proteins is essential for enabling pulmonary delivery of biotherapeutics as a non-invasive alternative to injections. Recently, a novel combination of two amino acids - L-arginine (L-Arg) and L-glutamic acid (L-Glu), has been reported to have synergistic protein-stabilizing effects on various protein solutions. Using spray-dried bovine serum albumin (BSA) reconstituted in solution as a model protein, we investigated the synergistic effect of these amino acids on the physical stability of proteins.

Five BSA solutions were prepared: (1) BSA with no amino acids (control); (2) with 50 mM L-Arg; (3) with 200 mM L-Arg, (4) with 50 mM L-Glu; and (5) with 25:25 mM of Arg:Glu. All solutions were spray-dried and accelerated studies at high temperatures were performed. Following accelerated studies, monomer BSA loss was measured using SE-HPLC.

We found that L-Arg significantly improved the physical stability of spray-dried BSA even at low concentrations, however, when combined with L-Glu, was ineffective at reducing monomer BSA loss. Our findings demonstrate the limitations in using Arg-Glu for the stabilization of spray-dried BSA. Furthermore, we found that a low concentration of L-Glu enhanced monomer BSA loss. These findings may have significant implications on the design of future biotherapeutic formulations

1. Introduction

The majority of current and emerging biotherapeutics are delivered parenterally due to their poor oral bioavailability and short half-lives in the gastrointestinal tract [1-3]. However, due to poor patient compliance to parenteral treatment and the increased likelihood of treatment failure, the development of non-invasive protein formulations has become critical [1, 4]. In recent years, following the success of insulin inhalers, pulmonary delivery of proteins has been recognized as a viable non-invasive alternative for the treatment of local and systemic conditions [5, 6]. The advantages of the pulmonary route include: improved compliance, potential to reduce dose and adverse effects, increased biological half-life, and enhanced efficacy for local lung diseases [2, 7].

For any biotherapeutic formulation, protein aggregation is particularly problematic as it leads to loss of protein activity and can induce an undesired immunogenic response in a patient [8, 9]. One method currently employed to suppress aggregation involves the addition of protein-stabilizing excipients to the formulation, such as various sugars - trehalose, sucrose and maltose; amino acids – arginine and leucine; and surfactants – tween 80 and poloxamer [4, 10-12]. In order for non-invasive formulations – such as inhalers - to become more practical, the physical stability of proteins must be enhanced further, without excessive use of excipients to maximize the potency of the formulation.

Recently, a combination of arginine and glutamic acid in equimolar concentrations has been used to stabilize a number of proteins prepared in aqueous solutions [9, 13, 14]. It was shown that the combination of the two amino acids had a synergistic effect on the suppression of protein aggregation in concentrations ranging from 50-200 mM [13, 14]. While the effect of amino acids on protein stability has been studied extensively, only a limited number of proteins have been tested with the Arg-Glu combination. Furthermore, the mechanism underlying the Arg-Glu synergy is poorly understood; thus, more research is required to understand the significance of these findings for the development of biotherapeutics. The aim of this study is to investigate the potential synergistic effects of L-Arg and L-Glu on the physical stability of protein formulations, using spray-dried BSA reconstituted in solution as a model system. BSA has good thermal stability and is widely used to model protein aggregation as it is well-characterized and readily available. Findings from our study may contribute to the use of a novel combination of amino acids as an effective protein-stabilizing excipient system for the formulation of therapeutically important proteins.

We used a 50 mM L-Glu concentration, due to the limited solubility of L-Glu. We observed minimal protein degradation due to spray-drying for all formulations. L-Arg suppressed heat-induced monomer loss of spray-dried BSA as previously reported [15, 16], however L-Glu enhanced monomer BSA loss, while the combination of Arg-Glu neither suppressed nor facilitated monomer loss. Our findings suggest that the synergistic mechanism observed in previous studies is protein-specific and it is possible that a minimum threshold concentration is required to observe synergistic action.

2. Materials and methods

2.1. Materials

Bovine serum albumin (Fraction V, A7906), L-arginine (A5006, reagent grade, ≥98%) and L-glutamic acid (G1251, ReagentPlus®, ≥99%) were purchased from Sigma Aldrich, Castle Hill, Australia. di-potassium hydrogen phosphate (105101, EMPROVE® Ph Eur, BP, E 340 grade) and potassium dihydrogen phosphate (104873, EMSURE® ISO grade) were purchased from Merck Millipore, MA, USA.

2.2. Preparation of BSA samples

All samples were prepared from a 40 mg/ml stock solution of BSA in 15 mM potassium phosphate buffer to a final [BSA] of 4 mg/mL. A 55.6 mM stock solution of L-Glu was used to make BG1 and BAG1 to a final [L-Glu] of 50 mM and 25 mM, respectively. A 200 mM stock solution of L-Arg was used to make BA1, BA2 and BAG1 to final [L-Arg] of 50 mM, 200 mM and 25 mM respectively (Table 1). 50 mL of each formulation was prepared and stored at 4 °C. All samples used in the study were adjusted to pH 6.5.

Table 1. Summary of preparations used in the study.

Samples	**[BSA] (mg/mL)**	**[L-arginine] (mM)**	**[L-glutamic acid] (mM)**	**[Potassium phosphate] (mM)**
BSA (Control)	4	-	-	15
BA1	4	50	-	15
BAG1	4	25	25	15
BG1	4	-	50	15
BA2	4	200	-	15

2.3. Spray-drying

All samples were spray dried using a Buchi Mini Spray-Dryer B-290 in open loop setting using compressed air. The operating conditions were: inlet temperature of 60 °C, outlet temperature of 39 °C, aspirator at 100%, liquid feed rate at 2.2 mL/min and an atomizing airflow of 742 NL/hr.

2.4. Laser diffraction (LD)

The particle size distribution of dry powders was measured by laser diffraction using a Malvern Mastersizer 2000 (Malvern, Worcestershire, UK). Approximately 5 mg of spray-dried powder was analyzed for each BSA sample, three times. The refractive index of BSA particles was 1.45 and the absorption value was 0.1. Size was assessed by the volume-weighted mean diameter and $D_{0.1}$, $D_{0.5}$ and $D_{0.9,}$ which represent the diameter at which, 10%, 50% and 90% of the volume distribution of particles (respectively), fall below. Size distribution was assessed by the span, which is a measure of the broadness of the distribution, calculated as $(D_{0.9}-D_{0.1})/D_{0.5}$.

2.5. Accelerated studies at elevated temperature

Accelerated studies at high temperatures were conducted as previously described [17]. Incubation of dry powders in the solid state was not feasible due to the powders sticking to the tubes at elevated temperatures, leading to significant loss of sample when dissolving the powders for SE-HPLC. Thus spray-dried BSA powders were first dissolved in 15 mM potassium phosphate buffer to a final [BSA] of 0.85 mg/mL, then 100 µL aliquots were incubated in a Thermal Cycler 2720 (Applied Biosystems, CA, USA) at 65 °C for 1 and 2 hours, and 70 °C for 15 and 30 minutes. Following incubation, the physical stability of the BSA samples was analyzed using size exclusion-high performance liquid chromatography (SE-HPLC).

2.6. SE-HPLC

Size exclusion-high performance liquid chromatography was used to quantify monomer loss of BSA following accelerated temperature studies. Analysis was performed using an Agilent 1200 Liquid Chromatography system with a TSKgel Super SW3000 column, at 22 °C, with 150 mM potassium phosphate mobile phase, at pH 6.5, and flow rate set at 0.2 mL/min. 85 µg of BSA was injected in each run (100 µL). Monomer peaks were detected at 280 nm by an in-line UV signal detector. The area under the curve (AUC) of the monomer peak was averaged over three runs and the mean monomer % was calculated for each sample. The standard deviation (SD) was plotted as error bars in the figures.

3. Results

3.1. Particle size distribution of powders by LD

The addition of L-Arg prior to spray-drying had no significant effect on the mean particle size of the spray-dried powders (Table 2), however the addition of L-Glu reduced the size of the particles generated from 2.75 ± 0.14 to 2.11 ± 0.16 µm (± SD), even when combined with arginine (BAG1; 2.27 ± 0.01 µm; Table 2). Despite the differences in the mean particle sizes, the particle size distribution of the powders was relatively comparable with a span ranging from 1.30 (BA1) to 1.71 (BG1) and $D_{0.5}$ from 1.90 (BG1) to 2.68 (BA2) (Table 2).

Table 2. Size distribution data of the spray-dried powders.

Powder	**Volume-weighted mean (µm) ± SD**	**$D_{0.1}$**	**$D_{0.5}$**	**$D_{0.9}$**	**Span**
BSA	2.75 ± 0.14	1.01	2.48	4.91	1.57
BA1	2.59 ± 0.05	1.21	2.38	4.30	1.30
BAG1	2.27 ± 0.01	0.86	2.04	4.04	1.56
BA2	2.87 ± 0.16	0.70	2.68	5.21	1.69
BG1	2.11 ± 0.16	0.66	1.90	3.89	1.71

3.2. SE-HPLC analysis of monomer BSA loss following spray-drying and accelerated temperature studies

SE-HPLC was used to measure changes in monomer BSA content following spray-drying and incubation at high temperatures (Fig. 1-7; Tables 3 and 4). Mean monomer % content and % loss of all samples following spray-drying and heat-treatment can be found in Tables 3 and 4. Since BSA exists predominantly in the monomer state, a loss of monomer AUC would indicate that the protein sample has either fragmented or formed aggregates. After spray-drying, a monomer loss between 1.1-2.8% is observed for all samples, except BA1 which had the lowest monomer loss (0.4%; Fig. 1 and 2; Table 3). Interestingly, the highest monomer loss post-spray drying was observed with BAG1 (2.8%), while the other formulations maintained a comparable monomer loss of ~1%. Incubation at 65 °C for 1 hour caused a significant decrease in monomer % for all samples (19-37% loss), except BA2 with only a 4.7% loss (Fig. 3 and 7; Table 4). Following incubation at 65 °C for 2 hours, all samples have a significantly lower monomer % (5.9-42.2% loss) when compared to the untreated control, however the smallest reductions in monomer % are observed with BA1 (23%) and BA2 (5.9%) (Fig. 4 and 7; Table 4). This trend continues for samples incubated at 70 °C for 15 minutes;

the highest monomer loss is observed with BG1 (51.4%), followed by BAG1 (45.5%), BSA-only (44.8%), BA1 (36.9%) and BA2 (16.5%) (Fig. 5 and 7; Table 4). Likewise, following incubation at 70 °C for 30 minutes, the highest monomer loss is observed with BG1 (54.2%), followed by BAG1 (49.9%), BSA-only (48.8%), BA1 (37.3%) and BA2 (22.7%) (Fig. 6 and 7; Table 4).

Table 3. Mean monomer % loss of BSA samples following spray-drying.

Sample	Monomer									
	BSA		BAG1		BG1		BA1		BA2	
	%	% loss	%	% loss	%	% loss	%	% loss	%	% loss
Pre-Spray	78.0	0	78.0	0	78.0	0	78.0	0	78.0	0
Post-Spray	76.9	1.1	75.2	2.8	76.9	1.1	77.6	0.4	76.3	1.7

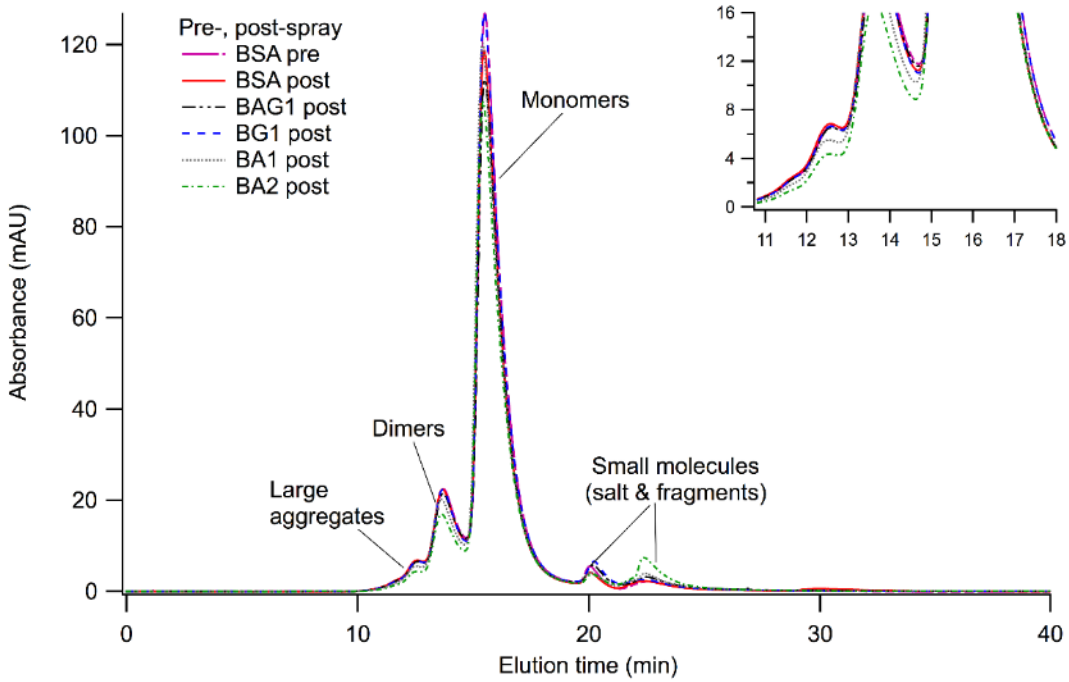

Figure 1. Representative SE-HPLC chromatogram of BSA and spray-dried BSA, BAG1, BG1, BA1 and BA2. [BSA] of all samples is 0.85 mg/mL. BAG1 = BSA + 5.3 mM L-Arg + 5.3 mM L-Glu; BG1 = BSA + 10.6 mM L-Glu; BA1 = BSA + 10.6 mM L-Arg; BA2 = BSA + 42.5 mM L-Arg. Inset figure represents a magnified region of the chromatogram between 10-25 minutes.

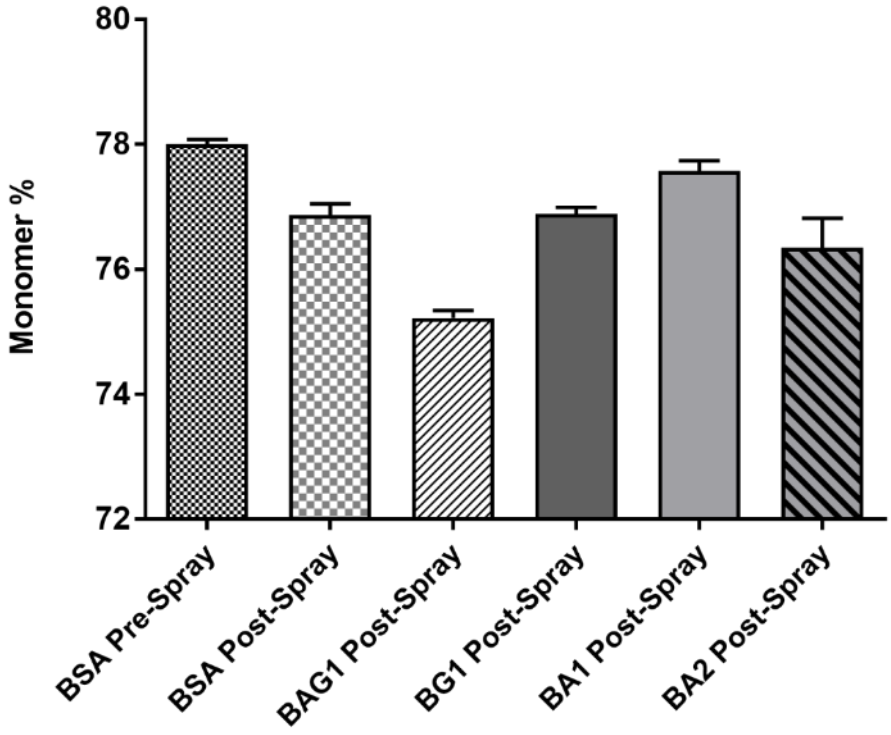

Figure 2. Mean monomer % of BSA samples following spray-drying. "BSA Pre-Spray" represents the monomer % for a BSA solution that has not been spray-dried. [BSA] of all samples is 0.85 mg/mL. BAG1 = BSA + 5.3 mM L-Arg + 5.3 mM L-Glu; BG1 = BSA + 10.6 mM L-Glu; BA1 = BSA + 10.6 mM L-Arg; BA2 = BSA + 42.5 mM L-Arg. The error bars represent the SD.

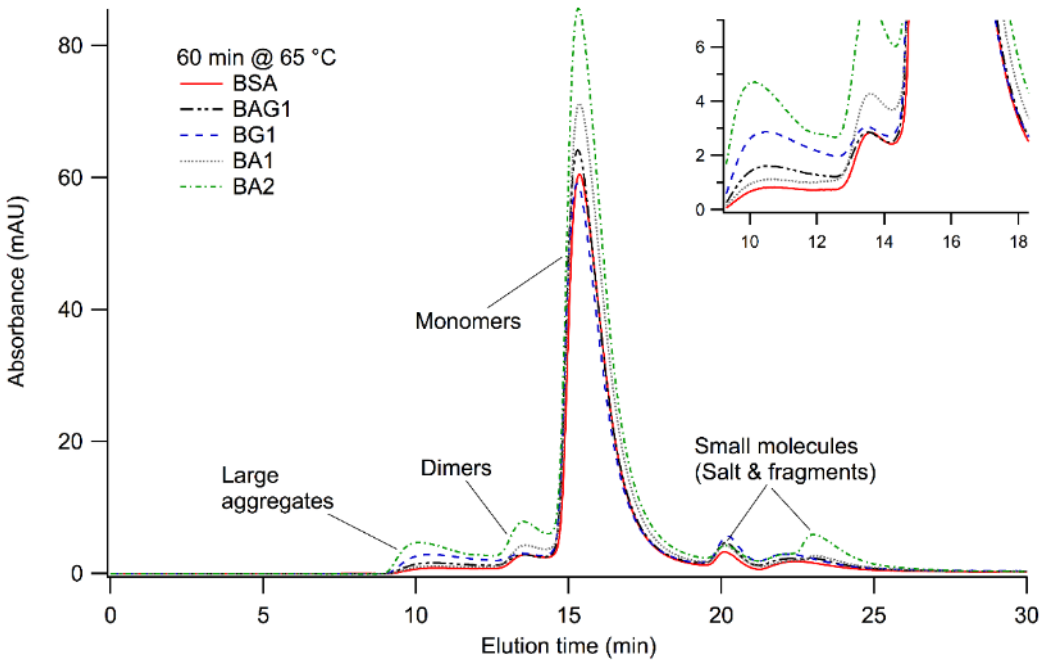

Figure 3. Representative SE-HPLC chromatogram of spray-dried BSA, BAG1, BG1, BA1 and BA2 following incubation at 65 °C for 60 minutes. [BSA] of all samples is 0.85 mg/mL. BAG1 = BSA + 5.3 mM L-Arg + 5.3 mM L-Glu; BG1 = BSA + 10.6 mM L-Glu; BA1 = BSA + 10.6 mM L-Arg; BA2 = BSA + 42.5 mM L-Arg. Inset figure represents a magnified region of the chromatogram between 9-25 minutes.

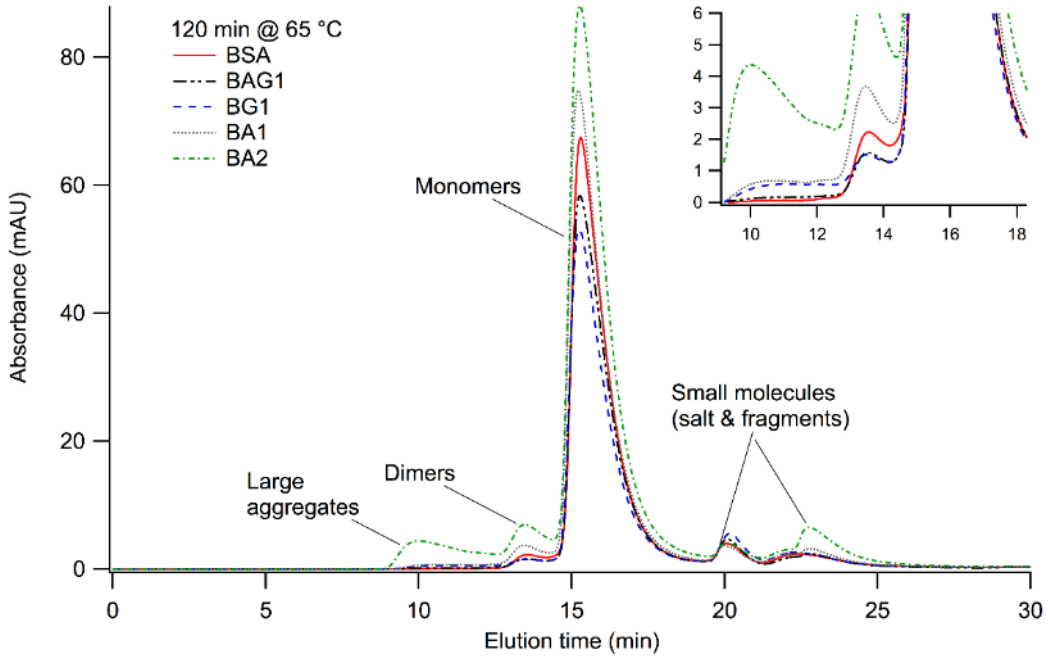

Figure 4. Representative SE-HPLC chromatogram of spray-dried BSA, BAG1, BG1, BA1 and BA2 following incubation at 65 °C for 120 minutes. [BSA] of all samples is 0.85 mg/mL. BAG1 = BSA + 5.3 mM L-Arg + 5.3 mM L-Glu; BG1 = BSA + 10.6 mM L-Glu; BA1 = BSA + 10.6 mM L-Arg; BA2 = BSA + 42.5 mM L-Arg. Inset figure represents a magnified region of the chromatogram between 9-25 minutes.

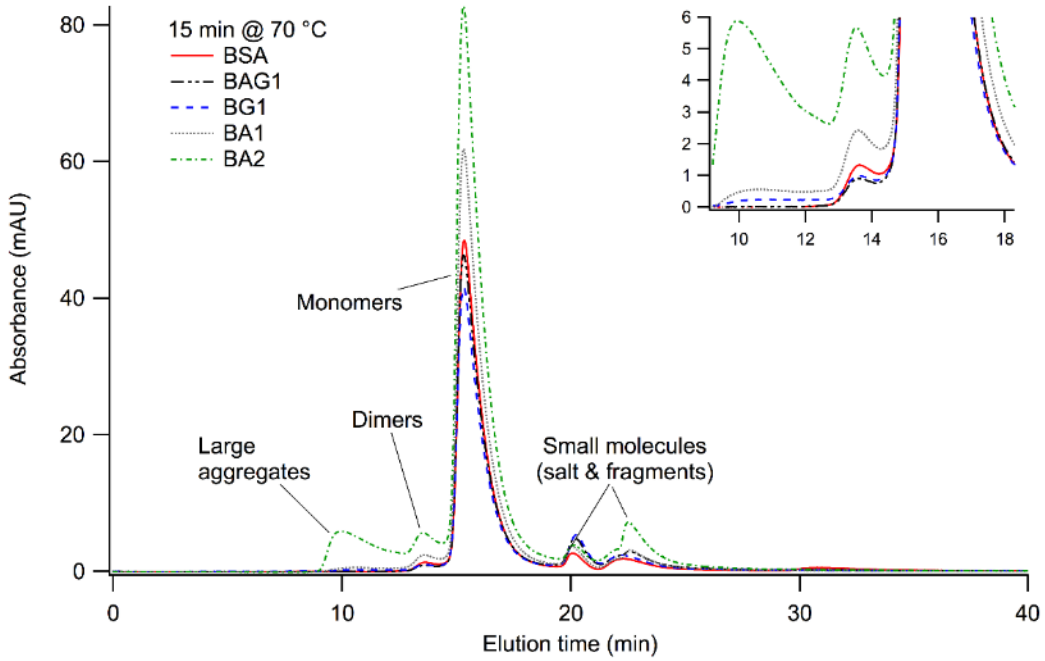

Figure 5. Representative SE-HPLC chromatogram of spray-dried BSA, BAG1, BG1, BA1 and BA2 following incubation at 70 °C for 15 minutes. [BSA] of all samples is 0.85 mg/mL. BAG1 = BSA + 5.3 mM L-Arg + 5.3 mM L-Glu; BG1 = BSA + 10.6 mM L-Glu; BA1 = BSA + 10.6 mM L-Arg; BA2 = BSA + 42.5 mM L-Arg. Inset figure represents a magnified region of the chromatogram between 9-26 minutes.

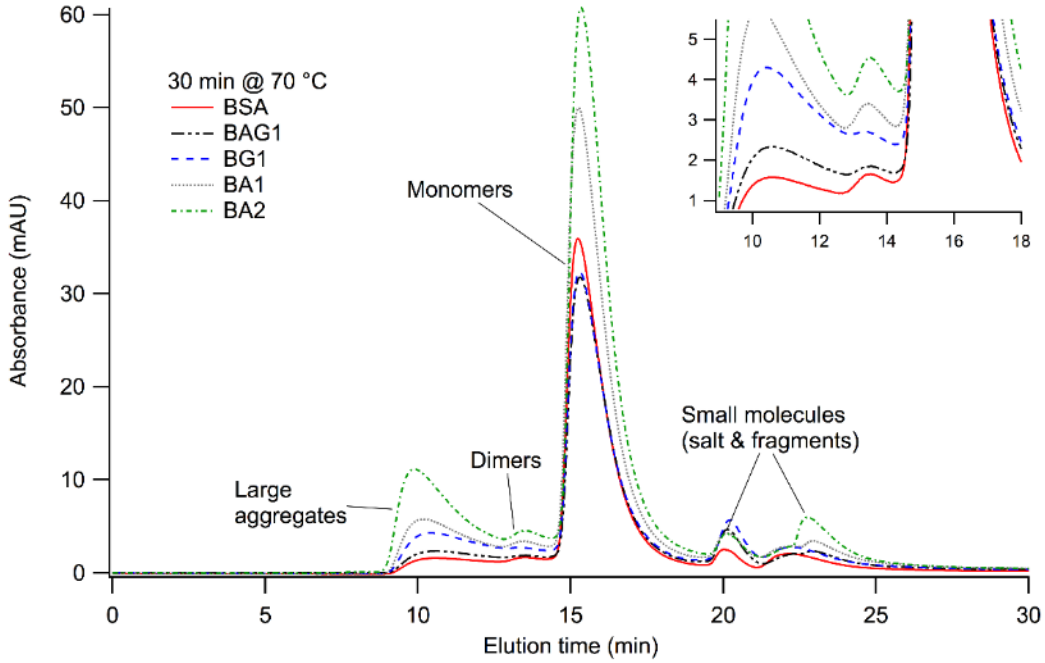

Figure 6. Representative SE-HPLC chromatogram of spray-dried BSA, BAG1, BG1, BA1 and BA2 following incubation at 70 °C for 30 minutes. [BSA] of all samples is 0.85 mg/mL. BAG1 = BSA + 5.3 mM L-Arg + 5.3 mM L-Glu; BG1 = BSA + 10.6 mM L-Glu; BA1 = BSA + 10.6 mM L-Arg; BA2 = BSA + 42.5 mM L-Arg. Inset figure represents a magnified region of the chromatogram between 9-26 minutes.

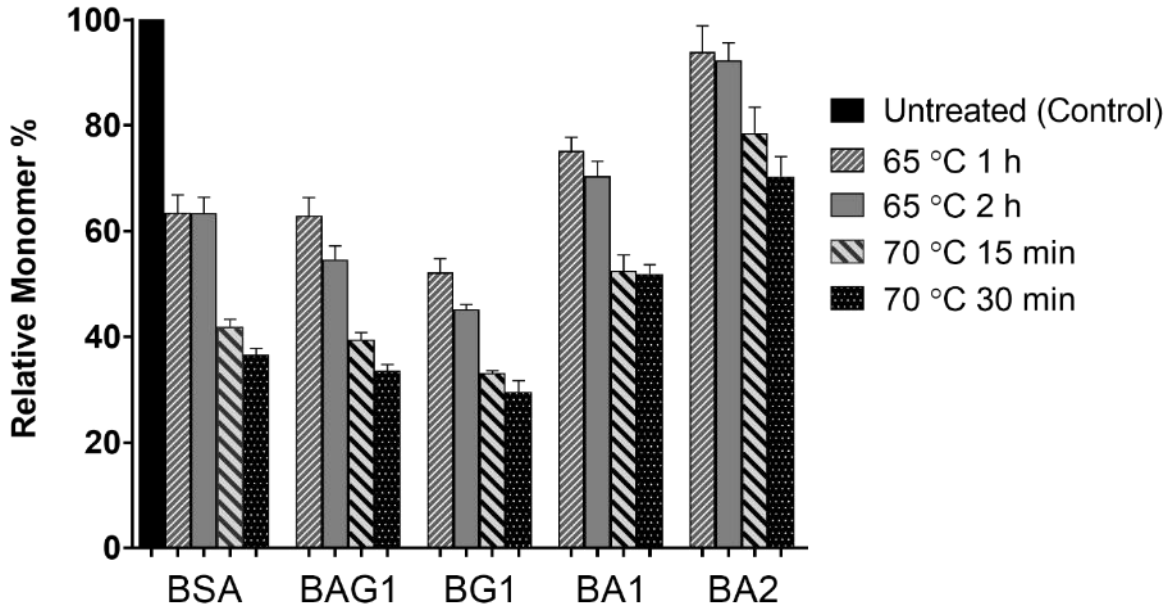

Figure 7. Mean relative monomer % of spray-dried BSA samples, prior to, and following incubation at 65 °C for 1 and 2 hours and 70 °C for 15 and 30 minutes. The "Untreated (Control)" represents a spray-dried sample prior to heat-treatment. [BSA] of all samples is 0.85 mg/mL. BAG1 = BSA + 5.3 mM L-Arg + 5.3 mM L-Glu; BG1 = BSA + 10.6 mM L-Glu; BA1 = BSA + 10.6 mM L-Arg; BA2 = BSA + 42.5 mM L-Arg. The error bars represent the SD.

Table 4. Mean monomer % loss of BSA samples following incubation at 65 °C for 1 and 2 hours and 70 °C for 15 and 30 minutes.

Sample	Monomer									
	BSA		BAG1		BG1		BA1		BA2	
	%	% loss	%	% loss	%	% loss	%	% loss	%	% loss
Post-Spray	76.9	0	75.2	0	76.9	0	77.6	0	76.3	0
65 °C 1 h	48.8	28.1	47.3	27.9	40.1	36.8	58.3	19.3	71.6	4.7
65 °C 2 h	48.7	28.2	41.1	34.1	34.7	42.2	54.6	23.0	70.4	5.9
70 °C 15 min	32.1	44.8	29.7	45.5	25.5	51.4	40.7	36.9	59.8	16.5
70 °C 30 min	28.1	48.8	25.3	49.9	22.7	54.2	40.3	37.3	53.6	22.7

When compared to BSA-only, BG1 has a significantly lower monomer % while BA1 and BA2 have a significantly higher monomer %, following all incubation conditions (Fig. 3-7; Table 4). For example, following incubation at 70 °C for 30 minutes, the monomer BSA content of BSA-only, BG1, BA1 and BA2 is 28.1%, 22.7%, 40.3% and 53.6%, respectively (Fig. 6 and 7; Table 4). There is no significant difference between BSA-only and BAG1 at any incubation conditions except at 65 °C after 2 hours, where BSA-only has a significantly higher monomer % (48.7% vs. 41.1%; Fig. 4 and 7; Table 4).

From the SE-HPLC chromatograms, a significant amount of the injected sample into the column is not recovered following heat-treatment as the total AUC decreases with incubation temperature. The low protein recovery is likely due to loss of aggregates that became trapped in the column owing to their large size. With this in mind, even though it appears that BA2 has the highest amount of aggregates after heat-treatment at all incubation conditions (Fig. 3-6), the total recovered protein with the BA2 sample is significantly higher than all other heat-treated samples (BSA, BAG1, BG1 and BA1) indicating that BA2 formed mostly smaller aggregates.

All samples containing amino acids had enlarged fragment peaks between ~19-26 minutes. BA2 had the largest fragment peak at ~24 minutes and the size of the peak remained unchanged following all incubation conditions (Fig. 3-6). Since L-Arg and L-Glu solutions eluted between 19-26 minutes in preliminary tests (data not shown), the

peaks observed were attributed to overlaps between the free amino acids, salt and the fragment BSA peaks, and therefore, were not considered in the final assessment of the physical stability of the samples.

4. Discussion

4.1. Particle size of BSA powders with amino acids

Particle size of spray-dried BSA was unchanged with the addition of L-Arg, however was significantly lowered when L-Glu was used. Faghihi, et al. [18] also found that spray-dried Immunoglobulin G (IgG) with 20% or 50% w/w arginine, did not significantly affect the size of particles produced when compared with excipient-free IgG. Conversely, they found that leucine, phenylalanine, cysteine and glycine significantly decreased the particle size of spray-dried IgG powders. They proposed that these amino acids would reside at the surface of IgG for extended periods of time due to either hydrophobicity or side-chain interactions, reducing agglomeration of IgG during spray-drying and thus resulting in smaller particle sizes. A similar phenomenon could be occurring here with L-Glu in our study. Firstly, BSA surface (pI 4.7) is expected to be predominantly negatively-charged at pH 6.5, and hence, the negatively-charged side chain of L-Glu is likely neutralizing the remaining positively-charged surface residues on BSA; increasing the net negative surface charge of BSA.

This would result in reduced agglomeration, due to increased electrostatic repulsion during particle formation, thereby causing the formation of smaller-sized BSA particles. Nonetheless, all samples prepared in our study maintained a satisfactory particle size for pulmonary delivery, (Table 3) and thus may be a feasible approach for the development and delivery of spray-dried biotherapeutics. We did not investigate the deposition performance of our powders since it is not the focus of our study.

4.2. Effect of spray-drying on protein stability

Spray-drying can introduce thermal and shear stress which can have unfavourable effects on the stability of protein powders [4, 19]. However, this is highly dependent on the protein studied and the spray-drying conditions used, particularly the inlet air temperature [20]. In our study, we chose a thermally stable protein and used a low

inlet temperature (60 °C) to ensure that the spray-drying process has a minimal effect on the stability of the powders, thus eliminating the contribution of the spray-drying process to changes observed following accelerated temperature studies. Nonetheless, BAG1 enhanced monomer loss during spray-drying when compared with the control and other formulations tested. Since this was not observed for BG1 nor BA1, the effect may be concentration-dependant, with lower concentrations facilitating protein aggregation during spray-drying. Despite this, monomer loss following spray-drying was still < 3% (Fig. 1 and 2; Table 3) and we consider such a loss to be not clinically or therapeutically significant.

4.3. Accelerated studies at high temperatures

We found that the addition of L-Arg at concentrations of 50 and 200 mM, significantly suppressed monomer loss of BSA, with a more prominent effect when higher [L-Arg] was used (Fig. 3-7; Table 4). Furthermore, using 200 mM of L-Arg may have suppressed the formation of insoluble aggregates or aggregates too large to be eluted with SE-HPLC, as there were higher amounts of smaller soluble aggregates eluting following heat-treatment and a higher total AUC (Fig. 3-6). Ajmera and Scherließ [21] investigated the effects of various amino acids including L-Arg on the enzymatic activity of catalase. In a 1:1 and 2:1 mass ratio with catalase, L-Arg significantly suppressed loss of activity of spray-dried catalase following storage at elevated temperate/humidity. However, Faghihi, et al. [18] found that the effects of L-Arg on IgG stability were not as significant. While the spray-dried powder containing 20 or 50% w/w L-Arg had a significantly lower soluble aggregate % than pure IgG, the aggregation rate constant was higher following storage for 2 months at 45 °C [18]. Shah, et al. [16] and Vagenende, et al. [22] illustrated that the relationship between the [L-Arg] added and changes in protein stability is non-linear; therefore it is likely that the concentrations of L-Arg used in our study lie on the high-end of the concentration-effect curve, where increasing [L-Arg] enhances its protein-stabilizing effect; while the [L-Arg] added to stabilize IgG [18] lies at the lower-end of the concentration-effect curve, where increasing [L-Arg] facilitates protein destabilization. Furthermore, Shiraki, et al. [15] found that lysozyme formulated with L-Arg had significantly higher soluble protein content following heat-induced degradation. These findings correlate well with our findings – higher protein content recovered in our SE-HPLC experiments

for samples containing L-Arg - thus suggesting that L-Arg suppresses the formation of insoluble or large aggregates.

On the other hand, we found that the addition of L-Glu alone increased monomer BSA loss significantly, even at the low concentration tested (Fig. 3-7; Table 4). Golovanov, et al. [23] reported no significant changes in protein solubility with the addition of L-Glu in concentrations of up to 50 mM for various proteins tested. Shiraki, et al. [15] tested the effects of L-Glu on the stability of several proteins including lysozyme and found that adding 50 mM of L-Glu resulted in a higher concentration of soluble protein following heat-treatment than the controls with no amino acids, with the exception of myoglobin, which had a lower protein concentration than the control. On the other hand, L-Glu was found to decrease soluble protein concentration of reduced carboxymethyl lysozyme that was denatured with urea and diluted 10-fold to induce aggregation [15]. The same findings were reported with L-Aspartic acid (L-Asp), which is also a negatively charged amino acid [15]. Based on the overall findings, it was concluded that the effect of negatively charged residues such as L-Glu and L-Asp on protein stability, depends on the nature of the equilibrium between the native and unfolded state and is determined by specific side-chain interactions with the protein [15]. This may explain why L-Glu promotes the aggregation of some proteins such as BSA or myoglobin, while suppressing aggregation of other proteins. It also explains why the effect observed varies according to the stress conditions applied [15].

In addition, contrary to the findings of previous studies, [13, 14, 23] the combination of Arg-Glu did not display synergistic-protein stabilizing effects for spray-dried BSA (Fig. 3-7; Table 4). Based on our findings, there are two possible scenarios; either the two amino acids interacted with each other and had no significant interactions with BSA, or each amino acid interacted with BSA separately (L-Arg suppressing aggregation; L-Glu promoting aggregation), and the net effect was neutral. There are a number of potential reasons for this; firstly, the synergy of Arg-Glu may be concentration-dependent and may not be effective for stabilizing spray-dried BSA in the low concentration we used - thus, for inhaled formulations where excipient concentration must be minimized, the use of these amino acids in high concentrations may not be feasible; secondly, the Arg-Glu interaction with proteins may be specific to the protein being tested, and may not be beneficial to BSA. The negative interaction between L-Glu and BSA observed in our study, may have contributed to the lack of effect

observed with the combination of Arg-Glu. Further research into the mechanism of destabilization of proteins by L-Glu is required to provide better understanding of the Arg-Glu synergy reported previously [13, 14, 23].

5. Conclusion

Our study investigated the synergistic effects of arginine and glutamic acid on the physical stability of spray-dried BSA. We found that the use of L-Arg alone, at low concentrations, improved the physical stability of BSA following heat-treatment, and the effect was more significant with higher concentrations of L-Arg. On the other hand, it was found that L-Glu facilitated monomer BSA loss when added alone, after heat-treatment. Finally, the combination of Arg-Glu in low concentrations neither enhanced nor worsened the physical stability of spray-dried BSA.

Our findings illustrate that the effect of L-Glu on protein stability varies according to the protein used, and the nature of the equilibrium conditions that govern the refolding or unfolding of a protein. Furthermore, how L-Glu interacts with the tested protein may determine whether the combination of Arg-Glu enhances the physical stability of a protein or not. Since the addition of these amino acids maintained acceptable particle size after spray-drying, they represent potential formulation approaches for the pulmonary delivery of proteins that are beneficially affected by the use of these amino acids. However, further investigation is required to provide insight into the mechanism of destabilization of BSA by L-Glu, and how this may affect the synergistic effects of Arg-Glu on protein stability.

Acknowledgement

The authors would like to acknowledge Dr. Nial Wheate for critical reading of the manuscript and the School of Pharmacy for financial support.

Declaration of interest

The authors declare no financial or commercial declarations of interest

References

[1] S.H. Lee, D. Heng, W.K. Ng, H.K. Chan, R.B. Tan, Nano spray drying: a novel method for preparing protein nanoparticles for protein therapy, International Journal of Pharmaceutics, 403 (2011) 192-200.

[2] S.A. Shoyele, A. Slowey, Prospects of formulating proteins/peptides as aerosols for pulmonary drug delivery, International Journal of Pharmaceutics, 314 (2006) 1-8.

[3] A. Hussain, J.J. Arnold, M.A. Khan, F. Ahsan, Absorption enhancers in pulmonary protein delivery, Journal of Controlled Release, 94 (2004) 15-24.

[4] F. Depreter, G. Pilcer, K. Amighi, Inhaled proteins: challenges and perspectives, International Journal of Pharmaceutics, 447 (2013) 251-280.

[5] K. Wadher, R. Kalsait, M. Umekar, Pulmonary Insulin Delivery: Challenges and Current Status, Journal of Pharmaceutical Sciences & Research, 3 (2011).

[6] A. Verma, N. Kumar, R. Malviya, P.K. Sharma, Emerging Trends in Noninvasive Insulin Delivery, Journal of Pharmaceutics, 2014 (2014) 9.

[7] S.W. Chung, T.A. Hil-lal, Y. Byun, Strategies for non-invasive delivery of biologics, Journal of Drug Targeting, 20 (2012) 481-501.

[8] S. Mitragotri, P.A. Burke, R. Langer, Overcoming the challenges in administering biopharmaceuticals: formulation and delivery strategies, Nature Reviews Drug Discovery 13 (2014) 655-672.

[9] M. Fukuda, D. Kameoka, T. Torizawa, S. Saitoh, M. Yasutake, Y. Imaeda, A. Koga, A. Mizutani, Thermodynamic and Fluorescence Analyses to Determine Mechanisms of IgG1 Stabilization and Destabilization by Arginine, Pharmaceutical Research, 31 (2014) 992-1001.

[10] K. Rajagopal, J. Wood, B. Tran, T.W. Patapoff, T. Nivaggioli, Trehalose limits BSA aggregation in spray-dried formulations at high temperatures: Implications in preparing polymer implants for long-term protein delivery, Journal of Pharmaceutical Sciences, 102 (2013) 2655-2666.

[11] D.A. Parkins, U.T. Lashmar, The formulation of biopharmaceutical products, Pharmaceutical Science & Technology Today, 3 (2000) 129-137.

[12] H.J. Lee, A. McAuley, K.F. Schilke, J. McGuire, Molecular origins of surfactant-mediated stabilization of protein drugs, Advanced Drug Delivery Reviews, 63 (2011) 1160-1171.

[13] P. Kheddo, M. Tracka, J. Armer, R.J. Dearman, S. Uddin, C.F. van der Walle, A.P. Golovanov, The effect of arginine glutamate on the stability of monoclonal antibodies in solution, International Journal of Pharmaceutics, 473 (2014) 126-133.
[14] D. Shukla, B.L. Trout, Understanding the Synergistic Effect of Arginine and Glutamic Acid Mixtures on Protein Solubility, The Journal of Physical Chemistry B, 115 (2011) 11831-11839.
[15] K. Shiraki, M. Kudou, S. Fujiwara, T. Imanaka, M. Takagi, Biophysical Effect of Amino Acids on the Prevention of Protein Aggregation, Journal of Biochemistry, 132 (2002) 591-595.
[16] D. Shah, A.R. Shaikh, X. Peng, R. Rajagopalan, Effects of arginine on heat-induced aggregation of concentrated protein solutions, Biotechnology Progress, 27 (2011) 513-520.
[17] V. Kayser, N. Chennamsetty, V. Voynov, B. Helk, K. Forrer, B.L. Trout, Evaluation of a Non-Arrhenius Model for Therapeutic Monoclonal Antibody Aggregation, Journal of Pharmaceutical Sciences, 100 (2011) 2526-2542.
[18] H. Faghihi, A. Vatanara, A.R. Najafabadi, V. Ramezani, K. Gilani, The use of amino acids to prepare physically and conformationally stable spray-dried IgG with enhanced aerosol performance, International Journal of Pharmaceutics, 466 (2014) 163-171.
[19] M. Adler, M. Unger, G. Lee, Surface Composition of Spray-Dried Particles of Bovine Serum Albumin/Trehalose/Surfactant, Pharmaceutical Research, 17 (2000) 863-870.
[20] M. Mumenthaler, C. Hsu, R. Pearlman, Feasibility Study on Spray-Drying Protein Pharmaceuticals: Recombinant Human Growth Hormone and Tissue-Type Plasminogen Activator, Pharmaceutical Research, 11 (1994) 12-20.
[21] A. Ajmera, R. Scherließ, Stabilisation of proteins via mixtures of amino acids during spray drying, International Journal of Pharmaceutics, 463 (2014) 98-107.
[22] V. Vagenende, A.X. Han, M. Mueller, B.L. Trout, Protein-Associated Cation Clusters in Aqueous Arginine Solutions and Their Effects on Protein Stability and Size, ACS Chemical Biology, 8 (2012) 416-422.
[23] A.P. Golovanov, G.M. Hautbergue, S.A. Wilson, L.-Y. Lian, A Simple Method for Improving Protein Solubility and Long-Term Stability, Journal of the American Chemical Society, 126 (2004) 8933-8939.

CHAPTER 3

“The Effect of Deuterium Oxide on the Conformational Stability and Aggregation of Bovine Serum Albumin”

Chapter 3 was published in the Pharmaceutical Development and Technology journal:

Reslan, M., Kayser, V. (2016). The effect of deuterium oxide on the conformational stability and aggregation of bovine serum albumin. Pharmaceutical Development and Technology, 1-7.

Abstract

Protein aggregation is a significant problem affecting the integrity of proteins and is a major hindrance to the development of biopharmaceutical products. Deuterium oxide (D_2O), widely used in protein characterization studies, has been shown to promote protein aggregation when used as a substitute for water in most buffered protein solutions; however, a few studies have reported minor improvements in melting point temperatures for some proteins. Our study aims to investigate the effect of D_2O on protein stability, using bovine serum albumin (BSA) as a model. We performed accelerated stability studies at high temperatures and assessed the physical and conformational stability of BSA using fluorescence spectroscopy, dynamic light scattering (DLS) and size-exclusion high performance liquid chromatography. Our findings reveal that D_2O enhances the conformational stability of monomeric BSA, reducing monomer loss and formation of small aggregates at high temperatures. There is also an increase in the formation of larger aggregates probed by thioflavin T, however the increase is not considered significant based on DLS results. Our findings demonstrate that exchanging water with D_2O can improve the stability of proteins in solution, by maintaining the stability of the monomeric form, which may be beneficial for the long-term storage of some biological products.

1. Introduction

Protein aggregation is a common and highly problematic degradative process affecting the long-term stability and integrity of a biological product and has been implicated in debilitating neurodegenerative diseases such as Alzheimer's, Parkinson's and Huntington's [1-4]. Our understanding of the aggregation process of biological products has developed tremendously in recent years, and is typically addressed by formulating purified proteins in aqueous buffers with various additives such as amino acids and surfactants which partially improve their long-term storage stability [3, 5-8]. However, as this approach alone is often inadequate, many biological products require additional steps such as lyophilization to form a dry powder, affording 1-2 years of shelf-life [5].

Over a decade ago, it was found that exchanging the solvent from water (H_2O) to deuterium oxide (D_2O) in various biological systems, affected the physical stability of different proteins studied [9-19]. The general consensus was that D_2O promoted

protein aggregation. Lee and Berns [10], reported that C-Phycocyanin formed a higher amount of hexamer aggregates in D_2O buffer when compared with H_2O buffer. It was suggested that D_2O enhances hydrophobic forces thought to contribute to the formation of the hexamer. Henderson, et al. [11], found that D_2O stabilized lactate dehydrogenase (LDH) at low ionic strength and inhibited monomer dissociation into subunits; however, for bovine liver glutamate dehydrogenase (GDH), D_2O promoted monomer association into larger polymers especially at larger concentrations. Since the studies were performed at a low temperature (8 °C), where the contribution of hydrophobic interactions is minimal, the findings were attributed to the greater strength of deuterium bonding to hydrogen bonding and the resultant strengthening of water bridges, which contributed to either decreased dissociation (LDH) or increased association (GDH), depending on the protein [11].

A series of other studies were performed with β-lactoglobulin [12], salmonella flagellin [13] and formyltetrahydrofolate synthetase [14] all of which found an increased extent of association in D_2O compared with H_2O, either due to increased hydrophobic interactions or formation of deuterium bonds, or both. A few studies reported that D_2O improved the melting point temperature of some proteins [13, 17], however the changes were not considered significant.

The effect of D_2O on protein stability is either facilitated by hydrogen-deuterium exchange of solvent-accessible NH or OH protons and, or a difference in the solvent-isotope effect/hydration shell due to the slightly heavier deuterium atom. In a study by Cioni and Strambini [19] they claimed that the effects observed were predominantly due to the latter of the two, at least for the majority of the proteins used in their study.

Nonetheless, the majority of previous work suggests that D_2O promotes protein aggregation by promoting hydrophobic interactions. Whether D_2O has the potential to stabilize proteins is unclear. D_2O is widely used in NMR, mass spectrometry and neutron scattering experiments for protein characterization and may be useful as a storage solution if found to improve the physical or conformational stability of proteins. Hereby, we investigated the effect of D_2O on protein aggregation propensity and conformational stability using BSA as a model protein. BSA is widely used in protein aggregation studies as it is well-characterized and readily available. Our results suggest that a simple exchange of solvents from H_2O to D_2O may increase its long-

term stability, without considerably increasing aggregation, by reducing the formation of small aggregates that are precursors of larger aggregates.

2. Materials and Methods

Bovine serum albumin (BSA; Fraction V, A7906), deuterium oxide (D_2O; 99.9 atom % D, 151882), 8-Anilino-1-naphthalenesulfonic acid (ANS; >97% HPLC grade, A1028), N-Acetyl-L-tryptophanamide (NATA; A6501), and Thioflavin T (ThT; T3516) were purchased from Sigma Aldrich (Castle Hill, Australia). Millex-GV syringe filter units (0.22 µm, PVDF, 33 mm, gamma sterilized, SLGV033RS), di-potassium hydrogen phosphate (EMPROVE® Ph Eur, BP, E 340 grade, 105101) and potassium dihydrogen phosphate (EMSURE® ISO grade, 104873) were purchased from Merck Millipore (MA, USA). Dimethyl sulfoxide (UNIVAR analytical grade, 2225) was purchased from Ajax Finechem (Taren Point, Australia).

2.1. Preparation of samples

5 mg/mL BSA solutions were prepared by dissolving BSA in double distilled H_2O (referred to as H_2O from here onwards) or D_2O. Samples were filter-sterilized using a 0.22 µm syringe filter and stored at 4 °C. The pH of BSA samples in H_2O was 6.7, while the pD of samples in D_2O was 7.1 (based on the equation: pD = pH measured + 0.4 [20]).

ANS and ThT dyes were prepared as 20 mM stock solutions in dimethyl sulfoxide (DMSO) and H_2O, respectively, and stored frozen at -20 °C. For dye binding studies, the stocks were diluted with either H_2O or D_2O to a working concentration of 300 µM. Working stock solutions were freshly prepared for each set of experiments.

2.2. Accelerated stability studies at elevated temperatures

Accelerated studies at elevated temperatures were conducted as previously described [8].100 µL aliquots of BSA solutions at a concentration of 5 mg/mL were incubated in a Thermal Cycler 2720 (Applied Biosystems, CA, USA) at 55, 60, 65 and 70 °C for various durations. Samples were immediately diluted and stored on ice following incubation, to 1 mg/mL for size exclusion-high performance liquid chromatography (SE-HPLC), 0.5 mg/mL for dynamic light scattering (DLS) and to 0.2 mg/mL for UV-vis absorbance and fluorescence studies, with either H_2O or D_2O.

2.3. Fluorescence Spectroscopy

Fluorescence measurements were performed using the Spectrophotometer Fluorolog 3 FL3-22 (HORIBA Jobin Yvon, Kyoto, Japan). BSA samples were diluted to 0.2 mg/mL in H_2O or D_2O and analyzed in an ultra-micro fluorescence quartz cuvette from Hellma at right-angled detection mode. NATA samples were diluted to 7.5 µg/mL for analysis. Data was analyzed using Igor Pro 6 software.

2.4. Tryptophan and NATA fluorescence

Tryptophan fluorescence of BSA was used to characterize BSA conformational stability by comparing differences in maximum fluorescence intensity and the maximum emission wavelength, which provide information on the environment surrounding the tryptophan residues. A decrease in tryptophan fluorescence and an increase in maximum emission wavelength usually suggest that there is increased solvent exposure near the tryptophan residue(s), which may be due to unfolding. On the other hand, a decrease in the maximum emission wavelength is due to the formation of a more hydrophobic local environment near the tryptophan residue(s) which may occur due to protein aggregation [21].

Fluorescence of NATA, an analogue of tryptophan, was measured to determine if D_2O had any solvent effects on tryptophan fluorescence, independent of its effect on the conformational stability of BSA.

Tryptophan fluorescence of BSA and NATA was detected in the emission wavelength range of 300-500 nm with an excitation wavelength of 295 nm. Both excitation and emission slit sizes were set at 3 nm. Samples were corrected by blank subtraction of H_2O or D_2O. All measurements were performed in triplicates and averaged, and the standard deviation (SD) was calculated.

2.5. ANS and ThT fluorescence

ANS fluorescence was used to determine the degree of solvent accessibility and unfolding following incubation at high temperatures. A significant increase in maximum ANS fluorescence is usually indicative of protein unfolding [22]. ANS fluorescence was detected in the emission wavelength range of 400-600 nm with an excitation wavelength of 385 nm. Both excitation and emission slit sizes were set at 2 nm.

ThT fluorescence was used to measure the degree of BSA aggregation following incubation at high temperatures. A significant increase in maximum ThT fluorescence

is usually associated with the formation of protein aggregates [22]. ThT emission was detected in the emission wavelength range of 425-600 nm with an excitation wavelength of 415 nm. Both excitation and emission slit sizes were set at 3 nm.

For both dyes, 5 µL of dye from a working stock of 300 µM was added to 495 µL of each sample to a final concentration of 3 µM. All samples were then incubated at room temperature for 20 minutes before analysis to allow for dye binding. Samples were corrected by blank subtraction of H_2O or D_2O (for dye-only samples) or a BSA sample dissolved in the respective solvent with no dye (for samples containing dye and BSA). All dye fluorescence measurements were performed in triplicates and averaged, and the SD was calculated.

2.6. SE-HPLC

Size exclusion-high performance liquid chromatography (SE-HPLC) was used to measure monomer loss of BSA following accelerated temperature studies. Analysis was performed using an Agilent 1200 Liquid Chromatography system (Agilent Technologies, California, USA) with a TSKgel Super SW3000 column (Tosoh Bioscience, Tokyo, Japan) at 22 °C, using a 150 mM potassium phosphate mobile phase, at pH 6.5, and a flow rate of 0.2 mL/min. 5 µL of each BSA sample at a concentration of 1 mg/mL was injected. Monomer peaks were detected using an in-line UV signal detector set at 280 nm. The area under the curve (AUC) of the monomer peak was averaged over three runs and the mean monomer % was calculated for each sample. The SD was plotted as error bars in the figures.

2.7. DLS

Monomer and aggregate size distributions of BSA samples were analysed by dynamic light scattering (DLS) using the Malvern Zetasizer Nano ZS (Malvern Instruments, Worcestershire, UK). The intensities of different-sized peaks were analysed qualitatively and compared across formulations for relative changes in monomer and aggregate intensities. Intermediates were defined as small-sized ‘aggregates’ that were distinct from the monomer or large aggregate population. The size range measured in each figure (x-axis) was modified to 1 nm – 1 µm as no particles were detected outside that range. The refractive index of BSA in H_2O or D_2O was set at 1.33 and the absorption value was 0.1. The viscosity of H_2O was set at 0.8879 mPa/s and

of D_2O at 1.095 mPa/s. Samples were diluted to 0.5 mg/mL in their respective solvents and measured three times each, in disposable plastic cuvettes at 25 °C.

2.8. UV-Vis Spectroscopy

UV-Vis absorbance was used to determine the concentration of soluble protein following accelerated temperature studies. Absorbance was measured at 280 nm over a wavelength range of 220-350 nm using a Shimadzu UV-2600 spectrophotometer (Shimadzu, Japan). Samples were corrected by blank subtraction of the respective solvent (H_2O or D_2O). Data was not included as the absorbance of all samples remained unchanged following incubation, and therefore no change in soluble protein concentration was observed.

3. Results

3.1. NATA and Tryptophan emission

Maximum NATA fluorescence at room temperature is almost 20% higher in D_2O compared with H_2O (Fig. 1A inset). Following incubation at 55 °C, NATA fluorescence decreases slightly in both H_2O and D_2O but remains ~20% higher in D_2O (Fig. 1A). At 60 °C, the fluorescence in both solvents is relatively unchanged. Following incubation at 65 and 70 °C, there is a slight increase in fluorescence in both solvents, however the ratio of NATA fluorescence in D_2O to H_2O decreases slightly to a difference of ~10% (Fig. 1A).

The maximum tryptophan fluorescence of BSA in H_2O and D_2O is the same at room temperature (Fig. 1B). Upon incubation at 55 °C for 2 hours, both samples have a decreased maximum fluorescence, with a larger decrease observed in the H_2O sample (Fig. 1B). This trend continues for 60, 65 and 70 °C – as the temperature become harsher, the maximum fluorescence continues to decrease - but the fluorescence of BSA dissolved in D_2O is consistently higher (Fig. 1B). From the ratio of tryptophan fluorescence of BSA in D_2O to BSA in H_2O, it can be determined that the difference ranges from approximately 10-16%, with the highest difference observed at 65 °C and the lowest at 70 °C (Fig. 1B inset). This difference is similar to that observed with NATA, except at room temperature, since D_2O does not appear to affect tryptophan fluorescence of BSA (Fig. 1A and B).

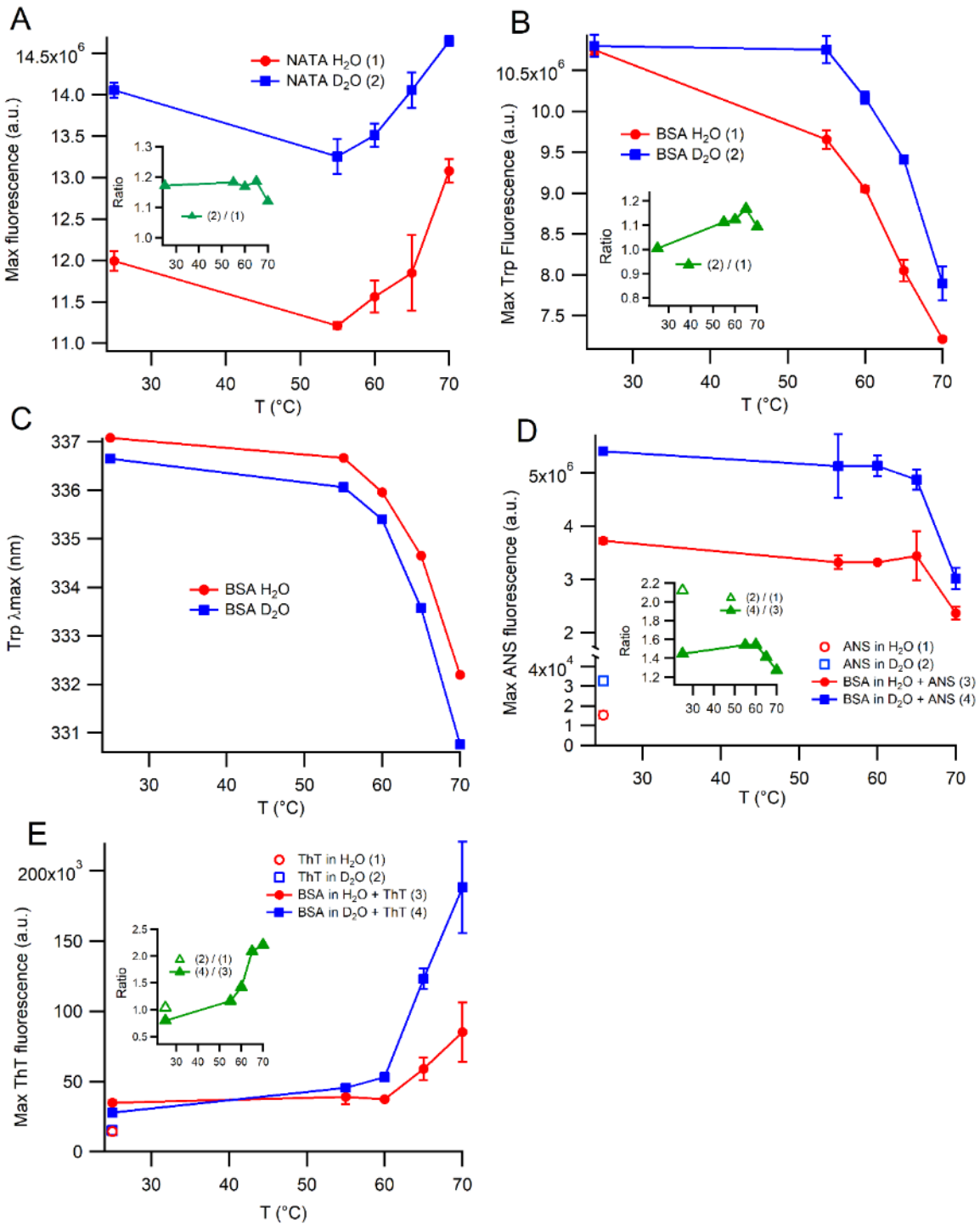

Figure 1. Maximum fluorescence emission spectra of NATA and BSA samples in H_2O or D_2O at 25 °C and following incubation at 55 °C (2 hours), 60 °C (1 hour), 65 °C (1 hour) and 70 °C (30 minutes). (A) Intrinsic fluorescence of NATA samples; (B) Tryptophan fluorescence of BSA samples; (C) Tryptophan maximum emission wavelength of BSA samples (D) Fluorescence of 3 μM ANS added following incubation; (E) Fluorescence of 3 μM Thioflavin T added following incubation. Insets: the fluorescence ratios of the respective samples in each figure, calculated by dividing the fluorescence of D_2O samples with H_2O samples. Error bars represent the SD.

~337 to ~332 nm following incubation at 55, 60, 65 and 70 °C (Fig. 1C). A similar shift is observed for BSA in D_2O, from ~336 nm at room temperature to ~331 nm following incubation at 70 °C. The difference between the max emission wavelengths of BSA in H_2O to BSA in D_2O at the different conditions suggests that the shift is slightly greater with increasing temperature for samples dissolved in D_2O, although this difference is not significant (Fig. 1C).

3.2. ANS Emission

The maximum fluorescence of ANS dye dissolved in H_2O or D_2O is minimal at room temperature in the absence of BSA (Fig. 1D). Interestingly, the fluorescence of ANS dye dissolved in D_2O is approximately 2-fold higher than that dissolved in H_2O (Fig. 1D inset). When BSA is added, ANS fluorescence increases significantly and is highest at room temperature in both solvents (Fig. 1D). The maximum fluorescence of ANS bound to BSA in D_2O remains higher by approximately 1.5-fold at room temperature (Fig. 1D inset). The maximum ANS fluorescence remains relatively unchanged following incubation at 55 °C, 60 °C and 65 °C in both H_2O and D_2O (Fig. 1D). Likewise, the ratio of maximum ANS intensity also remains relatively unchanged, only increasing slightly to approximately 1.6-fold at 55 °C and 60 °C then decreasing back to 1.4-fold at 65 °C (Fig. 1D inset). Following incubation at 70 °C, the maximum fluorescence of ANS bound to BSA dissolved in H_2O or D_2O significantly decreases and is lowest at this temperature (Fig. 1D). The ratio of ANS fluorescence is also lowest at 70 °C, decreasing to ~1.3-fold higher for samples dissolved in D_2O (Fig. 1D inset).

3.3. ThT Emission

The maximum fluorescence of ThT in H_2O or D_2O is minimal at room temperature, and almost identical when dissolved in either solvent (Fig. 1E). At 25 °C, BSA dissolved in H_2O or D_2O with ThT has low ThT fluorescence, and the fluorescence of ThT in D_2O is ~0.8-fold that of BSA dissolved in H_2O (Fig. 1E). After incubation at 55 °C, there is a small increase in the maximum fluorescence of ThT for BSA samples in both solvents, with a 1.2-fold higher fluorescence for BSA dissolved in D_2O (Fig. 1E). Following incubation at 60 °C, the maximum ThT fluorescence continues to increase for BSA in D_2O, but remains relatively unchanged for BSA in H_2O (Fig. 1E). The ThT fluorescence is approximately 1.4-fold higher at 60 °C for BSA in D_2O (Fig. 1E inset).

A significant increase in ThT fluorescence is observed for BSA in D_2O following incubation at 65 °C and again at 70 °C (Fig. 1E). The same trend is observed for BSA in H_2O, however the increase in ThT fluorescence following incubation at 65 and 70 °C is not as prominent as the increase observed for BSA in D_2O (Fig. 1E). At 65 °C, the maximum fluorescence of ThT bound to BSA in D_2O is 2.1-fold higher and at 70 °C it is 2.2-fold higher than the fluorescence of ThT bound to BSA in H_2O (Fig. 1E).

3.4. SE-HPLC

Following incubation at 55 °C, monomer loss is minimal in both BSA samples (Fig. 2 and 3). Although BSA in H_2O has a slightly higher mean monomer % at 55 °C, the SD is large and the difference is not significant (Fig. 3). There are minor losses after incubation at 60 °C, but again the difference between the monomer % of BSA in H_2O and BSA in D_2O remains insignificant (Fig. 2 and 3). A large decrease in monomer % is observed following incubation at 65 °C - the relative monomer % of BSA in H_2O decreases to ~75% while for BSA in D_2O the monomer % remains significantly higher at ~85% (Fig. 2 and 3). Likewise, following incubation at 70 °C, there is a large decrease in monomer % for both samples, dropping to ~35% for BSA in H_2O and ~40% for BSA in D_2O. Again, BSA in D_2O retains a higher monomer % (~5% higher) following heat-treatment at 70 °C (Fig. 2 and 3). We did not compare the changes in aggregate peaks, as the larger aggregates formed following incubation did not elute, possibly due to their size. Thus, we relied on ThT fluorescence and DLS results to compare aggregate populations.

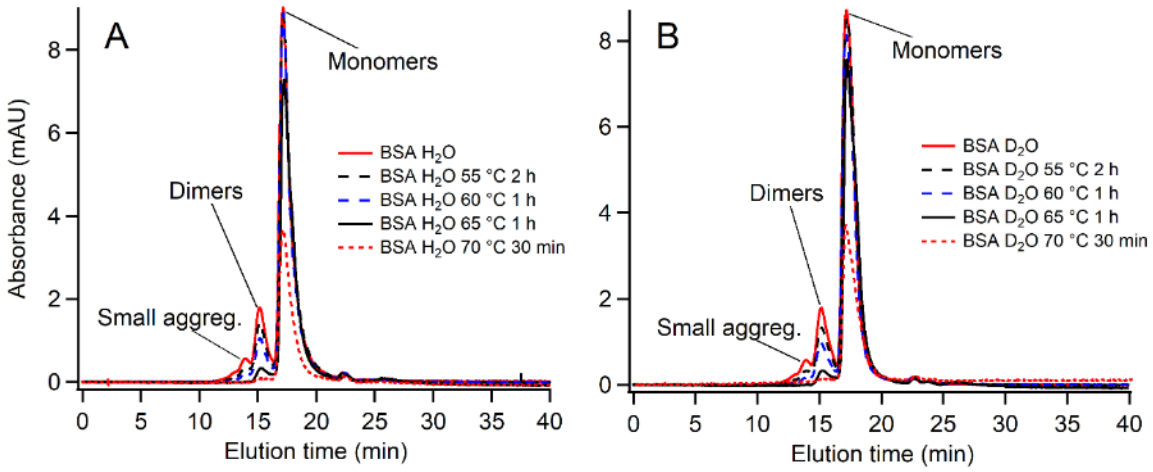

Figure 2. Representative SE-HPLC chromatograms of BSA samples in (A) H_2O or (B) D_2O, measured at 25 °C (control) and following incubation at 55 °C (2 hours), 60 °C (1 hour), 65 °C (1 hour) and 70 °C (30 minutes).

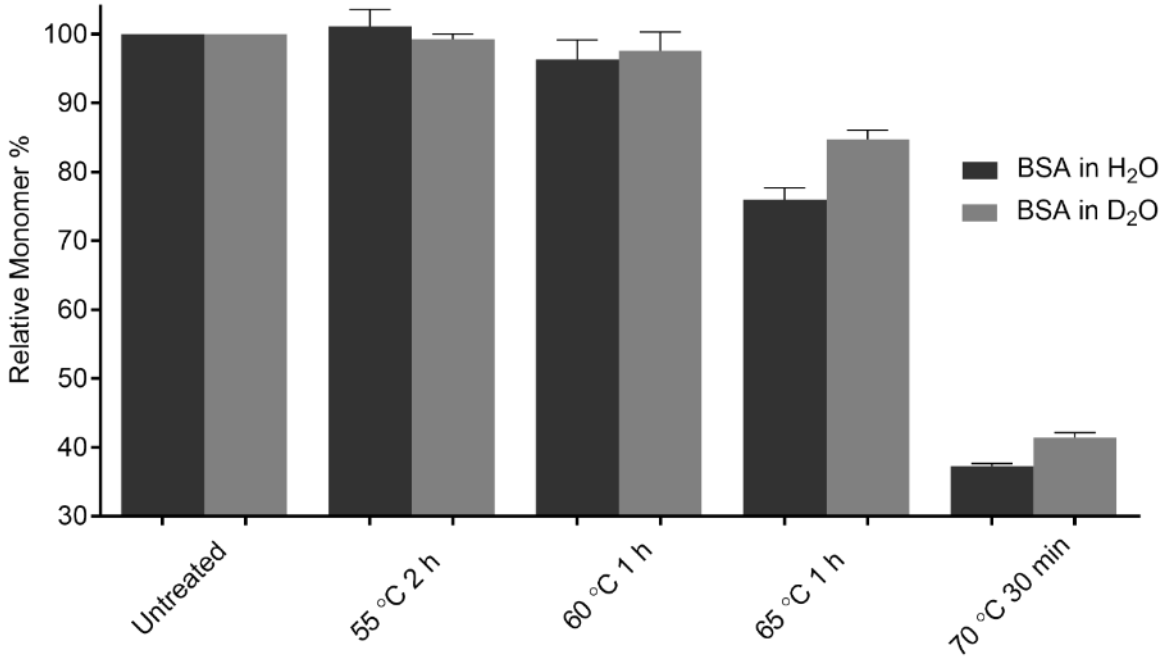

Figure 3. Relative mean monomer % of BSA samples in H_2O or D_2O measured at 25 °C ("Untreated") and following incubation at 55 °C (2 hours), 60 °C (1 hour), 65 °C (1 hour) and 70 °C (30 minutes). Incubated samples were adjusted to the control "Untreated", where "Untreated" represents 100% monomer, or no monomer loss. Error bars represent the SD.

3.5. DLS

At room temperature, there is no significant difference between the size distribution of BSA species in H_2O compared with D_2O (Fig. 4A). Monomer species at ~ 5 nm have the highest relative intensity for both solvents and smaller intensities are detected between 10-50 nm and 200-1000 nm (Fig. 4A). Following incubation at 55 °C, the relative intensity of the monomer species for both H_2O and D_2O remains unchanged, however an increased intensity at ~ 100 nm is detected for BSA in H_2O, suggesting the formation of larger intermediates (Fig. 4B). At 60 °C the size of these intermediates increases in H_2O with the peak broadening to ~ 700 nm (Fig. 4C). The monomer intensity also decreases correspondingly. Meanwhile, the large aggregate intensity of D_2O increases slightly, although the difference is not significant (Fig. 4C). At 65 °C there is a sharp decrease in monomer intensity for BSA in H_2O and D_2O, with corresponding increases in intermediates and large aggregates (Fig. 4D). All species are roughly the same size between samples, however there is a narrower distribution of intermediates and large aggregates in D_2O. Finally, at 70 °C, there is a further decrease in monomer intensity and an increase in intermediates (Fig. 4E). Large

aggregate intensity also decreases, possibly due to rapid sedimentation of large aggregates formed at this temperature or reduced incubation time. Again, the size distribution of intermediates is narrower in D_2O, suggesting that there is a less diverse population of intermediates in D_2O at 70 °C (Fig. 4E).

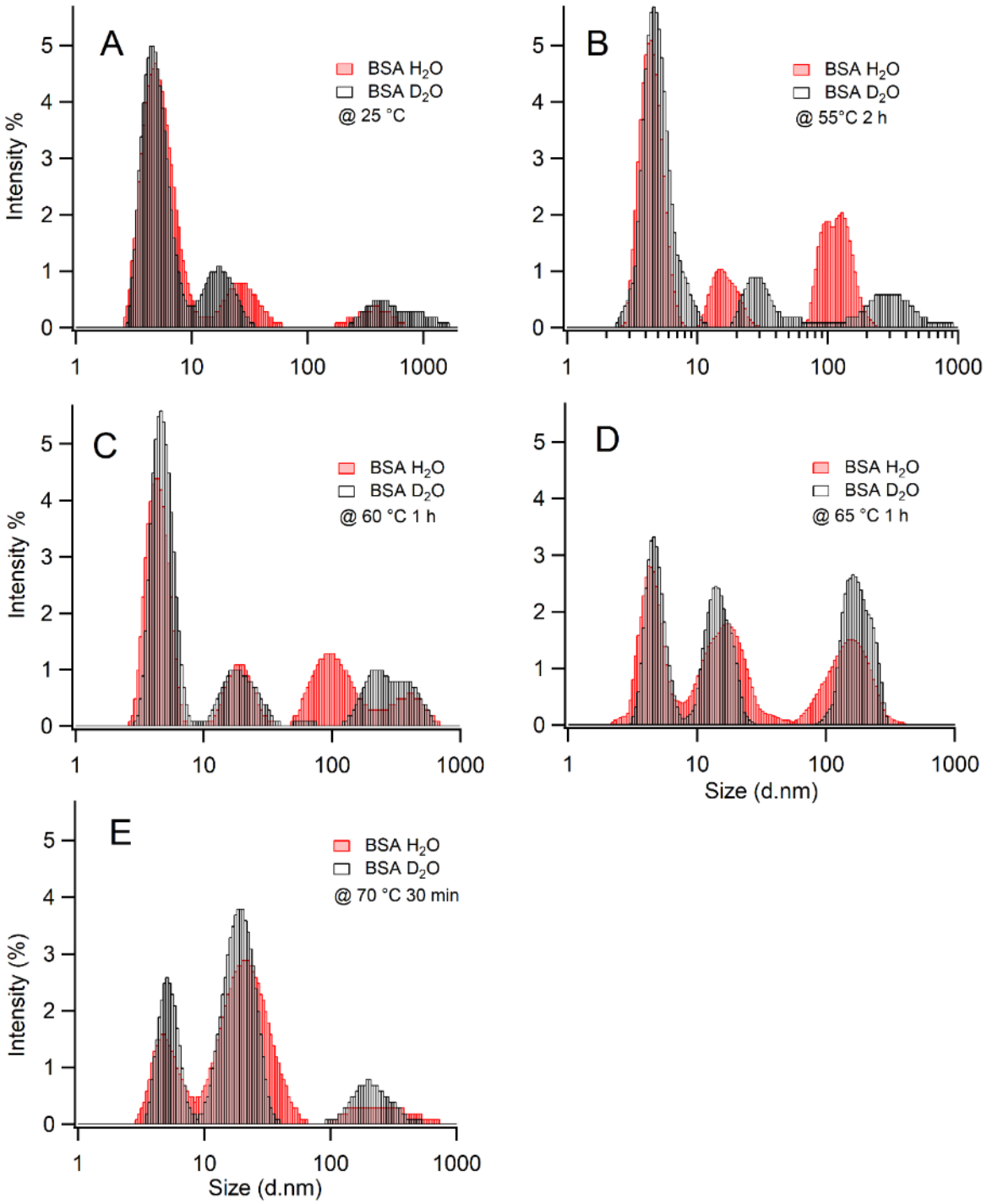

Figure 4. Mean intensity-based size distribution of BSA in H_2O or D_2O at (A) 25 °C and following incubation at (B) 55 °C (2 hours), (C) 60 °C (1 hour), (D) 65 °C (1 hour) and (E) 70 °C (30 minutes) using DLS. “Size” represents the measured hydrodynamic diameter in nm.

4. Discussion

4.1. Stability of BSA monomers in D_2O

Our findings suggest that BSA dissolved in D_2O compared with H_2O, has higher stability against heat-induced degradation, particularly at denaturing conditions at, or above, the melting temperature of BSA (≥65 °C) [23], since the monomer % was significantly higher in D_2O at these conditions (Fig. 2 and 3). There is also a slight blue-shift in the tryptophan max emission wavelength of all BSA samples in D_2O at all conditions, most prominently at 70 °C, which suggests that the local environment surrounding the tryptophan residues is more compact and less exposed in D_2O than in H_2O (Fig. 1C). This is further supported by the higher tryptophan intensity in D_2O following heat-treatment (Fig. 1B), although as demonstrated with NATA fluorescence (Fig. 1A), this may – at least partly - be due to enhanced emission of photons in D_2O [24], rather than structural protein changes. Although the enhanced fluorescence of tryptophan in D_2O is not apparent for BSA in D_2O at room temperature, this is most likely due to the inaccessibility of the tryptophan residues at this temperature, as the enhanced tryptophan fluorescence becomes apparent at higher temperatures (Fig. 1B), which expose the buried residues to D_2O.

Nonetheless, our findings are in accord with observations by Cioni and Strambini [19] who found that a number of proteins had a more rigid folded structure in D_2O over H_2O. They proposed that this is predominantly due to solvent effects, especially enhancement of hydrophobic interactions, with the exception of proteins such as LDH [19]. Therefore, the stabilizing effect of D_2O is amplified at higher temperatures and conditions which destabilize the folded state [19], as shown in our results. D_2O was first thought to enhance protein hydrophobic interactions based on previous observations with surfactant behaviour, where a lower critical micelle concentration was achieved in D_2O compared with H_2O [9]. This was explained by the increased cohesiveness of D_2O molecules, since solvent-solvent deuterium bonds were found to be stronger in D_2O than solvent-solvent hydrogen bonds in H_2O [9]. The enhancement of hydrophobic interactions explains the observed improvements in native monomer stability.

If we model BSA aggregation using a two-step model [25]:

$$\mathrm{M} \leftrightharpoons \mathrm{I} \longrightarrow \mathrm{A}$$

Scheme 1: A two-step model of protein aggregation

Where the native monomer state is represented by M, reversible partially-unfolded species and/or small pre-cursor aggregates (referred to as intermediates) are I, and A represents large irreversible aggregates – we can acknowledge that large aggregates are formed via the formation of reversible intermediates, usually due to exposure of previously inaccessible hydrophobic patches which facilitate aggregation. From our findings, we conclude that D_2O reduces the change from M to I, by strengthening the native structure and increasing its conformational stability. It is therefore, more thermodynamically favourable for the folded monomer structure to compact and minimise solvent exposure, resulting in stabilization of the monomer state.

4.2. Formation of intermediates and large aggregates in D_2O

Our results reveal that D_2O significantly increases the fluorescence of ANS dye by 2-fold without BSA, and approximately 1.5-fold when bound to BSA (Fig. 1D). Thus, we cannot conclude that the higher fluorescence observed in the D_2O samples is due to increased solvent-exposure, but rather due to the increased dye fluorescence in D_2O compared with H_2O, as was the case with tryptophan fluorescence (Fig. 1B).

Interestingly though, ANS fluorescence in both BSA in D_2O and H_2O does not increase at 65 °C and is lowest at 70 °C, despite the expected high degree of denaturation at these temperatures (Fig. 1D). This may be due to the formation of aggregates that occupy newly exposed hydrophobic patches, reducing available ANS binding sites on BSA and resulting in a decrease in the fluorescence at these high temperatures. The larger decrease in fluorescence at 70 °C for BSA in D_2O compared with the smaller decrease for BSA in H_2O, suggests that D_2O facilitates the formation of aggregates at high temperatures (Fig. 1D).

This is confirmed by the higher ThT fluorescence of BSA samples dissolved in D_2O compared with H_2O (Fig. 1E). Unlike tryptophan and ANS fluorescence, ThT fluorescence does not seem to be affected by D_2O itself, as the ThT fluorescence in both D_2O and H_2O is approximately the same even with BSA at room temperature (Fig. 1E).

It has been reported previously that BSA can form beta-sheet rich amyloid-like structures at high temperatures [23, 26] – the increasing ThT fluorescence when BSA

in H_2O is incubated at higher temperatures may be due to the formation of these aggregates which are known to bind ThT. If this is the case, then D_2O may accelerate the formation of these aggregates, resulting in the higher ThT fluorescence observed (Fig. 1E). However, ThT fluorescence is not quantitative and therefore it is not clear how significant this increase in aggregate formation is. Although DLS is not a quantitative technique either, it is well known that larger particles scatter light at much greater intensities, and therefore, if the quantity of large aggregates formed in D_2O was significantly higher, we would expect a much higher aggregate intensity in D_2O compared with in H_2O using DLS. However, the intensity of large aggregates observed in H_2O and D_2O was quite comparable at each temperature (Fig. 4) - this suggests that the quantity of aggregates formed in D_2O is not significantly higher. The difference in aggregate formation is likely due to the same monomer-stabilizing mechanism of D_2O – increased strength of hydrophobic interactions. At melting point temperatures, BSA is forced into significant unfolding, and the resulting exposure of hydrophobic patches in D_2O will therefore facilitate aggregation, as expected based on the two-step model (Scheme 1). In addition, since the hydrogen-deuterium rate is increased and higher solvent accessibility is expected at higher temperatures, the increased number and strength of deuterium bonds, results in stronger intra- and inter-molecular bonding which may have also contributed to the increased formation of these aggregates.

Since the monomer % remains higher in D_2O at the higher temperatures as seen with SE-HPLC (Fig. 2 and 3), and there is a minor increase in aggregates based on fluorescence measurements (Fig. 1D and E), then the total amount of intermediates in D_2O must be lower. Furthermore, from the DLS results at higher temperatures, it is apparent that the variety of intermediates in D_2O is also less (Fig. 4D and E). Based on the two-step model (Scheme 1), it is expected that the number of intermediates is lower in D_2O, as the refolding/dissociation of intermediates back to the monomer state is favoured in D_2O.

5. Conclusion

Our study reveals that D_2O has two main effects on BSA stability: (1) enhancing its conformational stability, resulting in reduced monomer loss and reduced formation of intermediates; (2) increasing the formation of aggregates that bind ThT. Both effects are predominantly due to an enhancement of hydrophobic interactions with possible

contribution from an increase in the strength of intra- or inter-molecular bonds, due to hydrogen-deuterium exchange. Further studies need to be performed to assess the quantity of large aggregates formed with D_2O and determine whether this is significant. Furthermore, long-term incubation may be useful to confirm if the reduction in intermediate formation will translate to even better overall stability. Nonetheless, it has been shown that a simple exchange of solvents increases the stability of a relatively stable protein such as BSA, thus there is great potential for D_2O to improve the stability of biotherapeutics that are more susceptible to degradation during storage in solution and warrants further investigation. Furthermore, it may be important to consider these changes when performing NMR or neutron scattering experiments which utilize D_2O.

Acknowledgments

The authors would like to acknowledge Professor Hak-Kim Chan for access to light scattering equipment and the School of Pharmacy for financial contribution.

Declaration of interest

The authors declare no conflicts of interest.

References

[1] A.R. Mazzer, X. Perraud, J. Halley, J. O'Hara, D.G. Bracewell, Protein A chromatography increases monoclonal antibody aggregation rate during subsequent low pH virus inactivation hold, Journal of Chromatography A, 1415 (2015) 83-90.
[2] M.E.M. Cromwell, E. Hilario, F. Jacobson, Protein aggregation and bioprocessing, The AAPS Journal, 8 (2006) E572-E579.
[3] F. Depreter, G. Pilcer, K. Amighi, Inhaled proteins: Challenges and perspectives, International Journal of Pharmaceutics, 447 (2013) 251-280.
[4] C.A. Ross, M.A. Poirier, Protein aggregation and neurodegenerative disease, Nature Medicine, 10 Suppl (2004) S10-17.
[5] S.J. Shire, Z. Shahrokh, J. Liu, Challenges in the development of high protein concentration formulations, Journal of Pharmaceutical Sciences, 93 (2004) 1390-1402.
[6] M. Reslan, Y.K. Demir, B.L. Trout, H.-K. Chan, V. Kayser, Lack of a synergistic effect of arginine–glutamic acid on the physical stability of spray-dried bovine serum albumin, Pharmaceutical Development and Technology, (2016) 1-7.

[7] Z. Sahin, Y.K. Demir, V. Kayser, Global kinetic analysis of seeded BSA aggregation, European Journal of Pharmaceutical Sciences, 86 (2016) 115-124.
[8] V. Kayser, N. Chennamsetty, V. Voynov, B. Helk, K. Forrer, B.L. Trout, Evaluation of a non-Arrhenius model for therapeutic monoclonal antibody aggregation, Journal of Pharmaceutical Sciences, 100 (2011) 2526-2542.
[9] G.C. Kresheck, H. Schneider, H.A. Scheraga, The Effect of D2O on the Thermal Stability of Proteins. Thermodynamic Parameters for the Transfer of Model Compounds from H2O to D2O1,2, The Journal of Physical Chemistry, 69 (1965) 3132-3144.
[10] J.J. Lee, D.S. Berns, Protein aggregation. The effect of deuterium oxide on large protein aggregates of C-phycocyanin, The Biochemical journal, 110 (1968) 465-470.
[11] R.F. Henderson, T.R. Henderson, B.M. Woodfin, Effects of D2O on the Association-Dissociation Equilibrium in Subunit Proteins, Journal of Biological Chemistry, 245 (1970) 3733-3737.
[12] P.A. Baghurst, L.W. Nichol, W.H. Sawyer, The Effect of D2O on the Association of β-Lactoglobulin A, Journal of Biological Chemistry, 247 (1972) 3199-3204.
[13] Y. Uratani, Polymerization of Salmonella Flagellin in Water and Deuterium Oxide Media, Journal of Biochemistry, 75 (1974) 1143-1151.
[14] J.A.K. Harmony, R.H. Himes, R.L. Schowen, Monovalent cation-induced association of formyltetrahydrofolate synthetase subunits. Solvent isotope effect, Biochemistry, 14 (1975) 5379-5386.
[15] F. Bonneté, D. Madern, G. Zaccai, Stability against Denaturation Mechanisms in Halophilic Malate Dehydrogenase "Adapt" to Solvent Conditions, Journal of Molecular Biology, 244 (1994) 436-447.
[16] H. Omori, M. Kuroda, H. Naora, H. Takeda, Y. Nio, H. Otani, K. Tamura, Deuterium oxide (heavy water) accelerates actin assembly in vitro and changes microfilament distribution in cultured cells, European Journal of Cell Biology, 74 (1997) 273-280.
[17] M. Verheul, S.P.F.M. Roefs, K.G. de Kruif, Aggregation of β-lactoglobulin and influence of D2O, FEBS Letters, 421 (1998) 273-276.
[18] G. Chakrabarti, S. Kim, M.L. Gupta, J.S. Barton, R.H. Himes, Stabilization of Tubulin by Deuterium Oxide, Biochemistry, 38 (1999) 3067-3072.
[19] P. Cioni, G.B. Strambini, Effect of Heavy Water on Protein Flexibility, Biophysical Journal, 82 (2002) 3246-3253.

[20] P.K. Glasoe, F.A. Long, Use of glass electrodes to measure acidities in deuterium oxide1,2, The Journal of Physical Chemistry, 64 (1960) 188-190.
[21] V. Kayser, N. Chennamsetty, V. Voynov, B. Helk, B.L. Trout, Tryptophan-Tryptophan Energy Transfer and Classification of Tryptophan Residues in Proteins Using a Therapeutic Monoclonal Antibody as a Model, Journal of Fluorescence, 21 (2011) 275-288.
[22] V. Kayser, N. Chennamsetty, V. Voynov, B. Helk, B.L. Trout, Conformational stability and aggregation of therapeutic monoclonal antibodies studied with ANS and Thioflavin T binding, mAbs, 3 (2011) 408-411.
[23] N.K. Holm, S.K. Jespersen, L.V. Thomassen, T.Y. Wolff, P. Sehgal, L.A. Thomsen, G. Christiansen, C.B. Andersen, A.D. Knudsen, D.E. Otzen, Aggregation and fibrillation of bovine serum albumin, Biochimica et Biophysica Acta (BBA) - Proteins and Proteomics, 1774 (2007) 1128-1138.
[24] W.Q. Ong, Y.R. Citron, J. Schnitzbauer, D. Kamiyama, B. Huang, Heavy water: a simple solution to increasing the brightness of fluorescent proteins in super-resolution imaging, Chemical Communications, 51 (2015) 13451-13453.
[25] R. Lumry, H. Eyring, Conformation Changes of Proteins, The Journal of Physical Chemistry, 58 (1954) 110-120.
[26] M. Bhattacharya, N. Jain, S. Mukhopadhyay, Insights into the Mechanism of Aggregation and Fibril Formation from Bovine Serum Albumin, The Journal of Physical Chemistry B, 115 (2011) 4195-4205.

CHAPTER 4

“Ionic Liquids as Biocompatible Stabilizers of Proteins”

Chapter 4 was published in the Biophysical Reviews journal:

Reslan, M., Kayser, V. (2018). Ionic liquids as biocompatible stabilizers of proteins. Biophysical Reviews. doi: 10.1007/s12551-018-0407-6

Abstract

Ionic liquids (ILs) have recently emerged as versatile solvents and additives in the field of biotechnology, particularly as stabilizers of proteins and enzymes. Of interest to the biotechnology industry is the formulation of stable biopharmaceuticals, therapeutic proteins and vaccines which have revolutionised the treatment of many diseases including debilitating conditions such as cancers and auto-immune diseases. The stabilization of therapeutic proteins is typically achieved using additives that prevent unfolding and aggregation of these proteins during manufacture, transport and long-term storage. To determine if ILs could be used in the formulation of stable therapeutic proteins, a thorough understanding of the effects of ILs on protein stability is needed, as well as understanding the toxicity of ILs on humans, and other considerations for formulation development such as viscosity and osmolarity. In this review, we summarise recent developments on the stabilization of proteins and enzymes using ILs, with emphasis on identifying biocompatible ILs that may be suitable for the formulation of stable biopharmaceuticals in the future.

1. Introduction

Ionic liquids (ILs) are organic salts with low melting points, typically below 100 ºC. The interest in IL research began shortly after the synthesis of the first air- and moisture-stable ILs in 1992 [1]. Initially developed as non-flammable alternatives to common organic solvents, ILs quickly found hundreds of applications spanning electrochemistry [2-4], energy [5-7], organic synthesis and catalysis [8, 9] to pharmaceutics [10-12], biotechnology [13-18] and more [19, 20]. It is estimated that there are over a million combinations of cations and anions that can form an IL [21]. Consequently, these versatile solvents which are often termed ‘designer solvents’ can access a wide range of physicochemical properties which can be tailored for almost any application; such properties include, low vapour pressure, high thermal stability, high conductivity, non-flammability, biocompatibility etc [22].

The use of ILs in biotechnology has gained significant attention recently, particularly for the enhanced stabilization of proteins, enzymes [19, 23, 24] and viruses [16]. Proteins are highly sensitive to changes in their vicinity induced by temperature, pH, humidity and salt concentration, in addition to any shear stress applied during manufacturing [25]. As they are exposed to these ‘stresses’, they undergo gradual

changes in structure, or unfold, and form protein aggregates over time [26]. In addition, the poor stability of proteins and enzymes might result in loss of function and activity, significantly limiting their use in biological processes and as biopharmaceuticals.

ILs have been utilized as ‘neat’ solvents or as solutes in an aqueous solution (“aqueous ILs”) to stabilize proteins [27, 28]. Although both approaches have led to improved protein stability, most neat ILs may not be suitable for biopharmaceutical applications due to the high viscosity of most ILs, and lack of solubility of proteins at high concentrations in neat ILs, which is particularly important for biologics. Consequently, dissolving ILs in an aqueous solution as an additive/co-solvent, has been a more favourable approach in this field and will be the focus of this review.

The emergence of ILs as potential stabilizers of proteins is a significant finding that requires review, particularly for the development of stable biopharmaceuticals, an application of ILs which has not been addressed adequately in previous literature. Biologics have revolutionised management of cancers, auto-immune diseases, infections and other difficult conditions to treat since their introduction as therapeutic products more than 30 years ago [25]. The stabilization of biopharmaceuticals is more challenging because of additional considerations required to determine the suitability of a formulation additive, such as the toxicity of the additive, and particularly in the case of ILs, the influence on the viscosity of the final protein solution, especially if the product is to be injected intravenously, which is the case for many biopharmaceuticals.

Our aim is to review the current literature on the application of ILs for the stabilization of proteins and assess the suitability of the promising IL candidates for the stabilization of biopharmaceuticals.

2. Current literature on the stabilisation of proteins using ILs

ILs are often classified as protic (PILs) or aprotic ILs (AILs). PILs act as hydrogen bond donors and often include ammonium or phosphonium derivatives as a cation, combined with a phosphate, sulfate or nitrate anion [24, 29, 30]. Examples of protic ILs include, ethylammonium nitrate (EAN) and choline dihydrogen phosphate ([Chol][DHP]) (Fig. 1). AILs act as hydrogen bond acceptors and typically include a bulky cation such as pyrrolidinium, pyridinium or imidazolium or their derivatives, in combination with a halide anion, or hexafluorophosphate, tetrafluoroborate or other such anions [29, 30]. Examples of AILs include 1-butyl-3-methyilimidazolium chloride

([BMIM][Cl]) and 1-benzyl-3-methylimidazolium tetrafluoroborate ([BzMIM][BF_4]) (Fig. 1). Of both classes of ILs, we will review some of the findings on imidazolium- and choline-based ILs which have received the most attention in recent years [19, 23]. Research on the imidazolium class of ILs, has helped to gain insight into the mechanism behind the observed effects on protein stability, as well as develop better ILs. Additionally, choline ILs have emerged as one of the most suitable candidates for stabilization of biopharmaceuticals due to their biocompatibility and pronounced effect on protein stability and are therefore of primary relevance to this review. For a quick summary of the literature findings see Table 1.

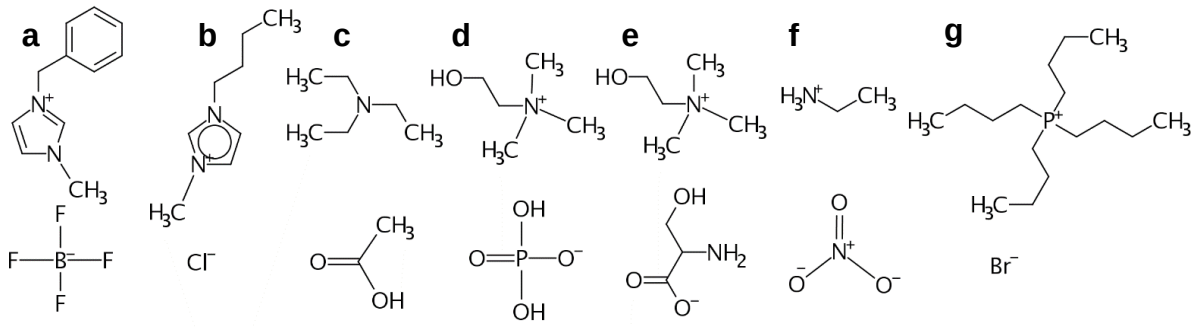

Figure 1. Examples of protic and aprotic ILs. a) 1-benzyl-3-methylimidazolium tetrafluoroborate ([BzMIM][BF_4]); b) 1-butyl-3-methyilimidazolium chloride ([BMIM][Cl]); c) Triethylammonium acetate (TEAA); d) Choline dihydrogen phosphate ([Chol][DHP]); e) Choline serinate ([Chol][Ser]); f) ethylammonium nitrate (EAN); g) tetrabutylphosphonium bromide (TBPBr)

2.1. Imidazolium-based ILs

Imidazolium-based ILs are the most extensively researched family of ILs until date and are widely used in many of the applications mentioned previously [31-33]. Many studies which investigated the use of imidazolium-ILs on protein stability have found that they act as protein denaturants or chaotropes; however, they have been extremely useful in gaining mechanistic insight into the complex interactions of ILs with proteins and are worth investigation [18, 34].

Kumar, et al. [35] studied the effect of three imidazolium-ILs - [BMIM][Cl], [BMIM][Br] and [BMIM][I] - on the conformational structure and thermal stability of stem bromelain. All three ILs were found to be denaturing above concentrations of 0.01 M, while having no stabilizing effect below that concentration. The order of thermal stability was: [BMIM][Cl] > [BMIM][Br] > [BMIM][I], with [BMIM][I] being the most denaturing.

Table 1. Summary of the literature on ILs and protein stability discussed in the review

Ionic liquid	Proteins tested	Effect on protein stability	References
Imidazolium-based ILs			
[MMIM][I]	Lysozyme crystals	+	[36]
[BMIM][Cl]	Stem bromelain, lysozyme, lysozyme crystals	-, -, +	[35-37]
[BMIM][Br]	Lysozyme crystals	+	[36]
[BMIM][I]	Stem bromelain	-	[35]
[BMIM][SCN]	Lysozyme, cyt C	-, -	[38]
[BMIM][BF_4]	Lysozyme crystals	+	[36]
[EMIM][Ac]	rPa^	~	[39]
[EMIM][Cl]	rPa^, lysozyme^	+, -	[37, 39]
[EMIM][$EtSO_4$]	rPa^	+	[39]
[EMIM][$MDEGSO_4$]	rPa^	+	
[EMIM][Et_2PO_4]	rPa^	+	
[EMIM][Tos]	rPa^	-	
[EMIM][$HexSO_4$]	rPa^	-	
[OH-EMIM][Cl]	Lysozyme	-	[37]
[OH-PMIM][Cl]	Lysozyme	-	
[HMIM][Cl]	Lysozyme	-	
[BzMIM][Cl]	CT	~	[40]
[BzMIM][BF_4]	CT	~	
Ammonium-based ILs			
EAN	Lysozyme, cyt C	-	[38]
TEAA	CT	++	[40]
TEAP	CT	++	
[Chol][Ac]	CT	++	[41]
[Chol][DHP]	CT, lysozyme, rHIL-2, cyt c	++, +, ++, +++	[41-46]
[Chol][Cit]	CT	-	[41]
[Chol][OH]	CT	-	[41]

[Chol][Cl]	CT, lysozyme	++	[41]
[Chol][TMA]	Lysozyme	+	[43]
[Chol][Lac]	Lysozyme	-	
[Chol][Prop]	Lysozyme	-	
[Chol][Hex]	Lysozyme	-	
[Chol][DMP]	Lysozyme	+	
[Chol][TFMS]	Lysozyme	-	
[Chol][TF_2N]	Lysozyme	-	
[Chol][Glu]	Cyt c	++	[44]
[Chol][Thr]	Collagen	-	[47]
[Chol][Ser]	Collagen	-	
[Chol][Lys]	Collagen	-	
[Chol][Phe]	Collagen	-	
Others			
TBPBr	CT	~	[40]
[EOOEMIM][$C_{12}SO_4$]	BSA	-	[17]
[EOOEMPy][$C_{12}SO_4$]	BSA	-	

^Only refolding was measured

Tertiary structure was also found to be disrupted at concentrations above 0.01 M and followed the same order; however, [BMIM][Cl] caused significantly less disruption of tertiary structure above 0.01 M than the other two ILs. The order of destabilization was found to follow the Hofmeister series; that is, the chaotropic (structure-breaking) anion - [I] - was the most destabilizing, while the kosmotropic (structure-making) [Cl] was the least destabilizing [35, 48].

Takekiyo, et al. [38] studied whether 1-butyl-3-methylimidazolium thiocyanate ([BMIM][SCN]) and ethylammonium nitrate (EAN) could be used as cryoprotectants of cytochrome complex (cyt C) and lysozyme. Both ILs significantly decreased the activity of cyt C and lysozyme and induced unfolding. However, following the removal of the ILs by dialysis after cryo-storage and subsequent heating, the activities of both cyt C and lysozyme returned to > 90% and structural changes were recovered (i.e. refolded) at IL concentrations > 10% [38]. This study demonstrated that the denaturant effect of imidazolium-ILs (and EAN) is predominantly reversible.

Some imidazolium-ILs have been shown to act as protein refolding agents. For example, Yamaguchi, et al. [49] investigated numerous hydrophobic imidazolium cations coupled with a Cl anion, and found that refolding was best achieved with short N-alkyl chain cations, with [BMIM][Cl] achieving the highest refolding yield of 84%. Increasing the length of the alkyl side-chain and hydrophobicity of the cation moiety of the ILs, reduced the refolding yield. The authors suggested that the hydrophobic moieties of these ILs with long alkyl side-chains strongly interact with hydrophobic patches of the protein structure driving destabilization and preventing intra-molecular interactions required for refolding. This was shown to be the case for bovine serum albumin (BSA) [50].

Buchfink, et al. [39] looked at the influence of the anion on the ability of EMIM-ILs to induce refolding of recombinant plasminogen activator (rPa) and stability of lysozyme. A series of anions were tested including: 2(2-methoxyethoxy)-ethyl sulfate ($MDEGSO_4$), ethyl sulfate ($EtSO_4$), and hexyl sulfate ($HexSO_4$), Cl, Ac, Tosylate (Tos) and diethyl phosphate (Et_2PO_4). The ability of the anion to promote refolding of rPa while coupled to EMIM followed the order of: [Cl] > [$MDEGSO_4$] > [$EtSO_4$] > [Ac] > [Tos] > [Et_2PO_4] > ≈ [$HexSO_4$]; [EMIM][Cl] was the only IL superior to ArgHCl as a refolding agent. Meanwhile the T_m of lysozyme in the same EMIM-ILs followed the order: [Cl] > [$EtSO_4$] ≈ [$MDEGSO_4$] > [Et_2PO_4] > [Ac] ≈ [Tos] > [$HexSO_4$]. Interestingly, this finding did not obey the Hofmeister series, which predicts that [Ac] is more stabilizing than [Cl] [48]. To some degree, the ability of the anion to promote refolding was related to the hydrophobicity of the anion. More specifically, the authors found that ILs which had intermediate ability to solubilize tryptophan were most effective at promoting refolding of rPa.

Interestingly, imidazolium-based ILs have been shown to act as denaturants, refolding enhancers and suppressors of insoluble aggregates at the same time. Lange, et al. [37] studied the effect of [BMIM][Cl], [OH-EMIM][Cl] and [OH-PMIM][Cl] on the stability of lysozyme and found that the melting temperature (T_m) of lysozyme decreased significantly with increasing alkyl chain length of the cation. The alkyl-ILs were found to be stronger denaturants than their OH-IL counterparts. They also tested the effects of [EMIM][Cl], [BMIM][Cl] and [HMIM][Cl], again confirming that increasing the alkyl chain length and hydrophobicity of the cation moiety, significantly decreases the conformational stability of lysozyme. However, insoluble aggregates were suppressed

in the presence of 2 M of each IL after denaturation of lysozyme and dilution into each IL, and at 0.5 M concentrations, [HMIM][Cl] was the most effective suppressor of insoluble aggregates, while less hydrophobic cations were not as effective. Additionally, [EMIM][Cl], [OH-EMIM][Cl], and [OH-PMIM][Cl] were found to be effective refolding enhancers, while [BMIM][Cl], [HMIM][Cl] and [OH-HMIM][Cl] were ineffective.

While imidazolium-ILs appear to act as protein denaturants, refolding enhancers and suppressors of insoluble aggregation, other studies have found that some imidazolium-ILs improved the thermal stability of proteins tested under certain conditions.

Wang, et al. [36] found that the T_m of lysozyme crystals produced in various imidazolium ILs as additives (1% w/v) increased from 65.6 to 71.4 °C ([BMIM][Cl]), 78.2 ([MMIM][I]), 81.2 ([BMIM][BF_4]) and 81.9 °C ([BMIM][Br]). Thus, the improved thermal stability obtained with the ILs followed the order of: [BMIM][Br] > [BMIM][BF_4] > [MMIM][I] > [BMIM][Cl] [36]. The enhanced thermal stability of lysozyme crystals was attributed to enhanced crystal contacts, changes in conformational stability and intermolecular interactions between lysozyme molecules, and lysozyme and each IL, which influenced lysozyme nucleation, and crystal growth and morphology [36].

Attri, et al. [40] studied the thermal stability of α-chymotrypsinogen (CT) in five ILs based on ammonium, phosphonium and imidazolium salts. Both imidazolium ILs tested (1-benzyl-3-methylimidazolium chloride ([BzMIM][Cl]), 1-benzyl-3-methylimidazolium tetrafluoroborate ([BzMIM][BF_4])) mildly improved the thermal stability of CT. On the other hand, triethyl ammonium acetate (TEAA) had the most stabilizing effect on CT increasing the T_m from 42 to 65 °C; followed by triethyl ammonium phosphate (TEAP) which increased its T_m to 62 °C. Tetra-butyl phosphonium bromide (TBPBr) only mildly improved thermal stability in comparison. However, all ILs reduced the activity of CT compared to buffer; TEAA retained the highest enzyme activity of all ILs. The stabilization of the native structure of CT was found to be due preferential expulsion of the ILs from the protein surface (the interaction between the ILs and disulfide bonds of CT is unfavourable) leading to the formation of a more compact CT structure which is more stable [40].

IL concentration is another critical factor as it determines the nature of interactions and subsequent effects of ILs on proteins and protein stability. For instance, Takekiyo, et

al. [51] found that at 5 M concentrations of [BMIM][NO_3] the tertiary structure of lysozyme was significantly disrupted, while at 6-10 M concentrations, partial refolding of the secondary structure was observed. At concentrations >10 M this partial refolding was maintained but the tertiary structure was significantly disrupted again. These observations were attributed to the changes in the spatial arrangement of water molecules around the protein structure, mediated by the concentration of IL in solution [51].

Thus, we can conclude that the effects of ILs on protein stability are multi-faceted; whether imidazolium-ILs act as protein denaturants, stabilizers or refolding agents depends on the type of protein being investigated, the anion coupled to the imidazolium ion, the hydrophobicity and length of the alkyl side chain of the cation and the concentration of the IL used, and these factors are most likely relevant to all families of ILs.

2.2. Choline-based ILs

The ammonium family of ILs especially choline ILs and their derivatives, have gained significant attention in the last decade for their pronounced effect on protein stability and apparent biocompatibility [24, 52, 53].

One of the earliest reports of the effect of choline-based ILs on protein stability by Fujita, et al. [45], Fujita, et al. [46] showed that the long-term stability of cyt C was significantly improved when dissolved in a solution of 80% w/v [Chol][DHP]. Even at this saturated concentration of [Chol][DHP], up to 37 mg/mL of protein was soluble. However, it is not necessary to use the saturated concentration of [Chol][DHP] or other choline-based ILs to observe significant improvements in protein stability, thus allowing for significantly higher protein solubility.

Bisht and Venkatesu [41] studied the effect of five choline-based ILs on the conformational stability, thermal stability and activity of CT. They tested 0.05-1.5 M concentrations of the following ILs: [Chol][Ac], [Chol][Cl], [Chol][Cit], [Chol][DHP] and [Chol][OH]. The conformational and thermal stability of CT in the different choline ILs followed the order: [Ac] > [Cl] > [DHP] || >> [Cit] >> [OH] with [Chol][Ac] having the most overall stabilizing effect on CT, increasing transition temperature from ~ 49 to 63 °C; those to the right of “||” reduced the stability of CT. The activity of CT in the choline ILs also followed a similar order, except [Chol][Cit] reduced the proteolytic

activity of CT more than [Chol][OH], and a mild increase in activity was observed with [Chol][Ac]; such that the order was as follows: [Ac] > [Cl] > [DHP] || >> [OH] >> [Cit]. The destabilizing effect of the [Cit] and [OH] anions was attributed to direct strong H-bonding with the CT structure, stripping off essential water molecules which normally stabilize the conformation of CT, while the stabilizing effect of anions such as [Ac], [Cl] and [DHP] was attributed to modification of water structuring around the protein, leading to its stabilization [41].

Weaver, et al. [42] studied the effect of [Chol][DHP] on the thermal and structural stability of lysozyme and recombinant human interleukin-2 (rHIL-2) at various [Chol][DHP] concentrations, and protein concentrations ≤ 1mg/mL. Increased concentrations of [Chol][DHP] (20 to 40% w/v) resulted in increased alpha-to-beta transition in the secondary structure of lysozyme at pH 4 and 7.2. On the other hand, increasing concentrations of [Chol][DHP] (0.5 to 12% w/v) improved the secondary order of rHIL-2 by decreasing the % of unordered content and increasing the % of alpha-helical content. The T_m of rHIL-2 was also found to be higher with increasing [Chol][DHP] concentrations, especially at the highest concentration tested (12% w/v or 680 mM), increasing from 61.7 to 74.2 °C. Lysozyme T_m was also increased with increasing concentrations of [Chol][DHP]; 40% w/v [Chol][DHP] at pH 7.2 shifted the T_m from 73.7 to 88.8 °C. At lower pH (e.g. 3.85), the increase in Tm was lower (76.5 to 84 °C), alluding to the importance of surface charge for stabilization with [Chol][DHP]. The results illustrate that [Chol][DHP] inhibits denaturation of lysozyme and rHIL-2 via interactions with charged residues on the protein surface but modifies the secondary structural elements in a favourable or unfavourable way depending on the protein. Additionally, thermal denaturation of rHIL-2 and lysozyme formulated with [Chol][DHP] resulted in the formation of irreversible aggregates.

Rodrigues, et al. [43] studied the stability of lysozyme in a series of choline-based ILs - choline trimethylacetate [Chol][TMA], choline lactate [Chol][Lac], choline propionate [Chol][Prop], choline hexanoate [Chol][Hex], choline dihydrogen phosphate [Chol][DHP], choline dimethyl phosphate [Chol][DMP], choline trifluoromethane sulfonate [Chol][TFMS], choline bis(trifluoromethylsulfonyl)amide [Chol][TF_2N], and choline chloride [Chol][Cl]. Lysozyme was best stabilized in [Chol][DHP] and destabilized in [Chol][TF_2N], following the order: [DHP] > [DMP] > [Lac] > [Cl] >> || [Prop] > [TFMS] ~ [TMA] > [Hex] > [TF_2N]. The effect of choline ILs was also found to

be concentration-dependant; for example, [Chol][DHP] had a stabilizing effect above 0.5 M and a destabilizing effect below this concentration [43].

Bisht, et al. [44] studied several choline ILs coupled to di/tri-carboxylate-based anions and dihydrogen phosphate as potential media for cyt C. Among the several ILs studied, >50-fold catalytic activity of cyt C was observed with choline glutarate ([Chol][Glu]) at 50% w/v of the IL, compared to PBS; and > 25-fold compared to [Chol][DHP] ~33% w/v. Additionally, the catalytic activity of cyt C was maintained against chemical denaturants (H_2O_2 and GuHCl) and temperatures of up to 120 °C, as well as long term storage of up to 21 weeks. It is important to note however, that the activity of cyt C is increased with partial unfolding of the tertiary structure, unlike most other proteins. Thus, it is not clear if the increased activity in this case is due to increased structural stability, although some secondary structural elements were stabilized in the presence of [Chol][Glu]. The authors concluded from molecular docking studies that the enhanced activity is due to H-bonding and electrostatic interactions between the ILs and specific residues in the active site of cyt C, as ILs which did not significantly enhance activity, such as [Chol][DHP], did not interact with the active site.

Mazid, et al. [54] published a short study characterizing the fragmentation of an Epidermal growth factor receptor (EGFR) monoclonal antibody (mAb) in the presence of buffered [Chol][DHP]. 20 and 50% w/v concentrations of buffered [Chol][DHP], prolonged the biological activity of the EGFR mAb and stabilized it against fragmentation in the presence of proteinase K. Higher stability was observed with 50% w/v buffered [Chol][DHP]. These effects were attributed to stabilization of the EGFR mAb alpha-helices in the presence of buffered [Chol][DHP]. This structural ordering is likely due to the [DHP] anion inducing water restructuring around the protein. Interestingly, the aggregation index of the formulations containing buffered [Chol][DHP] was found to be higher than control PBS by 20-30%, suggesting a modest increase in aggregation propensity.

Amino acid-based ILs are another promising class of biocompatible ILs that have received some interest in recent years [47, 55-57]. Amino acids have been mostly incorporated as anions, especially with imidazolium or choline cations to produce a biocompatible or ‘green’ IL. Guncheva, et al. [57] tested a series of choline-amino acid ILs on a hemocyanin and found that the thermal stability was lower in all ILs tested

than in the control. Tarannum, et al. [47] recently studied the effect of four choline-based amino acid ILs (choline serinate, threoninate, lysinate, and phenylalaninate) on the structural stability of collagen and had similar findings; they determined that competing hydrogen bonds between the ILs and OH groups on the collagen may be responsible for the destabilisation observed.

Unfortunately, research into the stabilization of proteins in amino acid-ILs is still in its early stages. Additionally, research is lacking on the formulation of ILs with therapeutically-relevant proteins such as mAbs, and other novel formats of antibodies such as antibody-drug conjugates and bi-specifics (antibody products that bind to two different epitopes), which are receiving considerable attention and undergoing intense research. Investigating the effect of ILs on such antibody formulations is important, as they are more complex multi-domain proteins with high therapeutic value and will certainly increase our understanding of the mechanisms behind protein stabilization with ILs.

3. Simulation studies of ILs: mechanisms of protein stabilization or destabilization

To determine the mechanism of stabilization or destabilization of ILs on proteins, an understanding of the interactions of ILs with water [58, 59] and ILs with proteins is necessary. Molecular dynamics (MD) simulations have been important in reaching some understanding of these interactions [58-60]. A comprehensive review of the findings of MD simulations is beyond the scope of this review; Schröder [61] and Smiatek [29] recently summarised important aspects. In brief, several important mechanisms of interaction and stabilization or destabilization of proteins have been identified with the help of MD simulations which will be discussed below.

As a solute, ILs share properties with inorganic salts and other stabilizing solutes, especially in how they interact with water and the protein surface [29, 58]. However, unlike simple inorganic salts which cannot typically form hydrogen bonds, IL interactions with water or proteins are in fact dominated by extensive hydrogen-bonding. Thus, the influence of ILs on protein stability is two-fold: the effect of the ions on water structure and direct hydrogen bonding to the protein surface residues.

IL interactions with water are based to some degree on the nature of the individual ions comprising the IL – i.e., if they are kosmotropic (structure-making/stabilizing) or

chaotropic (structure-breaking/destabilizing). In turn, the effects of IL ions on water structure affect protein solvation and stability. Although the Hofmeister series - which ranks anions based on their ability to precipitate proteins - is not always followed [62], understanding the effects of IL ions on water structure gives some insight into the complex mechanisms involved in protein stabilization or destabilization.

In most cases ILs are composed of a chaotropic cation such as imidazolium and a kosmotropic anion such as chloride or acetate. Interactions between ions and water are typically limited to their direct environment; i.e. they only influence the first hydration shell [63], however, these interactions may still impact protein stability. If there is strong involvement of the anions in the hydrogen bond network of water, the cations are often expelled from the water network, and then either accumulate at the surface of the protein (Fig. 2) [64, 65] or cluster together and form small aggregates

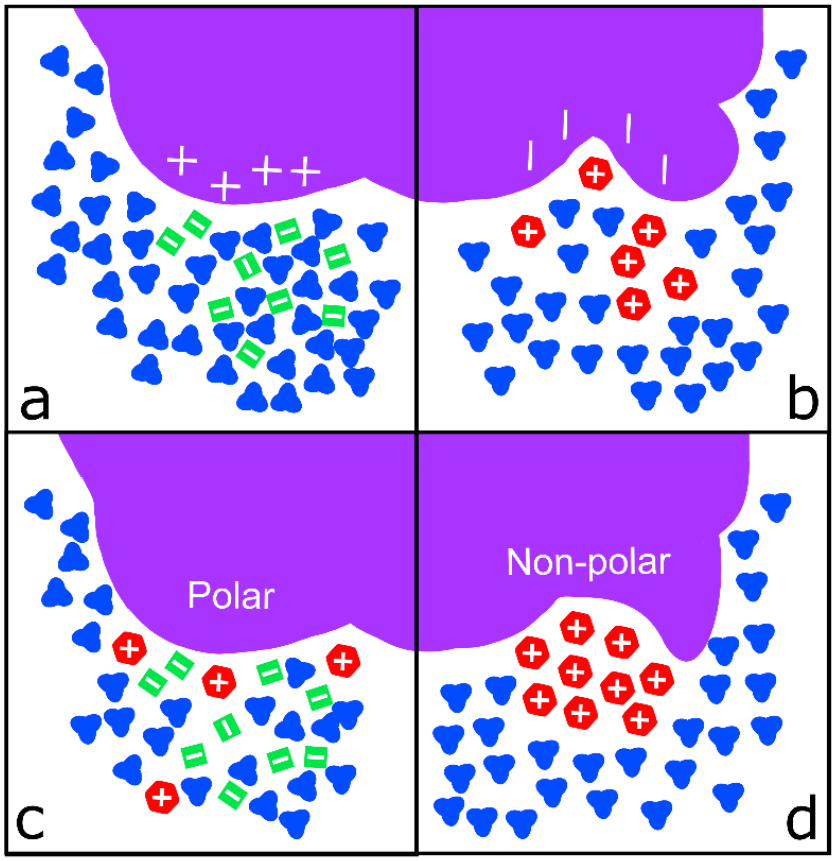

Figure 2. Ionic liquid (IL) interactions with water and the protein surface. Purple = protein; Red = IL cation; Green = IL anion; Blue = water. (a) Anions interact with water network and with positively charged regions on the protein surface electrostatically and via hydrogen bonding; (b) Cations interact electrostatically with negatively charged regions on the protein surface; (c) cations and anions interact with polar regions on the surface of the protein electrostatically; (d) IL cations expelled from water network cluster around non-polar or hydrophobic regions on the protein surface IL.

or micelles [66]; it is not clear if or how these micelles affect protein stability, but they do not disrupt the water network as significantly as individual ions dispersed throughout [61, 66].

Secondly, the observed effects on protein stability exhibited by ILs is significantly influenced by the type of interactions with the protein surface. IL cations which are expelled from the anion-water network, may directly interact with protein residues resulting in water removal from the surface, and increased or decreased stability (Fig. 2) [61, 67]. These cations may interact with polar, non-polar (through alkyl side chains) or negatively charged residues, while anions interact with positively charged and polar residues only (Fig. 2) [61]. MD simulations have shown that hydrophobic IL cations are inserted into phospholipid membranes through their alkyl side chains [68]. Micaêlo and Soares [67] performed molecular simulations on the interaction of two [BMIM] ILs formulated with low water content, with a serine protease cutinase enzyme. They found that the two ILs directly interacted with the enzyme surface, stripping off most of the water from the surface of the enzyme, and that the remaining water molecules formed many small clusters. Furthermore, molecular docking studies of BSA in various BMIM ILs revealed that the imidazolium cations of these ILs interact with hydrophobic residues in the subdomains of BSA via hydrophobic interactions causing protein unfolding [50]. Long alkyl chains would likely promote these hydrophobic interactions, contributing further to water removal from the surface, promoting further denaturation, as evident by the experimental results discussed in the previous section.

In cases where poorly soluble hydrophobic ILs have exhibited stabilizing effects, this stabilization has been attributed to the formation of two-phase systems, which results in less water depletion from the surface of the protein, enhancing its solubility and its overall stability [21].

MD simulations also show that the influence of the IL anion on protein stability, is stronger at higher concentrations of ILs. At higher concentrations, anions interact with positively charged residues of the protein, promoting refolding [69]. Additionally, because of the strong interaction of an anion with many positively charged residues, these residues are forced into a more compact conformation, facilitating the formation of H-bonds and restructuring of secondary structural elements, resulting in increased

thermal stability of the protein [69]; this is likely the case with choline ILs such as [Chol][DHP] which are better stabilizers at higher concentrations.

Recent computer simulations have suggested that the nucleophilicity and hydrogen bond basicity of the ions of an IL are the primary contributors to protein stability in ILs rather than their hydrophobicity, as postulated by numerous experimental studies, especially for enzymes. [29, 61]. The body of work on modelling IL interactions with proteins is in its early stages – as more computational studies are performed, a deeper understanding of the specific interactions of ILs on protein stability will be possible.

4. Considerations for IL use in formulations of biologics and vaccines

4.1. Toxicity of ILs

The widespread interest in the use of ILs, particularly as industrial solvents, necessitated studies into the toxicity of these compounds on environmental systems and various organisms, including humans. While the ecotoxicity of 'green' ILs has been studied extensively and summarised elsewhere [70], of significant interest in biological applications of ILs, is understanding their toxicity to humans, particularly their cytotoxicity [71]. Numerous cytotoxicity assays have been performed on animal cell lines, particularly mouse leukaemia cells (IPC-81) [72, 73] and various human cell lines [74, 75]. The high toxicity of some ILs is even being exploited for the development of IL-based cytotoxic drugs and anti-bacterial agents [76]. Given that ILs can exhibit a range of toxicities, it is important to identify which class of ILs may be considered biocompatible or 'safe' to use in formulations of biopharmaceuticals (Fig. 3).

The toxicity of ILs is a product of both the cation and anion [70, 71, 76], despite earlier claims that the cation moiety was a more significant determinant of toxicity. Both cation and anion toxicity is influenced by several factors; most significantly is the length of the alkyl side chain and branching, and the hydrophobicity of the ion. Several studies have shown that increasing the alkyl chain length of the cation significantly increases the toxicity of the IL [70, 74, 77, 78]. For example, Wang, et al. [74], found that the half maximal effective concentration (EC_{50}) of 1-ethyl-3-methylimidazolium bromide in a human cervical cancer cell line (HeLa), decreased from 8.4 mM to 2.8 mM when the ethyl was substituted for a butyl group, and further to 0.3 mM when substituted for an octyl group.

It has also been shown that introducing hydrophilic functional groups such as hydroxyls, nitriles and polar ethers to the side chains of ILs reduces the toxicity of the IL cation when compared with a non-functionalised alkyl side chain [78-80]. This is attributed to a reduction in hydrophobicity and ability to interact with and disrupt the lipid bilayer of cell membranes [81]. Additionally, some perfluorinated anions may be cytotoxic if they decompose and release fluoride ions [82]; however this is dependent on the organism tested and whether the anion is hydrolysable or not. Nonetheless, most AILs without modification, would not be an ideal choice of biocompatible ILs especially at high concentrations due to toxicity issues.

In most cases, PILs have been shown to exhibit less cytotoxicity than commonly-used AILs, as they typically lack the bulky hydrophobic cations and perfluorinated anions [77, 83]. Choline-based ILs are a promising class of biocompatible PILs for the stabilization of biopharmaceuticals. At least, the choline cation is significantly less toxic

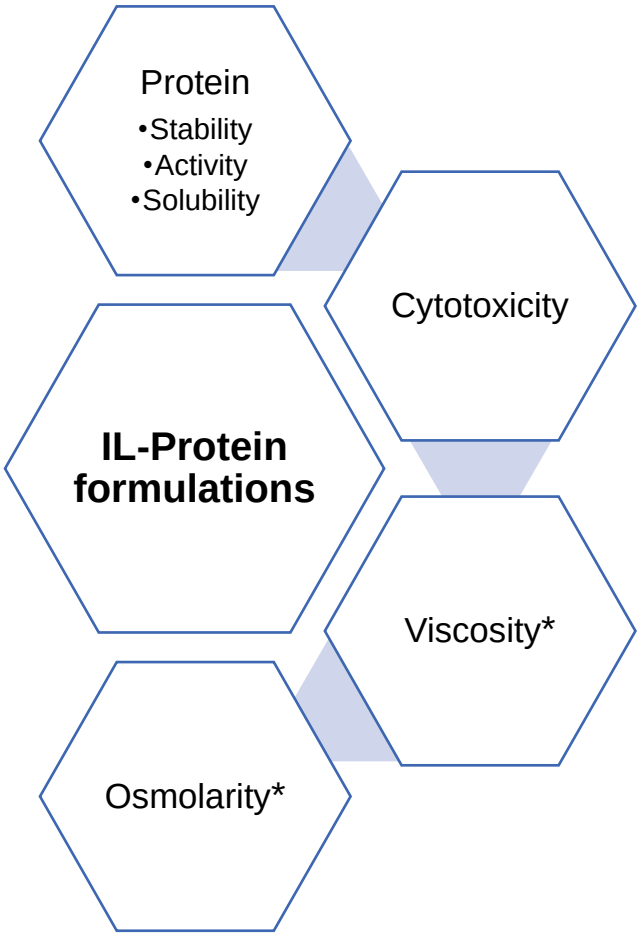

Figure 3. Important considerations for the use of ILs in protein formulations for therapeutic use. *considerations for injectable formulations

than an imidazolium or pyridinium-based cation as shown by [83]. The authors found that the EC_{50} of choline IL in HeLa cells were at least 10-fold lower than imidazolium and pyridinium ILs tested. Additionally, choline is an FDA approved molecule.

As the choline cation is typically considered a 'non-toxic' essential micronutrient, the overall cytotoxicity of choline ILs is mostly dependent on the anion it is coupled with.

Weaver, et al. [84] studied the cytotoxicity of choline cation paired with five phosphate-based anions; DHP, dibutyl phosphate (DBP), bis(2-ethylhexyl) phosphate (BEH), bis(2,4,4-trimethylpentyl) phosphinate (TMP), and O,O′-diethyl dithiophosphate (DEP). The cytotoxicity of the choline ILs was assessed on a J774 murine macrophage cell line. Of all the choline ILs tested, [Chol][DHP] exhibited the lowest cytotoxicity to J774; the EC_{50} values (mM) of the ILs were 0.25 [Chol][TMP], 0.3 [Chol][BEH], 8.2 [Chol][DEP], 9.1 [Chol][DBP], 20 [Chol][DHP] compared with values of 63 for NaCl and 34 for [Chol][Cl] [84]. Increased anion size and the presence of moderately long and/or branched alkyl chains increased the cytotoxicity of the IL, as previously shown with cations of AILs.

Following on from work by Weaver, et al. [42], Foureau, et al. [85] investigated the potential of [Chol][DHP] as a biocompatible additive for the stabilization and formulation of recombinant human interleukin-2 (rHIL-2). [Chol][DHP] *in vitro* concentrations < 80 mM were found to have no cytotoxic activity towards primary splenocytes nor mouse melanoma cells (B16-F10), suggesting that [Chol][DHP] is biocompatible at these physiological concentrations in an *in vitro* mouse model. Thus, it appears that the choline family of ILs is one of the most promising candidates for biocompatible ILs that exhibit a strong protein stabilizing effect.

4.2. Viscosity of ILs

ILs are typically quite viscous and range in viscosities from 10s to 1000s in cP (Table 2); thus, it is integral to assess the viscosity of typical IL solutions, to ensure they are below the acceptable viscosity for injectables (< ~20 cP), which is still one the most common methods of formulating and administering biopharmaceuticals (Fig. 3). Since these ILs are often used in concentrations ≤ 50% w/v their viscosity would be expected to be significantly lower than in their 'neat' form. Using [Chol][DHP] as an example, we observe that the viscosity of the 80% w/v as measured by Fujita, et al. [86] was 440 cP; however, at 65% w/v IL concentration, the viscosity decreases significantly to 25

cP (Table 2). Thus, it is expected that the viscosity of [Chol][DHP] solutions ≤ 50% w/v to be below 20 cP - the generally acceptable viscosity of IV formulations. However, it is important to consider the contribution of the high protein concentrations often formulated in these injectables to the total viscosity of the solution; the final formulation viscosity would need to be measured in a case-by-case basis to determine the suitability of the IL used.

Table 2. Viscosities of some common ILs

Ionic Liquid	**Viscosity (cP) @25 °C**	**Reference**
[BMIM][I]	1110	[87]
[BMIM][TF_2N]	69	
[BMIM][BF_4]	219	
[HMIM][Cl]	716	
[EMIM][TF_2N]	28	[88]
[Chol][DHP] 80% w/w	440	[86]
[Chol][DHP] 65% w/w	25	

4.3. Osmolarity of IL solutions for injection

When choosing ILs for use in IV formulations of biologics, the final solution osmolarity must be measured (Fig. 3). If ILs are used in large concentrations (for e.g. > 50% w/v), they would undoubtedly result in hypertonic formulations that may not be suitable for IV injection. For example, Foureau, et al. [85] measured the osmolarity of rHIL-2 formulations containing 680 mM (12% w/v) [Chol][DHP], and found that the solutions were hypertonic with an osmolarity of 1520 mOsm/L, approximately 2.5-5-fold higher than near-isotonic levels suitable for IV injection (~300-600 mOsm/L) [89]. Since ILs have concentration-dependant effects on protein stability, and are often stabilizing in higher concentrations, issues with osmolarity are inevitable. One approach to address the hypertonicity of the solutions is to introduce an intermediate dilution step prior to injection. Alternatively, if lower concentrations of IL are used as with Foureau, et al. [85], the product may be formulated in other types of injectables or infused; for example, Nony, et al. [90] reported that intramuscular injections comfortably administered 0.5 ml of up to 1100 mOsm/L hypertonic vaccine-like solutions. Such

considerations are becoming less significant as we head towards the development of non-invasive formulation routes for the administration of biopharmaceuticals.

5. Conclusion

ILs have demonstrated potential as novel versatile protein-stabilizing additives albeit with complex mechanisms of action. However, most studies up to date have focused on the thermal or chemical denaturation of proteins in IL solutions. While partial protein unfolding may lead to protein aggregation and influence overall protein stability, it is not sufficient to describe protein aggregation mechanism, as the aggregation process is distinct and is driven by protein-protein interactions. It is possible for an additive to inhibit unfolding while also promote aggregation, resulting in a limited overall benefit. Additionally, few of the studies on protein stability with ILs were performed on therapeutically-important and multi-domain proteins such as mAbs, which are extremely valuable, and few at high protein concentrations. With the development of biocompatible ILs, toxicity issues are becoming less of a concern for their use in therapeutic formulations. Additionally, the viscosity and osmolarity of protein-IL formulations is not an issue for long-term storage of biotherapeutics as long as the product is diluted prior to administration and only if the product is injected. ILs are exciting versatile liquids – with high potential yet to be exploited fully for rationally developed formulations of biologics and vaccines – certainly with more research in this field, as well as computational MD simulations for deeper mechanistic insights, we may see the incorporation of ILs in biotherapeutic formulations within the next decade.

References

[1] J.S. Wilkes, M.J. Zaworotko, Air and water stable 1-ethyl-3-methylimidazolium based ionic liquids, Journal of the Chemical Society, Chemical Communications, (1992) 965-967.

[2] M. Angell, C.-J. Pan, Y. Rong, C. Yuan, M.-C. Lin, B.-J. Hwang, H. Dai, High Coulombic efficiency aluminum-ion battery using an AlCl3-urea ionic liquid analog electrolyte, Proceedings of the National Academy of Sciences, 114 (2017) 834-839.

[3] M. Alvarez-Guerra, J. Albo, E. Alvarez-Guerra, A. Irabien, Ionic liquids in the electrochemical valorisation of CO2, Energy & Environmental Science, 8 (2015) 2574-2599.

[4] M.V. Fedorov, A.A. Kornyshev, Ionic Liquids at Electrified Interfaces, Chemical Reviews, 114 (2014) 2978-3036.
[5] D.R. MacFarlane, N. Tachikawa, M. Forsyth, J.M. Pringle, P.C. Howlett, G.D. Elliott, J.H. Davis, M. Watanabe, P. Simon, C.A. Angell, Energy applications of ionic liquids, Energy & Environmental Science, 7 (2014) 232-250.
[6] D.R. MacFarlane, M. Forsyth, P.C. Howlett, M. Kar, S. Passerini, J.M. Pringle, H. Ohno, M. Watanabe, F. Yan, W. Zheng, S. Zhang, J. Zhang, Ionic liquids and their solid-state analogues as materials for energy generation and storage, Nature Reviews Materials, 1 (2016) 15005.
[7] M. Smiglak, J.M. Pringle, X. Lu, L. Han, S. Zhang, H. Gao, D.R. MacFarlane, R.D. Rogers, Ionic liquids for energy, materials, and medicine, Chemical Communications, 50 (2014) 9228-9250.
[8] Z.S. Qureshi, K.M. Deshmukh, B.M. Bhanage, Applications of ionic liquids in organic synthesis and catalysis, Clean Technologies and Environmental Policy, 16 (2014) 1487-1513.
[9] Q. He, J.W. O'Brien, K.A. Kitselman, L.E. Tompkins, G.C.T. Curtis, F.M. Kerton, Synthesis of cyclic carbonates from CO2 and epoxides using ionic liquids and related catalysts including choline chloride-metal halide mixtures, Catalysis Science & Technology, 4 (2014) 1513-1528.
[10] M. Taha, M.R. Almeida, F.A.e. Silva, P. Domingues, S.P.M. Ventura, J.A.P. Coutinho, M.G. Freire, Novel Biocompatible and Self-buffering Ionic Liquids for Biopharmaceutical Applications, Chemistry – A European Journal, 21 (2015) 4781-4788.
[11] C. Jouannin, C. Tourne-Peteilh, V. Darcos, T. Sharkawi, J.-M. Devoisselle, P. Gaveau, P. Dieudonne, A. Vioux, L. Viau, Drug delivery systems based on pharmaceutically active ionic liquids and biocompatible poly(lactic acid), Journal of Materials Chemistry B, 2 (2014) 3133-3141.
[12] I.M. Marrucho, L.C. Branco, L.P.N. Rebelo, Ionic Liquids in Pharmaceutical Applications, Annual Review of Chemical and Biomolecular Engineering, 5 (2014) 527-546.
[13] M.V. Quental, M. Caban, M.M. Pereira, P. Stepnowski, J.A.P. Coutinho, M.G. Freire, Enhanced extraction of proteins using cholinium-based ionic liquids as phase-forming components of aqueous biphasic systems, Biotechnology Journal, 10 (2015) 1457-1466.

[14] A.M. da Costa Lopes, K.G. João, D.F. Rubik, E. Bogel-Łukasik, L.C. Duarte, J. Andreaus, R. Bogel-Łukasik, Pre-treatment of lignocellulosic biomass using ionic liquids: Wheat straw fractionation, Bioresource Technology, 142 (2013) 198-208.
[15] N.I. Haykir, E. Bahcegul, N. Bicak, U. Bakir, Pretreatment of cotton stalk with ionic liquids including 2-hydroxy ethyl ammonium formate to enhance biomass digestibility, Industrial Crops and Products, 41 (2013) 430-436.
[16] N. Byrne, B. Rodoni, F. Constable, S. Varghese, J.H. Davis, Enhanced stabilization of the Tobacco mosaic virus using protic ionic liquids, Physical Chemistry Chemical Physics, 14 (2012) 10119-10121.
[17] X. Wang, J. Liu, L. Sun, L. Yu, J. Jiao, R. Wang, Interaction of Bovine Serum Albumin with Ester-Functionalized Anionic Surface-Active Ionic Liquids in Aqueous Solution: A Detailed Physicochemical and Conformational Study, The Journal of Physical Chemistry B, 116 (2012) 12479-12488.
[18] M. Sivapragasam, M. Moniruzzaman, M. Goto, Recent advances in exploiting ionic liquids for biomolecules: Solubility, stability and applications, Biotechnology Journal, 11 (2016) 1000-1013.
[19] K.S. Egorova, E.G. Gordeev, V.P. Ananikov, Biological Activity of Ionic Liquids and Their Application in Pharmaceutics and Medicine, Chemical Reviews, 117 (2017) 7132-7189.
[20] W. Wei, N.D. Danielson, Fluorescence and Circular Dichroism Spectroscopy of Cytochrome c in Alkylammonium Formate Ionic Liquids, Biomacromolecules, 12 (2011) 290-297.
[21] H. Weingartner, C. Cabrele, C. Herrmann, How ionic liquids can help to stabilize native proteins, Physical Chemistry Chemical Physics, 14 (2012) 415-426.
[22] R.D. Rogers, K.R. Seddon, Ionic Liquids--Solvents of the Future?, Science, 302 (2003) 792-793.
[23] A. Kumar, M. Bisht, P. Venkatesu, Biocompatibility of ionic liquids towards protein stability: A comprehensive overview on the current understanding and their implications, International Journal of Biological Macromolecules, 96 (2017) 611-651.
[24] T.L. Greaves, C.J. Drummond, Protic Ionic Liquids: Evolving Structure–Property Relationships and Expanding Applications, Chemical Reviews, 115 (2015) 11379-11448.
[25] Z. Elgundi, M. Reslan, E. Cruz, V. Sifniotis, V. Kayser, The state-of-play and future of antibody therapeutics, Advanced Drug Delivery Reviews, 122 (2017) 2-19.

[26] V. Kayser, N. Chennamsetty, V. Voynov, B. Helk, K. Forrer, B.L. Trout, Evaluation of a Non-Arrhenius Model for Therapeutic Monoclonal Antibody Aggregation, Journal of Pharmaceutical Sciences, 100 (2011) 2526-2542.
[27] M. Persson, U.T. Bornscheuer, Increased stability of an esterase from Bacillus stearothermophilus in ionic liquids as compared to organic solvents, Journal of Molecular Catalysis B: Enzymatic, 22 (2003) 21-27.
[28] R.M. Vrikkis, K.J. Fraser, K. Fujita, D.R. MacFarlane, G.D. Elliott, Biocompatible Ionic Liquids: A New Approach for Stabilizing Proteins in Liquid Formulation, Journal of Biomechanical Engineering, 131 (2009) 074514-074514-074514.
[29] J. Smiatek, Aqueous ionic liquids and their effects on protein structures: an overview on recent theoretical and experimental results, Journal of Physics: Condensed Matter, 29 (2017) 233001.
[30] C.A. Angell, N. Byrne, J.-P. Belieres, Parallel Developments in Aprotic and Protic Ionic Liquids: Physical Chemistry and Applications, Accounts of Chemical Research, 40 (2007) 1228-1236.
[31] J. Fang, M. Lyu, X. Wang, Y. Wu, J. Zhao, Synthesis and performance of novel anion exchange membranes based on imidazolium ionic liquids for alkaline fuel cell applications, Journal of Power Sources, 284 (2015) 517-523.
[32] H.L. Ngo, K. LeCompte, L. Hargens, A.B. McEwen, Thermal properties of imidazolium ionic liquids, Thermochimica Acta, 357-358 (2000) 97-102.
[33] W.-W. Gao, F.-X. Zhang, G.-X. Zhang, C.-H. Zhou, Key factors affecting the activity and stability of enzymes in ionic liquids and novel applications in biocatalysis, Biochemical Engineering Journal, 99 (2015) 67-84.
[34] R. Patel, M. Kumari, A.B. Khan, Recent Advances in the Applications of Ionic Liquids in Protein Stability and Activity: A Review, Applied Biochemistry and Biotechnology, 172 (2014) 3701-3720.
[35] P.K. Kumar, I. Jha, P. Venkatesu, I. Bahadur, E.E. Ebenso, A comparative study of the stability of stem bromelain based on the variation of anions of imidazolium-based ionic liquids, Journal of Molecular Liquids, 246 (2017) 178-186.
[36] Z. Wang, L. Dang, Y. Han, P. Jiang, H. Wei, Crystallization Control of Thermal Stability and Morphology of Hen Egg White Lysozyme Crystals by Ionic Liquids, Journal of Agricultural and Food Chemistry, 58 (2010) 5444-5448.

[37] C. Lange, G. Patil, R. Rudolph, Ionic liquids as refolding additives: N '-alkyl and N '-(omega-hydroxyalkyl) N-methylimidazolium chlorides, Protein Science, 14 (2005) 2693-2701.
[38] T. Takekiyo, Y. Ishikawa, Y. Yoshimura, Cryopreservation of Proteins Using Ionic Liquids: A Case Study of Cytochrome c, The Journal of Physical Chemistry B, 121 (2017) 7614-7620.
[39] R. Buchfink, A. Tischer, G. Patil, R. Rudolph, C. Lange, Ionic liquids as refolding additives: Variation of the anion, Journal of Biotechnology, 150 (2010) 64-72.
[40] P. Attri, P. Venkatesu, A. Kumar, Activity and stability of [small alpha]-chymotrypsin in biocompatible ionic liquids: enzyme refolding by triethyl ammonium acetate, Physical Chemistry Chemical Physics, 13 (2011) 2788-2796.
[41] M. Bisht, P. Venkatesu, Influence of cholinium-based ionic liquids on the structural stability and activity of [small alpha]-chymotrypsin, New Journal of Chemistry, (2017).
[42] K.D. Weaver, R.M. Vrikkis, M.P. Van Vorst, J. Trullinger, R. Vijayaraghavan, D.M. Foureau, I.H. McKillop, D.R. MacFarlane, J.K. Krueger, G.D. Elliott, Structure and function of proteins in hydrated choline dihydrogen phosphate ionic liquid, Physical Chemistry Chemical Physics, 14 (2012) 790-801.
[43] J.V. Rodrigues, V. Prosinecki, I. Marrucho, L.P.N. Rebelo, C.M. Gomes, Protein stability in an ionic liquid milieu: on the use of differential scanning fluorimetry, Physical Chemistry Chemical Physics, 13 (2011) 13614-13616.
[44] M. Bisht, D. Mondal, M.M. Pereira, M.G. Freire, P. Venkatesu, J.A.P. Coutinho, Long-term protein packaging in cholinium-based ionic liquids: improved catalytic activity and enhanced stability of cytochrome c against multiple stresses, Green Chemistry, 19 (2017) 4900-4911.
[45] K. Fujita, M. Forsyth, D.R. MacFarlane, R.W. Reid, G.D. Elliott, Unexpected improvement in stability and utility of cytochrome c by solution in biocompatible ionic liquids, Biotechnology and Bioengineering, 94 (2006) 1209-1213.
[46] K. Fujita, D.R. MacFarlane, M. Forsyth, M. Yoshizawa-Fujita, K. Murata, N. Nakamura, H. Ohno, Solubility and Stability of Cytochrome c in Hydrated Ionic Liquids: Effect of Oxo Acid Residues and Kosmotropicity, Biomacromolecules, 8 (2007) 2080-2086.
[47] A. Tarannum, J.R. Rao, N.N. Fathima, Choline-Based Amino Acid ILs–Collagen Interaction: Enunciating Its Role in Stabilization/Destabilization Phenomena, The Journal of Physical Chemistry B, 122 (2018) 1145-1151.

[48] C.P. Schneider, D. Shukla, B.L. Trout, Arginine and the Hofmeister Series: The Role of Ion–Ion Interactions in Protein Aggregation Suppression, The Journal of Physical Chemistry B, 115 (2011) 7447-7458.
[49] S. Yamaguchi, E. Yamamoto, S. Tsukiji, T. Nagamune, Successful control of aggregation and folding rates during refolding of denatured lysozyme by adding N-methylimidazolium cations with various N '-substituents, Biotechnology Progress, 24 (2008) 402-408.
[50] Y. Shu, M. Liu, S. Chen, X. Chen, J. Wang, New Insight into Molecular Interactions of Imidazolium Ionic Liquids with Bovine Serum Albumin, The Journal of Physical Chemistry B, 115 (2011) 12306-12314.
[51] T. Takekiyo, K. Yamazaki, E. Yamaguchi, H. Abe, Y. Yoshimura, High Ionic Liquid Concentration-Induced Structural Change of Protein in Aqueous Solution: A Case Study of Lysozyme, Journal of Physical Chemistry B, 116 (2012) 11092-11097.
[52] M.M. Pereira, S.N. Pedro, M.V. Quental, Á.S. Lima, J.A.P. Coutinho, M.G. Freire, Enhanced extraction of bovine serum albumin with aqueous biphasic systems of phosphonium- and ammonium-based ionic liquids, Journal of Biotechnology, 206 (2015) 17-25.
[53] I. Jha, P. Attri, P. Venkatesu, Unexpected effects of the alteration of structure and stability of myoglobin and hemoglobin in ammonium-based ionic liquids, Physical Chemistry Chemical Physics, 16 (2014) 5514-5526.
[54] R.R. Mazid, R. Vijayaraghavan, D.R. MacFarlane, C. Cortez-Jugo, W. Cheng, Inhibited fragmentation of mAbs in buffered ionic liquids, Chemical Communications, 51 (2015) 8089-8092.
[55] G. Chevrot, E.E. Fileti, V.V. Chaban, Enhanced stability of the model mini-protein in amino acid ionic liquids and their aqueous solutions, Journal of Computational Chemistry, 36 (2015) 2044-2051.
[56] K. Sankaranarayanan, G. Sathyaraj, B.U. Nair, A. Dhathathreyan, Reversible and Irreversible Conformational Transitions in Myoglobin: Role of Hydrated Amino Acid Ionic Liquid, The Journal of Physical Chemistry B, 116 (2012) 4175-4180.
[57] M. Guncheva, K. Paunova, P. Ossowicz, Z. Rozwadowski, E. Janus, K. Idakieva, S. Todinova, Y. Raynova, V. Uzunova, S. Apostolova, R. Tzoneva, D. Yancheva, Modification of Rapana thomasiana hemocyanin with choline amino acid salts significantly enhances its antiproliferative activity against MCF-7 human breast cancer cells, RSC Advances, 5 (2015) 63345-63354.

[58] I. Khan, K.A. Kurnia, F. Mutelet, S.P. Pinho, J.A.P. Coutinho, Probing the Interactions between Ionic Liquids and Water: Experimental and Quantum Chemical Approach, The Journal of Physical Chemistry B, 118 (2014) 1848-1860.
[59] R. Hayes, S. Imberti, G.G. Warr, R. Atkin, How Water Dissolves in Protic Ionic Liquids, Angewandte Chemie International Edition, 51 (2012) 7468-7471.
[60] A. Benedetto, P. Ballone, Room temperature ionic liquids interacting with bio-molecules: an overview of experimental and computational studies, Philosophical Magazine, 96 (2016) 870-894.
[61] C. Schröder, Proteins in Ionic Liquids: Current Status of Experiments and Simulations, Topics in Current Chemistry, 375 (2017) 25.
[62] A. Kumar, P. Venkatesu, Does the stability of proteins in ionic liquids obey the Hofmeister series?, International Journal of Biological Macromolecules, 63 (2014) 244-253.
[63] J.D. Batchelor, A. Olteanu, A. Tripathy, G.J. Pielak, Impact of Protein Denaturants and Stabilizers on Water Structure, Journal of the American Chemical Society, 126 (2004) 1958-1961.
[64] M. Haberler, C. Schroder, O. Steinhauser, Solvation studies of a zinc finger protein in hydrated ionic liquids, Physical Chemistry Chemical Physics, 13 (2011) 6955-6969.
[65] M. Klahn, G.S. Lim, A. Seduraman, P. Wu, On the different roles of anions and cations in the solvation of enzymes in ionic liquids, Physical Chemistry Chemical Physics, 13 (2011) 1649-1662.
[66] R. Hayes, G.G. Warr, R. Atkin, Structure and Nanostructure in Ionic Liquids, Chemical Reviews, 115 (2015) 6357-6426.
[67] N.M. Micaêlo, C.M. Soares, Protein Structure and Dynamics in Ionic Liquids. Insights from Molecular Dynamics Simulation Studies, The Journal of Physical Chemistry B, 112 (2008) 2566-2572.
[68] G.S. Lim, J. Zidar, D.W. Cheong, S. Jaenicke, M. Klähn, Impact of Ionic Liquids in Aqueous Solution on Bacterial Plasma Membranes Studied with Molecular Dynamics Simulations, The Journal of Physical Chemistry B, 118 (2014) 10444-10459.
[69] C.A. Summers, R.A. Flowers, Protein renaturation by the liquid organic salt ethylammonium nitrate, Protein Science, 9 (2000) 2001-2008.
[70] T.P. Thuy Pham, C.-W. Cho, Y.-S. Yun, Environmental fate and toxicity of ionic liquids: A review, Water Research, 44 (2010) 352-372.

[71] R.F.M. Frade, C.A.M. Afonso, Impact of ionic liquids in environment and humans: An overview, Human & Experimental Toxicology, 29 (2010) 1038-1054.
[72] J. Ranke, A. Müller, U. Bottin-Weber, F. Stock, S. Stolte, J. Arning, R. Störmann, B. Jastorff, Lipophilicity parameters for ionic liquid cations and their correlation to in vitro cytotoxicity, Ecotoxicology and Environmental Safety, 67 (2007) 430-438.
[73] J.S. Torrecilla, J. García, E. Rojo, F. Rodríguez, Estimation of toxicity of ionic liquids in Leukemia Rat Cell Line and Acetylcholinesterase enzyme by principal component analysis, neural networks and multiple lineal regressions, Journal of Hazardous materials, 164 (2009) 182-194.
[74] X. Wang, C.A. Ohlin, Q. Lu, Z. Fei, J. Hu, P.J. Dyson, Cytotoxicity of ionic liquids and precursor compounds towards human cell line HeLa, Green Chemistry, 9 (2007) 1191-1197.
[75] A. Garcia-Lorenzo, E. Tojo, J. Tojo, M. Teijeira, F.J. Rodriguez-Berrocal, M.P. Gonzalez, V.S. Martinez-Zorzano, Cytotoxicity of selected imidazolium-derived ionic liquids in the human Caco-2 cell line. Sub-structural toxicological interpretation through a QSAR study, Green Chemistry, 10 (2008) 508-516.
[76] A. Pandey, M.K. Ekka, S. Ranjan, S. Maiti, C. Sachidanandan, Teratogenic, cardiotoxic and hepatotoxic properties of related ionic liquids reveal the biological importance of anionic components, RSC Advances, 7 (2017) 22927-22935.
[77] B. Peric, J. Sierra, E. Martí, R. Cruañas, M.A. Garau, J. Arning, U. Bottin-Weber, S. Stolte, (Eco)toxicity and biodegradability of selected protic and aprotic ionic liquids, Journal of Hazardous materials, 261 (2013) 99-105.
[78] R.A. Kumar, N. Papaiconomou, J.-M. Lee, J. Salminen, D.S. Clark, J.M. Prausnitz, In Vitro Cytotoxicities of Ionic Liquids: Effect of Cation Rings, Functional Groups, and Anions, Environmental Toxicology, 24 (2009) 388-395.
[79] M. Stasiewicz, E. Mulkiewicz, R. Tomczak-Wandzel, J. Kumirska, E.M. Siedlecka, M. Golebiowski, J. Gajdus, M. Czerwicka, P. Stepnowski, Assessing toxicity and biodegradation of novel, environmentally benign ionic liquids (1-alkoxymethyl-3-hydroxypyridinium chloride, saccharinate and acesulfamates) on cellular and molecular level, Ecotoxicology and Environmental Safety, 71 (2008) 157-165.
[80] S. Stolte, J. Arning, U. Bottin-Weber, A. Mueller, W.-R. Pitner, U. Welz-Biermann, B. Jastorff, J. Ranke, Effects of different head groups and functionalised side chains on the cytotoxicity of ionic liquids, Green Chemistry, 9 (2007) 760-767.

[81] B. Jing, N. Lan, J. Qiu, Y. Zhu, Interaction of Ionic Liquids with a Lipid Bilayer: A Biophysical Study of Ionic Liquid Cytotoxicity, The Journal of Physical Chemistry B, 120 (2016) 2781-2789.
[82] S. Steudte, J. Neumann, U. Bottin-Weber, M. Diedenhofen, J. Arning, P. Stepnowski, S. Stolte, Hydrolysis study of fluoroorganic and cyano-based ionic liquid anions - consequences for operational safety and environmental stability, Green Chemistry, 14 (2012) 2474-2483.
[83] W. Gouveia, T.F. Jorge, S. Martins, M. Meireles, M. Carolino, C. Cruz, T.V. Almeida, M.E.M. Araújo, Toxicity of ionic liquids prepared from biomaterials, Chemosphere, 104 (2014) 51-56.
[84] K.D. Weaver, H.J. Kim, J. Sun, D.R. MacFarlane, G.D. Elliott, Cyto-toxicity and biocompatibility of a family of choline phosphate ionic liquids designed for pharmaceutical applications, Green Chemistry, 12 (2010) 507-513.
[85] D.M. Foureau, R.M. Vrikkis, C.P. Jones, K.D. Weaver, D.R. MacFarlane, J.C. Salo, I.H. McKillop, G.D. Elliott, In Vitro Assessment of Choline Dihydrogen Phosphate (CDHP) as a Vehicle for Recombinant Human Interleukin-2 (rhIL-2), Cellular and Molecular Bioengineering, 5 (2012) 390-401.
[86] K. Fujita, N. Nakamura, K. Igarashi, M. Samejima, H. Ohno, Biocatalytic oxidation of cellobiose in an hydrated ionic liquid, Green Chemistry, 11 (2009) 351-354.
[87] J.G. Huddleston, A.E. Visser, W.M. Reichert, H.D. Willauer, G.A. Broker, R.D. Rogers, Characterization and comparison of hydrophilic and hydrophobic room temperature ionic liquids incorporating the imidazolium cation, Green Chemistry, 3 (2001) 156-164.
[88] A.B. McEwen, H.L. Ngo, K. LeCompte, J.L. Goldman, Electrochemical Properties of Imidazolium Salt Electrolytes for Electrochemical Capacitor Applications, Journal of the Electrochemical Society, 146 (1999) 1687-1695.
[89] W. Wang, Tolerability of hypertonic injectables, International Journal of Pharmaceutics, 490 (2015) 308-315.
[90] P. Nony, P. Girard, S. Chabaud, L. Hessel, C. Thébault, J.P. Boissel, Impact of osmolality on burning sensations during and immediately after intramuscular injection of 0.5 ml of vaccine suspensions in healthy adults, Vaccine, 19 (2001) 3645-3651.

CHAPTER 5

“Analysis of the Aggregation Kinetics of Herceptin® (Trastuzumab)”

Chapter 5 was submitted for publication to the European Journal of Pharmaceutics and Biopharmaceutics:

Reslan, M., Kayser, V. (2018). Analysis of the aggregation kinetics of Herceptin® (trastuzumab). European Journal of Pharmaceutics and Biopharmaceutics

Abstract

Monoclonal antibodies (mAbs) have dominated the pharmaceutical market in the last decade, with thousands more in the development pipeline. Despite rapid growth in the mAb industry, protein aggregation continues to plague the development of novel antibody therapies due to the immunogenicity of antibody aggregates, thus limiting the product's shelf-life. To combat protein aggregation more effectively, a mechanistic understanding of the aggregation process is needed; studying the aggregation kinetics of therapeutic antibodies provides mechanistic insight into the intricate processes that precede aggregation, with the possibility of developing predictive models to determine parameters such as shelf-life and establish a connection between accelerated studies with long-term storage conditions. Hereby, we thoroughly characterised the aggregation kinetics of Herceptin® (trastuzumab) using spectroscopic methods including fluorescence, dynamic and static light scattering (DLS, SLS), and size-exclusion chromatography (SE-HPLC) and at various temperatures to gain insight into the process of mAb aggregation. We have developed a simple model summarising the aggregation process of Herceptin® with mechanistic insight into the predominant steps in the aggregation process.

1. Introduction

Therapeutic monoclonal antibodies (mAbs) and antibody-based products have consistently led the biopharmaceutical market in the last ten years. Over 70 therapeutic antibody products have been approved by the FDA and EMA, and hundreds more are in clinical trials [1-4]. One of the most challenging facets of developing novel antibody biologics is protein aggregation [5]; a common physical degradation process that often causes adverse effects and leads to undesired immunogenicity and loss of antibody function [1, 6, 7]. The success of these novel therapeutic antibodies is heavily dependent on the aggregation propensity of the antibody and how effectively aggregation can be suppressed at high protein concentrations over the shelf-life of the product.

To combat aggregation more effectively, mechanistic insight into the pathways of antibody aggregation and molecular level protein-protein interaction is necessary. Studying the aggregation kinetics of antibodies allows us to expand our understanding of the aggregation process and more accurately determine important parameters such

as shelf-life [8-12]. Numerous kinetic models of different protein aggregation pathways have been described in the last fifty years [13-19]. We have previously summarised and discussed these elsewhere [15, 20]. Briefly, aggregation proceeds through a number of sequential processes as follows and shown in Scheme 1: (1) reversible transition from native (*M*) to partially unfolded monomers (assumed to be reactive monomers (M_u)); (2) addition of M_u to other reactive species such as other M_u and (3) aggregates (*A*); and (4) aggregate-aggregate association/clustering. It is worth nothing that these processes may be reversible or irreversible depending on the protein, excipients and experimental conditions. For example, the native monomer can unfold to an extent that it becomes irreversible. Additionally, precipitation of large aggregates can occur especially at high concentrations; however, therapeutic mAbs are relatively stable under standard long-term storage conditions and rarely unfold completely or precipitate at low temperatures. For simplicity, the model can be summarised as follows:

$$(1)\ M \overset{k_u}{\leftrightarrow} M_u$$

$$(2)\ M_u + M_u \overset{k_{di}}{\leftrightarrow} A_2$$

$$(3)\ M_u + A_2 \overset{k_{m1,1}}{\longleftrightarrow} A_3$$

$$\vdots$$

$$M_u + A_{n-1} \overset{k_{m1,n-2}}{\longleftrightarrow} A_n$$

$$(4)\ A_2 + A_2 \overset{k_{m2,1}}{\longleftrightarrow} A_4$$

$$A_2 + A_3 \overset{k_{m2,2}}{\longleftrightarrow} A_5$$

$$\vdots$$

$$A_x + A_y \overset{k_{m2,x}}{\longleftrightarrow} A_{x+y}$$

Note: (x+y) < n

Scheme 1. Model for protein aggregation

Such models are often reduced down further and analysed with 1-3 unknown parameters, often relying solely on monomer loss kinetic data to model aggregation

[15]. The above reaction rate constants that define each step are often obtained experimentally by analyzing protein folding/unfolding kinetics at either elevated temperatures or using chaotropic agents such as urea or guandine HCl (GuHCl), and performing accelerated-protein-aggregation studies. Kinetic data such as monomer loss and/or aggregate formation is determined using separation methods such as size exclusion-HPLC (SE-HPLC) and spectroscopic methods such as light scattering and fluorescence [16, 21, 22]. In general, kinetic data are analysed with (pseudo)first-order or second order functions although sometimes more complicated models are required to explain the data [13, 18, 21, 23]. Obtaining these rate constants can also be useful for predicting parameters such as shelf-life from accelerated data at elevated temperatures [21]. However, while some protein aggregation kinetics display the Arrhenius tendency, the aggregation of complex multi-domain proteins such as mAbs has been shown to be non-Arrhenius over a wide range of temperatures [21]. Thus, mathematical prediction of therapeutic antibody shelf-life remains a challenge [6, 21].

To our knowledge, limited kinetic analyses have been performed on the marketed mAb product Herceptin® in its original formulation. Hereby, we thoroughly investigated the conformational and colloidal stability of trastuzumab in its marketed formulation conditions (Herceptin®) as a model for IgG1 therapeutic antibodies using SE-HPLC, fluorescence spectroscopy, static (SLS) and dynamic light scattering (DLS) to develop a deeper understanding of the aggregation phenomenon of therapeutic mAbs. Our results provide mechanistic insight into the aggregation kinetics under accelerated and long-term storage conditions.

2. Materials and Methods

Herceptin® was generously donated by Genentech (San Francisco, US) and was used in its formulation buffer for all experiments at the reconstituted concentration of 21 mg/mL (except where otherwise mentioned). Millex-GV syringe filter units (0.22 µm, PVDF, 33 mm, gamma sterilized, SLGV033RS), di-potassium hydrogen phosphate (EMPROVE® Ph Eur, BP, E 340 grade, 105101) and potassium dihydrogen phosphate (EMSURE® ISO grade, 104873) were purchased from Merck Millipore (MA, USA). 8-anilino-1-naphthalenesulfonic acid (ANS; >97% HPLC) grade, A1028), thioflavin T (ThT; T3516), guanidium hydrochloride (GuHCl) and all other reagents were purchased from Sigma Aldrich (Castle Hill, Australia).

2.1. Accelerated stability studies at elevated temperatures

Accelerated studies at elevated temperatures were conducted as previously described [21]. 30 or 100 µL aliquots of Herceptin® (hereafter referred to as trastuzumab) at concentrations of 21 mg/mL (aggregation kinetics) or 0.2 mg/mL (for ANS unfolding kinetics) were incubated in a Thermal Cycler 2720 (Applied Biosystems, CA, USA) at temperatures between 65-75 °C for various durations based on incubation temperature. A thermal cycler was used to prevent sample evaporation during incubation (with heated lid cover). Heated samples were immediately stored on ice following incubation to halt further aggregation and characterized with or without dilution in either formulation buffer or 150 mM potassium phosphate buffer, pH 6.5.

2.2. SE-HPLC

Size exclusion-high performance liquid chromatography (SE-HPLC) was used to quantify monomer loss and aggregation of trastuzumab following accelerated stability studies. Analysis was performed using an Agilent 1200 Liquid Chromatography system (Agilent Technologies, California, USA) with a single or double column set-up of TSKgel Super SW3000 columns (Tosoh Bioscience, Tokyo, Japan) at 22 °C, using a 150 mM potassium phosphate mobile phase, at pH 6.5, and a flow rate of 1 mL/min. 5 µL of each Herceptin® sample at a concentration of 21 mg/mL was injected. Monomer and aggregate peaks were detected using an in-line UV signal detector set at 280 nm. The area under the curve (AUC) of the monomer and the aggregate peaks was averaged over three runs and the mean % of each species was calculated for each sample. The standard deviation (SD) was plotted as error bars in the figures. For fractionation of chromatogram peaks, 100 µL of Herceptin® at a concentration of 21 mg/mL was injected, and monomer and aggregate peaks were evenly fractionated into 4 aggregate samples (from 11 to 15 minutes), and 7 monomer samples (from 10 to 20 minutes).

2.3. Fluorescence spectroscopy

Fluorescence measurements were performed using the Fluorolog 3 FL3-22 Spectrophotometer (HORIBA scientific, New Jersey, USA). Herceptin® samples were diluted to 0.2 or 0.15 mg/mL (GuHCl unfolding) in formulation buffer (excluding polysorbate 20 for ANS measurements due to its fluorescence contribution) while SE-

HPLC fractions were kept in the mobile phase buffer (potassium phosphate 150 mM) and diluted if necessary to approximately 0.02 mg/mL, pH 6.5. All samples were measured in a Hellma® ultra-micro fluorescence quartz cuvette (Hellma® Analytics, Müllheim, Germany) at right-angled detection mode. Data was analyzed using Igor Pro 6 software.

2.4. Tryptophan fluorescence

Tryptophan fluorescence of trastuzumab was used to characterize conformational changes between monomer fractions and different-sized aggregate species separated by SE-HPLC, by comparing differences in maximum fluorescence intensity and the maximum emission wavelength, which provide information on the environment surrounding the tryptophan residues. A change in tryptophan fluorescence and an increase in maximum emission wavelength (termed red-shift) usually suggests that there is increased solvent exposure near the tryptophan residue(s), which may be due to unfolding. On the other hand, a decrease in the maximum emission wavelength (termed blue-shift) is due to the formation of a more hydrophobic local environment near the tryptophan residue(s) which may occur because of protein aggregation [22]. For unfolding studies, a stock of 8 M GuHCl was used to dilute trastuzumab samples to required concentrations of antibody and GuHCl (1-6 M). Trastuzumab samples were incubated overnight at room temperature with GuHCl prior to measurement. ΔG' at 0M GuHCl was calculated from the normalised maximum trp wavelength using the following equation:

$$\Delta G = -RT \ln K_{eq}$$

and K_{eq}:

$$K_{eq} = \frac{W_{Folded} - W}{W - W_{Unfolded}}$$

where W is maximum trp wavelength at different concentrations of GuHCl (folded = 0 M; unfolded = 6 M) and K_{eq} is the equilibrium constant of the unfolding process.

Tryptophan fluorescence of trastuzumab was detected in the emission wavelength range of 300-500 nm with an excitation wavelength of 295 nm. Both excitation and emission slit sizes were set at 3 nm. Samples were corrected by blank subtraction of

150 mM potassium phosphate, pH 6.5 or formulation buffer. All measurements were performed in triplicates and averaged, and the standard deviation (SD) was calculated.

2.5. ANS and ThT fluorescence

ANS fluorescence was used to characterize the unfolding behaviour of trastuzumab following incubation at elevated temperatures. A significant increase in maximum ANS fluorescence is usually indicative of protein unfolding [24]. This is often accompanied by a blue-shift, as unfolding allows ANS to bind to hydrophobic pockets of the protein, away from the polar solvent environment. ANS fluorescence was detected in the emission wavelength range of 400-650 nm with an excitation wavelength of 385 nm. Both excitation and emission slit sizes were set at 3 nm. ANS kinetic data was fit using the IGOR 6 in-built single exponential function.

ThT fluorescence was used to characterize different-sized trastuzumab aggregates following incubation at elevated temperatures. A significant increase in maximum ThT fluorescence is usually associated with the formation of protein aggregates [24], and the degree of increase is also dependent on the hydrophobicity of the environment and the aggregate structure. A change in the maximum emission wavelength may also be observed, based on the aggregate environment. ThT emission was detected in the emission wavelength range of 425-600 nm with an excitation wavelength of 415 nm. Both excitation and emission slit sizes were set at 3 nm.

For both dyes, 5 µL of dye from a working stock was added to 95 µL of each trastuzumab sample to a final concentration of 20 µM ANS for unfolding kinetics studies, 3.5 µM ANS for monomer fractions, and 3 µM ThT for aggregate fractions. All samples were then incubated while in ice for exactly 20 minutes before analysis to allow for dye binding. Samples were corrected by blank subtraction of H_2O (for dye-only samples) or a trastuzumab sample dissolved in the respective solvent with no dye (for samples containing dye and trastuzumab). All dye fluorescence measurements were performed in triplicates and averaged, and the SD was calculated.

2.6. Dynamic light scattering (DLS)

The hydrodynamic diameter of trastuzumab monomer and aggregate fractions were measured by DLS using the Malvern Zetasizer Nano ZS (Malvern Instruments, Worcestershire, UK). The size range cut-off was adjusted to 1nm–0.5 µm as no

antibody particles were detected outside that range, minimising unwanted scatter. The refractive index was set at 1.33 and the absorption value was 0.1. The viscosity was set at 0.8879 mPa/s. Samples were diluted to 0.5 mg/mL in their respective solvents and measured in triplicates.

2.7. UV-Vis spectroscopy

UV-Vis absorbance was used to measure the concentration of soluble Herceptin® following accelerated stability studies. Absorbance was measured at 280 nm over a wavelength range of 220-350 nm using a Shimadzu UV-2600 spectrophotometer (Shimadzu, Japan). Samples were corrected by blank subtraction of the respective solvent. Data was not included as the absorbance of all samples remained unchanged following incubation, and therefore no change in soluble antibody concentration was observed.

3. Results and discussion

3.1. Conformation of monomeric antibody and aggregates

The unfolding of trastuzumab was characterised by thermal and GuHCl-induced stress, using ANS and trp fluorescence, respectively (Fig. 1 and 2). The melting temperatures (T_m) of each trastuzumab domain are 68-70 °C for the C_H2 and 81-83 °C for both the Fab and C_H3 domains [25, 26]. This was confirmed for our samples using trp fluorescence (data not shown). Thermal unfolding kinetics of trastuzumab was achieved by incubating very low concentrations of antibody in order to minimise aggregation, and probing external dye-binding kinetics using ANS fluorescence as previously described [24]. As expected, at 65 °C (below the melting temperature (T_m) of C_H2 of trastuzumab) minor changes in the native structure occur, illustrated by the changes in ANS fluorescence (Fig. 1). At higher temperatures 70 and 75 °C, however, the max fluorescence intensity of ANS increases 3-fold, with a blue-shift of ~40 nm as the ANS dye buries itself within the exposed hydrophobic domains of trastuzumab. The rate of unfolding is very rapid at 70 and 75 °C, with an exponential rate of fluorescence change and near maximum occurring within an hour at 70 °C and 6 minutes at 75 °C (Fig. 1). Unfolding rate is significantly slower at 65 °C, but an exponential rate of change is still observed. The unfolding rate constants at 65, 70 and 75 °C based on a single exponential fit, are 0.0192, 0.0235 and 0.325 min^{-1} (Fig. 1A;

max fluorescence) and 0.0112, 0.0905 and 0.890 min^{-1} (Fig. 1B; max wavelength), respectively.

Chemical unfolding of trastuzumab with increasing concentrations of GuHCl allows us to determine the sensitivity of the trp max emission wavelength of trastuzumab to

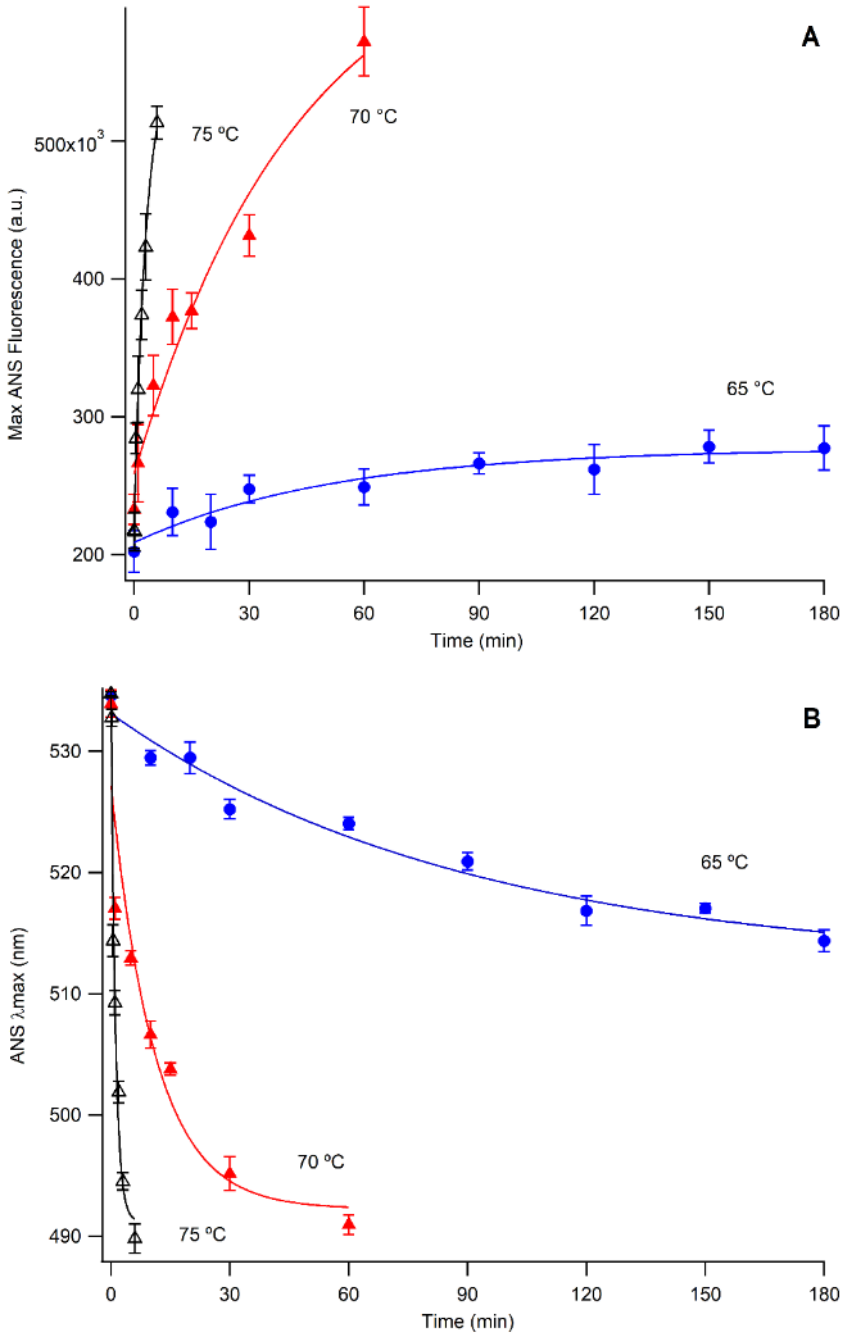

Figure 1. Trastuzumab unfolding kinetics measured with ANS fluorescence spectroscopy A) ANS max fluorescence plot with heat-stressed trastuzumab samples; B) ANS max emission wavelength shift with heat-stressed trastuzumab samples. Error bars represent the SD.

changes in its conformational structure and calculate ΔG' which was determined to be 14.7 kJ/mol at 0 M GuHCl. As can be seen, complete unfolding of trastuzumab domains is associated with a ~16 nm red-shift in the trp maximum emission

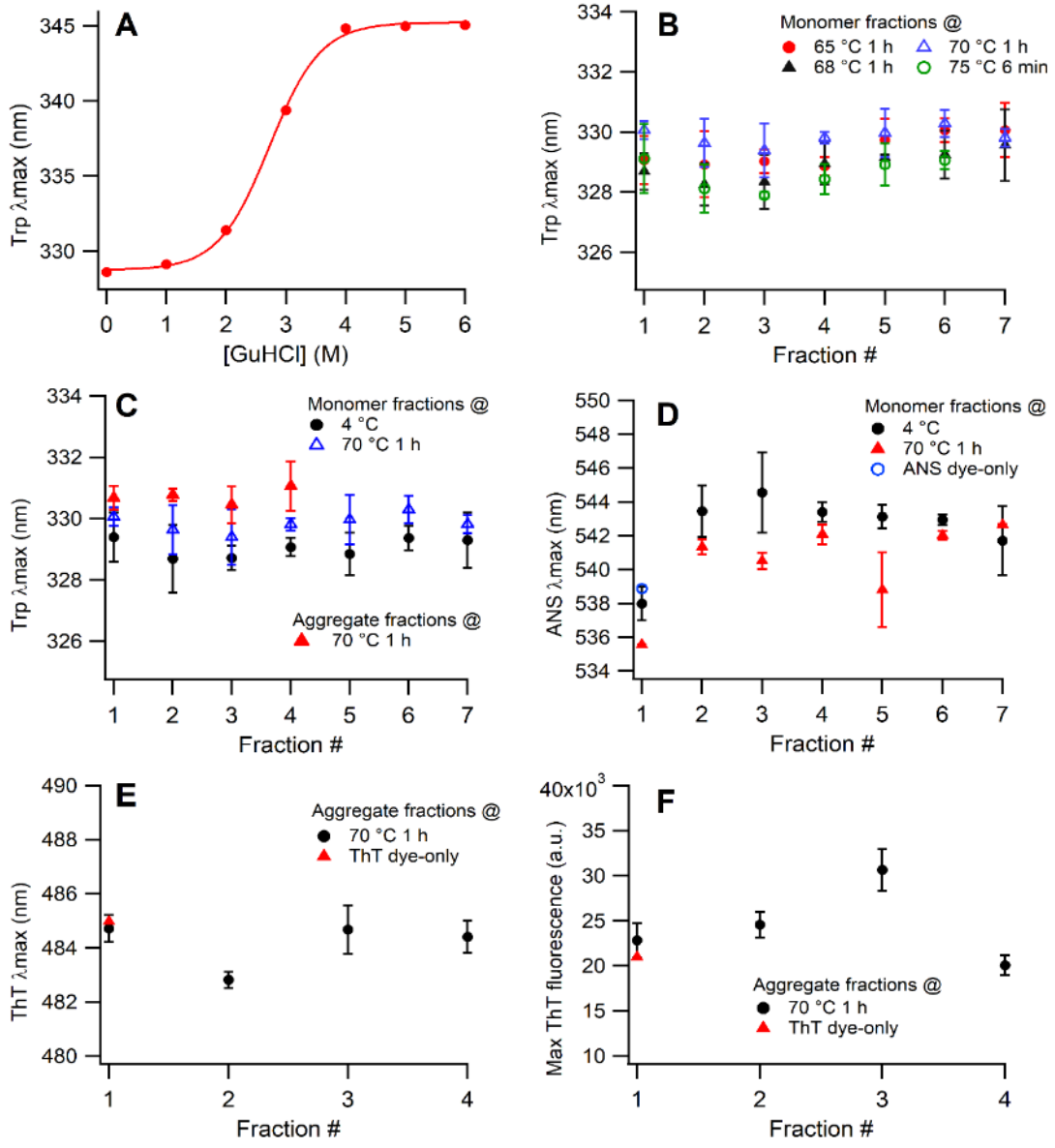

Figure 2. Characterisation of trastuzumab monomer and aggregate fractions from SE-HPLC by fluorescence spectroscopy; A) trp max emission wavelength shift of trastuzumab with increasing concentrations of GuHCl; B) trp max emission wavelength of monomer fractions from different sections of the chromatogram peak stressed at elevated temperatures; C) trp max emission wavelength of monomer and aggregate fractions stressed at 70 °C compared with 4 °C; D) max emission wavelength of ANS bound to monomer fractions stressed at 70 °C compared with fractions at 4 °C; E) max emission wavelength of ThT bound to aggregate fractions stressed at 70 °C; F) max fluorescence of ThT bound to aggregate fractions stressed at 70 °C. Error bars represent the SD.

wavelength, obtained with 6 M GuHCl (Fig. 2A). To determine whether there is any heterogeneity of eluted monomer species on SE-HPLC, we measured the trp max emission wavelength of 7 monomer fractions obtained from different sections of the eluted monomer peak, and from monomeric species incubated at different temperatures. We observed no difference in the trp max emission wavelength between monomer fractions taken at earlier or later sections of the elution peak, nor between these fractions and the corresponding fractions of monomer peaks from samples incubated at different temperatures (Fig. 2B).

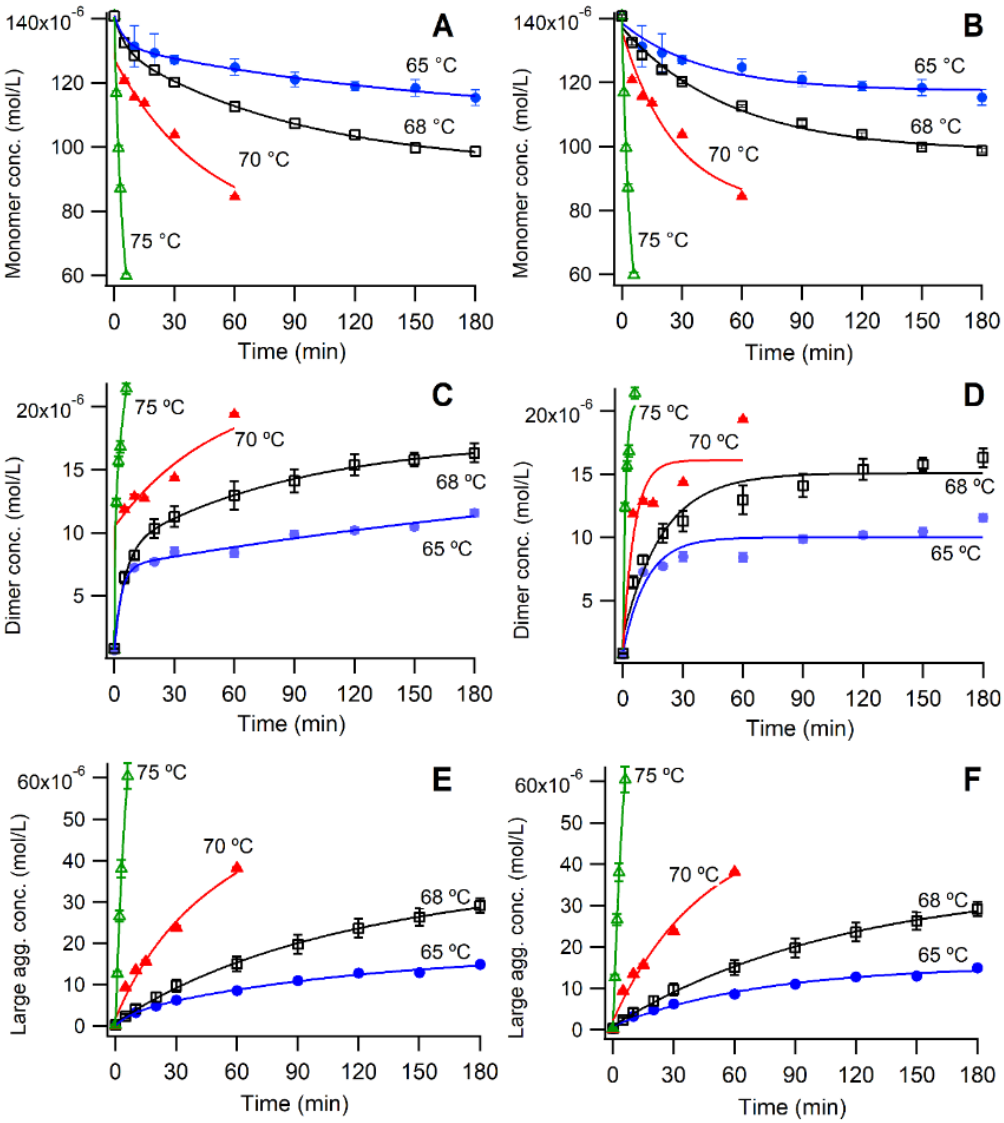

Figure 3. Aggregation kinetics of trastuzumab formulation at elevated temperatures (65, 68, 70 and 75C) A) monomer loss kinetics at elevated temperatures fit with a double exponential function; B) same as A) fit with a single exponential function; C) dimer formation kinetics at elevated temperatures fit with a double exponential function; D) same as C) fit with a single exponential function; E) large aggregate formation kinetics fit with a double exponential function; F) same as E) fit with a single exponential function. Aggregate concentration is determined based on monomeric concentration. Error bars represent the SD.

This suggests that the eluted monomer peak is at least predominantly made up of a single monomer species, that is native, and that the monomer species of incubated samples are similar in conformational structure with regards to their degree of unfolding. This allows us to confirm that the monomer concentration obtained from SE-HPLC at different temperatures is reflective of the native monomer concentration. However, since this is an *ex situ* analysis, it does not rule out the formation of other species during the reaction which are involved in aggregation; these species are either 'used' up to form aggregates or refold immediately upon cooling and dilution into the mobile phase, resulting in one native conformation that is eluted. Our results are consistent with observations in our previous study with BSA [15].

Surprisingly though, fractions 1-4 from the aggregate peak, also display no change in trp max emission wavelength (Fig. 2C). Aggregates are expected to bury trp residues in hydrophobic pockets, resulting in a blue-shift. The lack of any shift illustrates that trp environments are almost identical to that of trps in monomers. Furthermore, it suggests that the formation of the eluted aggregates is preceded by minimal changes in antibody conformation. That is, the formation of both dimers and large aggregate species proceeds with minimal structural rearrangement due to unfolding or otherwise. A similar observation with another mAb was reported by us using time-resolved trp fluorescence lifetime analysis [21], where individual antibody structures were somewhat different in very small and very large protein aggregates but were similar to each other if aggregate fractions were close to each other in size. However, these results are contrary to what we have previously found with BSA – whereby dimer and aggregate fractions from different incubation temperatures were found to have different conformations measured by trp fluorescence [15].

The lack of changes in conformational structure of monomer and aggregate species is further confirmed by ANS and ThT dye binding studies (Fig. 2D, E and F). Fractions 2-7 for both 4 and 70 °C samples are slightly red-shifted, compared to fraction 1 and ANS-dye only. However, when comparing the 4 °C fractions to the 70 °C fractions, no significant difference is observed. This illustrates that the monomeric species of heat-stressed samples have the same or very similar conformation to those samples which are not stressed. The apparent red-shift in fractions 2-7 compared to fraction 1 is likely due to the presence of a small amount of aggregate species in fraction 1, due to overlap between peaks.

Interestingly, no significant difference is observed when assessing the differences between aggregate fractions 1-4 with ThT (Fig. 2E and F), further demonstrating that the different-sized aggregates formed are conformationally similar in structure. This implies that beyond dimer formation, aggregates form via mechanisms which do not require further unfolding, such as aggregate-aggregate clustering/association. Based on DLS measurements of aggregate fractions, we can deduce that these findings apply up to the largest aggregate species detected which is approximately 8-10 times larger than the monomer – i.e. a decamer (Fig. 4B).

3.2. Accelerated trastuzumab aggregation studies and kinetics of aggregation

We further performed protein aggregation studies and measured the monomer, dimer and large aggregate concentration of trastuzumab to study its aggregation kinetics. Due to the large size of an antibody monomer (~148 kD) - and therefore the large size of its aggregates - it is difficult to resolve the different sized-aggregate species present in the elution. With a double column SE-HPLC set-up to assist separation, we achieved reasonable separation between dimer and larger aggregate species, which were fractionated and quantified (Fig. 2 and 3). Size-determination of the SE-HPLC fractions with DLS shows that the dimer peak fraction is predominantly dimer, with minimal heterogeneity (Fig. 4B). When trastuzumab is incubated at elevated temperature, we initially observe rapid dimer formation (Fig. 3C and D); the rate of formation of dimer species then begins to plateau reaching an equilibrium, as large aggregates ‘consume’ dimers and form more rapidly with increasing incubation time (Fig. 3E and F). Eventually, the rate of large aggregate formation also beings to decrease and the rate of formation of all aggregates (i.e. monomer loss) reaches a ‘plateau’ (Fig. 3A and B). As expected, little to no fragmentation was observed at elevated temperatures as fragmentation typically occurs slowly due to hydrolysis, or enzymatic digestion. The change in concentration of different-sized aggregates with incubation time confirms that large aggregates form by aggregate-aggregate association, utilizing dimers formed by monomer addition. Additionally, an equilibrium must exist between monomer and aggregate concentration, leading to the ‘plateau’ of monomer consumption. Altogether, a complex equilibrium between reversible and non-reversible species forms, leading to the steady rate of monomer loss observed after the rapid initial aggregation process at all temperatures.

Table 1. Rate constants of trastuzumab unfolding (k_u), monomer loss and aggregation from single (k) and double exponential equation fits (k_1 and k_2). N.D. denotes not determined.

T (°C)	Unfolding (min^{-1})	Monomer loss (min^{-1})			Dimer formation (min^{-1})			Large agg. formation (min^{-1})		
	k_u	k_1 (k_{m1}) n ≤ 3	k_2 (k_{m1}) n > 3	k (k_{m1})	k_1 (k_{di})	k_2	k	k_1 (k_{m2})	k_2	k
65	0.019	0.201	0.006	0.024	0.287	0.002	0.084	0.115	0.008	0.014
68	N.D.	0.202	0.011	0.019	0.201	0.011	0.05	0.017	0.004	0.009
70	0.024	10.53	0.022	0.038	71.71	0.019	0.175	0.023	0.166	0.023
75	0.325	0.365	0.089	0.246	2.443	0.147	0.711	0.138	0.184	0.155

3.3. Trastuzumab kinetic fits and aggregation mechanism

Several models of antibody aggregation have been previously proposed [6, 11, 13, 14, 16, 21, 27]. However, till-date most monomer loss kinetic data is fit with simple equations such as an exponential fit or a first/second order kinetic equation to derive a rate constant of aggregation. We compared the degree of 'fit' using in-built IGOR 6 single and double exponential functions and derived rate constants (k, and k_1 and k_2, respectively) of reactions contributing to monomer loss, dimer formation and large aggregate formation (Table 1). Since we did not obtain an ideal fit for monomer loss and dimer formation with a single exponential function, we used a double exponential function, while no significant difference was observed when fitting large aggregate formation kinetics (Fig. 3E and F). Analysis with a double exponential function suggests that monomer loss is involved in at least two different 'reactions' - a faster and slower reaction - defined by k_1 and k_2, respectively. Typically, the rate of small aggregate formation (e.g. dimer and trimer) is faster than the rate of monomer addition to larger aggregates as there is more accessibility to aggregation-prone regions, and therefore more possible combinations for association.

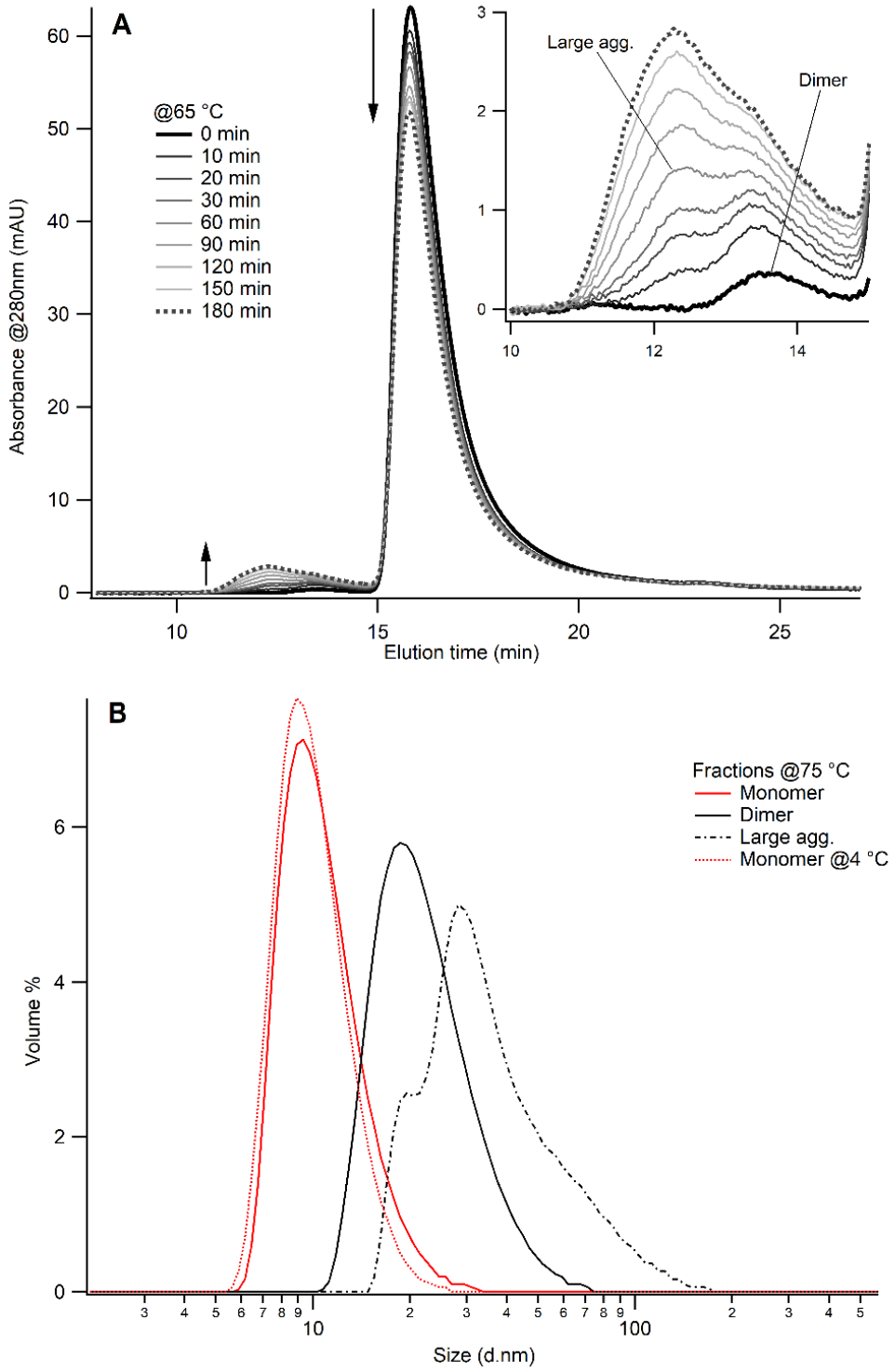

Figure 4. A) Representative SE-HPLC chromatogram of trastuzumab aggregation with inset showing the dimer and large aggregate peaks that were fractionated. B) DLS hydrodynamic diameter measurements of fractioned monomer, dimer and large aggregate species including monomer fractions from unstressed samples (4 °C).

The proportionally high concentration of dimers with respect to each other aggregate size, and the rapid formation of dimers initially (Fig. 3C and D) supports this idea. Thus, the first rate constant k_1 reflects the rapid initial rate of monomer loss due to dimer and possibly trimer formation (k_{m1}, $n \leq 3$), while k_2 reflects the slower rate of monomer loss due to addition of monomers to larger aggregates (k_{m1}, $n > 3$). Interestingly, although dimer formation is expected to proceed via monomer addition only, we did not obtain an ideal fit with a single exponential equation (Fig. 3C). It is not unusual to expect the formation of dimers to proceed via different pathways, or that conformationally-different dimer species are formed, as previously reported [21, 28]. Additionally, there may be small quantities of larger aggregates in the fraction that are unavoidable during fractionation. We can assume that k_1 derived from the dimer double exponential fit is k_{di}, while k_2 may be the average rate of formation of other dimer species and/or non-dimeric species present in the fraction. This is supported by the rate constants obtained from the monomer fits; i.e. k_{m1} for $n \leq 3$ is smaller than k_{di}, which supports our hypothesis, as it is expected that dimers form faster than trimers. The kinetics of large aggregate formation were fit well with both single and double exponential fits (Fig. 3E and F). Thus, we can assume that k_1 represents the average rate constant k_{m2} for all aggregate clustering steps in our model. Alternatively, the two mechanisms may proceed at a similar rate and are therefore indistinguishable from each other.

3.4. Arrhenius behaviour of trastuzumab aggregation and linearization of non-Arrhenius plot using VFT function

The Arrhenius equation is an empirical temperature-dependant function used to describe kinetic data of many processes including decomposition [29], oxidation rate [27] and chemical degradation [30, 31]. Arrhenius plots of reaction rate constants at accelerated conditions are often used to predict shelf-life of small molecule drugs at lower storage temperatures [30, 32-34]. Using rate constants of aggregation obtained with single and double-exponential fits, we extrapolated the accelerated conditions at elevated temperature to predict experimental rate constants for 45 °C (obtained from [26]) and 4 °C (Fig. 5A). $\ln(k_2)$ and $\ln(k)$ inverse temperature plots, appear linear up to 45 °C. Non-Arrhenius behaviour becomes apparent at temperatures below 45 °C as demonstrated by the data point for 4 °C. Because of the linearity of the aggregation kinetics at elevated temperatures, no adjustments were needed to extrapolate the data to lower temperatures such as 4 °C. However, as expected, the extrapolation of

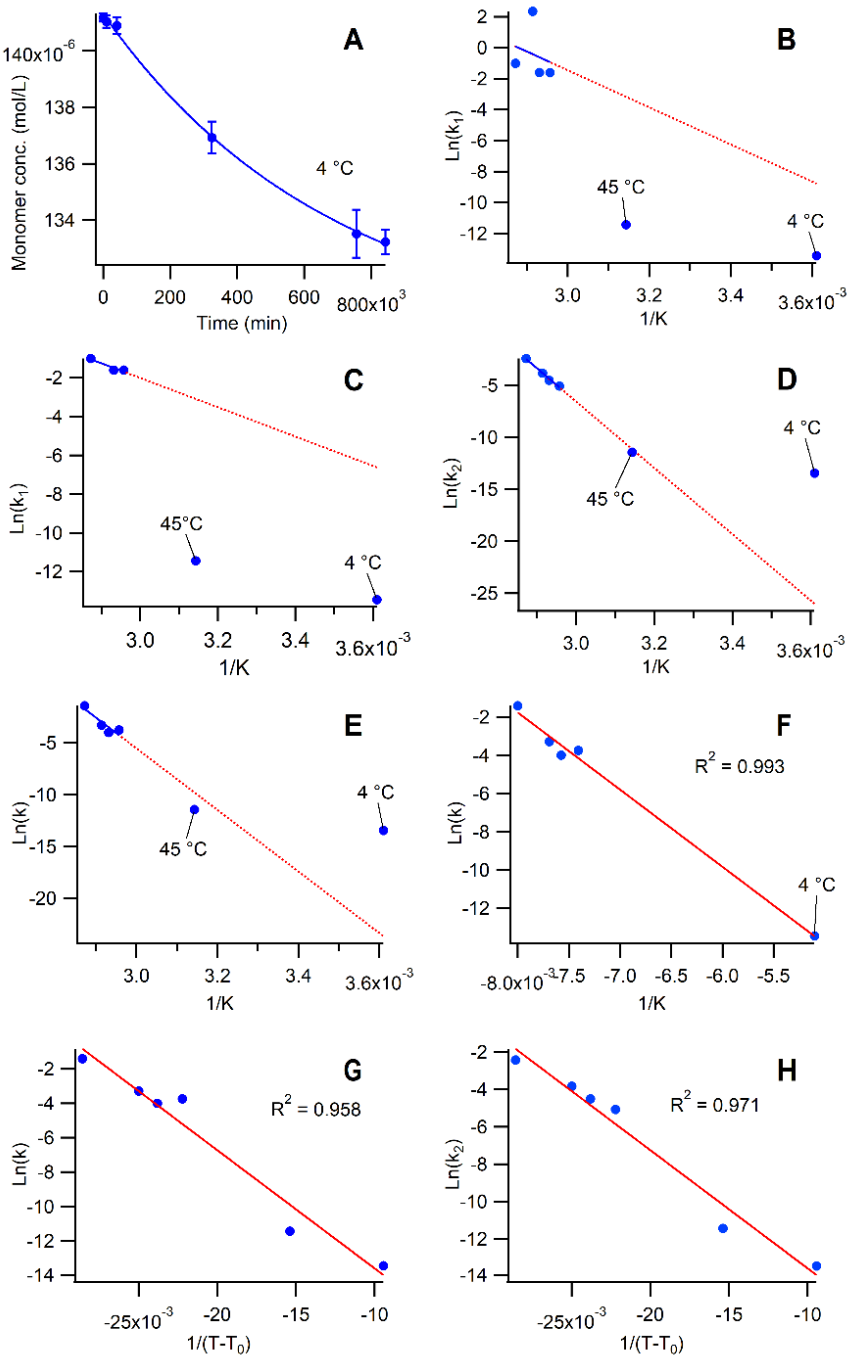

Figure 5. Arrhenius plots and extrapolations of accelerated monomer loss data to lower temperatures. A) Monomer loss kinetics at 4 °C; B) Arrhenius plot of the logarithm of k_1 vs. the inverse temperature in kelvins (rate constant derived from double exponential fit) extrapolated to 45 and 4 °C long-term data; C) Same as B) but excluding the k_1 data point for 70 °C; D) same as B) except plotting the logarithm of k_2 vs. inverse temperature in kelvins; E) Arrhenius plot of the logarithm of k vs. the inverse temperature in kelvins (rate constant derived from single exponential fit) extrapolated to 45 and 4 °C long-term data; F) VFT plot using a T_0 of 200 °C to linearize the non-Arrhenius data from E) at high and low temperatures (excluding rate constant at 45 °C); G) VFT plot using a T_0 of 110 °C to linearize data from E) including rate constant at 45 °C; H) VFT plot at 110 °C to linearize data from D)

accelerated data at elevated temperatures, did not accurately predict the rate constants at 4 °C using Arrhenius equation. Antibody aggregation is known to display non-Arrhenius behaviour [21]; in this case, the non-Arrhenius behaviour only became apparent when incorporating the data at 4 °C, making it difficult to use elevated temperatures as predictors of shelf-life. Several methods have been described in the literature to linearize non-Arrhenius data. Previously, the Vogel-Fulcher-Tammann (VFT) equation showed the most success in predicting mAb shelf-life at lower temperatures, when a T_0 larger than the melting temperature of the mAb was used [24]. The VFT equation is described by the following equation when used to derive Arrhenius parameters:

$$k = A_{VFT} e^{(\frac{B}{T-T_0})}$$

Whereby A_{VFT} is the pre-exponential factor, B is the activation energy and T_0 is the reference temperature. Although in this case we could not use VFT for prediction, we were able to derive a T_0 that fit the entire range of data from 75 to 4 °C. As predicted, this T_0 was greater than the T_m of trastuzumab (T_0 = 110 °C). We also obtained a better linear fit of the rate constants using k_2 values. In our case, more data points with a wider range of elevated temperatures were needed to observe the non-Arrhenius behaviour of trastuzumab aggregation more clearly and perform the prediction of the aggregation rate at lower temperatures. Nonetheless, we obtained an accurate reference temperature that allows prediction of shelf-life between a wide range of temperatures for this antibody formulation. With additional aggregation kinetic data from a large set of IgG1 antibodies, it may be possible to derive a relationship between the VFT reference temperature (T_0) and the T_m of the antibody, which can be used to link accelerated data with long-term storage conditions and predict long-term stability.

4. Conclusion

Protein aggregation continues to be the main complication for the development of novel biologics such as mAbs; a stronger mechanistic understanding of this process is required to elucidate important parameters such as shelf-life, and drive manufacturing decisions to ensure the most aggregation-resistant candidates are developed. We thoroughly analysed the aggregation kinetics of trastuzumab in its original formulation to gain insight into the process of aggregation for therapeutic antibodies. Our findings strengthen our mechanistic understanding of this complex

process by connecting the different steps in the aggregation process through a simple protein aggregation model with insight into utilising the VFT function to determine important parameters such as shelf-life and connection of experimental results from accelerated studies to the long-term storage behaviour.

Acknowledgements

The authors would like to thank Genentech Inc. for their generous donation of Herceptin® to conduct this study. M. Reslan is a recipient of the Research Training Program stipend provided by the University of Sydney on behalf of the Department of Education and Training.

References

[1] Z. Elgundi, M. Reslan, E. Cruz, V. Sifniotis, V. Kayser, The state-of-play and future of antibody therapeutics, Advanced Drug Delivery Reviews.
[2] C. Touzeau, P. Moreau, C. Dumontet, Monoclonal antibody therapy in multiple myeloma, Leukemia, 31 (2017) 1039.
[3] H.M. Shepard, G.L. Phillips, C. D Thanos, M. Feldmann, Developments in therapy with monoclonal antibodies and related proteins, Clinical Medicine, 17 (2017) 220-232.
[4] C. Klein, Special Issue: Monoclonal Antibodies, Antibodies, 7 (2018) 17.
[5] S. Zheng, D. Qiu, M. Adams, J. Li, R.V. Mantri, R. Gandhi, Investigating the Degradation Behaviors of a Therapeutic Monoclonal Antibody Associated with pH and Buffer Species, AAPS PharmSciTech, 18 (2017) 42-48.
[6] C.J. Roberts, Non-native protein aggregation kinetics, Biotechnology and Bioengineering, 98 (2007) 927-938.
[7] T.W. Randolph, J.F. Carpenter, Engineering challenges of protein formulations, AIChE Journal, 53 (2007) 1902-1907.
[8] R. van der Kant, A.R. Karow-Zwick, J. Van Durme, M. Blech, R. Gallardo, D. Seeliger, K. Aßfalg, P. Baatsen, G. Compernolle, A. Gils, J.M. Studts, P. Schulz, P. Garidel, J. Schymkowitz, F. Rousseau, Prediction and Reduction of the Aggregation of Monoclonal Antibodies, Journal of Molecular Biology, 429 (2017) 1244-1261.
[9] M.L. Fleischman, J. Chung, E.P. Paul, R.A. Lewus, Shipping-Induced Aggregation in Therapeutic Antibodies: Utilization of a Scale-Down Model to Assess Degradation in Monoclonal Antibodies, Journal of Pharmaceutical Sciences, 106 (2017) 994-1000.

[10] N. Michal, Ž. Gabriel, S.J. V., K. Florian, M. Pavol, P. Andreas, S. Erik, Analysis of IgG kinetic stability by differential scanning calorimetry, probe fluorescence and light scattering, Protein Science, 26 (2017) 2229-2239.
[11] N. Kim, R.L. Remmele, D. Liu, V.I. Razinkov, E.J. Fernandez, C.J. Roberts, Aggregation of anti-streptavidin immunoglobulin gamma-1 involves Fab unfolding and competing growth pathways mediated by pH and salt concentration, Biophysical Chemistry, 172 (2013) 26-36.
[12] H. Imamura, A. Sasaki, S. Honda, Fate of a Stressed Therapeutic Antibody Tracked by Fluorescence Correlation Spectroscopy: Folded Monomers Survive Aggregation, The Journal of Physical Chemistry B, 121 (2017) 8085-8093.
[13] P. Arosio, S. Rima, M. Lattuada, M. Morbidelli, Population Balance Modeling of Antibodies Aggregation Kinetics, The Journal of Physical Chemistry B, 116 (2012) 7066-7075.
[14] C.J. Roberts, Kinetics of Irreversible Protein Aggregation: Analysis of Extended Lumry−Eyring Models and Implications for Predicting Protein Shelf Life, The Journal of Physical Chemistry B, 107 (2003) 1194-1207.
[15] Z. Sahin, Y.K. Demir, V. Kayser, Global kinetic analysis of seeded BSA aggregation, European Journal of Pharmaceutical Sciences, 86 (2016) 115-124.
[16] J.M. Andrews, C.J. Roberts, A Lumry−Eyring Nucleated Polymerization Model of Protein Aggregation Kinetics: 1. Aggregation with Pre-Equilibrated Unfolding, The Journal of Physical Chemistry B, 111 (2007) 7897-7913.
[17] I.A. Iashchishyn, D. Sulskis, M. Nguyen Ngoc, V. Smirnovas, L.A. Morozova-Roche, Finke–Watzky Two-Step Nucleation–Autocatalysis Model of S100A9 Amyloid Formation: Protein Misfolding as “Nucleation” Event, ACS Chemical Neuroscience, 8 (2017) 2152-2158.
[18] A.M. Morris, M.A. Watzky, J.N. Agar, R.G. Finke, Fitting Neurological Protein Aggregation Kinetic Data via a 2-Step, Minimal/“Ockham's Razor” Model: The Finke−Watzky Mechanism of Nucleation Followed by Autocatalytic Surface Growth, Biochemistry, 47 (2008) 2413-2427.
[19] L. Nicoud, M. Sozo, P. Arosio, A. Yates, E. Norrant, M. Morbidelli, Role of Cosolutes in the Aggregation Kinetics of Monoclonal Antibodies, The Journal of Physical Chemistry B, 118 (2014) 11921-11930.

[20] V. Kayser, N. Chennamsetty, V. Voynov, B. Helk, K. Forrer, B.L. Trout, Evaluation of a Non-Arrhenius Model for Therapeutic Monoclonal Antibody Aggregation, Journal of Pharmaceutical Sciences, 100 (2011) 2526-2542.
[21] V. Kayser, N. Chennamsetty, V. Voynov, B. Helk, K. Forrer, B.L. Trout, Evaluation of a non-Arrhenius model for therapeutic monoclonal antibody aggregation, Journal of Pharmaceutical Sciences, 100 (2011) 2526-2542.
[22] V. Kayser, N. Chennamsetty, V. Voynov, B. Helk, B.L. Trout, Tryptophan-Tryptophan Energy Transfer and Classification of Tryptophan Residues in Proteins Using a Therapeutic Monoclonal Antibody as a Model, Journal of Fluorescence, 21 (2011) 275-288.
[23] J.S. Bee, M. Davis, E. Freund, J.F. Carpenter, T.W. Randolph, Aggregation of a monoclonal antibody induced by adsorption to stainless steel, Biotechnology and Bioengineering, 105 (2010) 121-129.
[24] V. Kayser, N. Chennamsetty, V. Voynov, B. Helk, B.L. Trout, Conformational stability and aggregation of therapeutic monoclonal antibodies studied with ANS and Thioflavin T binding, mAbs, 3 (2011) 408-411.
[25] A.A. Wakankar, M.B. Feeney, J. Rivera, Y. Chen, M. Kim, V.K. Sharma, Y.J. Wang, Physicochemical Stability of the Antibody−Drug Conjugate Trastuzumab-DM1: Changes due to Modification and Conjugation Processes, Bioconjugate Chemistry, 21 (2010) 1588-1595.
[26] K. Kristina, A. Jens, D. Roland, K. Thomas, R. Eva, S. Martin, Amino Acid‐Based Advanced Liquid Formulation Development for Highly Concentrated Therapeutic Antibodies Balances Physical and Chemical Stability and Low Viscosity, Biotechnology Journal, 0 (2018) 1700523.
[27] C. S., M. L., C. L.S., N. M.C., Application of a Modified Arrhenius Equation for the Evaluation of Oxidation Rate of Sunflower Oil at Subzero Temperatures, Journal of Food Science, 69 (2004) E361-E366.
[28] S. Krishnan, E.Y. Chi, J.N. Webb, B.S. Chang, D. Shan, M. Goldenberg, M.C. Manning, T.W. Randolph, J.F. Carpenter, Aggregation of Granulocyte Colony Stimulating Factor under Physiological Conditions: Characterization and Thermodynamic Inhibition, Biochemistry, 41 (2002) 6422-6431.

[29] D. Dollimore, P. Tong, K.S. Alexander, The kinetic interpretation of the decomposition of calcium carbonate by use of relationships other than the Arrhenius equation, Thermochimica Acta, 282-283 (1996) 13-27.
[30] K.C. Waterman, The Application of the Accelerated Stability Assessment Program (ASAP) to Quality by Design (QbD) for Drug Product Stability, AAPS PharmSciTech, 12 (2011) 932.
[31] V. La Saponara, Environmental and chemical degradation of carbon/epoxy and structural adhesive for aerospace applications: Fickian and anomalous diffusion, Arrhenius kinetics, Composite Structures, 93 (2011) 2180-2195.
[32] A. Patterson, A.P. Ferreira, E. Banks, K. Skeene, G. Clarke, S. Nicholson, C. Rawlinson-Malone, Modelling drug degradation in a spray dried polymer dispersion using a modified Arrhenius equation, International Journal of Pharmaceutics, 478 (2015) 348-360.
[33] I.T. Some, P. Bogaerts, R. Hanus, M. Hanocq, J. Dubois, Incorporating batch effects in the estimation of drug stability parameters using an Arrhenius model, International Journal of Pharmaceutics, 184 (1999) 165-172.
[34] M. Blessy, R.D. Patel, P.N. Prajapati, Y.K. Agrawal, Development of forced degradation and stability indicating studies of drugs—A review, Journal of Pharmaceutical Analysis, 4 (2014) 159-165.

CHAPTER 6

“Choline Ionic Liquid Enhances the Stability of Herceptin® (Trastuzumab)”

Graphical abstract

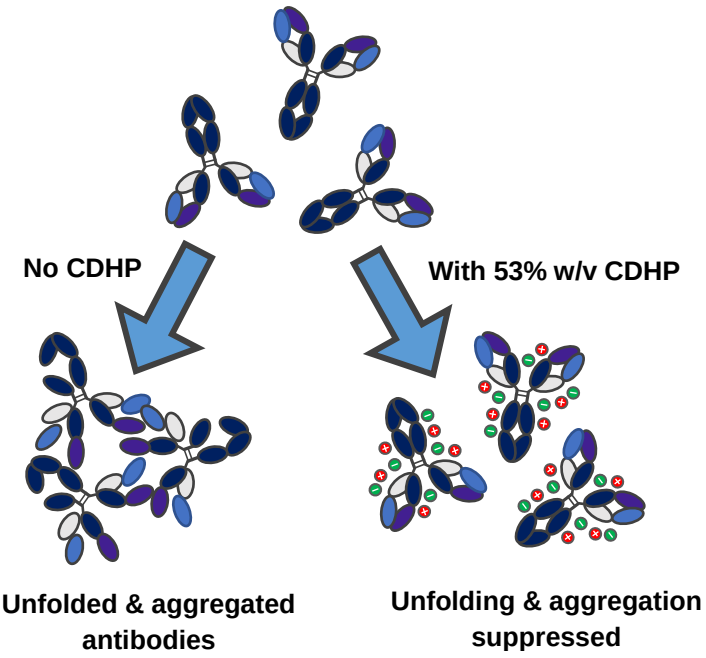

Chapter 6 was published as a communication article at Chemical Communications:

Reslan, M., Vijayaraghavan R., Macfarlane D. R., Kayser, V. (2018). Choline ionic liquid enhances the stability of Herceptin® (trastuzumab). Chemical Communications, 54:10622-10625.

Supplementary information was combined with the manuscript for the thesis chapter with other minor changes.

Short Abstract

We investigated the effect of an emerging biocompatible ionic liquid, choline dihydrogen phosphate (CDHP), on the stability of high-concentration formulations of Herceptin® (trastuzumab). Our results show that CDHP significantly suppresses unfolding and aggregation of trastuzumab, demonstrating great promise as an additive in the development of stable therapeutic antibody formulations.

1. Introduction

Therapeutic monoclonal antibodies (mAbs) are an ever-growing class of biologics widely used in diagnostics and in the treatment of a variety of ailments including cancer and auto-immune diseases. Antibodies have been used in various formats including, as whole antibodies and fragments, linked to other drugs as an antibody-drug conjugate [1], or modified to form a bispecific antibody which binds to two targets [2, 3]. Various novel antibody-based formulations are also in development, including nanobodies [4], nanoparticle formulations and more [2]. mAbs have dominated the list of top 10 best-selling drugs worldwide in the last decade, with more than 70 mAb products currently on the market and hundreds in the development pipeline [2, 5, 6]. Undoubtedly, mAbs are an extremely useful class of therapeutics; however, like other proteins, they pose several challenges for manufacturers during production, transport and storage, and patients who are administered these products.

One of the most significant challenges with the development of antibody products is protein aggregation, which not only results in the loss of activity and therapeutic efficiency but can also cause undesired immunogenic reactions to patients administered these products [7, 8]. Generally, protein aggregation is addressed either via mutational studies [9-11] or using stabilizing excipients which are added to the formulation [12-14]. If the protein stability and aggregation still pose a problem, then the final product can be freeze-dried to further extend the shelf-life of the product [15, 16]. Even though some antibody products have been developed as subcutaneous injections at high concentrations, there is still an urgent need for novel choices of stabilizing excipients to pave the way for the development of non-invasive drug delivery options, which are more convenient for patients and prolong the shelf-life of these products.

Ionic liquids (ILs) are a versatile class of compounds utilised in applications including electrochemistry [17], fuel production [18], bio-catalysis [19], analytics and biotechnology [20]. Put simply, ILs are 'molten' salts, typically having melting points below 100 °C, and possess several useful physicochemical properties determined by the combination of organic cation and anion [21]. These properties include, negligible vapor pressures, high thermal stabilities, high conductivities and non-flammability. ILs have been shown to influence the stability and activity of certain enzymes when added into the storage buffers or used as a solvent [22]. In particular, the choline family of ILs have exhibited protein-stabilizing effects in some cases. Some of the proteins that have been investigated using choline-ILs include cytochrome complex (cyt C) [23-25], α-chymotrypsinogen (CT) [26], lysozyme [27-29] and more [30, 31]. Mondal et al., [32] showed that aqueous biphasic systems based on choline ILs were excellent platforms for purification of antibodies, partly due to keeping antibodies stable during extraction.

Of several choline-ILs studied, choline dihydrogen phosphate (CDHP) appears to be the most suitable candidate for the stabilization of therapeutically important proteins such as mAbs, owing to its overall stabilizing potential and biocompatibility [33-35]. For instance, Foureau, et al. [36] found that recombinant human interleukin-2 (rHIL-2) had increased thermal stability with 12% CDHP and had no cytotoxicity in mouse melanoma and primary splenocytes at physiological concentrations of up to 80 mM. Additionally, Jagannath et al.[37] found that CDHP appears to reduce aggregation of capture probe antibodies.

We previously [38], showed that CDHP inhibits the fragmentation of an EGFR mAb and does not reduce antigen binding efficiency. Besides these few studies, research is lacking on the potential use of CDHP or other ILs for the stabilization of therapeutic mAbs and prevention of mAb aggregation. Hereby, we have studied the effect of CDHP on the stability of trastuzumab, a marketed therapeutic mAb used for the treatment of HER2+ breast cancer, as a model for IgG1 therapeutic mAbs and other antibody products. We are the first to assess the potential of CDHP to be used as an excipient for the stabilization of trastuzumab with and without other stabilizing excipients and determine its usefulness as a solvent or excipient for high concentration antibody formulations.

2. Materials and Methods

2.1. Materials

Herceptin® was obtained from Genentech (San Francisco, US) as freeze-dried powder containing (858.1 mg): 51.4% trastuzumab, 0.74% L-histidine, 1.15% L-histidine hydrochloride monohydrate, 46.7% trehalose dihydrate and 0.01% polysorbate 20. Millex-GV syringe filter units (0.22 µm, PVDF, 33 mm, gamma sterilized, SLGV033RS), Amicon® centrifugal filters (Ultracell® 50,000 NMWL), di-potassium hydrogen phosphate (EMPROVE® Ph Eur, BP, E 340 grade, 105101) and potassium dihydrogen phosphate (EMSURE® ISO grade, 104873) were purchased from Merck Millipore (MA, USA). All other reagents were obtained from Sigma Aldrich and used without further purification.

2.2. Synthesis and characterization of choline dihydrogen phosphate (CDHP)

CDHP was made by neutralization reaction involving 1 mole of choline hydroxide with 1 mole of phosphoric acid as given in the literature[35]. Typically, 10 g of CDHP was made by slow addition of an aqueous solution (85%) of phosphoric acid (5.7g, 58 mmoles) to 20% aqueous choline hydroxide solution (30.1g, 248 mmoles) in an ice bath. The contents were stirred for about 1 hour at room temperature and the mixture was roto-evaporated at reduced pressures to obtain crude CDHP. To the crude compound activated charcoal (approx. 1 g) was added, stirred with water and filtered. The filtrate was again evaporated to get pure white solid in 98% yield. The sample was characterized by Electrospray Mass spectrometry to reveal the presence of the cation and anion.

Electrospray Mass spectroscopy analysis, (cone ±35V): CDHP, *m/z* (relative intensity, %): ES^+, 103.9 ($Me_3N^+CH_2CH_2OH$, 100); ES^-, 96.9 ($H_2PO_4^-$, 100). The acid base stoichiometry was confirmed by determining the pH of a 0.1 M aqueous solution of the material. This was found to be in satisfactory agreement with a control aqueous sample (pH= 5.6).

^{13}C NMR (600 MHz, D_2O) δ: 67.3 (CH_2), 55.5 (CH_2), 53.8 (3 x CH_3)

^1H NMR (300.13 MHz in D_20, δ, ppm relative to TMS): 3.16(s,9H), 3.49-3.46(m,2H), 4.04-4.06(m, 2H). The choline OH proton and OH protons from dihydrogen phosphate appear to be exchanged with the solvent D_2O peak at 4.67 ppm.

The purity of the synthesised CDHP was determined to be 99.5% (based on 1H NMR spectrum) and observed only tiny impurities at around 2.7ppm (to an extent of ~0.5 %). The peak integral shows 9 protons (for 3 methyl groups of choline cation), 2 protons for methylene groups (attached to Nitrogen atom) and another 2 protons for methylene groups (attached to oxygen atom).

Elemental analysis (%), calculated: C 29.85, N 6.96, H 7.96; found: C 28.10, N 6.87, H 8.09.

2.3. Formulation preparation

Two sets of Herceptin® formulations were prepared: (1) 20 mg/mL antibody formulations containing no other excipients besides any added CDHP; and (2) 60 mg/mL antibody formulations containing the excipients present in the Herceptin® formulation as provided by the manufacturer in the same antibody:excipient ratio, in addition to any added CDHP (Table 1). The formulations prepared were designed to test:

1) The effect of CDHP alone on antibody stability, in addition to its effect in combination with excipients commonly used in marketed antibody products. This way, its compatibility and potential synergy with other stabilizing excipients can be tested.

2) The effect of CDHP on antibody stability in formulations containing high antibody concentrations

3) Whether the influence of CDHP on protein stability is related to the protein:ionic liquid ratio or the ionic liquid:solvent ratio, which would determine its practicality in more highly concentrated protein formulations.

Buffer exchange and concentration of Herceptin® solutions was performed using 50 kDa centrifugal filters to achieve the desired formulation. Due to the high viscosity of CDHP stock solutions concentrated Herceptin® solutions were diluted in CDHP to the desired antibody (20 mg/mL) and IL concentration to minimize unwanted aggregation. For 60 mg/mL formulations, the Herceptin® powder provided (containing the excipients listed in Materials section) was dissolved in water (control), a solution of 53% w/v CDHP or 30% w/v CDHP such that the final concentration of trastuzumab was 60 mg/mL in each formulation and the antibody:excipient ratio was maintained.

Table 1. Trastuzumab (TmAb) formulations prepared for this study

Formulation	[TmAb] mg/mL	[CDHP] % w/v	Buffer
Control	20	0	15 mM potassium phosphate
53% CDHP	20	53	Water
40% CDHP	20	40	
25% CDHP	20	25	
Control H	60	0	5.5 mM L-histidine, 6.4 mM L-histidine HCL monohydrate, 144 mM trehalose dihydrate and 0.001% w/v polysorbate 20
53% CDHP H	60	53	
30% CDHP H	60	30	

Dissolution was achieved by keeping each formulation at 4 °C overnight with gentle pipetting to assist dissolution of all the powder. When necessary, sodium hydroxide and phosphoric acid were used to adjust solution pH to 6 for all formulations. Solutions were filtered using 0.22 µm syringe filter units then the UV absorbance at 280 nm was checked to confirm the concentration of trastuzumab in each formulation was 60 mg/mL. All formulations were stored at 4 °C until needed.

2.4. Accelerated aggregation studies at elevated temperature

5 µL of each antibody formulation was pipetted into a 0.2 mL PCR vial and incubated at 68 °C in a Thermal Cycler (Applied Biosystems, CA, USA) for various durations to induce aggregation as previously described[39]. A thermal cycler was used to: 1) minimize sample amount; 2) prevent evaporation of the sample and consequent changes in antibody concentration during incubation (lid/cover of thermal cycler is heated above incubation temperature). Following incubation, incubated samples were removed and immediately stored on ice to halt aggregation and then characterized by size exclusion-high performance liquid chromatography (SE-HPLC). To investigate the nature of aggregates formed in the 60 mg/mL formulations, each of the 60 mg/ml formulations that were incubated at 68 °C were also kept for 20 hours at 4 °C after dilution, then monomer content was re-measured using SE-HPLC.

2.5. SE-HPLC

Size exclusion-high performance liquid chromatography (SE-HPLC) was used to quantify antibody monomer loss following incubation at 68 °C. Analysis was performed using an Agilent 1200 Liquid Chromatography system (Agilent Technologies, California, USA) with a Zorbax GF-250 column coupled to a guard column at 22 °C, using a 150 mM potassium phosphate mobile phase, at pH 6.5, and a flow rate of 0.5 mL/min. The incubated 5 µL samples of each trastuzumab formulation were diluted to 50 µL with mobile phase buffer prior to injection to prevent blockage of column with high amounts of protein. 10 µL of the diluted samples were then immediately injected and each injection was repeated three times. Stressed 60 mg/mL samples were re-injected after 20 hours at 4 °C. Monomer peaks were detected using an in-line UV signal detector set at 280 nm. The area under the curve (AUC) of the monomer peak was averaged over the three runs and the mean relative monomer % was calculated for each sample, by setting the monomer AUC of the unincubated samples as 100% and calculating the change in monomer AUC accordingly. The standard deviations (SD) were plotted as error bars in the figures.

2.6. Trastuzumab melting temperature (T_m) and onset temperature of aggregation (T_{agg})

Intrinsic tryptophan fluorescence and static light scattering (SLS) techniques were used to calculate the T_m and T_{agg} respectively, of each formulation. A linear temperature ramp from 15 to 95 °C at 1 °C/min scan rate was performed whilst measuring tryptophan fluorescence and SLS simultaneously through laser excitation at 473 nm using UNcle (Unchained Labs, CA, USA). 8.5 µL of each formulation was pipetted undiluted into the UNcle UNI (a sample holding unit containing 16 quartz cells) in triplicates. A holding time was not used to maximise the frequency of measurements. T_m and T_{agg} were determined by the UNcle Analysis software, and in some cases manually, by using the first derivative (for T_m determination). The barycentric mean (BCM) was used to plot the T_m curves, which is defined by the following equation:

$$\lambda_{BCM} = \frac{\sum_\lambda \lambda I(\lambda)}{\sum_\lambda I(\lambda)}$$

The equation is defined over the range 300-450 nm, whereby each wavelength value (λ) is multiplied by the tryptophan fluorescence intensity (*I*) at that wavelength, and the sum of that value for all wavelengths between 300 to 450 is divided by the sum of the intensities at those wavelengths. This results in an 'averaged' peak wavelength (λ_{BCM})

for a given spectrum which eliminates noise and accommodates for changes in the shape of the spectrum. Since antibodies are multi-domain proteins, up to three T_ms can be measured, corresponding to the C_H2, Fab and C_H3 domains. For trastuzumab only two T_ms are usually distinguishable as the Fab and C_H3 domain have approximately the same T_m, leading to overlap.

2.7. UV-Vis spectroscopy

UV-Vis spectroscopy was used to measure the concentration of soluble antibody after dissolution of powder to ensure complete dissolution and following incubation at elevated temperatures to confirm the lack of insoluble aggregates. Absorbance was measured at 280 nm over a wavelength range of 220-350 nm using a Shimadzu UV-2600 spectrophotometer (Shimadzu, Japan). Samples were corrected by blank subtraction of the respective solvent. Data was not included as the absorbance of all samples remained unchanged following incubation, and therefore no change in soluble antibody concentration was observed.

3. Results and discussion

Our results demonstrated for the first time, that CDHP significantly suppresses the unfolding of trastuzumab by stabilizing the C_H2, Fab and C_H3 domains as demonstrated by the significant improvements in all T_ms measured. The improvements in T_ms are seen in both formulations of trastuzumab (20 and 60 mg/mL) with and without other stabilizing-excipients, suggesting that the effect is additive. The T_ms of excipient-free trastuzumab measured in our study corresponds with literature values; DSC studies with separate Fab and Fc fragments of trastuzumab identified that the first transition corresponds to the unfolding of the C_H2 domain, and the second transition is an overlap of the Fab and C_H3 domain [40, 41]. In most excipient-free formulations containing CDHP, three distinct T_ms are identified, whereas only two are determined in the control (Fig. 1A and B; table 2). This suggests that CDHP improves the stability of all regions of trastuzumab but either the Fab or the C_H3 domain is stabilized more strongly than the other, leading to the separation of those two T_ms. Interestingly, the stabilizing effect is proportional to the concentration of CDHP in the formulation, with higher concentrations (53% w/v) increasing the T_ms the most. A similar trend is shown by [42] who found that CDHP had a destabilizing effect on lysozyme below 0.5 M and a stabilizing effect above this concentration. This protein

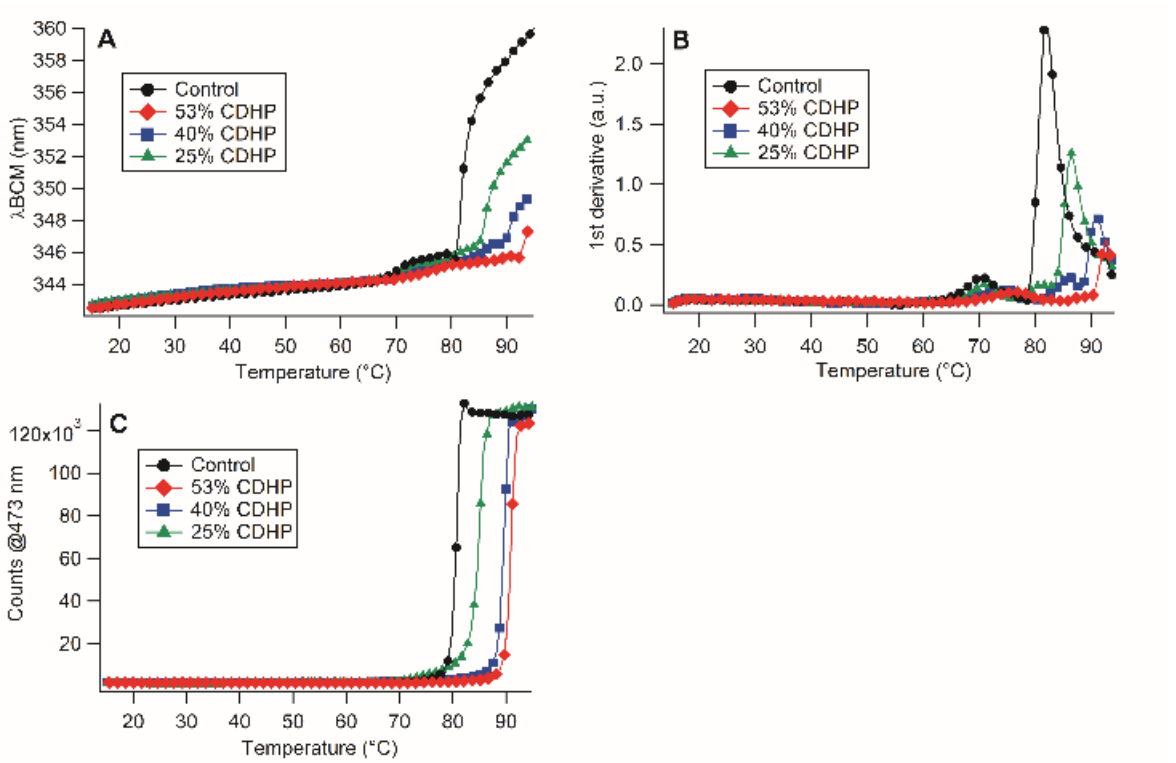

Figure 1. Representative T_m and T_{agg} curves of trastuzumab formulations (20 mg/mL) with and without CDHP. (A) The change in Trp BCM wavelength throughout the temperature ramp; (B) the 1st derivative of data in (A) showing the T_ms of each formulation at the peaks; (C) Changes in SLS counts at 473 nm throughout the temperature ramp showing the T_{agg} of each formulation

stabilizing effect has been attributed to the DHP anion inducing water restructuring around the protein [26]. Additionally, at higher concentrations each DHP anion may form strong interactions with many positively charged residues on the antibody surface forcing it into a more compact conformation and enhancing the antibody's thermal stability [43].

It is commonly believed that unfolding is a precursor to protein aggregation, and many models of protein aggregation kinetics incorporate unfolding as a crucial step in the protein aggregation pathway (see supplementary table by Kayser, et al. [39] for a summary of commonly used kinetic models) Accordingly, it is expected that CDHP would also inhibit protein aggregation, as it significantly suppresses trastuzumab unfolding. Indeed, we observed that in the presence of CDHP the T_{agg} of trastuzumab was also significantly increased in a concentration-dependant trend, demonstrating a strong inhibition of aggregation in formulations containing CDHP; however, T_{agg} is based on light scattering signals and therefore may only detect the formation of

insoluble aggregates (precipitates) which form in the late stages of antibody aggregation.

To reach a more complete understanding of the entire aggregation process, we measured the formation of soluble aggregates that typically form during storage or manufacturing through accelerated studies at 68 °C. This was achieved through short incubation times to limit the degree of aggregation. From these results, we identified that there is a strong initial suppression of aggregation (first ~10% of monomer loss) in formulations containing 53% CDHP at both concentrations of trastuzumab (Fig. 2 and 3). Interestingly however, monomer loss proceeds faster in CDHP formulations after this initial stage of antibody aggregation. The reversibility data of these aggregates provides valuable insight into the protein aggregation process in CDHP. After storing the stressed/incubated samples at 4 °C for 20 hours, we observed a significant recovery of monomeric species for formulations containing 53% CDHP, especially for the 90-minute-stressed samples which had significantly lower monomer content than the control (Fig. 3). The recovery is so significant that the final monomer content of these formulations is higher than the control after incubation at 4 °C.

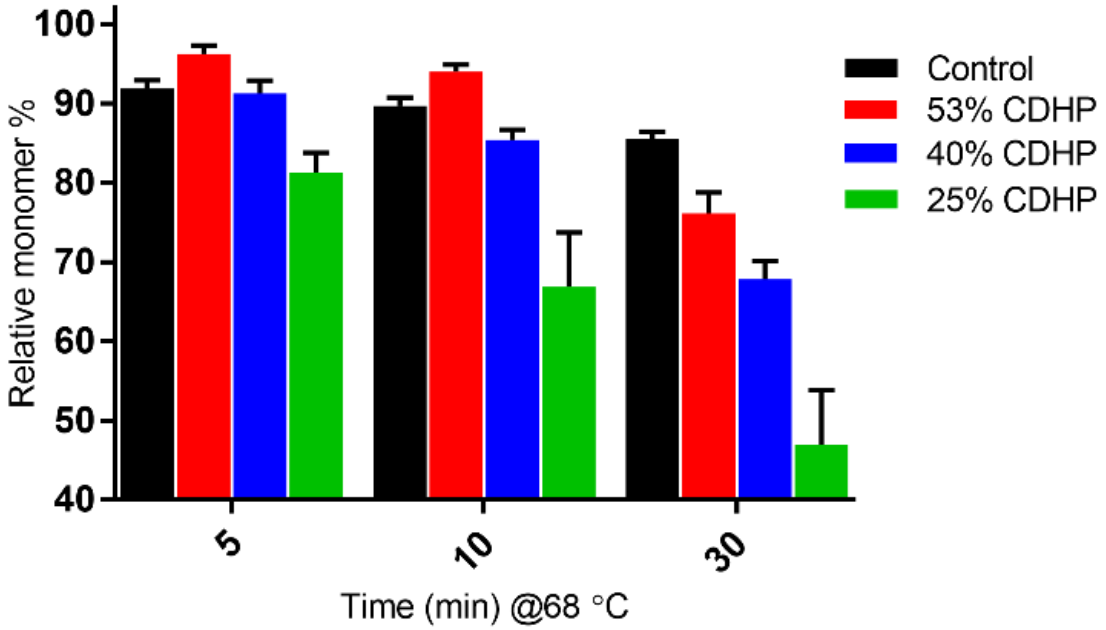

Figure 2. Mean relative monomer loss % of the 20 mg/mL trastuzumab formulations following incubation at 68 °C for 5, 10 and 30 minutes. Time point 'zero' is 100% monomer. The error bars represent the SD.

Table 2. The T_m and T_{agg} values of the 20 mg/mL trastuzumab formulations

Formulation	T_m1	T_m2	T_m3	T_{agg} @473 nm
Control	70.5 ± 0.4	-	82.2 ± 0.3	79 ± 0.5
53% CDHP	76.1 ± 0.4	86.6 ± 1.4	92 ± 0.3	89.4 ± 0.3
40% CDHP	73.7 ± 0.6	85.1 ± 0.4	89.9 ± 0.4	86.9 ± 0.5
25% CDHP	70.6 ± 0.4	-	85.8 ± 0.3	81.3 ± 0.2

Table 3. The T_m and T_{agg} values of the 60 mg/mL trastuzumab formulations

Formulation (60 mg/mL)	T_m1	T_m2	T_m3	T_{agg} @473 nm
Control H	72.9 ± 0.2	-	88.2 ± 0.9	81.2 ± 1.5
53% CDHP H	-	-	94.0± 0.5	90.3 ± 0.1
30% CDHP H	77.8 ± 1.4	-	89.7 ± 0.2	83.5 ± 0.1

This demonstrates that the significant monomer loss observed in CDHP formulations after the initial ~10% aggregation which occurs at 90 minutes of incubation is predominantly due to the formation of reversible species, which revert to monomers over time. We propose the following simplified model of trastuzumab aggregation:

$$M \leftrightarrow U \leftrightarrow rA \rightarrow pA$$
$$\downarrow$$
$$iA \rightarrow pA$$

Whereby M = monomer; U = partially unfolded monomer; rA = reversible small aggregates; iA = irreversible soluble aggregates; pA = irreversible insoluble aggregates (precipitates). Thus, in summary CDHP:

1) Suppresses trastuzumab unfolding (suppresses M→U reaction) especially at 53% CDHP
2) At 53% w/v: promotes reversible aggregation (promotes U→rA) and suppresses irreversible soluble aggregation (suppresses U→iA)
   At 30% w/v: promotes both reversible and irreversible soluble aggregation (U→rA and iA)

3) Inhibits formation of insoluble aggregates (suppresses rA/iA→pA) especially at 53% CDHP

At low [CDHP] unfolding is not as strongly suppressed, and irreversible aggregation dominates, thus, we observe significant monomer loss and minimal reversibility. While at 53% CDHP, both unfolding and irreversible aggregation are significantly suppressed, resulting in reduced monomer loss. Reversible aggregation dominates at later stages of aggregation.

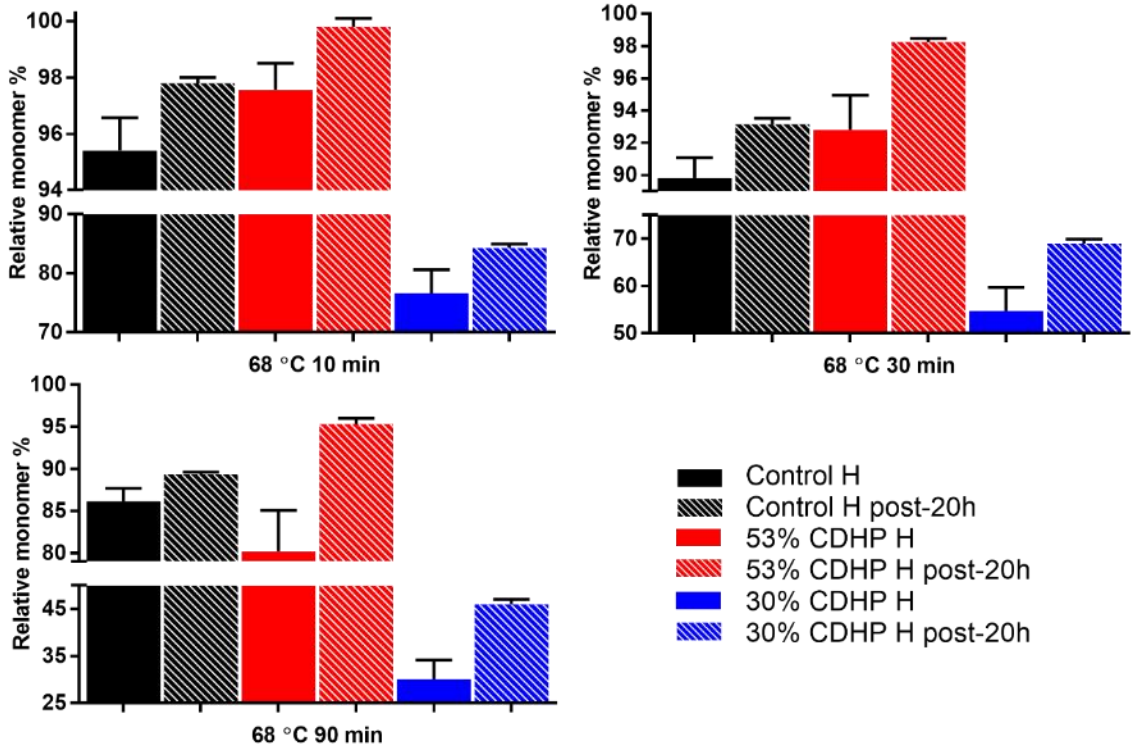

Figure 3. Mean relative monomer loss of the 60 mg/mL trastuzumab formulations following incubation at 68 °C for 10, 30 and 90 minutes. Time point 'zero' is 100% monomer. 'post-20h' are the stressed samples re-measured after 20 hours at 4 °C. The error bars represent the SD.

It is generally accepted that therapeutic antibody formulations must not exceed >5% aggregates to minimize the risk of immunogenicity [44, 45]. At 53% w/v, CDHP acts as a strong stabilizer against aggregation in the initial stages of monomer loss up to ~90% relative monomer %. Even if the formation of reversible aggregates after this stage is undesirable, the strong suppression of aggregation up to ~10% is extremely useful in the context of developing safe therapeutic antibody formulations.

The fact that the trends observed are consistent in both the 20 mg/mL (excipient-free) and 60 mg/mL formulations illustrates that:

1) Stability is based on ionic liquid:solvent ratio rather than protein:ionic liquid ratio
2) The effects observed are due to CDHP and not other excipients only
3) The stabilizing effect of CDHP is maintained when combined with other stabilizing excipients and may be strategically incorporated in a formulation to enhance formulation stability further, even for relatively stable antibodies such as trastuzumab
4) CDHP can be used to stabilize antibodies against aggregation at high antibody concentrations

4. Conclusion

Ionic liquids have emerged as versatile solvents and additives in a wide range of applications and industries spanning organic chemistry and biotechnology. Amongst the many applications within the biotechnology industry, is the use of ILs for protein stabilization, whereby CDHP has emerged as one of the most promising biocompatible ILs for the stabilization of biopharmaceuticals. We have demonstrated for the first time that CDHP can be used to stabilize trastuzumab in high concentrations and in combination with other excipients, against unfolding and irreversible aggregation. Our results pave the way for utilising ILs such as CDHP as stabilizing additives in much needed rationally engineered formulations of therapeutic mAbs.

Acknowledgements

The authors would like to thank Genentech, Inc. for their generous supply of Herceptin® to perform our studies. M. Reslan is a recipient of the Research Training Program stipend provided by the University of Sydney on behalf of the Department of Education and Training to support his research training.

References

[1] S.M. Lehar, T. Pillow, M. Xu, L. Staben, K.K. Kajihara, R. Vandlen, L. DePalatis, H. Raab, W.L. Hazenbos, J. Hiroshi Morisaki, J. Kim, S. Park, M. Darwish, B.-C. Lee, H. Hernandez, K.M. Loyet, P. Lupardus, R. Fong, D. Yan, C. Chalouni, E. Luis, Y. Khalfin, E. Plise, J. Cheong, J.P. Lyssikatos, M. Strandh, K. Koefoed, P.S. Andersen, J.A.

Flygare, M. Wah Tan, E.J. Brown, S. Mariathasan, Novel antibody–antibiotic conjugate eliminates intracellular S. aureus, Nature, 527 (2015) 323.
[2] Z. Elgundi, M. Reslan, E. Cruz, V. Sifniotis, V. Kayser, The state-of-play and future of antibody therapeutics, Advanced Drug Delivery Reviews, 122 (2017) 2-19.
[3] M. Bacac, T. Fauti, J. Sam, S. Colombetti, T. Weinzierl, D. Ouaret, W. Bodmer, S. Lehmann, T. Hofer, R.J. Hosse, E. Moessner, O. Ast, P. Bruenker, S. Grau-Richards, T. Schaller, A. Seidl, C. Gerdes, M. Perro, V. Nicolini, N. Steinhoff, S. Dudal, S. Neumann, T. von Hirschheydt, C. Jaeger, J. Saro, V. Karanikas, C. Klein, P. Umaña, A Novel Carcinoembryonic Antigen T-Cell Bispecific Antibody (CEA TCB) for the Treatment of Solid Tumors, Clinical Cancer Research, 22 (2016) 3286-3297.
[4] A. Desmyter, S. Spinelli, A. Roussel, C. Cambillau, Camelid nanobodies: killing two birds with one stone, Current Opinion in Structural Biology, 32 (2015) 1-8.
[5] D.M. Ecker, S.D. Jones, H.L. Levine, The therapeutic monoclonal antibody market, mAbs, 7 (2015) 9-14.
[6] H. Kaplon, J.M. Reichert, Antibodies to watch in 2018, mAbs, 10 (2018) 183-203.
[7] C.J. Roberts, Protein aggregation and its impact on product quality, Current Opinion in Biotechnology, 30 (2014) 211-217.
[8] E.M. Moussa, J.P. Panchal, B.S. Moorthy, J.S. Blum, M.K. Joubert, L.O. Narhi, E.M. Topp, Immunogenicity of Therapeutic Protein Aggregates, Journal of Pharmaceutical Sciences, 105 (2016) 417-430.
[9] N. Chennamsetty, V. Voynov, V. Kayser, B. Helk, B.L. Trout, Design of therapeutic proteins with enhanced stability, Proceedings of the National Academy of Sciences, 106 (2009) 11937-11942.
[10] N. Chennamsetty, B. Helk, V. Voynov, V. Kayser, B.L. Trout, Aggregation-Prone Motifs in Human Immunoglobulin G, Journal of Molecular Biology, 391 (2009) 404-413.
[11] S. Kuyucak, V. Kayser, Biobetters From an Integrated Computational/Experimental Approach, Computational and Structural Biotechnology Journal, 15 (2017) 138-145.
[12] M. Reslan, V. Kayser, The effect of deuterium oxide on the conformational stability and aggregation of bovine serum albumin, Pharmaceutical Development and Technology, (2016) 1-7.
[13] M. Reslan, Y.K. Demir, B.L. Trout, H.-K. Chan, V. Kayser, Lack of a synergistic effect of arginine–glutamic acid on the physical stability of spray-dried bovine serum albumin, Pharmaceutical Development and Technology, 22 (2017) 785-791.

[14] K.M. Forney-Stevens, R.H. Bogner, M.J. Pikal, Addition of Amino Acids to Further Stabilize Lyophilized Sucrose-Based Protein Formulations: I. Screening of 15 Amino Acids in Two Model Proteins, Journal of Pharmaceutical Sciences, 105 (2016) 697-704.
[15] J.D. Andya, C.C. Hsu, S.J. Shire, Mechanisms of aggregate formation and carbohydrate excipient stabilization of lyophilized humanized monoclonal antibody formulations, AAPS PharmSci, 5 (2015) 21.
[16] E.D. Breen, J.G. Curley, D.E. Overcashier, C.C. Hsu, S.J. Shire, Effect of Moisture on the Stability of a Lyophilized Humanized Monoclonal Antibody Formulation, Pharmaceutical Research, 18 (2001) 1345-1353.
[17] M. Angell, C.-J. Pan, Y. Rong, C. Yuan, M.-C. Lin, B.-J. Hwang, H. Dai, High Coulombic efficiency aluminum-ion battery using an AlCl3-urea ionic liquid analog electrolyte, Proceedings of the National Academy of Sciences, 114 (2017) 834-839.
[18] P. Fan, S. Xing, J. Wang, J. Fu, L. Yang, G. Yang, C. Miao, P. Lv, Sulfonated imidazolium ionic liquid-catalyzed transesterification for biodiesel synthesis, Fuel, 188 (2017) 483-488.
[19] E. Husson, C. Hadad, G. Huet, S. Laclef, D. Lesur, V. Lambertyn, A. Jamali, S. Gottis, C. Sarazin, A. Nguyen Van Nhien, The effect of room temperature ionic liquids on the selective biocatalytic hydrolysis of chitin via sequential or simultaneous strategies, Green Chemistry, 19 (2017) 4122-4131.
[20] K.S. Egorova, E.G. Gordeev, V.P. Ananikov, Biological Activity of Ionic Liquids and Their Application in Pharmaceutics and Medicine, Chemical Reviews, 117 (2017) 7132-7189.
[21] H. Weingartner, C. Cabrele, C. Herrmann, How ionic liquids can help to stabilize native proteins, Physical Chemistry Chemical Physics, 14 (2012) 415-426.
[22] A. Kumar, M. Bisht, P. Venkatesu, Biocompatibility of ionic liquids towards protein stability: A comprehensive overview on the current understanding and their implications, International Journal of Biological Macromolecules, 96 (2017) 611-651.
[23] M. Bisht, D. Mondal, M.M. Pereira, M.G. Freire, P. Venkatesu, J.A.P. Coutinho, Long-term protein packaging in cholinium-based ionic liquids: improved catalytic activity and enhanced stability of cytochrome c against multiple stresses, Green Chemistry, 19 (2017) 4900-4911.

[24] K. Fujita, M. Forsyth, D.R. MacFarlane, R.W. Reid, G.D. Eiliott, Unexpected improvement in stability and utility of cytochrome c by solution in biocompatible ionic liquids, Biotechnology and Bioengineering, 94 (2006) 1209-1213.
[25] M. Jaganathan, C. Ramakrishnan, D. Velmurugan, A. Dhathathreyan, Understanding ethylammonium nitrate stabilized cytochrome c - Molecular dynamics and experimental approach, Journal of Molecular Structure, 1081 (2015) 334-341.
[26] M. Bisht, P. Venkatesu, Influence of cholinium-based ionic liquids on the structural stability and activity of [small alpha]-chymotrypsin, New Journal of Chemistry, (2017).
[27] T. Takekiyo, K. Yamazaki, E. Yamaguchi, H. Abe, Y. Yoshimura, High Ionic Liquid Concentration-Induced Structural Change of Protein in Aqueous Solution: A Case Study of Lysozyme, Journal of Physical Chemistry B, 116 (2012) 11092-11097.
[28] K.D. Weaver, R.M. Vrikkis, M.P. Van Vorst, J. Trullinger, R. Vijayaraghavan, D.M. Foureau, I.H. McKillop, D.R. MacFarlane, J.K. Krueger, G.D. Elliott, Structure and function of proteins in hydrated choline dihydrogen phosphate ionic liquid, Physical Chemistry Chemical Physics, 14 (2012) 790-801.
[29] L. Christian, P. Ganesh, R. Rainer, Ionic liquids as refolding additives: N′-alkyl and N′-(ω-hydroxyalkyl) N-methylimidazolium chlorides, Protein Science, 14 (2005) 2693-2701.
[30] V.F. Curto, S. Scheuermann, R.M. Owens, V. Ranganathan, D.R. MacFarlane, F. Benito-Lopez, D. Diamond, Probing the specific ion effects of biocompatible hydrated choline ionic liquids on lactate oxidase biofunctionality in sensor applications, Physical Chemistry Chemical Physics, 16 (2014) 1841-1849.
[31] T. Arakawa, D. Ejima, Refolding Technologies for Antibody Fragments, Antibodies, 3 (2014) 232.
[32] D. Mondal, M. Sharma, M.V. Quental, A.P.M. Tavares, K. Prasad, M.G. Freire, Suitability of bio-based ionic liquids for the extraction and purification of IgG antibodies, Green Chemistry, 18 (2016) 6071-6081.
[33] K.D. Weaver, H.J. Kim, J. Sun, D.R. MacFarlane, G.D. Elliott, Cyto-toxicity and biocompatibility of a family of choline phosphate ionic liquids designed for pharmaceutical applications, Green Chemistry, 12 (2010) 507-513.
[34] M. Reslan, V. Kayser, Ionic liquids as biocompatible stabilizers of proteins, Biophysical Reviews, 10 (2018) 781-793.

[35] R. Vijayaraghavan, B.C. Thompson, D.R. MacFarlane, R. Kumar, M. Surianarayanan, S. Aishwarya, P.K. Sehgal, Biocompatibility of choline salts as crosslinking agents for collagen based biomaterials, Chemical Communications, 46 (2010) 294-296.
[36] D.M. Foureau, R.M. Vrikkis, C.P. Jones, K.D. Weaver, D.R. MacFarlane, J.C. Salo, I.H. McKillop, G.D. Elliott, In Vitro Assessment of Choline Dihydrogen Phosphate (CDHP) as a Vehicle for Recombinant Human Interleukin-2 (rhIL-2), Cellular and Molecular Bioengineering, 5 (2012) 390-401.
[37] B. Jagannath, S. Muthukumar, S. Prasad, Electrical double layer modulation of hybrid room temperature ionic liquid/aqueous buffer interface for enhanced sweat based biosensing, Analytica Chimica Acta, 1016 (2018) 29-39.
[38] R.R. Mazid, R. Vijayaraghavan, D.R. MacFarlane, C. Cortez-Jugo, W. Cheng, Inhibited fragmentation of mAbs in buffered ionic liquids, Chemical Communications, 51 (2015) 8089-8092.
[39] V. Kayser, N. Chennamsetty, V. Voynov, B. Helk, K. Forrer, B.L. Trout, Evaluation of a Non-Arrhenius Model for Therapeutic Monoclonal Antibody Aggregation, Journal of Pharmaceutical Sciences, 100 (2011) 2526-2542.
[40] A.A. Wakankar, M.B. Feeney, J. Rivera, Y. Chen, M. Kim, V.K. Sharma, Y.J. Wang, Physicochemical Stability of the Antibody−Drug Conjugate Trastuzumab-DM1: Changes due to Modification and Conjugation Processes, Bioconjugate Chemistry, 21 (2010) 1588-1595.
[41] R.M. Ionescu, J. Vlasak, C. Price, M. Kirchmeier, Contribution of Variable Domains to the Stability of Humanized IgG1 Monoclonal Antibodies, Journal of Pharmaceutical Sciences, 97 (2008) 1414-1426.
[42] J.V. Rodrigues, V. Prosinecki, I. Marrucho, L.P.N. Rebelo, C.M. Gomes, Protein stability in an ionic liquid milieu: on the use of differential scanning fluorimetry, Physical Chemistry Chemical Physics, 13 (2011) 13614-13616.
[43] C.A. Summers, R.A. Flowers, Protein renaturation by the liquid organic salt ethylammonium nitrate, Protein Science, 9 (2000) 2001-2008.
[44] O. Obrezanova, A. Arnell, R.G. de la Cuesta, M.E. Berthelot, T.R.A. Gallagher, J. Zurdo, Y. Stallwood, Aggregation risk prediction for antibodies and its application to biotherapeutic development, mAbs, 7 (2015) 352-363.
[45] A.S. Rosenberg, Effects of protein aggregates: An immunologic perspective, The AAPS Journal, 8 (2006) E501-E507.

CHAPTER 7

“Laboratory Scale Production and Purification of a Therapeutic Antibody”

Chapter 7 was published in the Journal of Visualized Experiments:

Elgundi, Z., Sifniotis, V., Reslan, M., Cruz, E., Kayser, V. (2017). Laboratory Scale Production and Purification of a Therapeutic Antibody. Journal of Visualized Experiments, 119: e55153.

Abstract

Ensuring the successful production of a therapeutic antibody begins early on in the development process. The first stage is vector expression of the antibody genes followed by stable transfection into a suitable cell line. The stable clones are subjected to screening in order to select those clones with desired production and growth characteristics. This is a critical albeit time-consuming step in the process. This protocol considers vector selection and sourcing of antibody sequences for the expression of a therapeutic antibody. The methods describe preparation of vector DNA for stable transfection of a suspension variant of human embryonic kidney 293 (HEK-293) cell line, using polyethylenimine (PEI). The cells are transfected as adherent cells in serum-containing media to maximize transfection efficiency, and afterwards adapted to serum-free conditions. Large scale production, setup as batch overgrow cultures is used to yield antibody protein that is purified by affinity chromatography using an automated fast protein liquid chromatography (FPLC) instrument. The antibody yields produced by this method can provide sufficient protein to begin initial characterization of the antibody. This may include *in vitro* assay development or physicochemical characterization to aid in the time-consuming task of clonal screening for lead candidates. This method can be transferable to the development of an expression system for the production of biosimilar antibodies.

I. Introduction

The success of therapeutic antibodies continues to drive substantial investment into antibody development as a wave of next generation therapeutics begins. The antibody market is expected to be reshaped by antibody fragments [1], antibody-drug conjugates [2], bispecific antibodies [3] and engineered antibodies with favorable properties [4]. Another class gaining pharmaceutical interest are biosimilars. Biosimilar antibodies are ‘highly similar’ replicate products of a therapeutic antibody that has already received regulatory approval. A proposed biosimilar must be comparable with the originator antibody with respect to its structure, function, animal toxicity, clinical safety and effectiveness, human pharmacokinetics (PK), pharmacodynamics (PD) and immunogenicity [5, 6].

The approval rates of biosimilar antibodies have been slow due to the strict constraints on the final quality of the product. The exact manufacturing processes such as specific

cell lines and culturing conditions through to the final processing steps can remain proprietary. What is more, the manufacturing of antibodies inherently involves a degree of variability which can add to the challenge of producing a highly similar product. A comprehensive physiochemical and biophysical characterization and comparison is quite difficult, yet a number of studies demonstrating the characteristics of biosimilar antibodies are emerging in the literature [7-9].

Generating a therapeutic antibody begins with transfection of mammalian host cells with a vector carrying the genes for the respective antibody. Vector design, cell line and culture conditions are key considerations for setting up the expression system.

The DNA sequences of antibodies can be sourced from Drug Bank (www.drugbank.ca), IMGT (www.igmt.org) or research publications including patents. For example, the sequence of trastuzumab is available through Drug Bank (DB ID: DB00072). The amino acid sequence of the variable regions can undergo gene design and optimization for synthesis in the desired host species. It is important for a biosimilar antibody that no modification is made to the amino acid sequence. Once synthesized, antibody genes can be subcloned into the appropriate vector of choice.

Human IgG antibodies consist of two identical heavy chains and two identical light chains. Tightly regulated expression of both chains is essential for optimal production of heterologous IgG protein in mammalian cells [10]. Intra- as well as inter-chain disulfide bonds have to be formed and a number of post-translational modifications have to be introduced during protein biosynthesis. A number of vectors are available that have been designed specifically to express antibody genes (refer to Table S1 in supplementary information). These antibody-specific vectors usually express the constant regions for both heavy and light chains so only the variable regions of each chain require cloning.

Transfection of cells with two independent constructs (co-transfection) is the most common approach for delivering heavy and light chain-encoding genes. That is, each gene is driven by its own promoter and transcribed as separate antibody chains before being assembled in the endoplasmic reticulum. On the other hand, multi-cistronic vectors have internal ribosome entry site (IRES) elements incorporated that allow expression of multiple genes as a single mRNA transcript with translation permitted from internal regions of the mRNA [11]. In this instance, the heavy and light chain-

encoding genes are coupled in an arrangement to achieve co-expression of both antibody chains [10, 12].

While transiently transfected cells yield sufficient protein to perform a limited number of experiments, stably transfected cell lines that have undergone selection for genome integration can deliver higher yields. Higher protein amounts allow for assay development relating to *in vitro* characterization and can provide an indication of antibody quality in consideration for downstream applications such as clonal cell line and lead candidate selection.

The goal of this article is to describe the stable expression and purification of a therapeutic antibody produced in a mammalian expression system. Indeed, this method can be applied to the expression of a biosimilar antibody. The method can be used for the initial characterization of antibodies before proceeding on to the critical, albeit time-consuming steps of identifying a desirable clone for larger scale manufacturing. Moreover, this method can be used to express other proteins and not just antibodies.

The following detailed protocol describes the expression of therapeutic antibody trastuzumab. This consists of preparation of vector DNA followed by stable transfection in HEK-293 cell line and purification of antibody protein by an automated chromatographic method.

II. Protocol

Note: A suitable mammalian expression vector must be used for this protocol. Here, a single construct containing two expression cassettes is used (i.e. heavy and light chain expression is driven by separate promoters). Trastuzumab heavy and light chains were previously cloned into the vector. This vector was a gift from Andrew Beavil, obtained through a not-for-profit plasmid repository [13].

1. Recovery and Scale-up of Vector DNA

Note: Vector DNA was received as a soft agar stab culture in *Escherichia coli* XL-1 Blue strain; vector carries hygromycin resistance.

1.1. Insert a sterile inoculation stab or loop into the soft agar of the stab culture then streak a Luria Bertani (LB) agar plate prepared with 75 µg/ml hygromycin for isolated colonies. Incubate the plate at 37 °C for 18-24 h.

1.2. Inoculate a single colony into 5 ml Terrific broth (TB) containing 75 µg/ml hygromycin. Incubate the culture at 37 °C for 18-24 h with 225 rpm shaking.

1.3. Use the overnight culture to prepare a glycerol stock of vector DNA by gently mixing 800 µl of culture with 200 µl 80% glycerol in a cryovial and freeze at -80 °C.

1.3.1. Add 100 µl of the overnight culture to 100 ml TB containing 75 µg/ml hygromycin in a baffled shaker flask (i.e. 1/1000 dilution). Incubate the culture at 37 °C for 18-24 h with 225 rpm shaking.

1.4. After overnight culture, extract and purify the DNA according to manufacturer's instructions of midi/maxi preparation kit with the following exception; during the final step, elute or resuspend DNA with water (pH 7.0-8.5).

1.5. Check concentration and purity of DNA by absorbance readings at 260 and 280 nm then store DNA at -20 °C.

Note: Optional (highly recommended): Sequence DNA using vector-specific primers to confirm identity.

2. Stable Transfection of HEK-293 Cells

a) PEI Transfection and clone selection

2.1 Grow and maintain HEK-293 cells (suspension cells) according to standard protocols in serum-free media supplemented with 0.1% non-ionic surfactant in baffled flasks. Maintain at $2x10^5$ cells/ml and subculture every fourth day. Culture cells at 37 °C with 5% CO_2 and 120 rpm rotation.

Note: Cells should have been in culture for no less than 4 days and no more than 4 weeks prior to transfection. HEK-293 cells grown as monolayers in serum-containing media can also be used for this procedure.

2.2. On the day prior to transfection, seed HEK-293 cells at $3x10^5$ cells/ml in wells of a 12-well plate in 2 ml of Dulbecco's Modified Eagle Media (DMEM) supplemented with 10% heat-inactivated fetal bovine serum (FBS). On the day of transfection, check that cells have reached 80-90% confluency

2.3. Dilute DNA and polyethylenimine (PEI) separately in transfection media then mix together.

2.3.1. Dilute 1.25 µg vector DNA per well (15 µg for 12 wells) in 300 µl transfection media. Incubate at room temperature for 5 min.

2.3.2. Dilute 2.5 µl of 1 mg/ml PEI solution (30 µl for 12 wells; i.e. 1:2 ratio of DNA to PEI) in 300 µl transfection media. Incubate at room temperature for 5 min.

2.3.3. Add diluted DNA to diluted PEI, gently mix and incubate at room temperature for 15 min.

2.4. Add 50 µl of DNA/PEI mixture dropwise to each well of the plate. Rock the plate gently to distribute the transfection mixture then place the plate at 37 °C, 5% CO_2 for 24 h.

2.5. Add 50 µg/ml hygromycin B per well and return plate to 37 °C, 5% CO_2 for 10 days.

Note: By Day 10, un-transfected cells will have died and detached from the surface of the plate, whereas stably-transfected cells will be viable and attached to the plate.

b) Adaptation of stable clones to serum-free media

2.6. Replace the media in wells with 1/4 volume serum-free media and 3/4 volume DMEM supplemented with 10% FBS (i.e. 0.5 ml serum-free media + 1.5 ml DMEM = 7.5% final serum concentration) and incubate for 4 days.

2.7. Replace the media in wells with 1/2 volume serum-free media and 1/2 volume DMEM supplemented with 10% FBS (i.e. 1 ml serum-free media + 1 ml DMEM = 5% final serum concentration) and incubate for 4 days.

2.8. Replace the media in wells with 3/4 volume serum-free media and 1/4 volume DMEM supplemented with 10% FBS (i.e. 1.5 ml serum-free media + 0.5 ml DMEM = 2.5% final serum concentration) and incubate for 4 days.

2.9. Replace the media in wells with 2 ml of serum-free media supplemented with 0.1% non-ionic surfactant (i.e. 0% final serum concentration) and incubate for 4 days.

Note: Maintain 50 µg/ml hygromycin B selective pressure on cells during serum-free adaptation. Cells adapted to serum-free media detach from the surface of wells and may cluster in suspension. Refer to step 2.1 for culture conditions with the additional supplement of 50 µg/ml hygromycin B.

2.10. Using a pipette, gently mix the suspension cultures in the 12-well plate and pool cells into a separate tube.

2.10.1. Using a hemocytometer, enumerate pooled cells and seed in 30 ml serum-free media in a baffled flask at $2x10^5$ cells/ml. Culture cells at 37 ˚C with 5% CO_2 and 120 rpm rotation. Subculture and expand every fourth day.

2.11. Continue to expand culture size to required cell density to obtain 10 vials at $1x10^7$ cells/vial for cryopreservation in liquid nitrogen. Freeze the cells in serum-free media containing 10% dimethylsulfoxide (DMSO).

Note: Conditioned media containing antibody can be harvested at each subculture to confirm protein production or used to optimize purification conditions. To harvest conditioned media and maintain cells for subculture, centrifuge the culture at 300 x g for 5 min then filter-sterilize supernatant through a 0.22 µm filter. Filtered supernatant may be kept at 4 ºC for 1-2 weeks or -20 ºC for longer term storage.

3. Large Scale Antibody Production from Batch Overgrow Culture

Note: Antibody production can be followed on from step 2.11 where existing cells are expanded to the required cell density based on the batch overgrow culture volume to be setup. Otherwise, cells that have been thawed from cryopreservation begin at this stage once expanded to an appropriate cell density and volume. Various culture supplements may be used to optimize antibody production; the use of tryptone to increase antibody yield is demonstrated in this protocol.

3.1. Seed cells at $2x10^5$ cells/ml in 100 ml serum-free media in two baffled flasks (to compare antibody yields from un-supplemented and nutrient-supplemented cultures). Culture at 37 ºC, 5% CO_2 and 120 rpm.

3.2. After 24 h, add tryptone to a final concentration of 0.5% to nutrient-supplemented culture. Equalize volume of un-supplemented culture with serum-free media.

3.3. From day 8, perform cell counts of the cultures daily using a hemocytometer to monitor cell viability. Harvest the culture supernatants once cell viability is less than 80%.

3.3.1. Harvest supernatant by centrifugation of the cultures at 3000 x g for 15 min then filter-sterilize the supernatant (containing antibody) through a 0.22 µm filter. Store the supernatants at 4 ^{o}C (short-term) or freeze at -20 ^{o}C (long-term).

4. Antibody Purification by Affinity Chromatography Using an Automated Fast Protein Liquid Chromatography (FPLC) System

Note: The following procedure can generally be applied to most automated systems. Purification can be performed at room temperature or at 4 °C (if FPLC system is kept in a cool room). A series of scouting tests can be performed to identify the optimal purification conditions including appropriate column matrix, binding buffer, elution buffer and pH to ensure maximum recovery of purified antibody from conditioned media (refer to Results section). The optimal conditions are dependent on the antibody or protein being purified. Purifications were performed on an automated FPLC system. Purifications were performed at room temperature using a 5 ml Protein A column.

4.1. Prepare the following buffers using ultrapure water and adjust to the recommended pH then filter through a 0.22 µm filter.

4.1.1. Prepare 1 L of phosphate buffered saline (PBS) pH 7.4 (binding buffer) by mixing the following: 0.14 M NaCl, 0.0027 M KCl, 0.01 M Na_2HPO_4 and 0.001 M KH_2PO_4. Adjust pH if necessary before filtering the buffer.

4.1.2. Prepare 500 ml of 0.1 M glycine-HCl pH 2.7 (elution buffer). Adjust pH before filtering the buffer.

4.1.3. Prepare 50 ml of 1 M Tris pH 9.0 (neutralization buffer).

4.2. Ensure all system power and communication connections with computer are made. Devices should be visible in the software ‘System Control’ module. Ensure UV cell is set at 280 nm wavelength. Optional: Calibrate pH meter if connected and to be used.

4.3. Immerse inlet tubes of A, B and sample pump in ultrapure water to wash the system. Purge the pumps with a syringe if there is air in the tubing or a suspicion of air in the system. Wash the system with water by manual operation via the system controller or via an automated method. Observe that pressure, conductivity, UV280

tracing and pH remain consistent and that the pressure limit for the column is not exceeded as per manufacturer's specification.

Note: Abnormalities may indicate air or blockage in the system that should be addressed before proceeding.

4.4. In the system controller module, start the flowrate at 1 ml/min manually via pump A in either load (bypassing sample loop) or inject (through the sample loop) position to begin connecting the column. Disconnect system tubing at the column position inlet and remove the stopper connected to the column inlet.

4.4.1. Allow water to flow from the system tubing dropwise on top of the column then attach the system tubing to the column. Having the column inlet and inlet fitting overflowing with drops of water ensures a connection free of air bubbles.

4.5. Attach the column outlet at the downstream outlet and verify all fittings are tightly fastened. With the column now attached to the system, do not exceed limits for maximum pressure limit and flowrate as outlined in column specifications.

4.6. Wash column with 5 column volumes (CV) of water. If necessary, continue column wash until UV280 tracing has stabilized.

4.7. Immerse inlet tubes of A in Binding buffer, B in Elution buffer and sample pump in Binding buffer to equilibrate the system in correct buffers. Fill the inlet tubes with buffer using PumpWash by manual operation.

4.8. In the 'Method Editor' module of the software, use the method wizard to setup an affinity chromatography method for the column that is intended to be used.

Note: Automated FPLC systems come with methods pre-filled with the recommended settings (i.e. flowrate and pressure limit) and run steps based on the column (manufacturer, matrix and size) selected for purification.

4.8.1. Use the following run steps for Protein A affinity chromatography:

4.8.1.1 Equilibrate system with 5 CV of Binding buffer and collect flowthrough into waste container.

4.8.1.2. Load sample onto the column (volume to be loaded is specified manually in the method) and collect flowthrough into a separate container.

4.8.1.3. Wash system with 5 CV of Binding buffer and collect flowthrough into a separate container.

4.8.1.4. Elute column with 5 CV isocratic fractionation using Elution buffer and collect purified antibody sample as fractions by fraction collector.

4.8.1.5. Equilibrate system with 5 CV of Binding buffer and collect flowthrough into waste container.

4.9. Once the method has been setup, specify the volume of conditioned media to be applied to the column and save the method.

Note: The specified volume in the method should be 5-10 ml less than the actual volume to avoid introduction of air during the sample run. The specified volume used in this protocol is 90-120 ml.

4.10. Submerge the sample pump tubing into the vessel containing the conditioned media.

4.11. Prepare a separate container to collect sample flowthrough via the specified outlet tubing.

Note: It is important to collect the flowthrough in the case an error occurs during the run or the binding capacity of the column is exceeded requiring the flowthrough to be reapplied to the column or the purification repeated.

4.12. Prepare collection tubes in the fraction collector. Add 100 µl of neutralization buffer per 1 ml fraction volume. The FPLC system will automatically elute the fractions into the collection tubes.

4.13. In the ‘System Control’ module of the software, open the method to be run.

Note: The method run is initiated in a series of pages that include checking the variables of the method, fraction collector setup and defining result file name and storage location.

4.14. Click START to initiate the run. The run can be monitored in the ‘System Control’ module.

4.15. At the completion of the purification run, check the resulting chromatogram in the ‘Evaluation’ module in the system software.

4.16. Combine all protein-containing fractions into a separate tube, buffer exchange and concentrate in PBS using a centrifugal filter device with 30 kDa molecular weight cut off. Perform centrifugation steps according to manufacturer's instructions.

4.17. Measure antibody concentration using bicinchoninic acid assay (BCA) according to manufacturer's instructions.

4.18. If another purification run is to be performed, prime the sample pump tubing in Binding buffer and repeat steps 4.9-4.14.

4.19. At the completion of purification runs, immerse inlet tubes of A, B and sample pump in ultrapure water and wash the system and column as performed in step 3.

4.20. Submerge A, B and sample pump tubing in 20% ethanol and repeat wash procedure for storage of the system and column.

4.21. Disconnect the column from the downstream outlet and replace column stopper, then disconnect column at the inlet and replace stopper, reconnect tubing to the system. Store the column at 4 °C.

III. Representative results

Stable production of trastuzumab by transfected HEK-293 cells was confirmed using bio-layer interferometry (BLI) as presented in Figure 1. An IgG standard curve was generated by measuring the binding rate between an IgG antibody standard and protein A biosensor (Fig. 1A). The crude supernatant sample was similarly measured, then its concentration interpolated from the standard curve (Fig. 1B). The supernatant concentration was measured to be approximately 25 µg/ml (sampled from 50 ml collected at subculture) two weeks after serum-free adaptation and prior to setting up cells for overgrow batch cultures. Supernatant collected at each subculture after serum-free adaptation was pooled and used to optimize purification conditions; scouting of binding and elution buffers was performed as shown in Figure 2. The steps of purification are depicted in Figure 2A based on UV280 signal. Once the Protein A column equilibrates, an increase in UV280 signal represents sample loading; this increase is due to supernatant flowthrough passing through the column (containing unbound proteins which absorb UV light at this wavelength), while antibodies have been captured by the column. Once the sample has finished loading, the UV280 signal returns to baseline as any remaining unbound proteins are washed away. Elution

occurs as pH decreases to the optimal pH to release the antibodies captured by the column, depicted by an increase in UV280 signal with eluted antibodies fractionated and collected by the fraction collector. Throughout the sample run, conductivity changes based on the salt concentration in the buffers whereas system pressure should remain relatively constant.

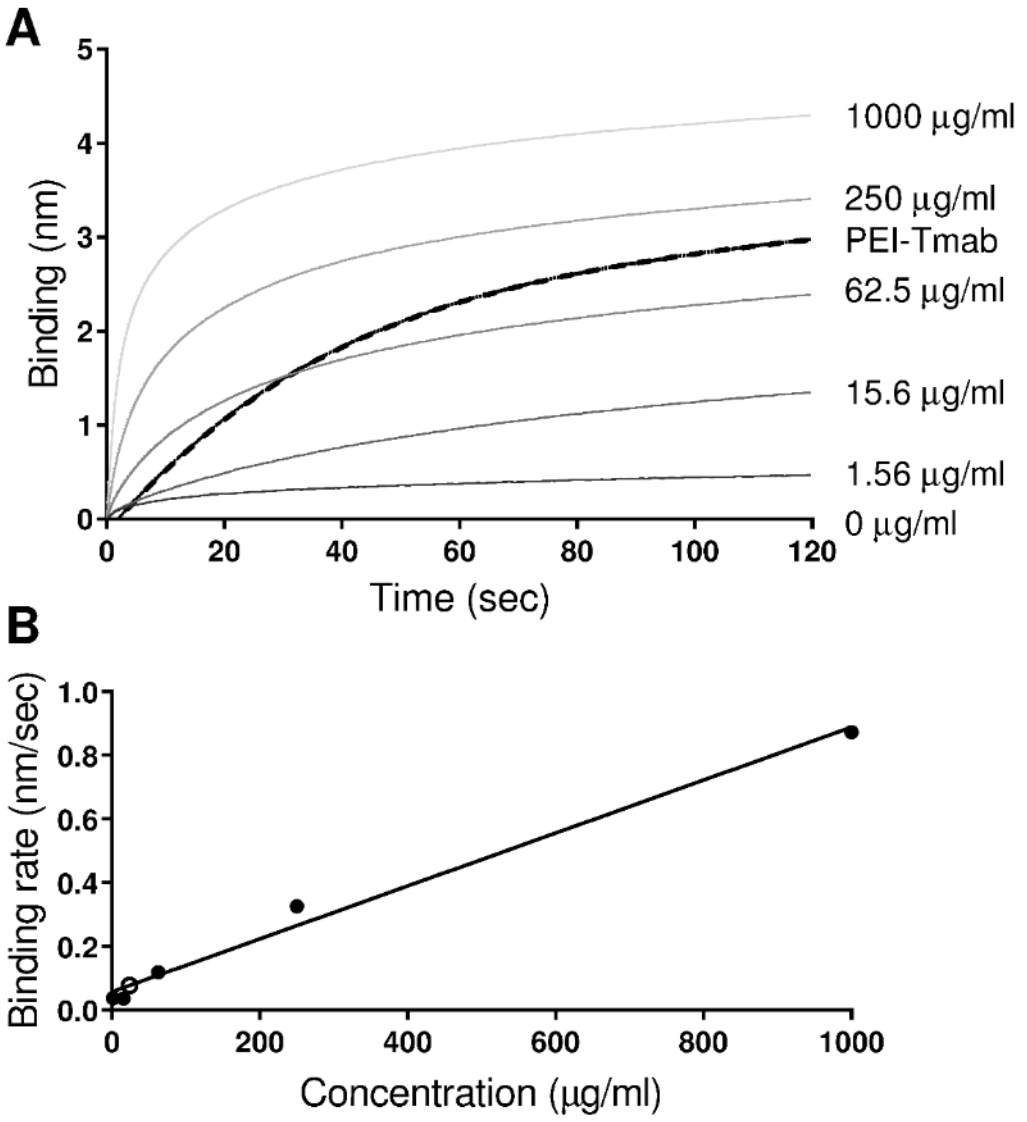

Figure 1. Confirmation of protein production by stably transfected HEK-293 cells using bio-layer interferometry (BLI). (A) Standard curve was generated by measuring binding rate of IgG antibody standard to protein A biosensor over 120 seconds (grey) followed by crude supernatant sample of PEI-transfected trastuzumab (PEI-Tmab; black). (B) Concentration of antibody protein in crude supernatant (open black circle) was interpolated from standard curve (closed black circles) by plotting IgG antibody standard concentration versus binding rate.

Optimal elution, pH and buffer were scouted first (Fig. 2B); it was observed that antibody eluted more efficiently off the column at lower pH using either 0.1 M glycine HCl or citric acid. However, below pH 2.7 there was no further improvement in the elution profile. In addition, elution peaks with 0.1 M glycine HCl appeared less broadened when compared with 0.1 M citric acid at similar pH (Fig. 2B). Subsequently, 0.1 M glycine-HCl pH 2.7 buffer was used to optimize binding buffer conditions (Fig. 2A). The effect of different binding buffers on elution was also compared (Fig. 2A). It was observed that PBS pH 7.4 and 20 mM sodium phosphate pH 7 had comparable elution profiles, while the addition of 3 M NaCl to sodium phosphate buffer (to enhance antibody binding to the column) was not favorable. Due to the ease of PBS buffer preparation, PBS pH 7.4 was selected as the binding buffer for future purifications.

The purification chromatograms of batch overgrow cultures are shown in Figure 3; tryptone-supplemented culture is compared to un-supplemented culture. It was noted that the addition of tryptone to the supplemented culture resulted in an increased UV280 signal during the sample loading step, compared to the un-supplemented culture. The tryptone-supplemented culture yielded 3.8 mg and the un-supplemented culture 1.7 mg of trastuzumab, based on protein recovered after buffer exchange and concentration. Quality control of the purified antibody was confirmed by sodium dodecyl sulfate polyacrylamide gel electrophoresis (SDS-PAGE) (Fig. 4). Trastuzumab grown in un-supplemented and tryptone-supplemented conditions results in similar antibody profiles under non-reducing and reducing conditions. As expected, a prominent band at approximately 150 kDa confirms correctly folded antibody; other bands represent fragmented forms of the antibody, a result of disulfide bond breakage and a method-induced artefact. Likewise, two bands at 50 and approximately 25 kDa confirm the presence of antibody heavy and light chains, respectively.

IV. Discussion

This protocol details the transfection, stable expression and purification of a therapeutic antibody in HEK-293 cells. Stable expression of antibody genes is the first step in generating an antibody-producing cell line for the development and manufacture of a therapeutic antibody. While Chinese hamster ovary (CHO) cells remain the expression platform of choice for therapeutic proteins, the HEK-293 cell

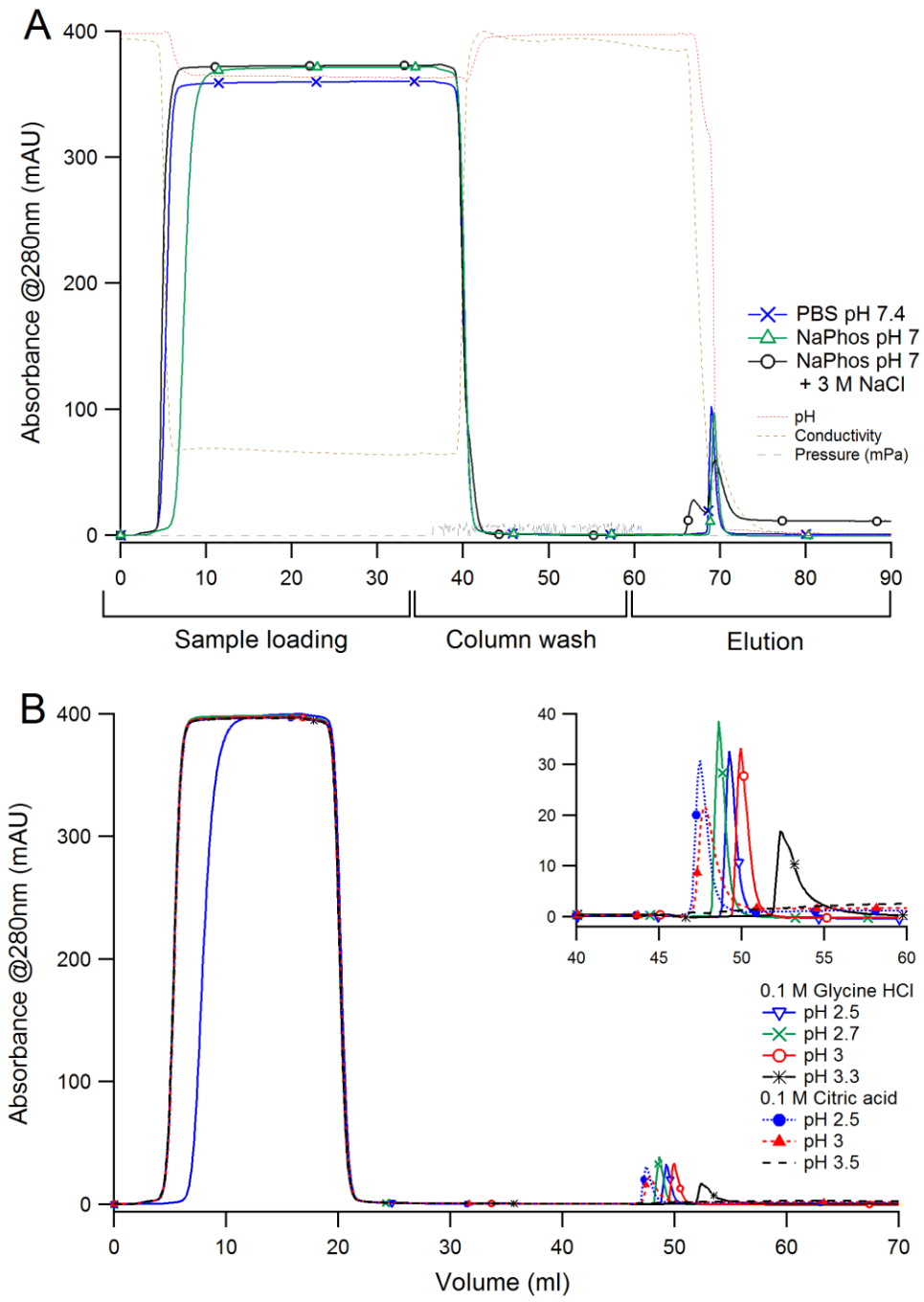

Figure 2. Purification chromatograms of elution and binding buffer scouting experiments. (A) The steps of purification are depicted according to UV280 signal (blue, green or black lines); sample loading onto the column followed by column wash to wash away unbound proteins then elution of bound protein from the column. Measurement of pH (red line), conductivity (brown line) and system pressure (grey line) is monitored throughout the run. Three buffers were tested for optimal binding of trastuzumab to the column and washing away of unbound protein to maximize elution yield. (B) 0.1 M glycine-HCl (pH 2.5-3.3) and 0.1 M citric acid (pH 2.5-3.5) buffers were tested for optimal elution of trastuzumab from protein A column.

line is gaining prominence with the realization that proteins produced in these cells are a closer match to naturally occurring human proteins, in terms of post-translational modifications and function [14, 15].

Mammalian cell lines including CHO (e.g., CHO-DG44 and CHO-K1) as well as non-immunoglobulin secreting murine B cell lines NS0 and SP2/0 are predominantly used in biopharmaceutical production. Expression systems based on these cell lines are based on selection processes whereby high producing clones are induced and selected through incremental addition of a specific selective drug [16, 17]. The selection process for a stable clone can therefore be arduous and time-consuming. In comparison to these existing methods, the HEK-293 cell line robustly transfects with high efficiency. The selection process is simplified and very easily adapts to serum-free suspension culture, making it an ideal expression system for laboratory scale production of proteins [18].

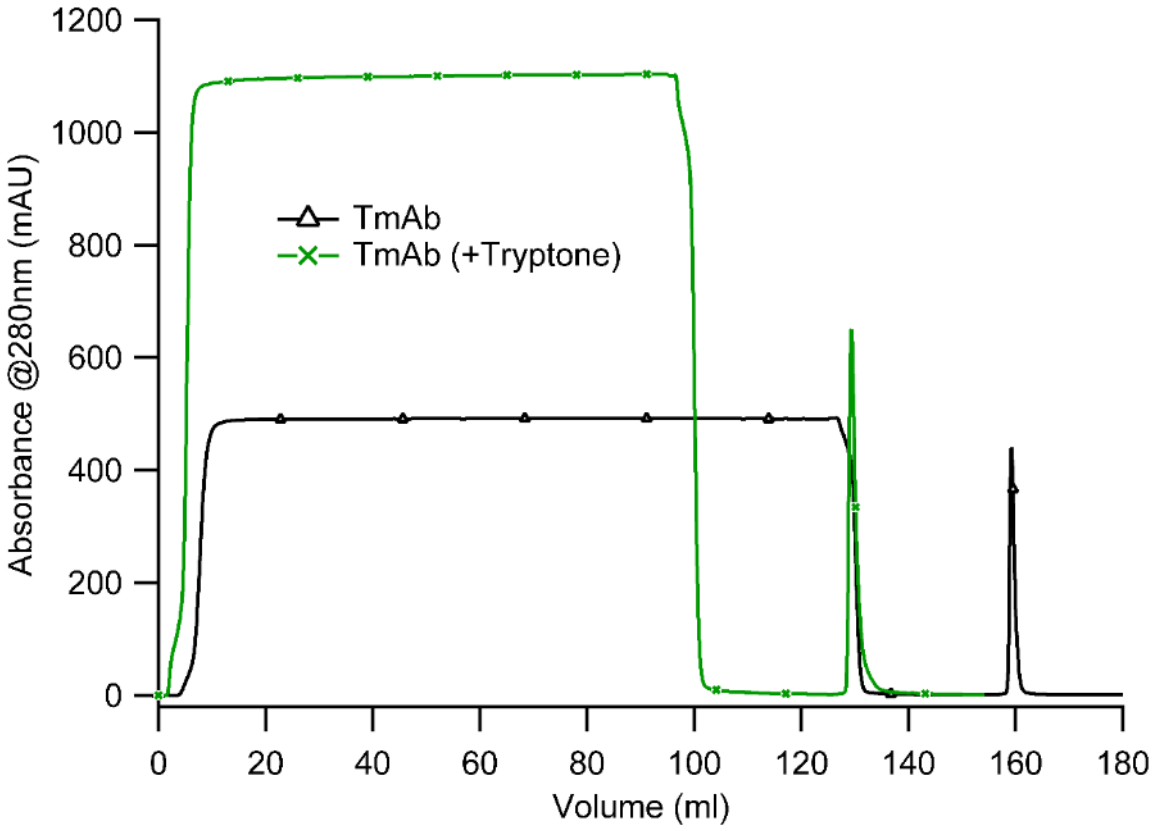

Figure 3. Purification chromatograms of trastuzumab (TmAb) batch overgrow cultures grown with no supplement or supplemented with tryptone. Stably transfected HEK-293 cells were setup at $2x10^5$ cells/ml and cultured for 8 days either un-supplemented (120 ml; black line) or supplemented with 0.4% tryptone (90 ml; green line). After harvesting, supernatants were purified using PBS pH 7.4 (binding buffer) and 0.1 M glycine-HCl pH 2.7 (elution buffer).

A limitation of stable transfection is time in which a practical amount of protein can be produced and utilized in experiments. To try and overcome this, the current protocol describes a culturing step that can achieve substantial amounts of protein within 3-6 weeks of transfection. The batch overgrow cultures (large scale production) provide the opportunity to produce substantial amounts of antibody for the setup of *in vitro* characterization experiments in the lead up to selection of a clonal cell line and lead candidates. This has clear advantages over transient transfection, which can require higher amounts of DNA and reagents. In addition, the protein yield is not reproducible from batch to batch since expression is only temporary and determined by transfection efficiency.

The addition of tryptone in this protocol provided an increased yield in protein expression. Addition of tryptone to transfection cultures has previously been shown to improve protein synthesis [19, 20]. The tryptone supplemented culture resulted in improved trastuzumab antibody yields of 40 mg/L versus the un-supplemented culture

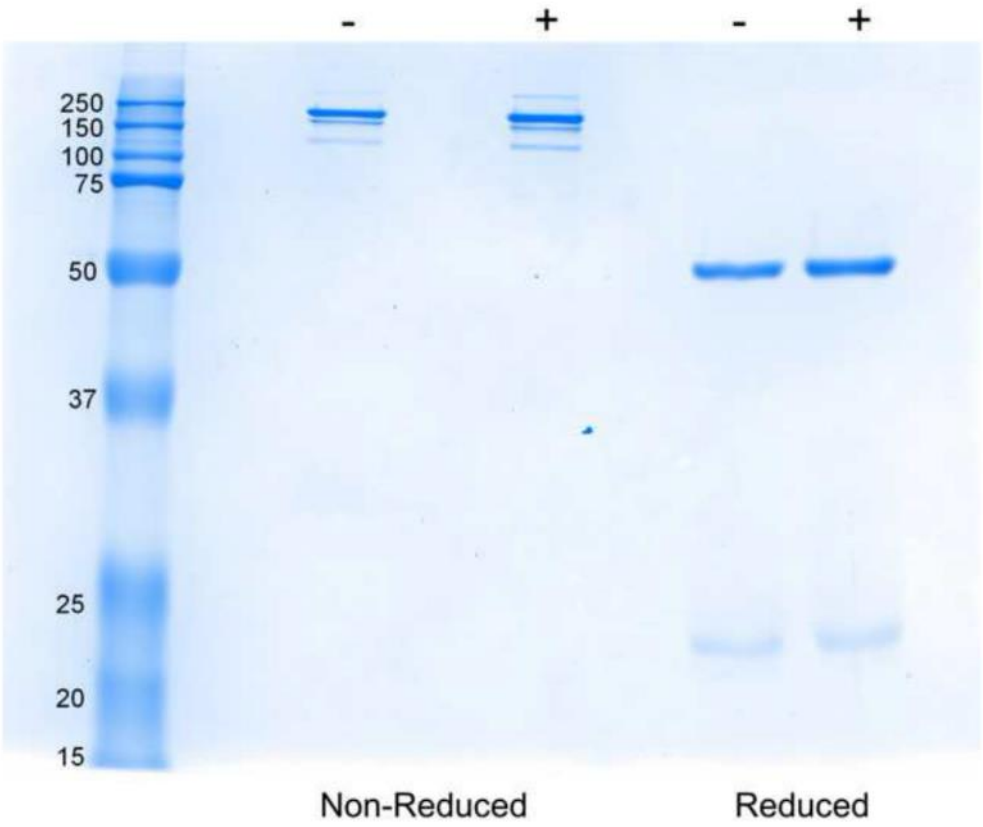

Figure 4. Analysis of purified trastuzumab by SDS-PAGE. Approximately 2 µg of trastuzumab purified from un-supplemented (-) or tryptone-supplemented (+) cultures was sampled by 10% SDS-PAGE under non-reduced or reduced conditions. The gel is stained with coomassie R-250.

of 14 mg/L (Fig. 3). SDS-PAGE verified that: (1) the antibody was being produced correctly; and (2) the addition of tryptone did not alter structure based on comparison of the antibody bands under non-reducing and reducing conditions (Fig. 4). The addition of tryptone to the cultures is optional and is particularly used to achieve higher protein yields. Other supplements have been considered to enhance protein expression such as sodium butyrate and valproic acid [21-23].

The first checkpoint of the protocol is the confirmation that protein is being produced by the transfected cell line. This step may be performed any time after the two-week period of selective pressure used to select stable transformants. A number of methods may be used to confirm protein production including bio-layer interferometry (Fig. 1) or the similar approach of an IgG ELISA. Alternatively, a western blot may be performed using an anti-IgG detection antibody to identify antibody protein in the crude supernatant or purified sample.

Other researchers have shown that higher transfection efficiency is achieved using adherent cells in serum-containing media [24]. The presence of supplements from animal origin is undesirable for biopharmaceutical production. Therefore, the sequential adaptation to serum-free media is a critical step in the protocol requiring patience and careful monitoring of cell viability. The 4-day turnover period suggested in this protocol is a guide and so if problems are encountered at a certain serum concentration, it is recommended that the cells be subcultured 2-3 times in the previous ratio of serum-containing to serum-free media before continuing with the next ratio. Prior to setting up batch cultures and cryopreservation of cells, consider that most cell lines are deemed fully adapted after three subcultures in 100% serum-free media.

One of the most crucial steps at the purification stage is the scouting for optimal conditions and buffers to ensure efficient binding of the antibody to the column and then complete elution off the column (Fig. 2). The conditioned media collected at each subculture is useful for this purpose. In this case, the elution buffer of citric acid pH 3.5 generally recommended for protein A affinity chromatography was unsuitable for elution of trastuzumab from the column. The scouting experiment using two different elution buffers at various pH clearly showed that even within the narrow range of pH tested, the degree of elution was affected (Fig. 2B).

In terms of downstream processing of the antibody fractions after purification, the antibody can be buffer-exchanged using a desalting column either by manual or automated operation. Alternatively, dialysis membrane can also be used. Final protein concentration can be determined by other protein quantification methods including measurement of the absorbance signal at 280 nm with concentration deduced from Beer Lambert's Law based on the extinction coefficient of the antibody.

This protocol has successfully produced the antibody protein of trastuzumab by stable transfection of HEK-293 cells. The antibody was purified and characterized to confirm integrity. The steps in this protocol detailing DNA preparation, stable transfection followed by serum-free adaptation, large scale production and automated purification can be transferred to producing other proteins.

Acknowledgements

The research was supported by the University of Sydney. pVITRO1-Trastuzumab-IgG1/κ was a gift from Andrew Beavil (Addgene plasmid # 61883). We thank Tihomir S. Dodev for useful discussions regarding pVITRO1-Trastuzumab-IgG1/κ.

Disclosures

The authors declare that they have no competing financial interests.

References

[1] A.L. Nelson, J.M. Reichert, Development trends for therapeutic antibody fragments, Nature Biotechnology, 27 (2009) 331-337.

[2] P.M. Drake, D. Rabuka, An emerging playbook for antibody-drug conjugates: lessons from the laboratory and clinic suggest a strategy for improving efficacy and safety, Curr Opin Chem Biol, 28 (2015) 174-180.

[3] R.E. Kontermann, U. Brinkmann, Bispecific antibodies, Drug Discov Today, 20 (2015) 838-847.

[4] A. Beck, T. Wurch, C. Bailly, N. Corvaia, Strategies and challenges for the next generation of therapeutic antibodies, Nat Rev Immunol, 10 (2010) 345-352.

[5] Food and Drug Administration, Quality Considerations in Demonstrating Biosimilarity of a Therapeutic Protein Product to a Reference Product

Guidance for Industry, in: U.S.D.o.H.a.H. Services, F.a.D. Administration, C.f.D.E.a.R. (CDER), C.f.B.E.a.R. (CBER) (Eds.), 2015, pp. 22.

[6] European Medicines Agency, Guideline on similar biological medicinal productsncontaining biotechnology-derived proteins as active substance: non-clinical and clinical issues, in: E.M.A. (EMA), C.f.M.P.f.H.U. (CHMP) (Eds.), 2014, pp. 13.
[7] C.A. Lopez-Morales, M.P. Miranda-Hernandez, L.C. Juarez-Bayardo, N.D. Ramirez-Ibanez, A.J. Romero-Diaz, N. Pina-Lara, V.R. Campos-Garcia, N.O. Perez, L.F. Flores-Ortiz, E. Medina-Rivero, Physicochemical and biological characterization of a biosimilar trastuzumab, Biomed Res Int, 2015 (2015) 427235.
[8] S.K. Jung, K.H. Lee, J.W. Jeon, J.W. Lee, B.O. Kwon, Y.J. Kim, J.S. Bae, D.I. Kim, S.Y. Lee, S.J. Chang, Physicochemical characterization of Remsima, mAbs, 6 (2014) 1163-1177.
[9] J. Visser, I. Feuerstein, T. Stangler, T. Schmiederer, C. Fritsch, M. Schiestl, Physicochemical and functional comparability between the proposed biosimilar rituximab GP2013 and originator rituximab, BioDrugs, 27 (2013) 495-507.
[10] J. Li, C. Menzel, D. Meier, C. Zhang, S. Dubel, T. Jostock, A comparative study of different vector designs for the mammalian expression of recombinant IgG antibodies, J Immunol Methods, 318 (2007) 113-124.
[11] K.D. Fitzgerald, B.L. Semler, Bridging IRES elements in mRNAs to the eukaryotic translation apparatus, Biochimica et Biophysica Acta, 1789 (2009) 518-528.
[12] S.C. Ho, M. Bardor, H. Feng, Mariati, Y.W. Tong, Z. Song, M.G. Yap, Y. Yang, IRES-mediated Tricistronic vectors for enhancing generation of high monoclonal antibody expressing CHO cell lines, Journal of Biotechnology, 157 (2012) 130-139.
[13] T.S. Dodev, P. Karagiannis, A.E. Gilbert, D.H. Josephs, H. Bowen, L.K. James, H.J. Bax, R. Beavil, M.O. Pang, H.J. Gould, S.N. Karagiannis, A.J. Beavil, A tool kit for rapid cloning and expression of recombinant antibodies, Sci Rep, 4 (2014) 5885.
[14] G. Walsh, Post-translational modifications of protein biopharmaceuticals, Drug Discov Today, 15 (2010) 773-780.
[15] G. Backliwal, M. Hildinger, S. Chenuet, S. Wulhfard, M. De Jesus, F.M. Wurm, Rational vector design and multi-pathway modulation of HEK 293E cells yield recombinant antibody titers exceeding 1 g/l by transient transfection under serum-free conditions, Nucleic Acids Research, 36 (2008) e96.
[16] C.R. Bebbington, G. Renner, S. Thomson, D. King, D. Abrams, G.T. Yarranton, High-level expression of a recombinant antibody from myeloma cells using a glutamine synthetase gene as an amplifiable selectable marker, Biotechnology (N Y), 10 (1992) 169-175.

[17] R.J. Kaufman, L.C. Wasley, A.J. Spiliotes, S.D. Gossels, S.A. Latt, G.R. Larsen, R.M. Kay, Coamplification and coexpression of human tissue-type plasminogen activator and murine dihydrofolate reductase sequences in Chinese hamster ovary cells, Mol Cell Biol, 5 (1985) 1750-1759.
[18] A.C. Dalton, W.A. Barton, Over-expression of secreted proteins from mammalian cell lines, Protein Science, 23 (2014) 517-525.
[19] P.L. Pham, S. Perret, B. Cass, E. Carpentier, G. St-Laurent, L. Bisson, A. Kamen, Y. Durocher, Transient gene expression in HEK293 cells: peptone addition posttransfection improves recombinant protein synthesis, Biotechnology and Bioengineering, 90 (2005) 332-344.
[20] P.L. Pham, S. Perret, H.C. Doan, B. Cass, G. St-Laurent, A. Kamen, Y. Durocher, Large-scale transient transfection of serum-free suspension-growing HEK293 EBNA1 cells: peptone additives improve cell growth and transfection efficiency, Biotechnology and Bioengineering, 84 (2003) 332-342.
[21] W.C. Yang, J. Lu, N.B. Nguyen, A. Zhang, N.V. Healy, R. Kshirsagar, T. Ryll, Y.M. Huang, Addition of valproic acid to CHO cell fed-batch cultures improves monoclonal antibody titers, Molecular Biotechnology, 56 (2014) 421-428.
[22] G. Backliwal, M. Hildinger, I. Kuettel, F. Delegrange, D.L. Hacker, F.M. Wurm, Valproic acid: a viable alternative to sodium butyrate for enhancing protein expression in mammalian cell cultures, Biotechnology and Bioengineering, 101 (2008) 182-189.
[23] Z. Jiang, S.T. Sharfstein, Sodium butyrate stimulates monoclonal antibody over-expression in CHO cells by improving gene accessibility, Biotechnology and Bioengineering, 100 (2008) 189-194.
[24] M. Jordan, F. Wurm, Transfection of adherent and suspended cells by calcium phosphate, Methods, 33 (2004) 136-143.

CHAPTER 8

“Enhancing the Stability of Adalimumab by Engineering Additional Glycosylation Motifs”

Chapter 8 was prepared for publication to the European Journal of Pharmaceutics and Biopharmaceutics:

Reslan, M., Sifniotis, V., Cruz, E., Sumer-Bayraktar, Z., Kayser, V. (2018). Enhancing the stability of adalimumab by engineering additional glycosylation motifs. European Journal of Pharmaceutics and Biopharmaceutics.

Abstract

Monoclonal antibodies (mAbs) are of high value in the diagnostic and treatment of many debilitating diseases such as cancers, auto-immune disorders and infections. Unfortunately, protein aggregation is one of the ongoing challenges, limiting the development and application of mAbs as therapeutic products by decreasing half-life, increasing immunogenicity and reducing activity. We engineered an aggregation-prone region of adalimumab, the top selling mAb product worldwide - with additional glycosylations to enhance its resistance to aggregation by steric hindrance as a next generation biologic. We found that the addition of N-glycans in the Fab domain significantly enhanced its conformational stability, with some variants increasing the melting temperature of the Fab domain by more than 6 °C. The mutations tested had minimal impact on antigen binding affinity, or affinity to Fcγ receptors responsible for effector function. Our findings highlight the significant utility of this rational engineering approach for enhancing the conformational stability of therapeutic mAbs and other next-generation antibody formats.

1. Introduction

Monoclonal antibodies (mAbs) are amongst the top-selling therapeutic prescription products worldwide. In 2017, Humira® (adalimumab) alone, generated over 18 billion US dollars, maintaining its position as the top-selling drug worldwide [1, 2]. mAbs are revolutionary biopharmaceuticals used to treat cancers, auto-immune and inflammatory conditions, and even some types of asthma. Approximately 80 antibody products have been approved and marketed by the FDA and EMA with hundreds more in early and advanced clinical trials [3]. Advances in antibody engineering technology have led to the development of a multitude of novel, next-generation antibody-derived products often termed biobetters, which include bispecifics, nanobodies, antibody-drug conjugates, and nanoparticles functionalised with antibodies [3, 4].

Despite the four-decade-long progress and ever-growing interest in antibody research, one of the major challenges in the development of antibody therapeutics remains unsolved: protein aggregation [4-7]. Protein aggregation is one of the most common form of antibody degradation, having significant implications for a therapeutic product under development; aggregation can result in reduced therapeutic efficacy, and may trigger severe immunogenic side effects when administered [8, 9]. Formulations of

biologics including mAbs and other protein products are stabilized with the use of additives such as salts, sugars, amino acids and surfactants [10-12]. Some novel formulation additives have also been investigated to inhibit protein aggregation, including deuterated solvents [13], hydrogels [14, 15], peptide dendrons [16] and ionic liquids [17]. However, the type and amount of additives allowed in any given formulation is limited, especially in parenteral formulations – which are often used to administer mAbs. Thus, other approaches to enhance the aggregation-resistance of mAbs are needed.

Another approach to significantly enhance the stability of a mAb is to modify the antibody structure itself. A single amino acid mutation in an aggregation-prone region (APR) can be sufficient to significantly improve the stability of an antibody against aggregation and/or increase its melting temperature. Predictions of aggregation-prone regions are often aided by computational tools – these include TANGO, AGGRESCAN3D, SAP [18-20], docking studies and/or molecular dynamics simulations [21]. For instance, the spatial aggregation propensity (SAP) tool has previously been used to guide mutations of aggregation-prone motifs of rituximab. These motifs predicted by SAP were ‘neutralised’ by single-point mutations, and multiple mutations were then combined to increase the overall antibody stability [22].

A variation of this approach, involves engineering an additional N-glycosylation site in a spatially proximate region to an APR, to sterically hinder aggregation in that APR [23, 24]. Naturally occurring N-linked glycans in the Fc domain are known to significantly influence antibody stability and effector function and to increase half-life in patient serum. The introduction of extra N-linked glycosylation sites in the Fab domain may not only improve resistance to aggregation, but also enhance solubility and conformational stability of the antibody, offering additional benefits to a single-point mutation in a hydrophobic region.

Courtois, et al. [23] recently tested a series of Fab-glycosylated bevacizumab variants and reported significant improvements in overall stability. Nakamura, et al. [24] also tested a glycan-introducing mutation in the Fab of adalimumab expressed in *Pichia pastoris* and found that it inhibited protease digestion and precipitation under pH stress. However, its impact on soluble aggregation of the full antibody is not clear.

In this study, we report on and discuss the stability of Fab-glycosylated adalimumab variants that have spatial proximity to a previously determined APR in the IgG1 C_H1 region of rituximab [22] and bevacizumab [23]. Specifically, the amino acid of the APR transposed to the adalimumab IgG1 peptide sequence is leucine 178. The substitution of this hydrophobic amino acid to lysine in bevacizumab [23], or to serine in rituximab [22] in the equivalent position, had experimentally demonstrated increased stability. This amino acid can also be substituted with asparagine (e.g. L178N) to introduce an N-linked glycosylation site. For this study, surface exposed amino acids were identified that can be substituted to asparagine to introduce N-linked glycosylation sites i.e. Asn-X-Ser/Thr, where X is any amino acid except proline (Fig. 1). All substitutions except T199N, were previously identified to have 10 Angstrom spatial proximity to the APR of

Table 1. Surface exposed amino acid (AA) residues identified in adalimumab Fab region for substitution

AA Residue	**Position**	**Region**	**Mutation**	**Proposed Function**
L	178	C_H1	K	Remove APR by introducing polar amino acid [23]
			N	Remove APR and introduce glycosylation site [23]
Q	160	C_{kappa}		Sterically hinder APR by introducing glycosylation site [23]
L	116	C_{join}		
T	118			
A	122	C_H1		Improve solubility by introducing glycosylation site [25]
Q	179			Sterically hinder APR by introducing glycosylation site [23, 25]
L	183			
T	199			Improve solubility and sterically hinder self-association by introducing glycosylation site [25, 26]

interest [22, 23]. T199N was specifically chosen as it had been reported to dramatically increase the solubility of a poorly soluble antibody [25], however it does not have spatial proximity to the APR. This particular substitution also has the potential to sterically hinder reversible self-association [26] which warranted further investigation through this study. The substitutions that were identified and pursued for this study are listed in Table 1.

.

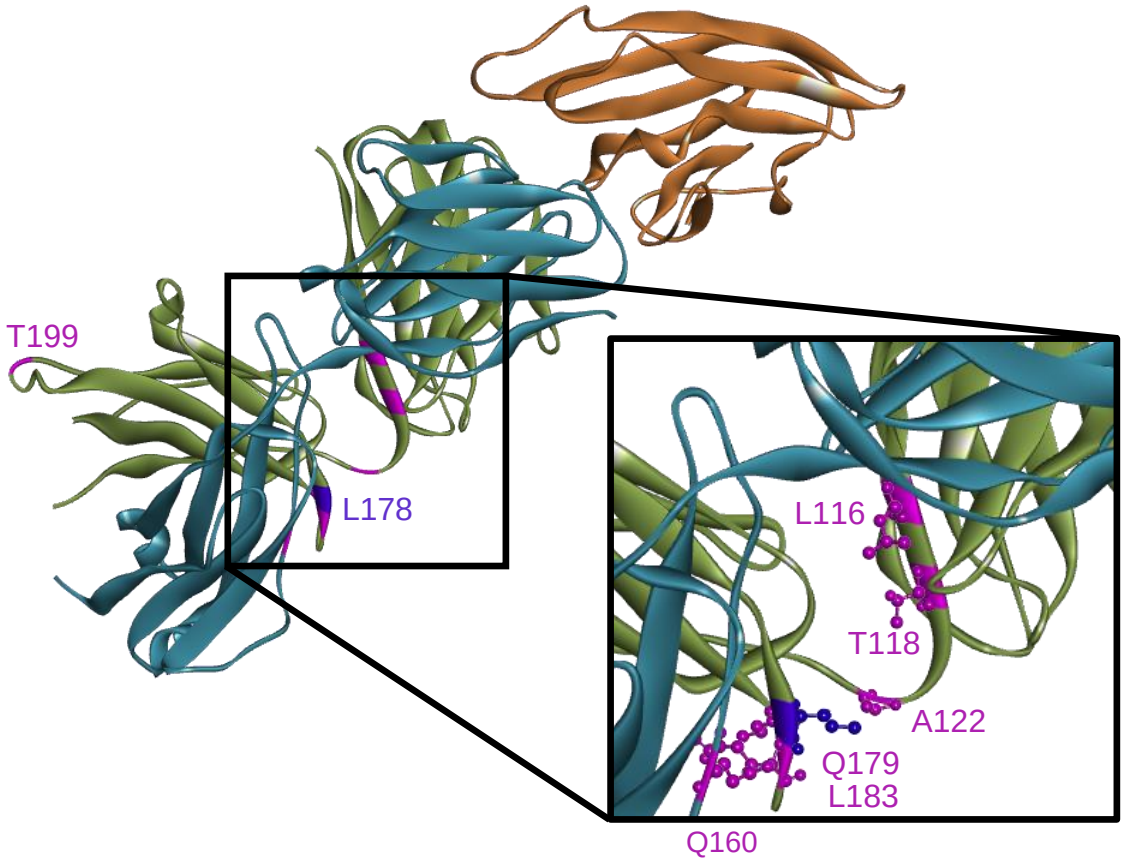

Figure 1. Crystal structure 3wd5 of adalimumab Fab fragment complexed to partial TNF-α fragment. Adalimumab V_H/C_H1 (green), V_L/C_L (aqua), TNF-α fragment (orange), APR site (purple) and surface exposed amino acids identified for substitution to an N-linked glycosylation site (pink).

In addition to studying the effect of these Fab N-linked glycosylations on the aggregation propensity of adalimumab, we also investigated the conformational stability of the variants, and characterised their binding affinity to TNF-α, and Fcγ receptors (FcγRs) responsible for effector function, to understand the broader impact of these additional glycans.

2. Materials and methods

2.1. Materials

Humira® subcutaneous injections (40 mg/0.8 mL) were purchased from Symbion (VIC, Australia) and used as a reference. Adalimumab (AdmAb) wild-type (WT) and mutant variants were expressed transiently in FreeStyle™ human embryonic kidney cells adapted for serum-free media (HEK293F). The expression vector gWiz (blank) was obtained from Genlantis (CA, USA) and vector pVITRO1-trastuzumab-IgG1/κ was a gift from Andrew Beavil (Addgene plasmid # 61883). Primers and synthetic AdmAb variable region gene constructs were purchased from Integrated DNA Technologies (Singapore). In-Fusion cloning kit was obtained from Scientifix (Australia). FreeStyle™ 293 Expression Medium, OptiPRO™ Serum Free Medium (SFM) and HIS-tagged FcRγ1A receptor were purchased from Life Technologies Pty Ltd (VIC, Australia). Polyethylenimine (PEI), Linear, MW 25 kDa was purchased from BioScientific (Australia). 0.22 µm PVDF filters), 50 kDa centrifugal filters, trypsin and chymotrypsin were purchased from Sigma Aldrich (Australia). PCR kits and all other enzymes were purchased from GeneSearch (Australia). Phosphate Buffered Saline (PBS) was purchased from Astral Scientific Pty Ltd (NSW, Australia). HiTrap MabSelect SuRe column, Biacore CM5 and ProA chips, amine coupling kit and HIS capture kit were purchased from GE Healthcare (Australia). All other receptors, chemicals, consumables and reagents were obtained from Sigma Aldrich (Australia).

2.2. Cloning and mutation of AdmAb WT and variants

The blank gWiz expression vector was used to construct separate AdmAb IgG1 and kappa chain expression vectors. The secretion signalling genes, IgG1 and kappa chain genes were sourced from genes contained in pVITRO1_trastuzumab_IgG1/κ vector; they were cloned separately into the empty gWiz vector through conventional restriction cloning techniques. The variable regions of AdmAb genes were designed and synthetically produced; they were exchanged with the trastuzumab variable regions in the gWiz vectors through In-Fusion cloning to produce gWiz AdmAb IgG1 and gWiz AdmAb kappa vectors.

Mutations were then introduced to the gWiz AdmAb IgG1 and kappa vectors through high fidelity inverse PCR to produce a library of AdmAb mutant expression vectors.

AdmAb WT and mutant variants were confirmed through sequencing and expressed through transfection of vector pair combinations.

2.3. Expression and Purification of AdmAb WT and variants

AdmAb WT and mutants were transiently expressed in suspension HEK293F culture. HEK293F culture was maintained and transfected in Freestyle 293F media, 120 rpm, 37 °C, 5% CO_2, humidified incubation conditions. 24 hours prior to transfection, HEK293F culture was seeded to 6 - 7 x 10^5 cells/mL in a 60 mL culture and the culture was adjusted to 1 x 10^6 cells/mL on the day of transfection.

The complexing DNA for transfection was prepared as 1 µg total DNA per 1 x 10^6 cells. The gWiz AdmAb IgG1 and kappa vectors were combined in a w/w ratio of 1:1, and the complexing w/w ratio of PEI to total DNA was 2:1. The vector DNA and PEI were separately diluted in OptiPRO SFM. The dilutions were combined and left to complex for 15 minutes before adding dropwise to the transfection culture.

After 24-hour incubation of the transfection culture, the culture was scaled up to 120 mL with Freestyle 293F media and supplemented to a total concentration of 0.5% Tryptone w/v. After a further 24 hours of incubation, the culture was scaled up to 240 mL with Freestyle 293F media and supplemented to a total concentration of 0.5% Tryptone w/v. The transfection culture remained in incubation for a total of 8 days before the media containing secreted antibody was harvested by centrifugation, and the culture supernatant was clarified by filtration.

AdmAb WT and variants were purified from the culture supernatants using protein A affinity with a 1mL HiTrap MabSelect SuRe column. PBS pH 7.4 was used as the binding and wash buffer, and glycine HCL pH 3 was used to elute bound antibody. Eluted antibody samples were neutralised in 1 M Tris-HCl pH 8 and concentrated to <1 mL using 50 kDa centrifugal filters. To purify the samples from any aggregates and obtain pure monomer samples, concentrated samples were fractioned using size-exclusion chromatography (as per 2.6) and the monomer fractions were collected and concentrated in 150 mM potassium phosphate buffer, pH 6.5, for analysis.

2.4. LC-MS/MS analysis of AdmAb variants

Successful mutation and introduction of glycosylation motifs of the AdmAb variants was confirmed through site-specific liquid chromatography tandem mass spectrometry (LC-MS/MS). Briefly, AdmAb variants were separated on reducing SDS-PAGE and

digested with trypsin and chymotrypsin. A fraction of the digestions was further treated with PNGase F for glycan release. The digestion products were analysed by LC-MS/MS using higher-energy collisional dissociation (HCD), collision induced dissociation (CID) and electron transfer dissociation (ETD) methods.

The AdmAb variants (10 µg) were run on a reducing SDS-PAGE, in-gel trypsin digestion was performed on the heavy chain band (50 - 60 kDa) of variants L116N, T118N, A122N, L178K, L178N, Q179N, L183N, T199N and the light chain band (25 - 30 kDa) of Q160N. The bands were excised, diced and washed with 50% (v/v) acetonitrile (MeCN) in 100 mM NH_4HCO_3. The gel pieces were then reduced with 10 mM DTT at 56 °C for 45 min, followed by alkylation by addition of 55 mM iodoacetamide (IAA) in 100 mM NH_4HCO_3, and incubation at 25 °C for 30 minutes. The samples were subsequently washed with 50% (v/v) MeCN in 100 mM NH_4HCO_3.

The alkylated polypeptides were incubated with trypsin (T6567) (1 µg trypsin per 50 µg antibody) in 50 mM NH_4HCO_3, pH 6.8 at 37 °C overnight. The resulting tryptic peptides were further digested with chymotrypsin (11418467001) in 100 mM Tris-HCl, 10 mM $CaCl_2$, pH 7.8 at room temperature overnight.

Glycan release was performed to confirm amino acid substitution; a fraction of the chymotryptic peptides (excluding L178K) was incubated with recombinant PNGase F (P0708S) (400 units per 1 µg of peptide) in 50 mM sodium phosphate buffer pH 7.5 at 37 °C overnight. The chymotryptic peptides and the de-glycosylated fractions were desalted with C18 ZipTips (Millipore), eluted in 80% (v/v) MeCN, dried by vacuum centrifugation then redissolved in 0.1% formic acid (FA) for LC-MS/MS analysis.

Glycopeptides and de-glycosylated peptides were separated on an in-house packed 20 cm × 75 µm Reprosil-Pur C18AQ (3 µm, 120 A; Dr. Maisch GmbH) column using a Dionex 3500RS HPLC over a 90-minute 0-40% solvent B gradient at a flow rate of 300 nL/min, at 60°C (solvent A was 0.1% (v/v) formic acid; solvent B was 80% (v/v) acetonitrile and 0.1% formic acid). MS analysis was performed on an Orbitrap Fusion MS (Thermo Scientific) in positive mode. Instrument parameters were set up as follows: source voltage = 2.3 kV, S-lens RF level = 68%, and capillary temperature = 275 °C. The initial MS scan was acquired in the Orbitrap mass analyzer (350–2000 m/z; MS AGC = 6×10^5) with a resolution of 60,000 at 400 m/z. MS1 was followed by data-dependent HCD using top speed, where as many dependant scans as possible

are acquired in a specified time. HCD fragmentation was followed by re-isolation of the top two most intense precursors, and fragmentation with CID and ETD MS/MS. HCD parameters were as follows: activation time = 0.1 ms, resolution = 30,000, maximum injection time = 200 ms, dynamic exclusion = enabled with repeat count 1, normalized energy = 40, exclusion duration = 20 s, default charge state = 2, and MSn AGC 2.0e5. CID parameters were as follows: 30,000 resolution in orbitrap, activation time = 10 ms, max injection time = 300 ms, dynamic exclusion = enabled with repeat count 1, normalized energy = 35, exclusion duration = 20 s, default charge state = 2, and MSn AGC 5.0e4. ETD parameters were as follows: 30,000 resolution in orbitrap, 5.0e4 AGC, ETD reaction time = 50 ms, Max injection time = 300 ms.

The peptide spectrum matches (PSM) were generated through a search against the corresponding fasta file (wild-type or variant Adalimumab amino acid sequence) utilising the search engine Byonic (Protein Metrics Inc.). Annotation of the HCD and ETD spectra were automated through Byonic and the PSM assignments were validated by manually annotating the aforementioned spectra and the complementary CID spectrum. Further confirmation of the identity assignment was achieved through analysis of the de-glycosylated chymotryptic peptides utilising the same LC-MS/MS approach as for the glycosylated fraction.

2.5. Accelerated stability at elevated temperatures

We performed accelerated studies at an elevated temperature as previously described [7]. Briefly, 20 µL of each AdmAb variant (1 mg/mL) was pipetted into a 0.2 mL PCR vial and incubated at 65 °C for 1, 2 or 3 hours in a Thermal Cycler (Applied Biosystems, CA, USA) to induce aggregation. Each experiment was repeated three times. A thermal cycler was used to minimize sample amount and prevent evaporation of the sample and consequent changes in antibody concentration during incubation (lid/cover of thermal cycler is heated above incubation temperature). Following incubation, incubated samples were removed and immediately stored on ice to halt aggregation and then characterized by size exclusion-high performance liquid chromatography (SE-HPLC).

2.6. SE-HPLC analysis of monomer loss

Size exclusion-high performance liquid chromatography (SE-HPLC) was used to quantify AdmAb monomer loss following incubation at elevated temperature as

previously described [7]. Analysis was performed using an Agilent 1200 Liquid Chromatography system (Agilent Technologies, California, USA) with a Zorbax GF-250 column coupled to a guard column at 22 °C, using a 150 mM potassium phosphate pH 6.5 mobile phase, and a flow rate of 0.5 mL/min. 5 µL of each incubated sample was then immediately injected and each injection was repeated three times. Monomer peaks were detected using an in-line UV signal detector set at 280 nm. The area under the curve (AUC) of the monomer peak was averaged over the three runs and the mean relative monomer % was calculated for each sample, by setting the monomer AUC of the non-incubated samples as 100% and calculating the change in monomer AUC accordingly. The standard deviations (SD) were plotted as error bars in the figures.

2.7. AdmAb melting temperature (T_m) and onset temperature of aggregation (T_{agg})

The T_m and T_{agg} of Humira®, AdmAb WT, and variants were simultaneously measured using intrinsic tryptophan fluorescence and static light scattering (SLS), respectively, on the UNcle system (Unchained Labs, CA, USA). A linear temperature ramp from 15 to 95 °C at a 1 °C/min scan rate was performed whilst measuring tryptophan fluorescence and SLS simultaneously through laser excitation at 266 nm. 8.5 µL of each AdmAb sample (1 mg/mL) was pipetted undiluted into the UNcle UNI (a sample holding unit containing 16 quartz cells) in triplicates. A holding time was not used to maximise the frequency of measurements. T_m and T_{agg} were determined by the UNcle Analysis software. The barycentric mean (BCM) was used to plot the T_m curves, which is defined by the following equation:

$$\lambda_{BCM} = \frac{\sum_\lambda \lambda I(\lambda)}{\sum_\lambda I(\lambda)}$$

The equation is defined over the range 300-450 nm; each wavelength value (λ) is multiplied by the tryptophan fluorescence intensity (I) at that wavelength, and the sum of that value for all wavelengths between 300-450 is divided by the sum of the intensities at those wavelengths. This results in an 'averaged' peak wavelength (λ_{BCM}) for a given spectrum.

2.8. Binding kinetics (K_D) to TNFα and Fc_γ receptors ($Fc_\gamma Rs$)

The binding kinetics of Humira®, AdmAb WT and variants were assessed to TNF-α and $Fc_\gamma R1A$, 2B and 3A through surface plasmon resonance (SPR) to confirm that the

mutations did not contribute to a loss of biological function. Briefly, a Biacore T200 system (GE Healthcare, Australia) was used, running single cycle kinetic assays. Monomeric AdmAb samples were captured on a ProA chip and increasing dilutions of TNF-α were injected, with a 60-minute dissociation. HIS-tagged FcγR1A, 2B and 3A were captured on an anti-HIS chip and increasing dilutions of monomeric AdmAb samples were injected, with a 30-minute dissociation. The sensograms were analysed to determine association (K_a), dissociation (K_d) and equilibrium binding constants (K_D). All runs were performed at 25 °C with running buffer HBS-T (10 mM HEPES, 150 mM NaCl, 0.05% v/v Tween 20, pH adjusted to 7.4).

Soluble homotrimeric TNF-α (H8916) was assayed against monomeric AdmAb samples on a ProA chip under continuous flow rate of 20 µL/min. Monomeric AdmAb samples were prepared to 10 nM and captured on the sensor chip surface with a contact time of 10 seconds. TNF-α was injected in 2-fold increasing concentrations (2.5 – 40 nM) with a contact time of 120 seconds at each concentration, then a dissociation time of 60 minutes. The chip surface was regenerated with 50 mM NaOH for 30 seconds at a flow rate of 30 µL / min.

Monomeric AdmAb samples were assayed against HIS tagged FcR_γ receptors. Anti-HIS antibody was covalently attached to a CM5 biosensor chip using an amine coupling kit and HIS capture kit. HIS tagged FcγR1A (10256H08H), FcγR2B (SRP6396) and FcγR3A (SRP6436) were prepared to 4 nM and captured to the sensor chip surface with a contact time of 300 seconds at 5 µL/min flow rate. AdmAb samples were injected on FcγR1A coated surface in 2-fold increasing concentrations (2.5 – 40 nM) at a flow rate of 20 µL/min with a contact time of 120 seconds at each concentration, followed by 30-minute dissociation time. AdmAb samples were injected on FcγR2B and FcγR3A-coated surfaces in 2-fold increasing concentrations (25 – 400 nM unless otherwise stated) at a flow rate of 10 µL/min with a contact time of 120 seconds at each concentration, followed by 1800 second dissociation time. The chip surface was regenerated with 10 mM Glycine HCl, pH 1.5 for 60 seconds at a flow rate of 30 µL/min.

The sensograms were analysed globally using a Langmuir 1:1 binding model to determine K_a, K_d and K_D. All samples were conducted in duplicate to obtain average values and standard deviation. Kinetic rate and binding constants determined from

sensograms were accepted if the goodness of fit value (χ^2) was within 5% of the maximum response level (R_{max}) of the sensograms and K_D was calculated as K_d/K_a.

3. Results

3.1. Confirmation of mutation and glycan attachment through LC-MS/MS

Detailed analysis of LC-MSMS data confirmed that all AdmAb variants had successful amino acid substitution. Incorporation of HCD, ETD and CID fragmentation techniques further provided compositional glycan information of the new *N*-glycosylation sites. Except for Q160N mutant, all other AdmAb glycosylation-site variants were found to contain an *N*-glycan (data not shown).

Here, we show the characterization of glycan site-engineered AdmAb variant T199N as a representation of the analysis performed for all AdmAb variants.

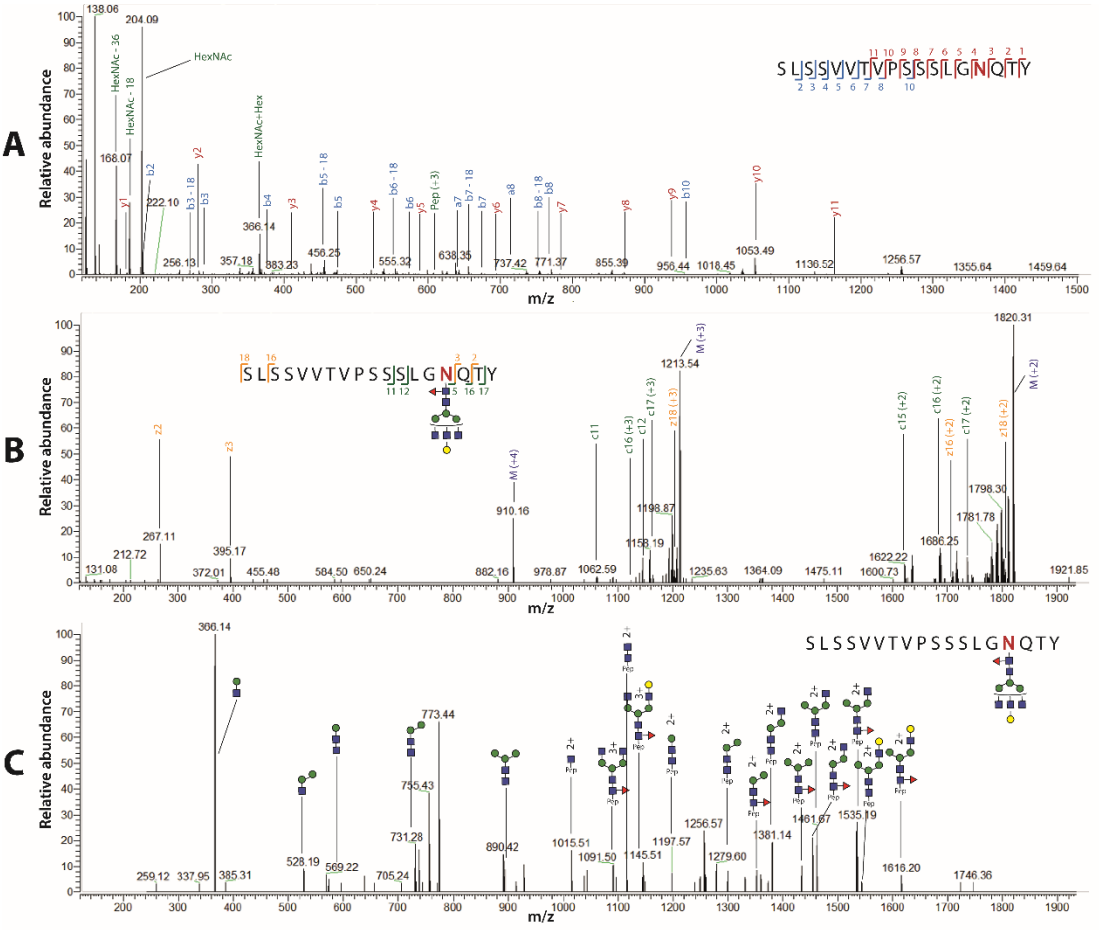

Figure 2. (A) HCD, (B) ETD and (C) CID spectra of chymotryptic T199N glycopeptide observed at m/z 909.65 (4+). Peptide sequence SLSSVVTVPSSSLGNQTY and attached complex type *N*-glycan $HexNAc_5Hex_4Fuc_1$ are shown. Blue square; *N*-acetylglucosamine, red triangle; fucose, green circle; mannose, yellow circle; galactose, Hex; hexose, HexNAc; N-acetylhexosamine, M; precursor ion.

HCD spectrum of SLSSVVTVPSSSLG*N*QTY peptide observed at m/z 909.65(4+) showed b- and y-ion series confirming amino acid sequence and the asparagine substitution was shown specifically by y4-y11 fragment ions (Fig. 2A). HCD of T199N mutant also contained diagnostic HexNAc (*m/z* 204.09) and HexNAcHex (*m/z* 366.14) oxonium ions, strongly indicating glycosylation on the mutant peptide (Fig. 2**Figure**A). ETD further confirmed the structure of T199N glycopeptide by multiple fragment ions corresponding to dissociated peptide backbone with intact glycan (Figure 2B, c-15, c-16, c-17 and z-16 ions). Theoretical monosaccharide composition of the *N*-glycan was derived using Byonic (Protein Metrics) search results and GlycoMod (https://web.expasy.org). CID data in Figure 2C shows sequential loss of monosaccharides from glycopeptide fragments of T199N mutant and contains complementary oxonium ions m/z 366.14, m/z 528.19, and m/z 569.22 of the observed glycan in the low mass region. Extensive glycosidic bond cleavages (Fig. 2C, y-ions, m/z 1616.2(2+), m/z 1535.19(2+), m/z 1461.67(2+)) observed in CID confirmed that SLSSVVTVPSSSLG*N*QTY peptide is occupied by a complex type *N*-glycan with $HexNAc_5Hex_4Fuc_1$ composition. CID spectra of deglycosylated T199N peptide m/z 609.64(3+) showed enhanced peptide backbone fragmentation and provided additional information for the expected mass shift from threonine to asparagine (y4-y18 ions and b17 ion, Fig. 3). Same ion series also displayed deamidation (+1Da) of the new asparagine residue which is a characteristic result of PNGaseF treatment of a formerly *N*-glycosylated peptide.

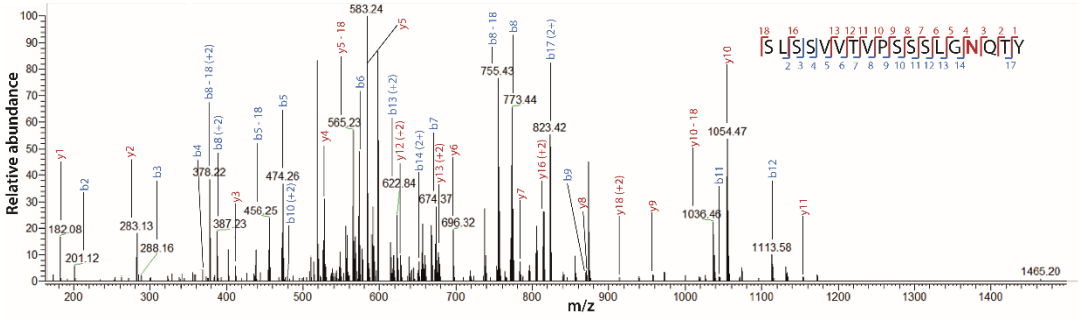

Figure 3. CID spectrum of de-glycosylated chymotryptic T199N mutant peptide SLSSVVTVPSSSLGNQTY observed at m/z 609.64(3+). b- and y- ions show CID fragments of the peptide.

3.2. Monomer loss following accelerated studies at elevated temperature

Incubation at 65 °C revealed modest differences in aggregation propensity between the reference Humira®, WT and single-mutant variants (Fig. 4). Variants L116N and T118N were completely degraded after an hour of incubation and were therefore not

included in the figure (Fig. 4). Variant Q160N had very similar monomer loss data at all incubation temperatures to the WT, while L183N had a noticeably higher monomer loss. Variants A122N, Q179N and T199N retained higher monomer content than the control at most incubation conditions, with A122N having the least monomer loss (Fig. 4). While Q179N had comparable monomer loss after 1 hour, monomer loss was lower at 2 and 3 hours, when compared to the WT. Interestingly, variants L178N and L178K had comparable monomer loss profiles which were not significantly different to the WT (Fig. 4). Humira® reference had slightly lower monomer loss than the WT.

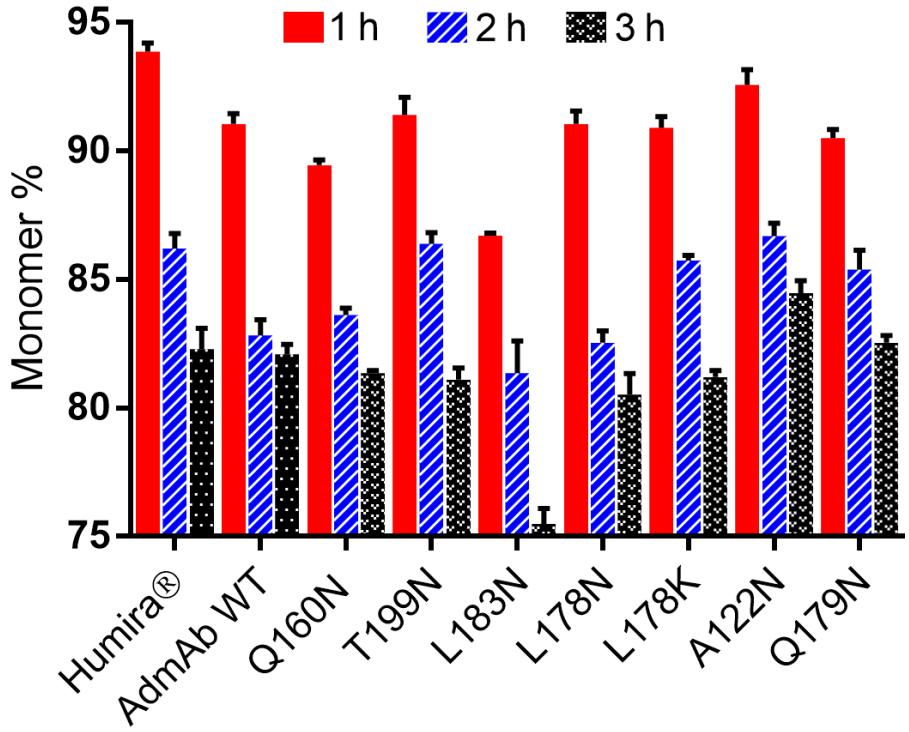

Figure 4. Monomer loss of Humira®, AdmAb wild-type (WT) and variants following incubation at 65 °C for 1, 2 and 3 hours. Error bars represent the SD.

3.3. T_m and T_{agg}

The WT AdmAb had a very similar T_m1 and T_m2 to the Humira® reference product; a slightly lower T_m1 was measured at 69.6 °C (WT) compared with 70.8 °C (Table 2). The T_m2 was comparable at 82 °C compared with 82.5 °C for Humira®. Variant Q160N had a similar melting profile to the WT, with an identical T_m1 and comparable T_m2 of 69.6 and 82 °C, respectively. Variants T118N and L116N had a significantly lower T_m1 at 59.7 and 63.6 °C, respectively; the T_m2 was also lower at 68 and 78.6 °C, respectively. Interestingly, a third T_m was recorded for variants T118N and L116N at 87.8 and 88.3 °C, respectively. Variants L178K, A122N and Q179N had similar T_ms

and were comparable to the WT. Variants T199N and L178N had similar T_m1 values to the WT (70.6 and 69.9 °C, respectively), but significantly higher T_m2 values (88.2 and 89.3 °C, respectively). Variant L183N had a similar T_m1 to the WT, but had a consistent minor unfolding event at ~65 °C (not shown); T_m2 was higher than the WT (88.3 °C, Table 2). The T_{agg} of the WT and variants ranged from 70.6 to 72.5 °C, except for variants T118N and L116N, which had significantly lower T_{agg} values (61.7 and 64.7 °C, respectively; Table 2). Most variants had a slightly higher T_{agg} than the WT (70.7 °C) by approximately 1-2 °C, while the T_{agg} of Q160N and L178K were unchanged. Compared with L178K, the T_{agg} of glycosylated variant L178N was 1.7 °C higher.

Table 2. The melting (T_m) and onset of aggregation temperatures (T_{agg}) of the AdmAb variants compared with the wild-type (WT) and reference Humira® product. ^see discussion

AdmAb	**T_m1 (°C)** ± SD	**T_m2 (°C)**	**T_m3 (°C)**	**T_{agg} @266 nm**
Humira®	70.8 ± 0.2	82.5 ± 0.8	-	71.3 ± 0.4
WT	69.6 ± 0.5	82 ± 1.4	-	70.7 ± 0.1
Q160N	69.6 ± 0.3	81.1 ± 1.4	-	71 ± 0.4
T199N	70.6 ± 0.2	88.2 ± 2.2	-	71.7 ± 0.1
T118N	59.7 ± 0.5	68 ± 0.7	87.8 ± 2.5	61.7 ± 0.6
L178K	68.4 ± 0.6	83.5 ± 0.5	-	70.6 ± 0.3
L178N	69.9 ± 0.5	89.3 ± 0.2	-	72.3 ± 0.3
A122N	69.7 ± 0.5	83.4 ± 0.7	-	71.8 ± 0.4
Q179N	69.4 ± 0.2	82.7 ± 0.9	-	71.7 ± 0.5
L118N	63.6 ± 0.5	78.6 ± 0.5	88.3 ± 1.2	64.7 ± 0.3
L183N	70^ ± 0.5	88.3 ± 1.1	-	72.5 ± 0.7

3.4. Binding kinetics of AdmAb to TNF-α and FcγRs

The binding kinetics of reference Humira®, monomeric AdmAb WT and variants to TNF-α and $Fc_\gamma R1A$, 2B and 3A were assessed using SPR single cycle kinetic analysis. Samples were run in duplicate and sensograms were fitted to a Langmuir 1:1 binding model to obtain K_a, K_d and K_D values for comparison as per previous studies [27, 28]. It was determined that in general, the majority of AdmAb variants did not experience a significant loss of biological activity.

The K_D range determined for monomeric AdmAb variants binding to soluble homotrimeric TNF-α spanned 36.69 – 110.27 pM, while Humira® had a mean K_D of 30.77 pM (Table 3). Monomeric AdmAb WT had a K_D of 66.43 ± 2.37 pM which lies within the range, with no significant outlier (Table 3). Of all variants tested, T199N had the strongest K_D to TNF-α (36.69 pM) - approximately 1.8-fold stronger than the WT - while Q179N had the weakest K_D (110.27 pM).

The K_D range determined for FcγR1A binding to monomeric AdmAb variants spanned 2.1 – 6.81 nM, while Humira® had a mean K_D of 1.84 nM (Table 4). Monomeric AdmAb WT had a K_D of 4.4 ± 0.01 nM which lies within the range with no significant outlier (Table 4). Of all variants tested, the strongest K_D was recorded for mutant T118N (2.1 nM), while the weakest K_D was recorded for L178N (6.81 nM).

Due to sample limitations, monomeric AdmAb Q160N was not tested for the cycle assays against FcγR2B (Table 4).

The K_D range determined for FcγR2B binding to monomeric AdmAb variants spanned 1.81 – 9.61 nM, while Humira® had a mean K_D of 2.55 nM. Monomeric AdmAb WT had a K_D of 4.47 ± 0.1 nM which lies within the range with no significant outlier (Table 4). T199N had the strongest K_D to FcγR2B (1.81 nM), while T118N had the weakest K_D (9.61 nM). However, due to the large variation in K_D values for the WT and several mutants, most differences were not deemed significant.

The K_D range determined for FcγR3A binding to monomeric AdmAb variants spanned 1.48 – 18.01 nM, while Humira® had a mean K_D of 1.84 nM. Monomeric AdmAb WT had a K_D of 5.96 ± 1.62 nM which lies within the range with no significant outlier (Table 4). The strongest K_D was recorded for L183N (1.48 nM), while the weakest K_D was recorded for A122N (18.01 nM) with large ranges. Overall, all differences in K_D recorded compared to the WT, were no larger or smaller than 3-fold for TNF-α and all receptors tested.

4. Discussion

We rationally designed and produced a library of glycan-engineered AdmAb variants to enhance stability through steric hindrance of an APR. Successful mutation and glycan addition was confirmed for all mutants aside from Q160N, through LC-MS/MS. Consequently, the stability and binding kinetics results for the Q160N variant are

directly related to the amino acid substitution alone. Since Q160N had similar stability and antigen binding affinity to the WT, it was concluded that the amino acid substitution did not have any significant impact on the antibody properties tested. The K_D values for the AdmAb WT produced in our study (Table 3 and 4) are comparable to Humira® K_D values observed, and as reported in the literature; TNF-α (30-110 pM), FcγR1A (15-23 nM), FcγR2B (4.3-14.2 nM) and FcγR3A (5.8-7.9 nM) [29, 30].

Table 3. Kinetics and binding affinity of reference (Humira®) and monomeric AdmAb mutants to soluble homotrimeric TNF-α (± SD).

AdmAb	TNF-α		
	K_a (x 10^5) $M^{-1}.s^{-1}$	**K_d** (x 10^{-5}) s^{-1}	**K_D** (pM)
Humira®	11.7 ± 0.01	3.59 ± 0.80	30.77 ± 6.83
WT	6.08 ± 0.07	4.04 ± 0.10	66.43 ± 2.37
L178K	4.84 ± 0.01	4.61 ± 0.64	95.33 ± 13.3
L178N	5.33 ± 0.03	5.42 ± 0.67	101.7 ± 12.1
Q160N	6.2 ± 0.07	2.86 ± 0.05	46.05 ± 1.31
L116N	5.19 ± 0.09	2.84 ± 0.1	54.77 ± 2.87
T118N	5.04 ± 0.02	3.59 ± 0.21	71.19 ± 4.50
A122N	6.47 ± 0.03	2.87 ± 0.05	44.32 ± 0.57
Q179N	5.02 ± 0.40	5.53 ± 0.1	110.3 ± 6.56
L183N	5.58 ± 0.14	3.05 ± 0.03	55.37 ± 0.86
T199N	7.15 ± 0.69	2.62 ± 0.01	36.69 ± 3.54

Likewise, most measured K_D values for the mutants tested lay within a close range to reported literature values for the reference AdmAb, showing that these mutations had minimal impact on binding properties.

The highest improvement in resistance to aggregation was observed in mutant A122N with a slight increase in T_{agg} and reduction in monomer loss (Table 2 and Fig. 4). The A122N mutation resulted in 1.5-fold increased binding affinity to TNF-α with slightly reduced binding to $Fc_{\gamma}Rs$ tested and with no impact on conformational stability. Pepinsky, et al [25] reported that a mutation equivalent in position to AdmAb variant. A122N significantly improved the solubility of an anti-LINGO antibody, with no impact

on binding affinity or conformational stability. Improvements in solubility often correlate with reduced precipitation and insoluble aggregate formation.

This may explain the minor improvement in T_{agg} we observed with mutant A122N which reflects a higher resistance to precipitation at higher temperatures. Although only a minor improvement in monomer loss, the improvement is consistent at higher concentrations tested (15 mg/mL, data not shown) and is significant in a clinical setting, where typically no more than 5% of aggregates are considered acceptable by regulatory standards.

Table 4. Binding affinity of reference Humira® and monomeric AdmAb mutants to FcγR1A, FcγR2B and FcγR3A.

AdmAb	K_D (nM)		
	FcγR1A	**FcγR2B**	**FcγR3A**
Humira®	1.84 ± 0.18	2.55 ± 1.67	1.84 ± 0.68
WT*	4.4 ± 0.01	4.47 ± 1.00	5.96 ± 1.62
L178K	4.14 ± 0.06	9.16 ± 6.86	2.37 ± 1.19
L178N	6.81 ± 0.45	3.67 ± 0.93	2.15 ± 0.73
Q160N	5.3 ± 0.01	N.D.	16.2 ± 3.05
L116N	3.87 ± 0.14	6.15 ± 1.10	6.71 ± 1.91
T118N	2.1 ± 0.01	9.61 ± 1.38	13.3 ± 0.45
A122N	5.58 ± 0.18	7.53 ± 2.74	18.01 ± 7.4
Q179N	2.74 ± 0.01	5.27 ± 0.11	2.92 ± 0.16
L183N	2.6 ± 0.04	2.52 ± 2.05	1.48 ± 0.84
T199N	6.49 ± 0.06	1.81 ± 1.25	11.80 ± 0.2

No significant improvements in monomer loss were observed with other mutants (e.g. T199N and Q179N). Courtois, et al [22] hypothesised that a mutant equivalent in position to Q179N in bevacizumab could not be glycosylated as it was inaccessible to glycosylases. However, we confirmed that Q179N was glycosylated; likewise, Pepinsky, et al. [25] were able to express a glycosylated variant with a mutation in an equivalent position to Q179N which mildly improved antibody solubility. Accessibility to glycosylases does not determine whether the initial glycan is added or not, as this addition occurs in the endoplasmic reticulum prior to the folding of the protein. Thus,

it may have been possible to introduce a glycan in this position with bevacizumab as well. Nevertheless, with the additional N-glycan, Q179N was expected to sterically hinder Fab-mediated aggregation in the targeted APR; while T199N was reported to significantly improve solubility [25] and sterically hinder self-association [26], however this was not observed for AdmAb. The Q179N mutation also mildly reduced antigen binding affinity by ~1.6-fold. Interestingly, Pepinsky, et al. [25] reported no change in the T_m of the mutation equivalent in position to AdmAb variant T199N, while we observed a significant improvement in Fab T_m with variant T199N (~6 degrees higher). Additionally, T199N had 1.8-fold improved K_D to TNF-α with minimal differences in K_D to $Fc_\gamma Rs$. The lack of improvement in resistance to aggregation, despite the improvement in Fab stability, may be related to the mechanism of aggregation in AdmAb. Since the C_H2 has the lowest T_m in most IgG1s, it is expected that most aggregation steps are at least initiated with unfolding of the C_H2; thus, an improvement in Fab stability may not significantly impact overall resistance to soluble aggregation.

Similarly, we observed an improvement in Fab T_m for mutants L178N and L183N. L178N is an interesting example, because when compared to the non-glycosylated variant L178K, there is an improvement in T_{agg} and Fab T_m through glycosylation. This emphasises the impact of the N-glycans added via mutation on the conformational stability of the Fab and its resistance to precipitation, and highlights that these changes are not due to the amino acid substitution. The mutation significantly improved the conformational stability of the Fab domain. Furthermore, despite suppressing pH-induced precipitation when tested on the Fab alone [24], the L178N mutation had minimal impact on soluble aggregation when tested on the full AdmAb. Surprisingly, the non-glycosylated variant L178K which was reported to significantly suppress aggregation in bevacizumab [23], but enhance aggregation in rituximab [22], also had minimal impact on the stability of AdmAb. This finding highlights that framework regions differ significantly between IgG1 antibodies despite having identical sequences.

Variants L116N and T118N had multiple T_ms, with a lower T_m1, higher T_m3 and a significantly reduced T_{agg}; additionally, they were completely degraded at 65 °C. The T_ms of these mutants are harder to interpret, and do not necessarily represent the C_H2, Fab and C_H3 in that order. As previously reported [31], disturbances in the joining region between the Fab domains can create additional T_ms for each separate domain.

Thus, we expect that the T_m1 value of these mutants is representative of only part of the Fab (for e.g. the C_H1 or V_L); since the T_m of this part of the Fab is now less stable than the C_H2, aggregation proceeded more rapidly at 65 °C. Again, our results do not correspond with findings reported for the mutation equivalent to AdmAb L116N in bevacizumab, which showed improved resistance to aggregation with no destabilization of the Fab [23]. Some perturbation in Fab stability was also observed with mutant L183N, resulting in increased monomer loss. The perturbation was minor and hard to detect; however consistently appeared in temperature ramps for T_m measurement. It is likely that the amino acid substation in this position impaired the conformational stability of part of the Fab domain as observed with mutants L116N and T118N.

5. Conclusion

Protein aggregation is a complex challenge hindering the development and long-term stability of therapeutic mAbs. Using advanced computational tools, we identified aggregation prone regions and engineered adalimumab, a marketed therapeutic mAb, with additional N-glycans in the Fab domain, with the aim to sterically hinder aggregation and increase long-term stability. Our glycan-engineered variants displayed a range of different stabilities, with some mutations increasing susceptibility to aggregation, others enhancing the conformational stability of the Fab domain, and one showing minor improvements in resistance to aggregation. This approach has potential application for other antibodies where the Fab domain has poor stability or is a pre-cursor to aggregation. We demonstrated that the conformational stability of blockbuster therapeutic antibodies such as AdmAb can still be improved with glycan-engineering without compromising its antigen and Fc receptor binding affinity; these findings highlight the significant value of this engineering approach in the quest for developing more stable therapeutic mAbs with improved half-lives and therapeutic outcomes.

Acknowledgements

The authors would like to acknowledge the Bosch Institute, Australia for technical help. E. Cruz would like to acknowledge the Ministry of Science, Technology and Telecommunications of the Republic of Costa Rica for the awarded postgraduate scholarship. M. Reslan is a recipient of the Research Training Program stipend

provided by the University of Sydney on behalf of the Department of Education and Training to support his research training.

References

[1] L. Urquhart, Top drugs and companies by sales in 2017, Nature Reviews Drug Discovery, 17 (2018) 232.
[2] D.M. Ecker, S.D. Jones, H.L. Levine, The therapeutic monoclonal antibody market, mAbs, 7 (2015) 9-14.
[3] C. Klein, Special Issue: Monoclonal Antibodies, Antibodies, 7 (2018) 17.
[4] Z. Elgundi, M. Reslan, E. Cruz, V. Sifniotis, V. Kayser, The state-of-play and future of antibody therapeutics, Adv. Drug Delivery Rev., 122 (2017) 2-19.
[5] M.L. Fleischman, J. Chung, E.P. Paul, R.A. Lewus, Shipping-Induced Aggregation in Therapeutic Antibodies: Utilization of a Scale-Down Model to Assess Degradation in Monoclonal Antibodies, J. Pharm. Sci., 106 (2017) 994-1000.
[6] A. Beck, L. Goetsch, C. Dumontet, N. Corvaïa, Strategies and challenges for the next generation of antibody–drug conjugates, Nature Reviews Drug Discovery, 16 (2017) 315.
[7] V. Kayser, N. Chennamsetty, V. Voynov, B. Helk, K. Forrer, B.L. Trout, Evaluation of a Non-Arrhenius Model for Therapeutic Monoclonal Antibody Aggregation, J. Pharm. Sci., 100 (2011) 2526-2542.
[8] J. Bessa, S. Boeckle, H. Beck, T. Buckel, S. Schlicht, M. Ebeling, A. Kiialainen, A. Koulov, B. Boll, T. Weiser, T. Singer, A.G. Rolink, A. Iglesias, The Immunogenicity of Antibody Aggregates in a Novel Transgenic Mouse Model, Pharm. Res., 32 (2015) 2344-2359.
[9] M. Ahmadi, C.J. Bryson, E.A. Cloake, K. Welch, V. Filipe, S. Romeijn, A. Hawe, W. Jiskoot, M.P. Baker, M.H. Fogg, Small Amounts of Sub-Visible Aggregates Enhance the Immunogenic Potential of Monoclonal Antibody Therapeutics, Pharm. Res., 32 (2015) 1383-1394.
[10] M. Reslan, Y.K. Demir, B.L. Trout, H.-K. Chan, V. Kayser, Lack of a synergistic effect of arginine–glutamic acid on the physical stability of spray-dried bovine serum albumin, Pharm. Dev. Technol., (2016) 1-7.
[11] J. Zhang, V. Frey, M. Corcoran, J. Zhang-van Enk, J.A. Subramony, Influence of Arginine Salts on the Thermal Stability and Aggregation Kinetics of Monoclonal Antibody: Dominant Role of Anions, Molecular Pharmaceutics, 13 (2016) 3362-3369.

[12] R. Respaud, D. Marchand, C. Parent, T. Pelat, P. Thullier, J.-F. Tournamille, M.-C. Viaud-Massuard, P. Diot, M. Si-Tahar, L. Vecellio, N. Heuzé-Vourc'h, Effect of formulation on the stability and aerosol performance of a nebulized antibody, mAbs, 6 (2014) 1347-1355.
[13] M. Reslan, V. Kayser, The effect of deuterium oxide on the conformational stability and aggregation of bovine serum albumin, Pharm. Dev. Technol., (2016) 1-7.
[14] B.V. Sridhar, J.R. Janczy, Ø. Hatlevik, G. Wolfson, K.S. Anseth, M.W. Tibbitt, Thermal Stabilization of Biologics with Photoresponsive Hydrogels, Biomacromolecules, 19 (2018) 740-747.
[15] J. Lee, J.H. Ko, K.M. Mansfield, P.C. Nauka, E. Bat, H.D. Maynard, Glucose-Responsive Trehalose Hydrogel for Insulin Stabilization and Delivery, Macromolecular Bioscience, 18 (2018) 1700372.
[16] R. Bansal, S. Dhawan, S. Chattopadhyay, G.P. Maurya, V. Haridas, A.S. Rathore, Peptide Dendrons as Thermal-Stability Amplifiers for Immunoglobulin G1 Monoclonal Antibody Biotherapeutics, Bioconjugate Chem., 28 (2017) 2549-2559.
[17] M. Reslan, V. Kayser, Ionic liquids as biocompatible stabilizers of proteins, Biophys. Rev., 10 (2018) 781-793.
[18] N. Chennamsetty, V. Voynov, V. Kayser, B. Helk, B.L. Trout, Design of therapeutic proteins with enhanced stability, Proc. Natl. Acad. Sci., 106 (2009) 11937-11942.
[19] S. Kulshreshtha, V. Chaudhary, G.K. Goswami, N. Mathur, Computational approaches for predicting mutant protein stability, J. Comput. Aided Mol. Des., 30 (2016) 401-412.
[20] R. Zambrano, M. Jamroz, A. Szczasiuk, J. Pujols, S. Kmiecik, S. Ventura, AGGRESCAN3D (A3D): server for prediction of aggregation properties of protein structures, Nucleic Acids Res., 43 (2015) W306-W313.
[21] S. Kuyucak, V. Kayser, Biobetters From an Integrated Computational/Experimental Approach, Comput. Struct. Biotechnol. J., 15 (2017) 138-145.
[22] F. Courtois, C.P. Schneider, N.J. Agrawal, B.L. Trout, Rational Design of Biobetters with Enhanced Stability, J. Pharm. Sci., 104 (2015) 2433-2440.
[23] F. Courtois, N.J. Agrawal, T.M. Lauer, B.L. Trout, Rational design of therapeutic mAbs against aggregation through protein engineering and incorporation of glycosylation motifs applied to bevacizumab, mAbs, 8 (2016) 99-112.

[24] H. Nakamura, N. Oda-Ueda, T. Ueda, T. Ohkuri, Introduction of a glycosylation site in the constant region decreases the aggregation of adalimumab Fab, Biochem. Biophys. Res. Commun., (2018).
[25] R.B. Pepinsky, S. Laura, B.S. A., F. Graham, L. Alexey, W. Lee, E. John, C. Allan, M. Sha, G. Christilyn, G. Ellen, Improving the solubility of anti-LINGO-1 monoclonal antibody Li33 by isotype switching and targeted mutagenesis, Protein Sci., 19 (2010) 954-966.
[26] T.F. Lerch, P. Sharpe, S.J. Mayclin, T.E. Edwards, E. Lee, H.D. Conlon, S. Polleck, J.C. Rouse, Y. Luo, Q. Zou, Infliximab crystal structures reveal insights into self-association, mAbs, 9 (2017) 874-883.
[27] R. Karlsson, E. Pol, Å. Frostell, Comparison of surface plasmon resonance binding curves for characterization of protein interactions and analysis of screening data, Anal. Biochem., 502 (2016) 53-63.
[28] J.M. Hayes, A. Frostell, R. Karlsson, S. Muller, S.M. Martín, M. Pauers, F. Reuss, E.F. Cosgrave, C. Anneren, G.P. Davey, P.M. Rudd, Identification of Fc Gamma receptor glycoforms that produce differential binding kinetics for rituximab, Molecular and Cellular Proteomics, 16 (2017) 1770-1788.
[29] Z. Kaymakcalan, P. Sakorafas, S. Bose, S. Scesney, L. Xiong, D.K. Hanzatian, J. Salfeld, E.H. Sasso, Comparisons of affinities, avidities, and complement activation of adalimumab, infliximab, and etanercept in binding to soluble and membrane tumor necrosis factor, Clinical Immunology, 131 (2009) 308-316.
[30] L. Magnenat, A. Palmese, C. Fremaux, F. D'Amici, M. Terlizzese, M. Rossi, L. Chevalet, Demonstration of physicochemical and functional similarity between the proposed biosimilar adalimumab MSB11022 and Humira®, mAbs, 9 (2017) 127-139.
[31] R.M. Ionescu, J. Vlasak, C. Price, M. Kirchmeier, Contribution of Variable Domains to the Stability of Humanized IgG1 Monoclonal Antibodies, J. Pharm. Sci., 97 (2008) 1414-1426.

CONCLUSION, FINAL REMARKS AND FUTURE DIRECTION

Antibodies have dominated the therapeutic market for the last decade as treatments for cancers, auto-immune disorders, inflammatory conditions and infections. The antibody landscape continues to evolve beyond the use of mAbs and fragments, with novel formats being developed including bispecifics, antibody-drug conjugates and nanobodies. Each of these formats also benefits from antibody engineering, whereby rational structural changes are made to enhance the biophysical properties of the antibody product, including antigen binding, cytotoxicity and stability. Some Fc-engineered antibodies have already entered the market as therapeutic products such as benralizumab in 2017.

Antibodies, like all proteins, undergo chemical and physical degradation, often leading to protein aggregation. These degradation processes can occur during manufacturing, processing, transport, and long-term storage. Because of the negative impact of antibody aggregation on both manufacturing success and the efficacy and safety of the treatment, it is critical that we continue to develop multi-faceted approaches that tackle protein aggregation. In this thesis, we explored two approaches of combating aggregation: 1) modifications to the formulation (Chapter 2-4 and 6); 2) modifications to the antibody (Chapter 8).

Through the investigation of protein-stabilizing excipients such as L-Arg and L-Glu, D_2O and ionic liquid (CDHP) we shed light on previously unknown issues and demonstrated that such excipients can be incorporated in protein formulations to enhance protein stability. We showed that common stabilizing additives do not stabilize proteins in a general way; each protein must be tested, as the effects are often protein- and concentration-specific (Chapter 2). We demonstrated a novel approach for stabilizing protein formulations by modifying the solvent from H_2O to D_2O to strengthen intramolecular interactions and enhance the conformational stability of the protein. However, this also led to enhanced intermolecular interactions and increased aggregation (Chapter 3). We saw a boom in research on the biological applications of ionic liquids, triggering an invited review of their potential use as antibody-stabilizing agents (Chapter 4). This literature review concluded by identifying several ionic liquids with significant potential as formulation excipients – one of which was CDHP – a biocompatible and effective protein stabilizer. Following an investigation of the aggregation kinetics of mAbs (Chapter 5) which uncovered novel mechanistic insights into the aggregation process, we were successful in stabilizing

trastuzumab at high concentrations (3-fold higher than marketed product) in CDHP (Chapter 6) demonstrating that the stability of these commercial therapeutic products can be taken to new heights with ionic liquids. These results will promote the development of pre-filled syringes with high antibody concentrations that allow convenient administration of antibodies to patients from their homes.

Our second approach to tackling antibody aggregation required an understanding of their production process. We developed a simple and cost-effective method to maximise antibody expression yield and optimise purification (Chapter 7). Following this, we engineered the top-selling therapeutic antibody adalimumab with additional N-linked glycans in the Fab domain and succeeded in improving its conformational stability further, without compromising its antigen or FcγR binding affinity (Chapter 8). Overall, the present work highlighted the unlimited potential to optimise the biophysical properties of therapeutic antibodies through formulation and engineering approaches.

Our work stimulates further research into the optimisation of antibody stability and other important biophysical properties. In addition to screening other novel excipients with high-throughput methods and testing novel formulation modifications, there is more work to be pursued with antibody engineering. We showed that with the addition of a single extra glycan pair in the Fab domain, the stability of the entire domain is significantly improved without compromising antigen binding affinity. Moreover, there may be additional unexplored benefits of this additional glycan pair. Naturally occurring N-linked glycans are known to impact stability, effector function and pharmacokinetics. Engineering additional glycans may introduce new immune functions and properties to the engineered antibodies yet to be discovered.

Future work may also involve characterising the identity of the added glycans in the Fab domain, to establish a possible relationship between the changes in stability and the composition of the glycan added. Modifying the composition of the added glycan via cellular engineering or enzymatic methods and observing its impact on stability is another area of future investigation.

Furthermore, there are several other aggregation-prone regions in other domains such as the Fc domain, that can be engineered to enhance the stability of IgG1 antibodies. A combination of a few mutations in multiple APRs may result in more significant improvements to antibody stability. New or advanced computational techniques are

expected to play a key role in the development of more stable biologics such as antibodies.

Protein aggregation is an ongoing hurdle to the development of biopharmaceuticals such as mAbs. The work presented in this thesis contributes to a detailed understanding of this complex process and provides methods to prevent it in therapeutic mAbs. As the antibody market continues to expand, research into ways of combating protein aggregation becomes increasingly important, especially as we move towards the development of novel antibody formats, which are often less stable than the original mAbs. Addressing protein aggregation will lead to reduced immunogenicity, improved pharmacokinetics, reduced tolerance to treatment and less manufacturing hurdles. The maximal potential of antibody therapeutics is yet to be unlocked.

APPENDICES

Appendix 1A: Supplementary data from chapter 7

Table S1. List of reagents and equipment used in the protocol and their source

Product	Catalogue Number	Company	Web Address	Comments
pFUSE vector series	N/A	InvivoGen	www.invivogen.com	Heavy and light antibody genes expressed in separate vectors that require co-transfection.
mAbXpress vector series	N/A	ACYTE Biotech Pty Ltd.	www.acyte.com	Heavy and light antibody genes expressed in separate vectors that require co-transfection. Refer to: Jones, M. L. et al. A method for rapid, ligation-independent reformatting of recombinant monoclonal antibodies. J Immunol Methods. 354 (1-2), 85-90, doi:10.1016/j.jim.2010.02.001, (2010).
pVITRO1 vector	N/A	N/A	N/A	Heavy and light antibody genes are each driven by a separate promoter in a single vector. Refer to: Dodev, T. S. et al. A tool kit for rapid cloning and expression of recombinant antibodies. Sci Rep. 4 5885, doi:10.1038/srep05885, (2014).
GS vector series	N/A	Lonza	www.lonza.com	Multi-cistronic vector with heavy and light antibody genes co-expressed and translated as single transcript.
Multi-cistronic vector series 1	N/A	N/A	N/A	Multi-cistronic vector with heavy and light antibody genes co-expressed and translated as single transcript. Refer to: Li, J. et al. A comparative study of different vector designs for the mammalian expression of recombinant IgG antibodies. J Immunol Methods. 318 (1-2), 113-124, doi:10.1016/j.jim.2006.10.010, (2007).

Multi-cistronic vector series 2	N/A	N/A	N/A	Multi-cistronic vector with heavy and light antibody genes co-expressed and translated as single transcript. Refer to: Ho, S. C. et al. IRES-mediated Tricistronic vectors for enhancing generation of high monoclonal antibody expressing CHO cell lines. J Biotechnol. 157 (1), 130-139, doi:10.1016/j.jbiotec.2011.09.023, (2012).
pVITRO1-Trastuzumab-IgG1/κ	61883	Addgene	www.addgene.org	Mammalian expression vector containing trastuzumab antibody genes with hygromycin resistance gene; pVITRO1-Trastuzumab-IgG1/κ was a gift from Andrew Beavil.
Fast-Media Hygro Agar	fas-hg-s	Jomar Life Research	www.liferesearch.com	Used to prepare low salt LB agar containing 75 µg/ml hygromycin.
Fast-Media Hygro TB	fas-hg-l	Jomar Life Research	www.liferesearch.com	Used to prepare low salt TB broth containing 75 µg/ml hygromycin.
Glycerol, BioXtra, ≥99%	G6279	Sigma-Aldrich	www.sigmaaldrich.com	Prepare to 80% with water and autoclave. Store at room temperature.
Jestar 2.0/LFU Plasmid Maxi Kit	G221020	Astral Scientific	www.astralscientific.com.au	Plasmid Maxi Prep Kit; elute or resuspend DNA in water (pH 7.0-8.5).
FreeStyle 293-F Cells	R790-07	Life Technologies	www.lifetechnologies.com	HEK-293 cell line adapted to suspension culture in serum-free media.
FreeStyle 293 Expression Medium	12338-018	Life Technologies	www.lifetechnologies.com	Serum-free media specially formulated for maintaing 293-F cell line and high protein expression.
Kolliphor P188	K4894	Sigma-Aldrich	www.sigmaaldrich.com	Non-ionic surfactant; pluronic F-68; prepare to 10% in water and filter-sterilize using 0.22 µm filter. Store at 4°C.
DMEM, high glucose	11995-065	Life Technologies	www.lifetechnologies.com	
Heat-Inactivated Foetal Bovine Serum	10082-147	Life Technologies	www.lifetechnologies.com	

Polyethylenimine, Linear, MW 25,000	23966	Polysciences, Inc.	www.polysciences.com	Prepare to 1 mg/ml in water. Adjust to pH 7.0 with 1 M HCl (solution becomes clear) and filter-sterilize using 0.22 µm filter. Store at -80^{o}C until use.
OptiPro SFM	12309-050	Life Technologies	www.lifetechnologies.com	Transfection formulated serum-free media
Hygromycin B Solution	ant-hg-1	Jomar Life Research	www.liferesearch.com	
Dimethylsulphoxide (DMSO)	AJA2225	Thermo Fisher Scientific	www.thermofisher.com	
Tryptone (casein peptone)	LP0042B	Thermo Fisher Scientific	www.thermofisher.com	Prepare to 20% in PBS and filter-sterilize using 0.22 µm filter. Store at 4^{o}C.
Phosphate Buffered Saline (PBS) Tablets, pH 7.4, 100 ml	09-2051-100	Astral Scientific	www.astralscientific.com.au	
HiTrap Protein A High Performance, 1 x 5 ml column	GE17-0403-01	Sigma-Aldrich	www.sigmaaldrich.com	
AKTApurifier 100	28406266	GE Healthcare	www.gelifesciences.com	Automated FPLC system, which can include a P-960 sample pump and Frac-920 fraction collector.
Glycine-HCl	G2879	Sigma-Aldrich	www.sigmaaldrich.com	
Citric Acid, monohydrate	BIOC2123	Astral Scientific	www.astralscientific.com.au	
Sodium Citrate, trisodium salt dihydrate	BIOCB0035	Astral Scientific	www.astralscientific.com.au	
1 M Tris-HCl solution pH 9.0	BIOSD8146	Astral Scientific	www.astralscientific.com.au	
Amicon Ultra Centrifugal Filters (30 MWCO)	UFC803008/UFC903008	Merck Millipore	www.merckmillipore.com	Used to buffer exchange and concentrate purified protein.

Pierce Bicinchoninic Acid (BCA) Assay Kit	23227	Thermo Fisher Scientific	www.thermofisher.com	
BLItz System	45-5000	fortéBIO	www.blitzmenow.com	Instrument used for bio-layer interferometry (BLI) measurements.
Protein A biosensors	18-5010	fortéBIO	www.blitzmenow.com	
Acrylamide/Bisacrylamide (37.5:1), 40% solution	786-502	Astral Scientific	www.astralscientific.com.au	
Ammonium Persulfate (APS)	AM0486	Astral Scientific	www.astralscientific.com.au	
TEMED	AM0761	Astral Scientific	www.astralscientific.com.au	
Coomassie Brilliant Blue R-250	786-498	Astral Scientific	www.astralscientific.com.au	
Precision Plus Dual-Color Protein Standard	1610374	Bio-Rad	www.bio-rad.com	

Appendix 1B: Supplementary data from chapter 8

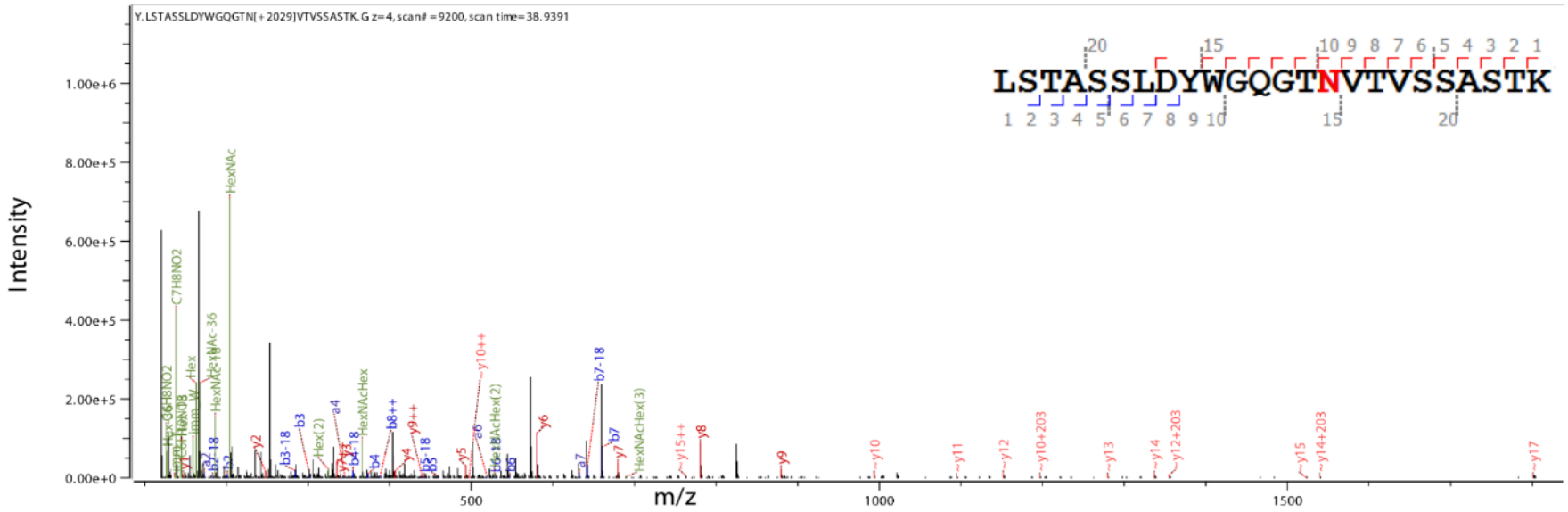

Figure S1. HCD spectrum of the chymotryptic peptide LSTASSLDYWGQGTNVTVSSASTK for the L116N mutant

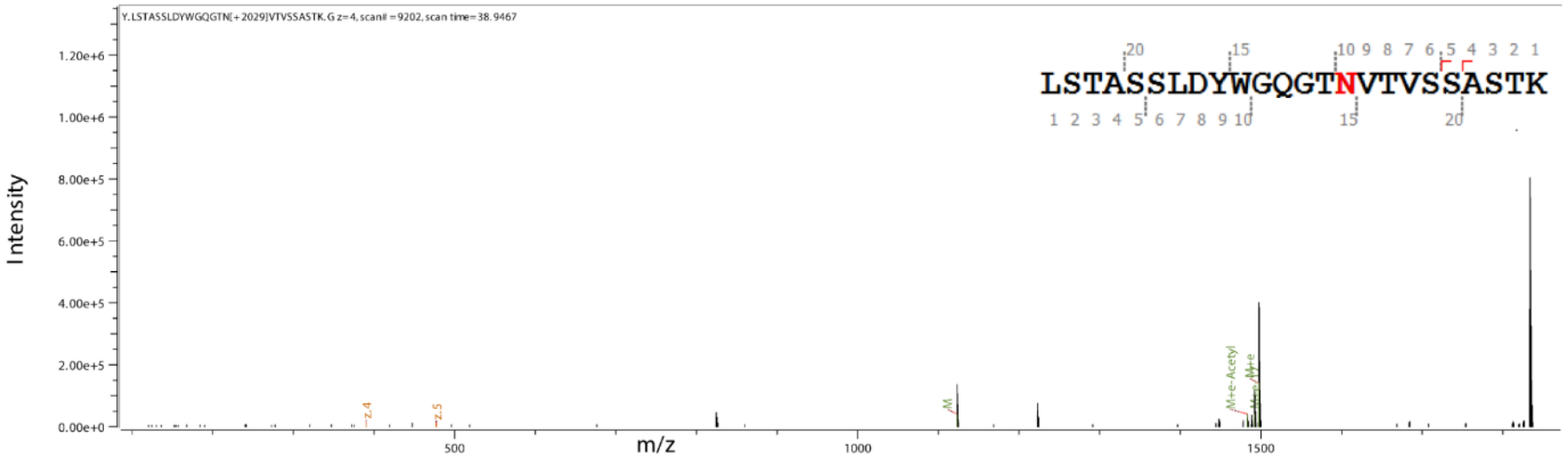

Figure S2. ETD spectrum of the chymotryptic peptide LSTASSLDYWGQGTNVTVSSASTK for the L116N mutant.

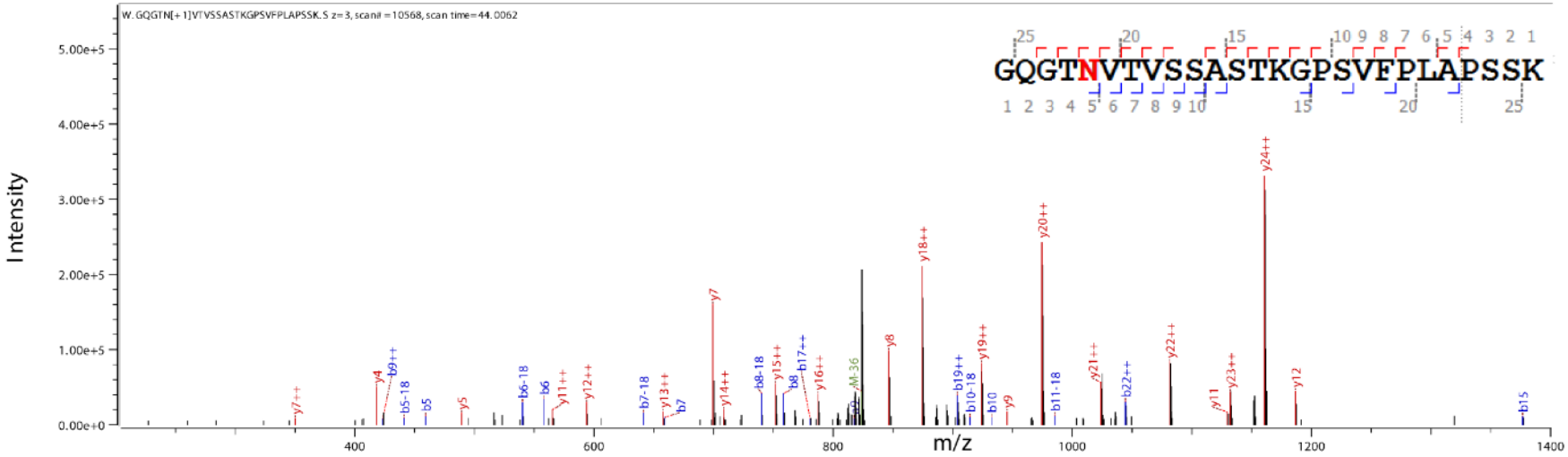

Figure S3. HCD spectrum of the de-glycosylated chymotryptic peptide GQGTNVTVSSASTKGPAVFPLAPSSK for the L116N mutant.

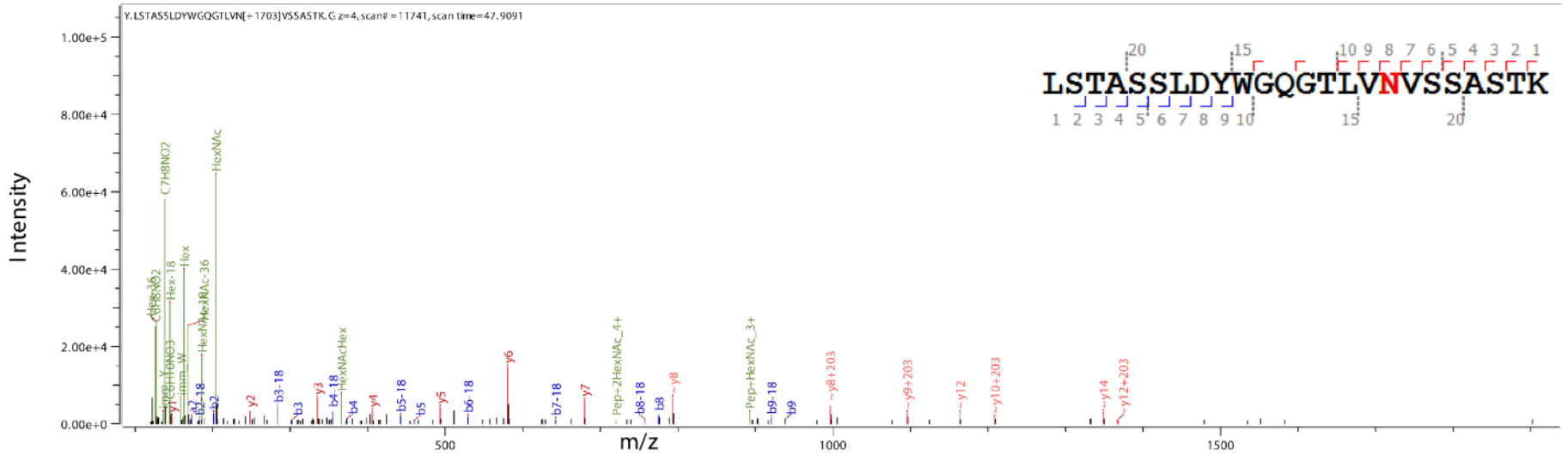

Figure S4. HCD spectrum of the chymotryptic peptide LSTASSLDYWGQGTLVNVSSASTK for the T118N mutant.

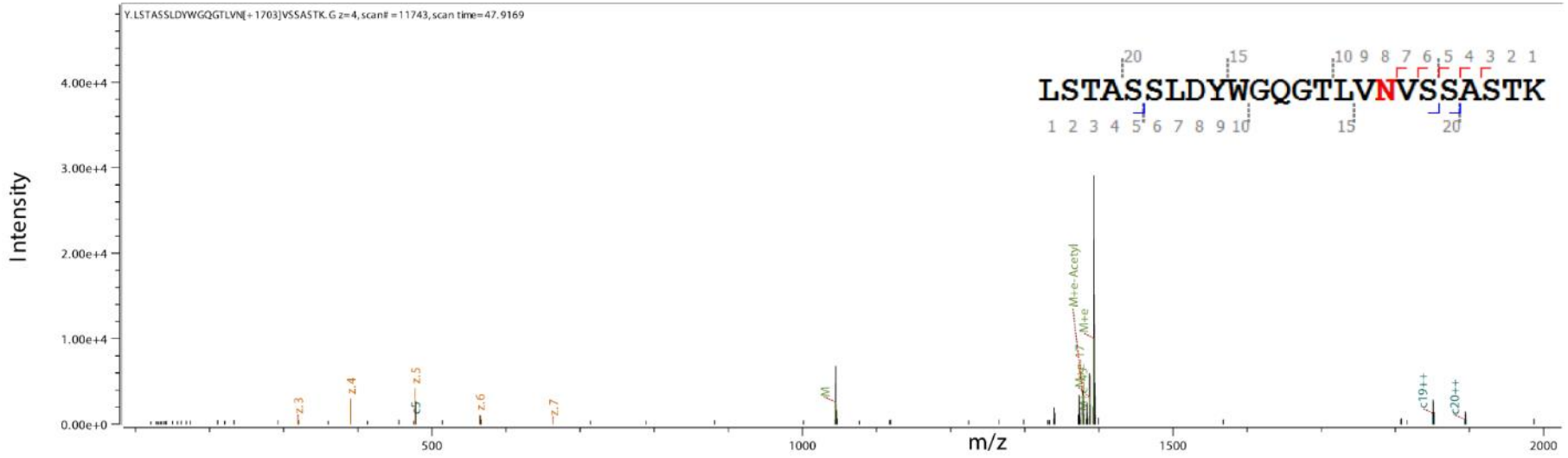

Figure S5. ETD spectrum of the chymotryptic peptide LSTASSLDYWGQGTLVNVSSASTK for the T118N mutant.

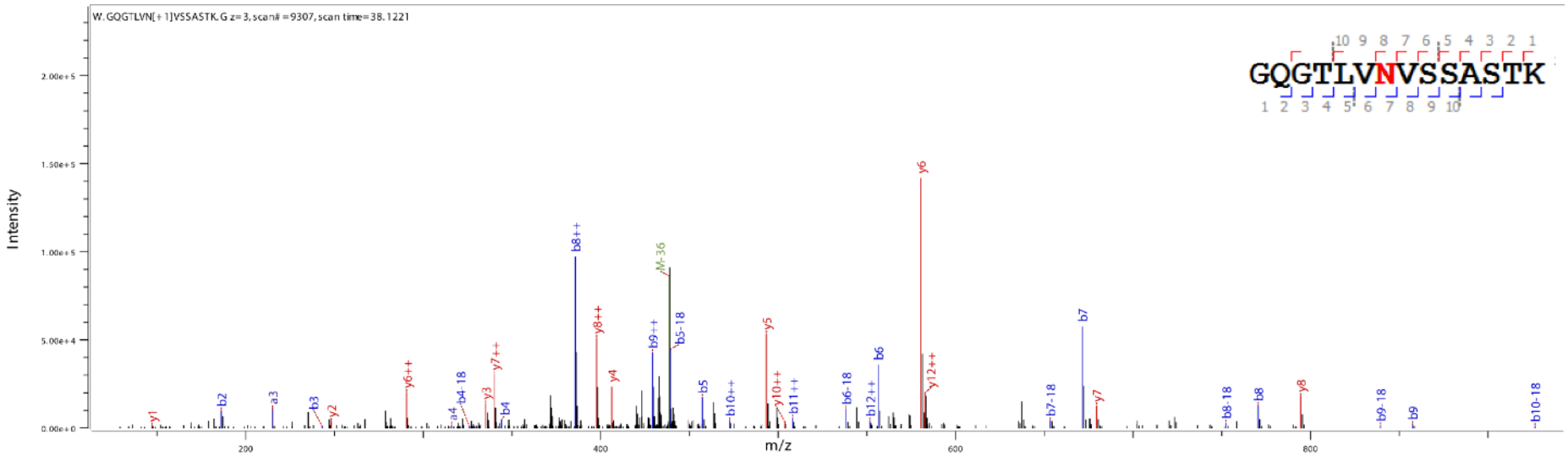

Figure S6. CID spectrum of the de-glycosylated chymotryptic peptide LSTASSLDYWGQGTLVNVSSASTK for the T118N mutant.

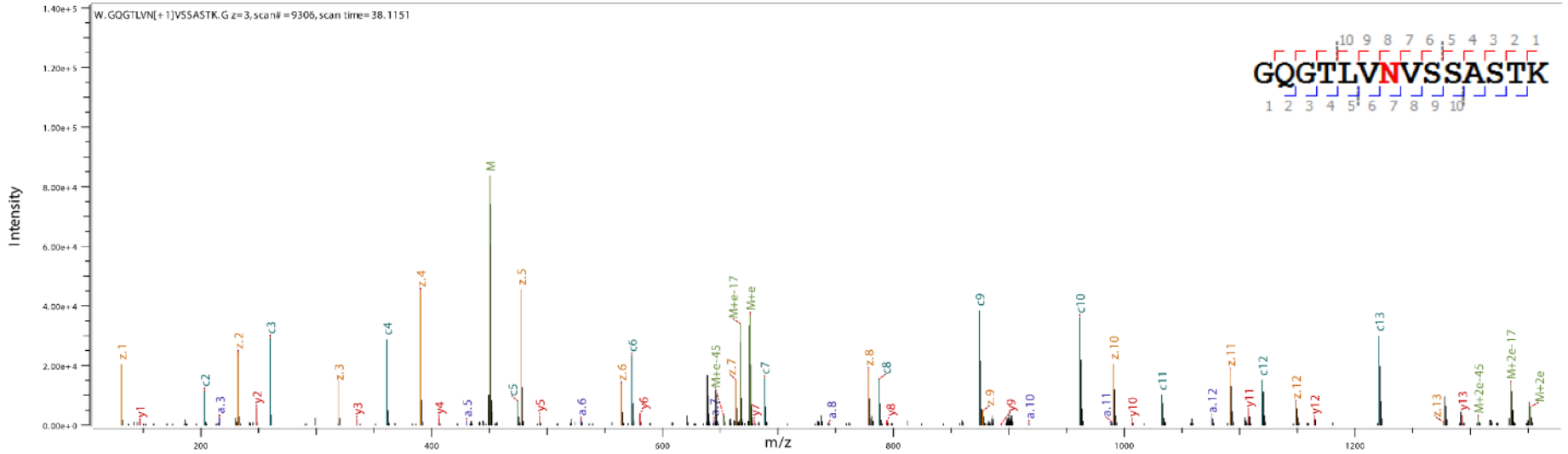

Figure S7. ETD spectrum of the de-glycosylated chymotryptic peptide LSTASSLDYWGQGTLVNVSSASTK for the T118N mutant.

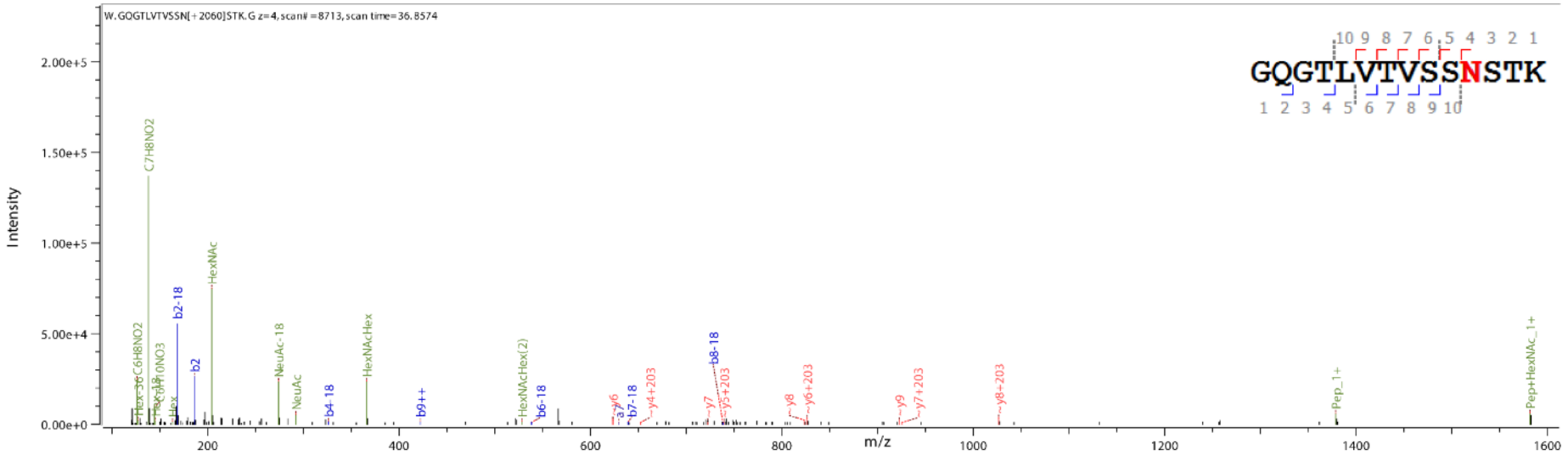

Figure S8. HCD spectrum of the chymotryptic peptide GQGTLVTVSSNSTK for the A122N mutant.

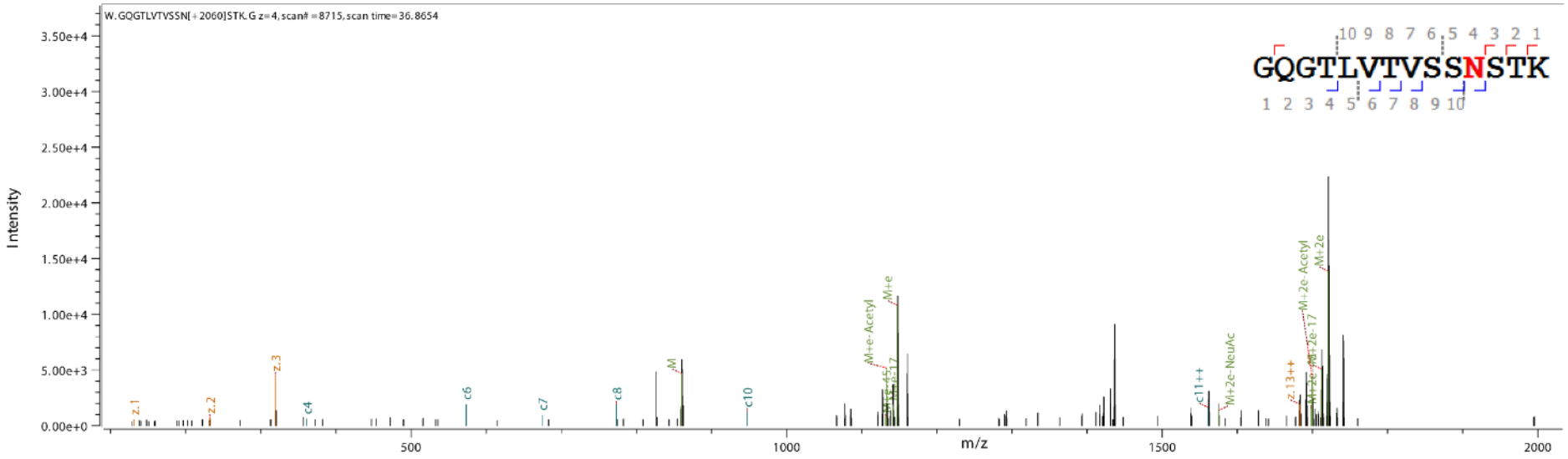

Figure S9. ETD spectrum of the chymotryptic peptide GQGTLVTVSSNSTK for the A122N mutant.

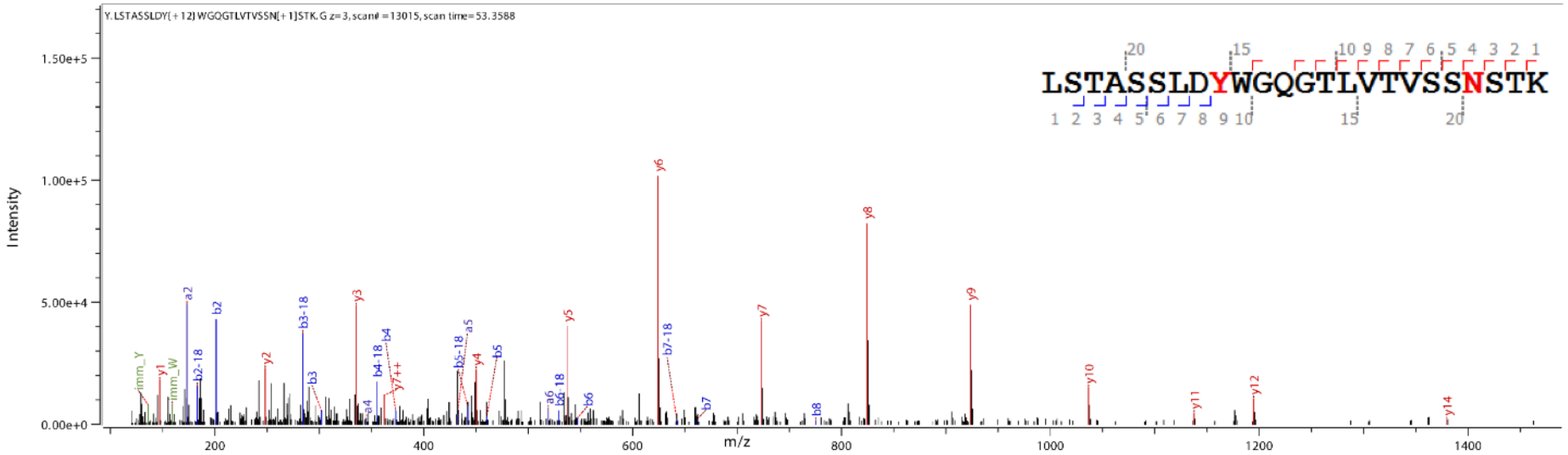

Figure S10. CID spectrum of the de-glycosylated chymotryptic peptide LSTASSLDYWGQGTLVTVSSNSTK for the A122N mutant.

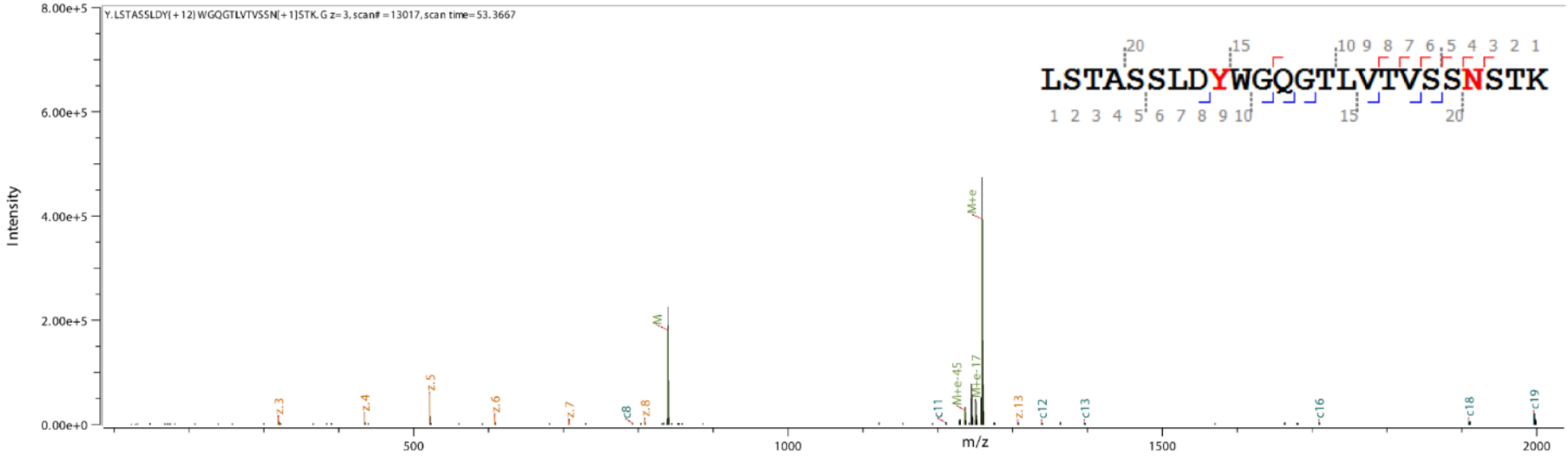

Figure S11. ETD spectrum of the de-glycosylated chymotryptic peptide LSTASSLDYWGQGTLVTVSSNSTK for the A122N mutant.

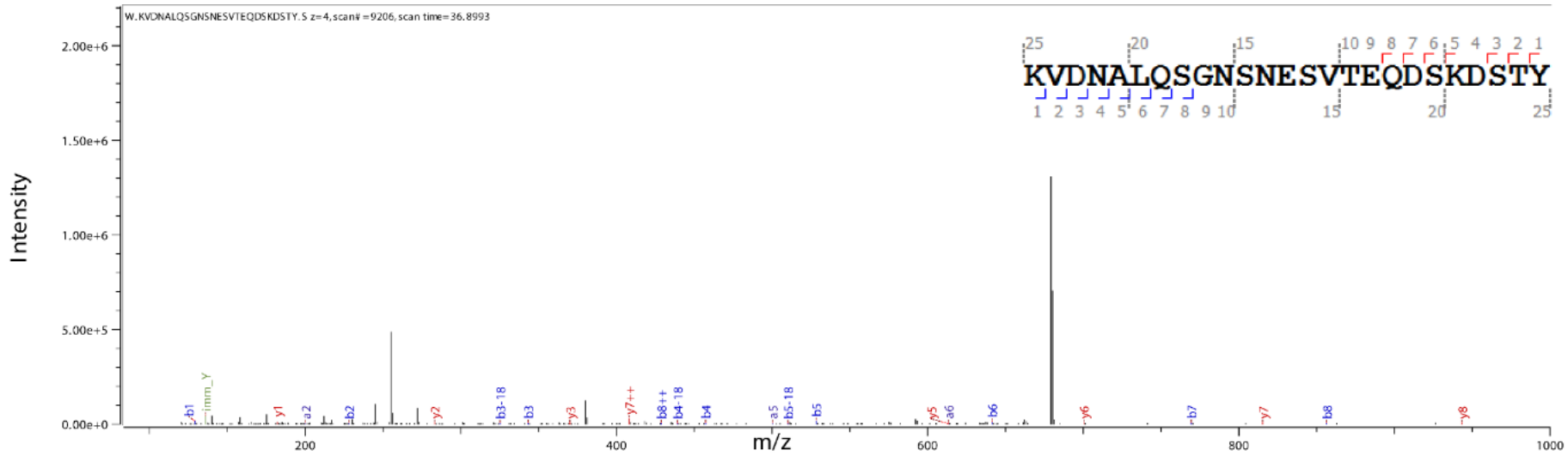

Figure S12. HCD spectrum of the chymotryptic peptide KVDNALQSGNSNESSVTEQDSKDSTY for the Q160N mutant

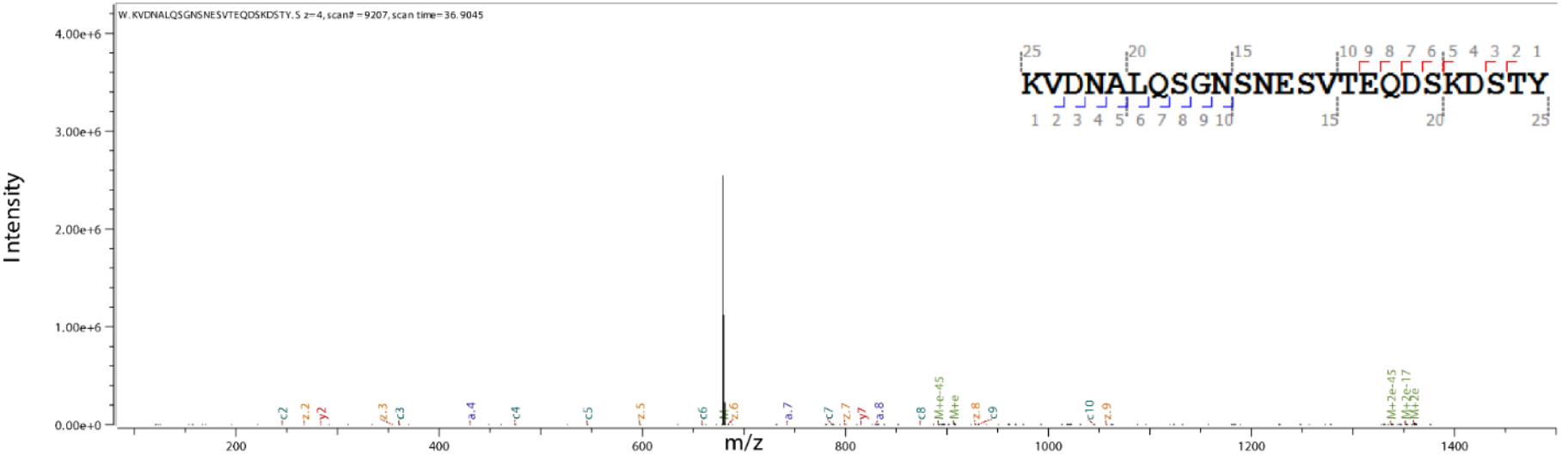

Figure S13. ETD spectrum of the chymotryptic peptide KVDNALQSGNSNESSVTEQDSKDSTY for the Q160N mutant

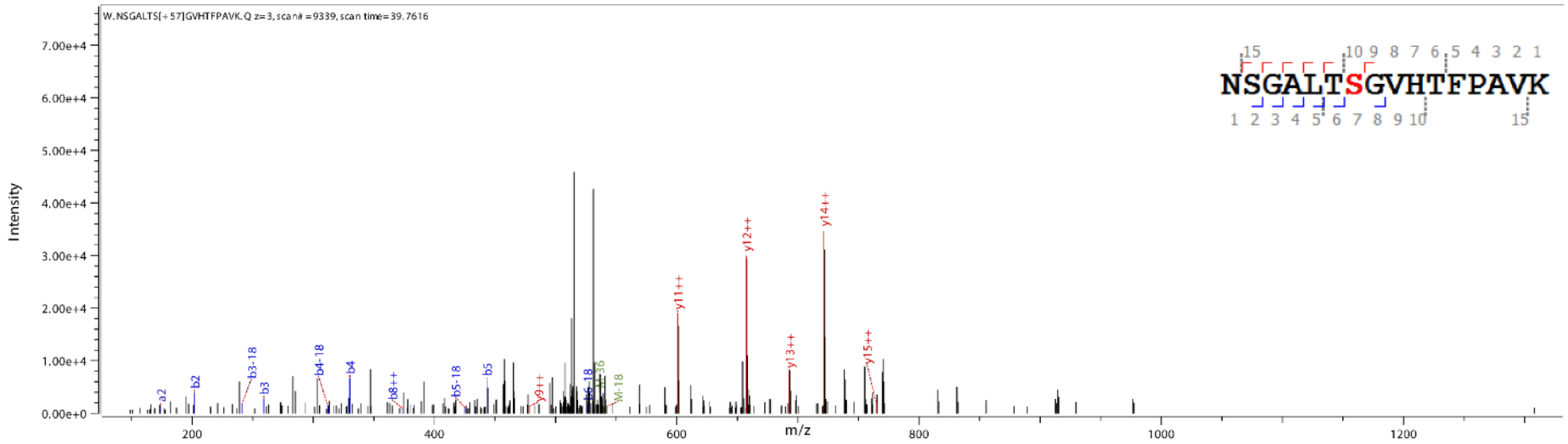

Figure S14. CID spectrum of the chymotryptic peptide NSGALTSGVHTFPAVK for the L178K mutant.

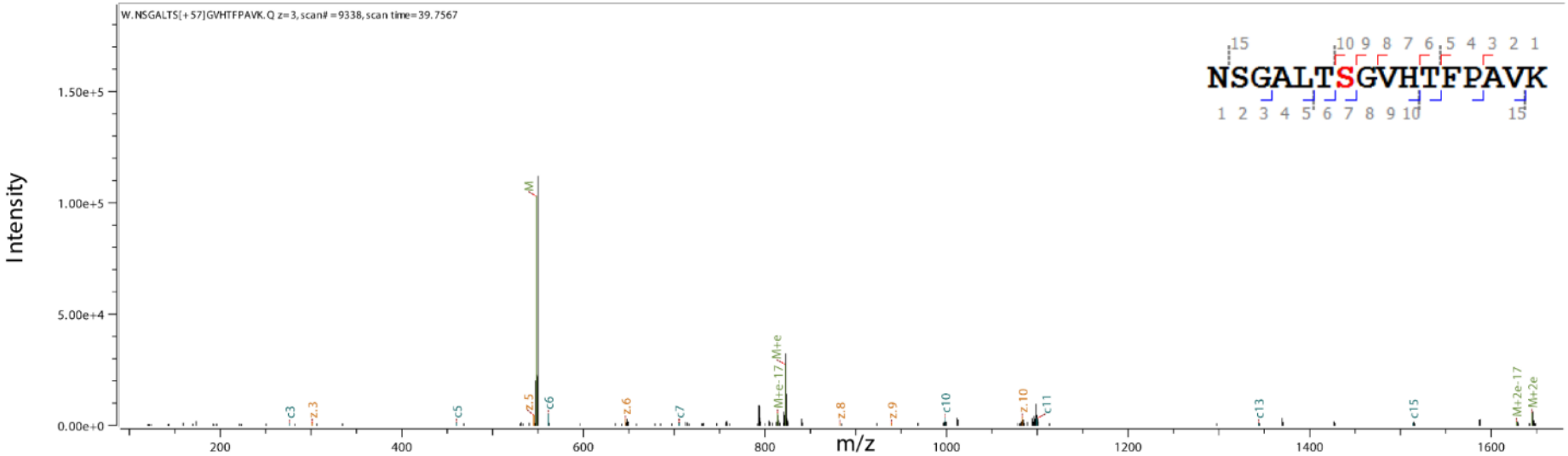

Figure S15. ETD spectrum of the chymotryptic peptide NSGALTSGVHTFPAVK for the L178K mutant.

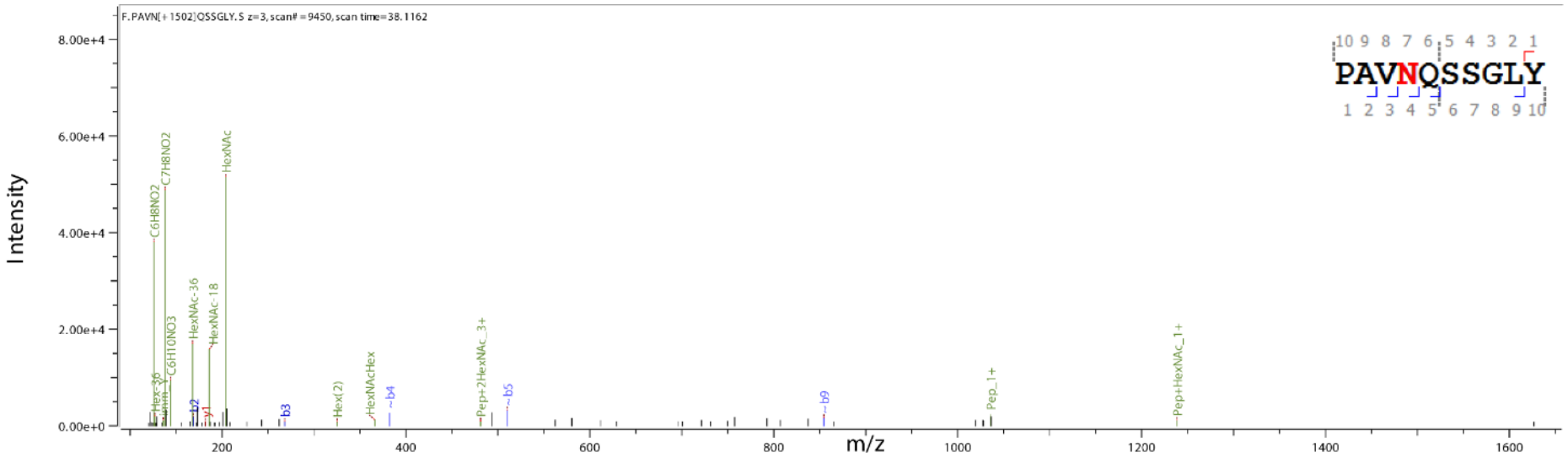

Figure S16. HCD spectrum of the chymotryptic peptide PAVNQSSGLY for the L178N mutant.

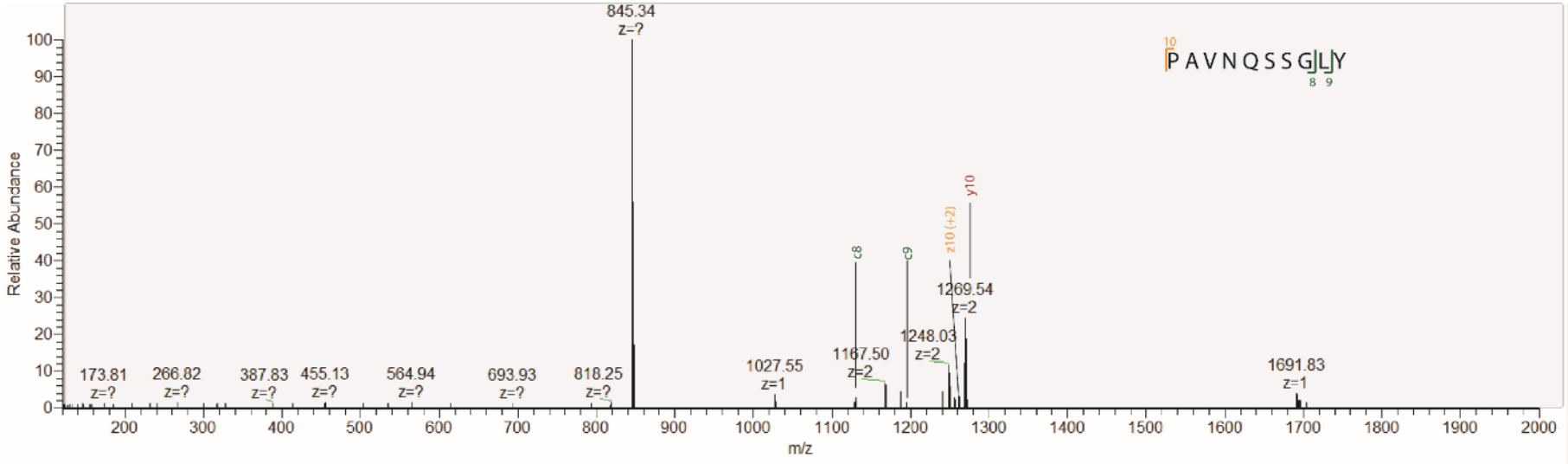

Figure S17. ETD spectrum of the chymotryptic peptide PAVNQSSGLY for the L178N mutant.

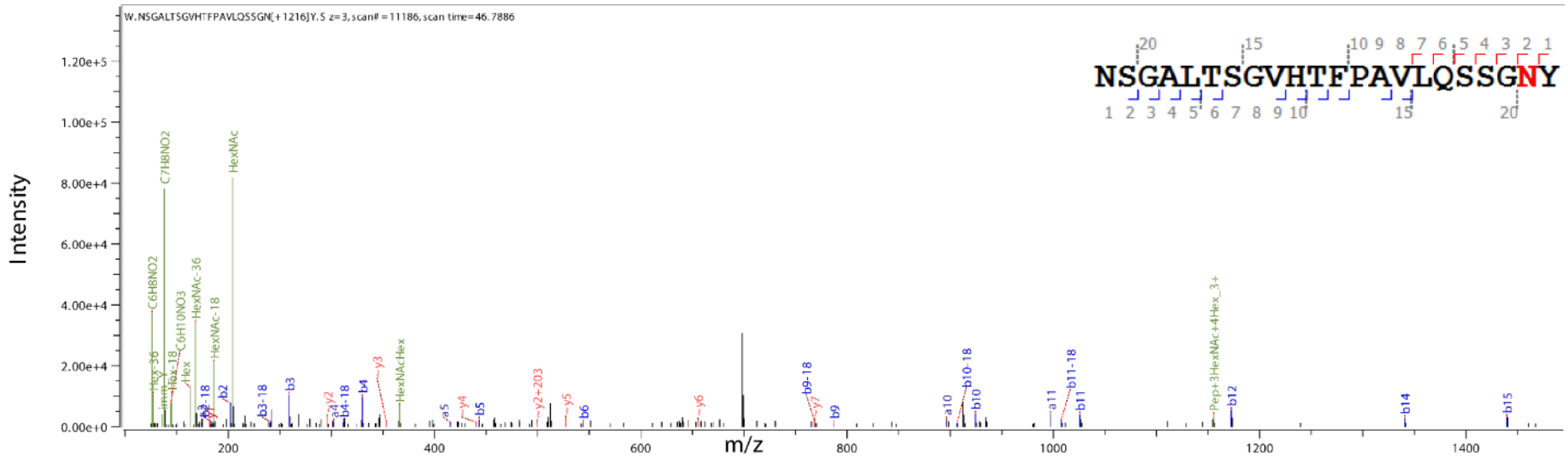

Figure S18. HCD spectrum of the chymotryptic peptide NSGALTSGVHTFPAVLQSSGNY for the L183N mutant.

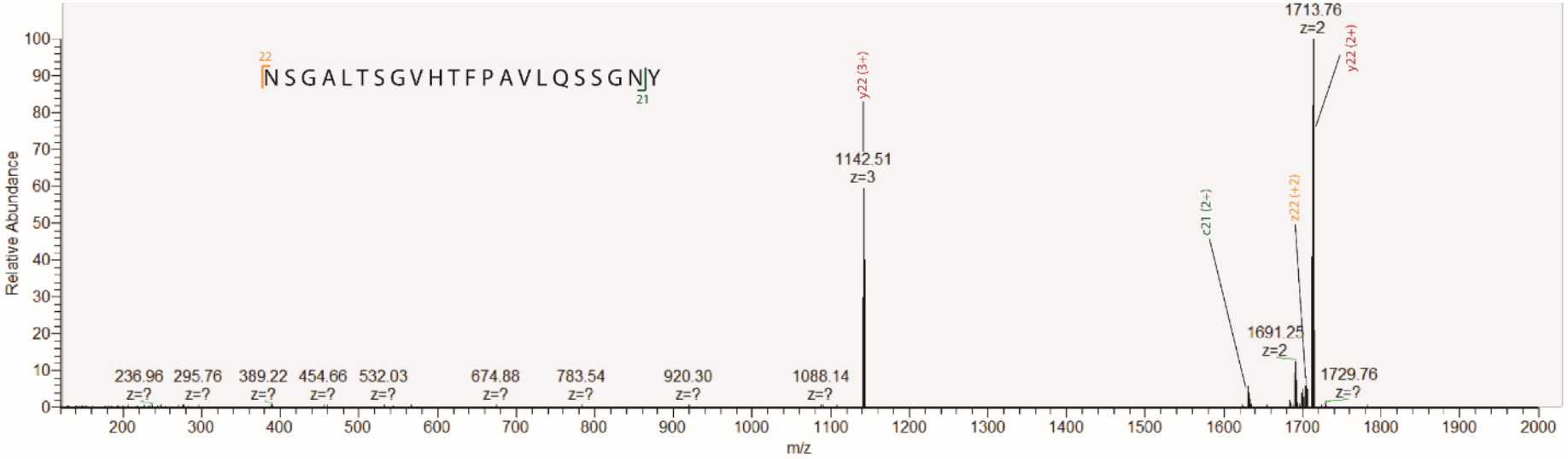

Figure S19. ETD spectrum of the chymotryptic peptide NSGALTSGVHTFPAVLQSSGNY for the L183N mutant.

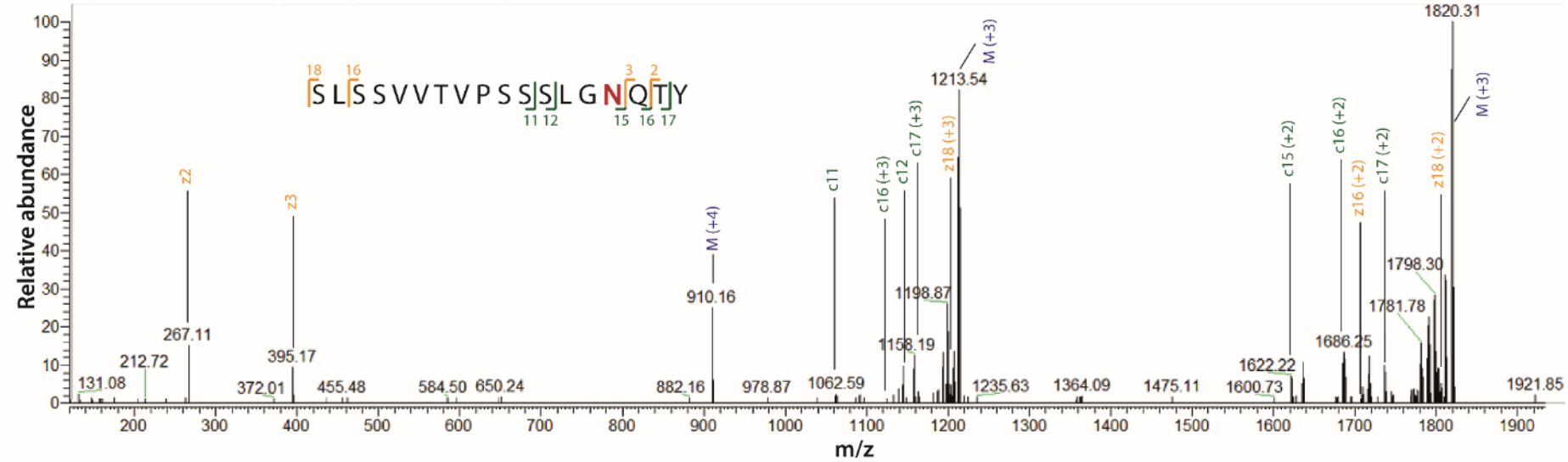

Figure S20. ETD spectrum of the chymotryptic peptide SLSSVVTVPSSSLGNQTY for the T198N mutant.

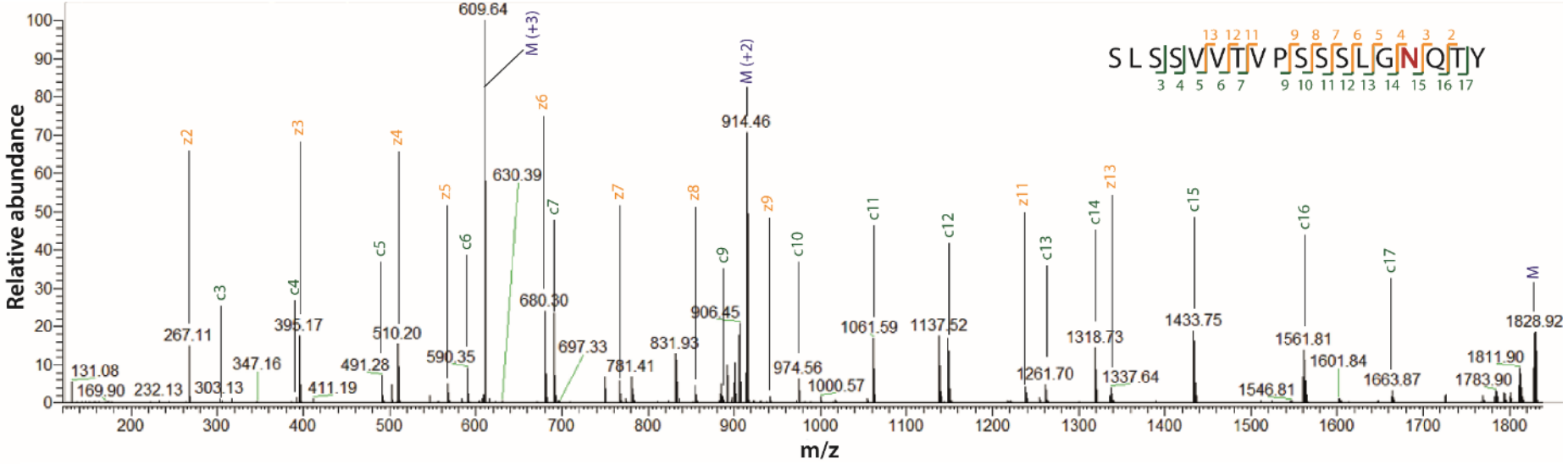

Figure S21. ETD spectrum of the de-glycosylated chymotryptic peptide SLSSVVTVPSSSLGNQTY for the T198N mutant.

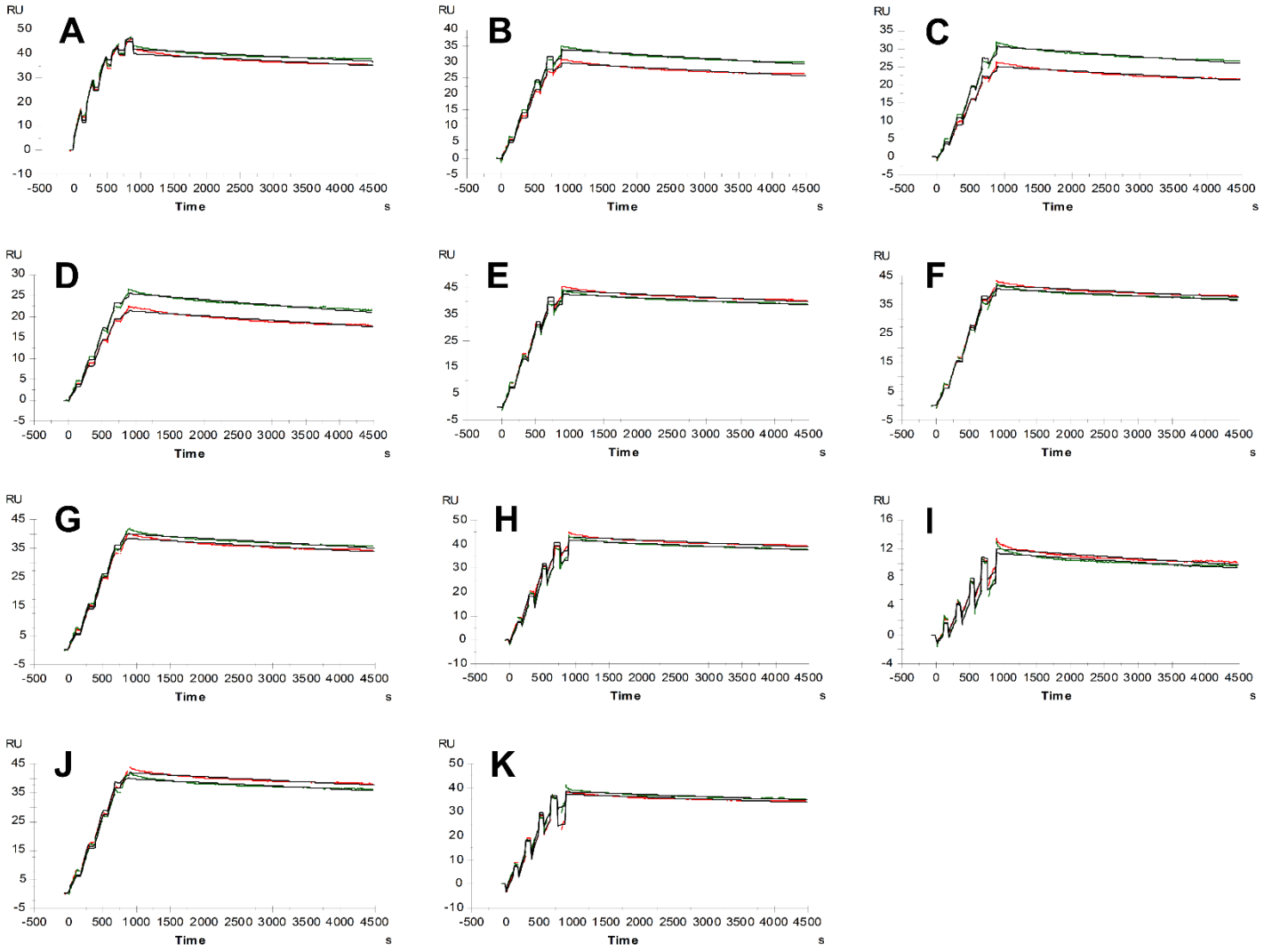

Figure S22. Single cycle kinetic sensograms of monomeric AdmAb variants binding to soluble homotrimeric TNF-α. Humira® (A), AdmAb WT (B), L178K (C), L178N (D), Q160N (E), L116N (F), T118N (G), A122N (H), Q179N (I), L183N (J) and T199N (K).

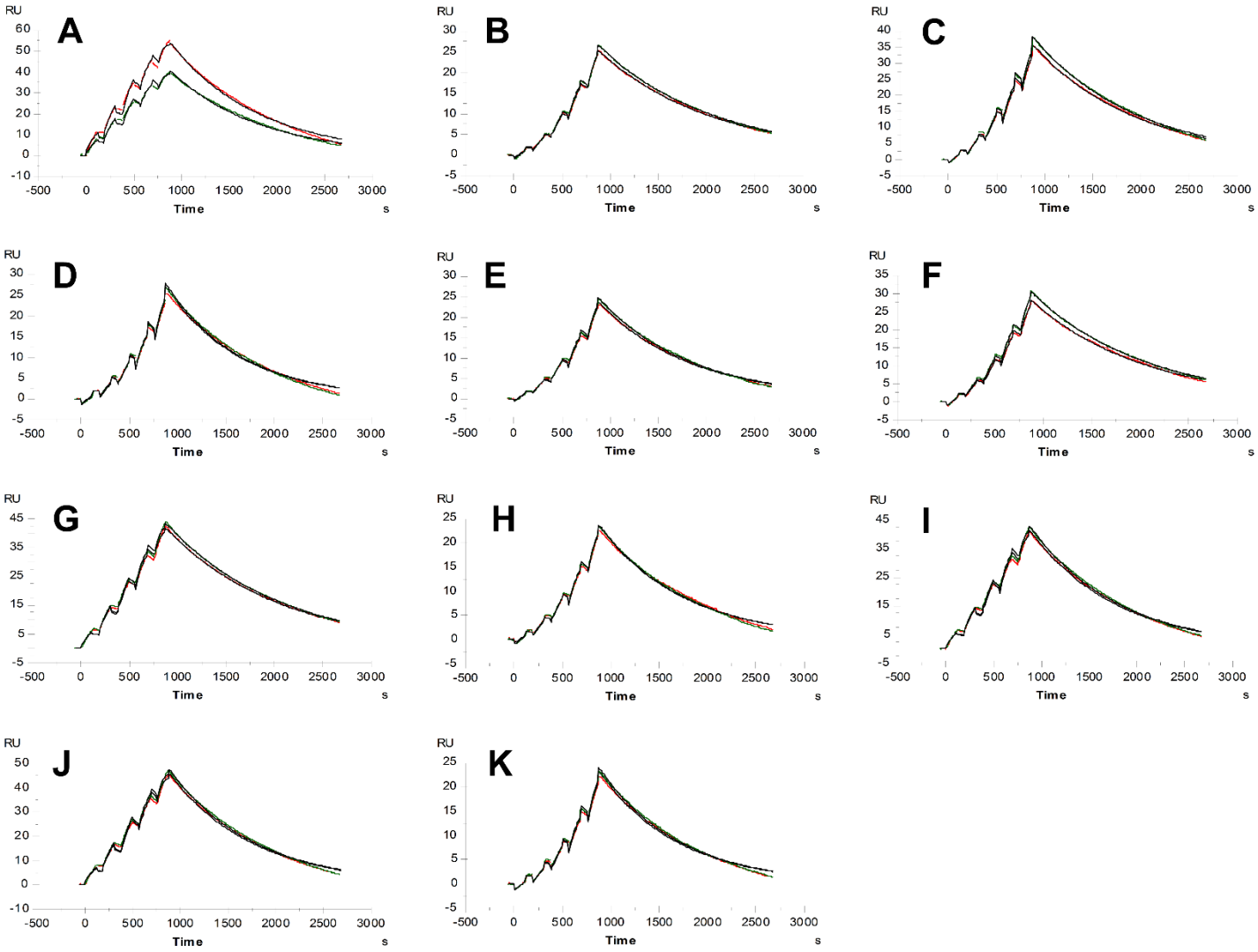

Figure S23. Single cycle kinetic sensograms of monomeric AdmAb variants binding to $Fc_{\gamma}R1A$. Humira® (A), AdmAb WT (B), L178K (C), L178N (D), Q160N (E), L116N (F), T118N (G), A122N (H), Q179N (I), L183N (J) and T199N (K).

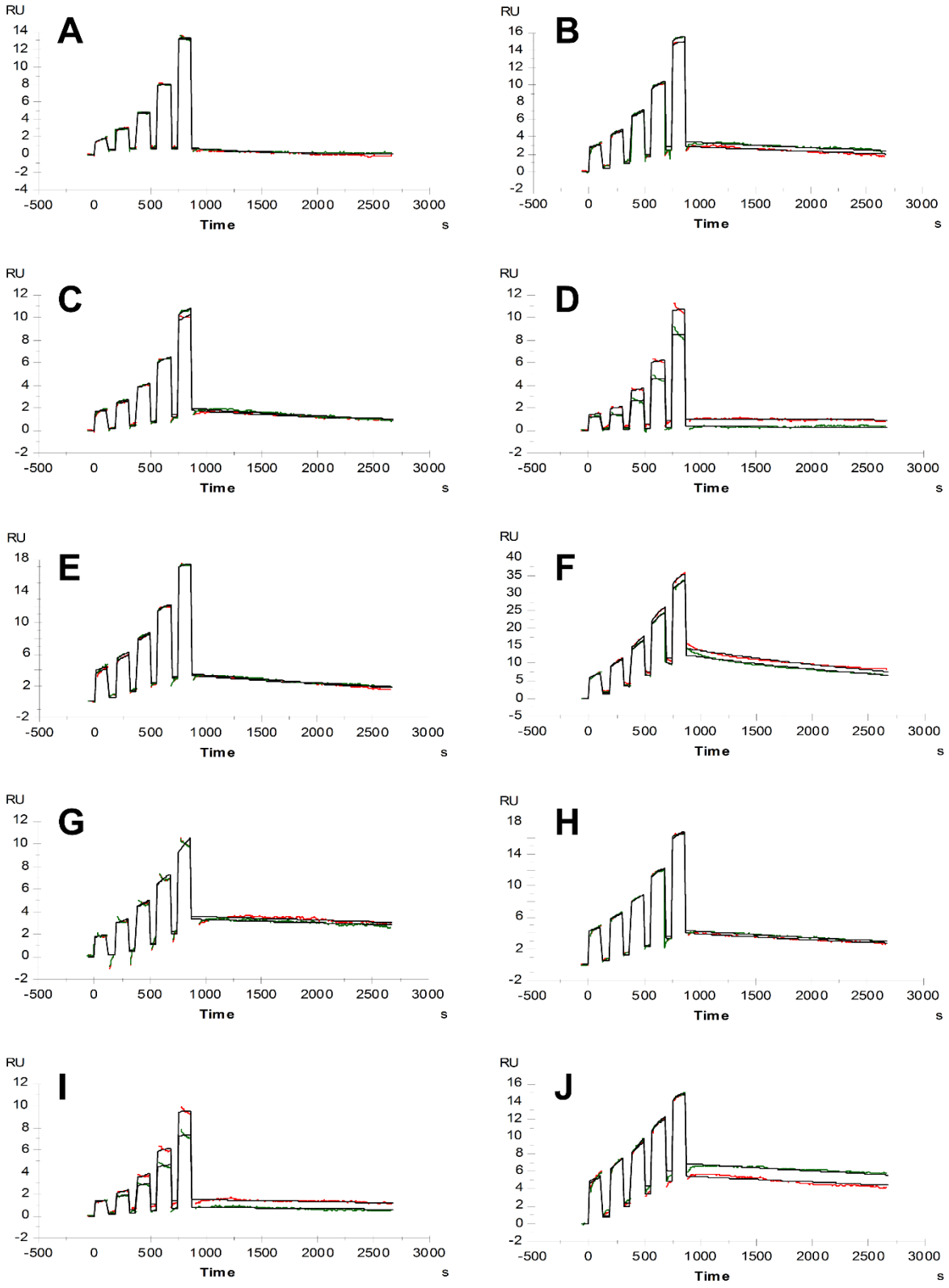

Figure S24. Single cycle kinetic sensograms of monomeric AdmAb variants binding to $Fc_{\gamma}R2B$. Humira® (A), AdmAb WT (B), L178K (C), L178N (D), L116N (E), T118N (F), A122N (G), Q179N (H), L183N (I) and T199N (J).

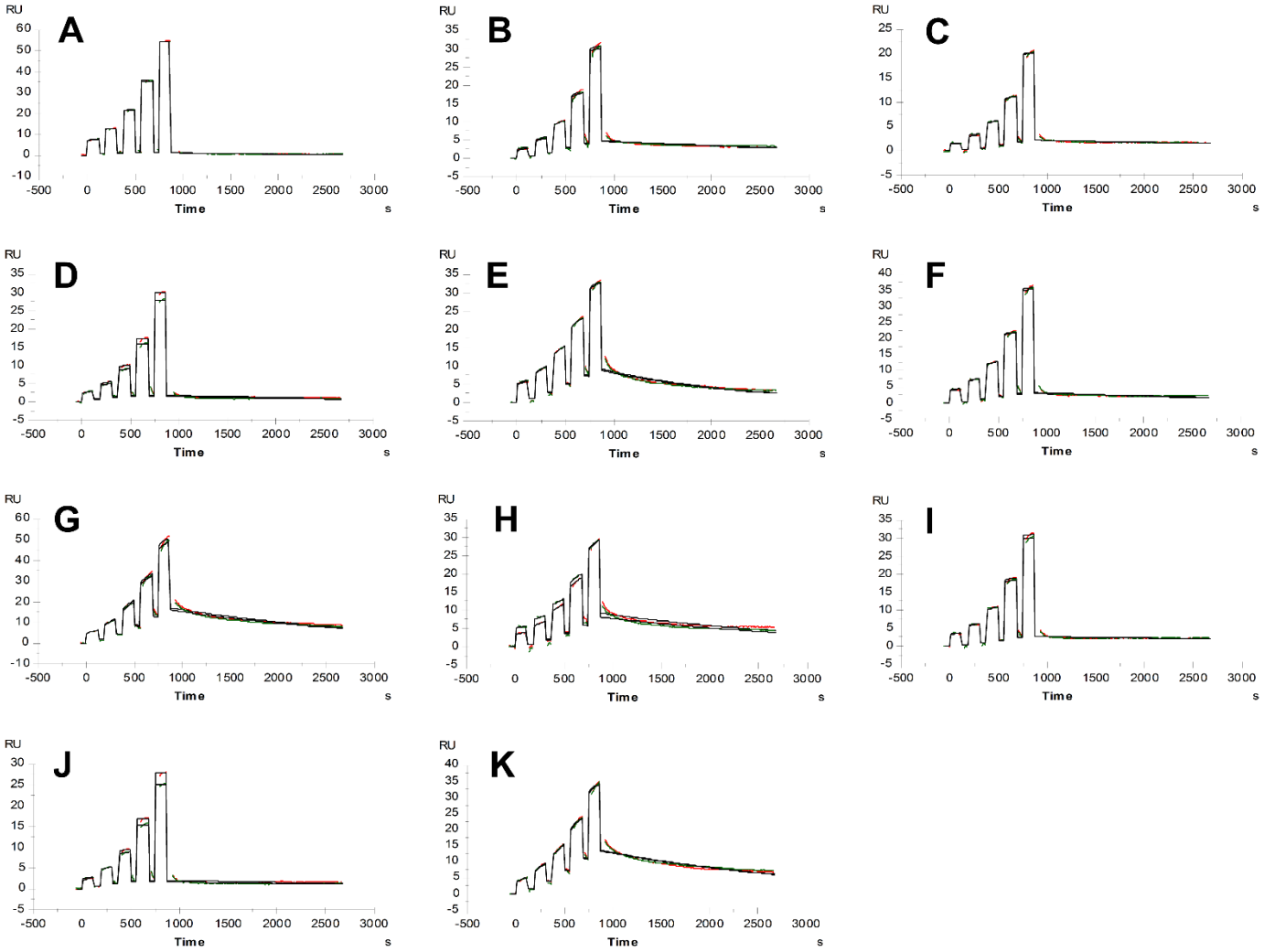

Figure S25. Single cycle kinetic sensograms of monomeric AdmAb variants binding to $Fc_{\gamma}R3A$. Humira® (A), AdmAb WT (B), L178K (C), L178N (D), Q160N (E), L116N (F), T118N (G), A122N (H), Q179N (I), L183N (J) and T199N (K).